Chlorpyrifos and chlorpyrifos oxon induce neurite retraction and cytoskeletal disruption in mouse N2a cells and human neural progenitor stem cells

Ramya A. Sindi

A thesis submitted in partial fulfilment of the
requirements of Nottingham Trent University
for the degree of Doctor of Philosophy

December 2015

Copyright statement:

Declaration

I, Ramya Sindi, hereby declare that the work presented in this thesis was conducted by myself. Exceptions to this have been clearly stated in the text.

Acknowledgments

'All thanks and praise be to Allah'

I am very grateful to my supervisors Dr. Alan Hargreaves and Dr. Chris Lloyd Mills, for their continuous support, guidance, patience and supervision during the course of this work. Without their support, this work will not be completed. I only hope my effort have matched their input.

A special thank to Wayne Harris, for his endless support and help during my lab work. You are truly an exceptional teacher and lab advisor. Many thanks for my lab mate Biola, Falguni, Al-Anood, Najyah and Reham for their support and comments. Special thanks to my second family in Nottingham Mai, Wesam, Ohoud, Rwa`a and Samar, who supported me during this journey.

I acknowledge the fund and support of King Abdullah Scholarship Program and Umm Al-Qura University (Faculty of Applied Medical Science) during my course work.

I am forever in debt to my Mum and my role model Prof. Houriyah Turkustani. My warmest thanks also go to my Dad Ahmed Sindi, the greatest father in the world. My thanks are also extended to my sisters and brothers. Thank you all for your praying, understanding, endless patience and encouragement. Because of you and your confidence in me I am who I am today. Love you all from the bottom of my heart.

To my treasure Abdulrahman and Anan, thank you for all the happy wishes and patience you showed during my work. Your smiles encourage me to finish this mission. I knew I was far away and missed a lot of play time but I promise that I will make it up to you and join you in every little thing you do.

I would like to express my deepest gratitude and appreciation to my husband, my love and my all, Dr. Ayman Alsaegh for all the sacrifices, understanding, advices, endless love, care, confidence and support to overcome all the difficulties encountered me during the years of my study. Your success motivated me and where would I be without you! You were always there for me and gave me the strength when I did not believe in myself. No words in the world can describe my appreciation to you. It is only because of you that I was able to finish this thesis and this degree! I am really sorry for all those hard times and sad nights we passed through. I hope I`ve made you proud.

Thank you Allah for making this dream possible. .

Abstract

The widespread use of the organophosphorous insecticide chlorpyrifos (CPF) over recent decades has posed major concerns about its toxicity in humans. Sub-cytotoxic concentrations of CPF and its metabolite CPF-oxon (CPO) were known to inhibit neurite outgrowth in differentiating neural cells but little was known about their ability to cause neurite retraction. The main aims of this study were to investigate the effects of CPF and CPO on the stability of neurites in pre-differentiated mouse N2a neuroblastoma and human ReNcell CX neural stem cells, and to relate toxicity to the regulation of cytoskeletal proteins involved in neural differentiation.

At 3 µM, both compounds reduced the numbers of axon-like processes in pre-differentiated N2a cells, as indicated by morphometric analysis of carboxyfluorescein succinimidyl ester-labelled cells. Retraction of neurites was observed within 2 h of exposure by live cell imaging. Neurofilament disruption was detected in treated cells, by indirect immunofluorescence with anti-phosphorylated neurofilament heavy chain (pNFH) monoclonal antibody SMI34, while the microtubule network was unaffected. Western blotting analysis revealed transiently increased levels of reactivity of Ta51 after 2 h exposure but reduced levels of reactivity following 8 h treatment with both compounds, whereas reactivity of anti-total NFH or anti-tubulin were unaffected. Altered NFH phosphorylation at 2 h exposure was associated with increased activation of extracellular signal-regulated protein kinase ERK 1/2. Increased levels of phosphatase activity were observed following 8 h treatment, suggesting that organophosphate-induced neurite retraction in N2a cells is associated with early transient increases in NFH phosphorylation and ERK1/2 activation.

High content analysis of immunofluorescently stained N2a cells showed that the induction of neurite retraction by both compounds was concentration-dependent. The same concentrations of CPF and CPO also caused retraction of neurites in differentiating neuronal and glial populations of human ReNcells.

Using a cell ELISA technique changes observed in Western blot analysis were confirmed and found to be concentration-dependent in N2a cells. In pre-differentiated ReNcells, reduced levels of NFH phosphorylation were observed, whereas total NFH, βIII-tubulin and ERK1/2 activation were unaffected. Acetylcholinesterase assays suggested that inhibition was not required for neurite retraction but could affect the severity of such effects.

List of Abbreviations

AChE	Acetylcholinesterase
ACh	Acetylcholine
ACP	Advisory Committee on Pesticides
ADHD	Attention deficit hyperactivity disorder
AIDA	Advanced Image Data Analysis software
ALP	Alkaline phosphatase
ANOVA	Analyses of variance
APS	Ammonium persulphate
ATCH	Acetylthiocholine iodide
ATP	Adenosine triphosphate
ATSDR	Agency for Toxic Substances and Disease Registry
B512	Monoclonal antibody recognising α-tubulin
BCA	Bicinchoninic acid
BSA	Bovine serum albumin
Ca^{+}	Calcium
cAMP	Cyclic AMP
CANP	Calcium activated neutral protease
CBB	Coomassie Brilliant Blue
CD	Compact disc
CFSE	5-Carboxy fluorescein diacetate N-succinimidyl ester
ChAT	Choline acetyltransferase
COPIND	Chronic organophosphate induced neuropsychiatric disorder
CPF	Chlorpyrifos
CPO	Chlorpyrifos oxon
CYP	Cytochrome P
DAPI	4',6-Diamidino-2-phenylindole
dbcAMP	dibutyryl cyclic 3', 5'-monophosphate
DEP	Diethylphosphate
DETP	Diethylthiophosphate
DMEM	Dulbecco's modified Eagle's medium
DMSO	Dimethylsulphoxide
DNA	Deoxyribonucleic acid
DTNB	5, 5 Dithiobis 2-nitrobenzoic acid
DZ	Diazinon
DZO	Diazinon oxon
ECL	Enhanced chemiluminescence
ECM	Extracellular matrix
EGF	Epidermal growth factor
ELISA	Enzyme linked immunosorbent assay
EPA	Environmental Protection Agency
ERK1/2	Extracellular-signal regulated kinases
FBS	Foetal bovine serum
FGFb	Basic fibroblast growth factor
FITC	Fluorescein isothiocyanate

GAP	Growth associated protein-43
GDNF	Glial-derived neurotrophic factor
GFAP	Glial fibrillary acidic protein
GTP	Guanosine triphosphate
h	Hour
HEPES	4-(2-Hydroxyethyl)peperazine-1-ethanesulfonic acid
HRP	Horseradish peroxidase
HSP(s)	Heat shock protein(s)
HSP60	Heat shock protein 60
HSP70	Heat shock protein 70
HSP90	Heat shock protein 90
IF(s)	Intermediate filament(s)
IQ	Intelligence quotient
JNK	JUN N-terminal kinases
kDa	kilo Dalton
KSR	Kinase suppressor of Ras
LAS AF	Leica Application Suite Advanced Fluorescence Lite
LC_{50}	Lethal concentration 50
LD_{50}	Lethal dose 50
Lys40	Lysine at position 40
MAPK(s)	Mitogen activated protein kinase(s)
MAPKK	MAPK kinase
MAPKKK	MAPK kinase kinase
MAPs	Microtubule associated proteins
min	Minute
ml	Millilitre
MT(s)	Microtubule(s)
MTOC(s)	Microtubule organising centre(s)
MTT	3-(4,5-dimethylthiazol-2-yl)-2,5 diphenyltetrazolium bromide
N2a	Mouse neuroblastoma cell line
N52	Monoclonal antibody recognising total NFH
NaOH	Sodium hydroxide
NF(s)	Neurofilament(s)
NFH	NF heavy chain
NFL	NF light chain
NFM	NF medium chain
nm	Nanometers
nM	Nano molar
NOEL	No-observed-effect level
NTE	Neuropathy target esterase
OP	Organophosphorous
OPIDN	Organophosphate-induced delayed neuropathy
PBS	Phosphate buffered saline
pERK	phosphorylated ERK
pNPP	p-Nitrophenyl phosphate
PON1	Paraoxonase 1
PSP	Phenyl saligenin phosphate
RBC	Red blood cell

ReNcell CX	Human neural progenitor stem cell line
RNA	Ribonucleic acid
RT-PCR	Real time polymerase chain reaction
SCG	Superior cervical ganglia
SDS	Sodium dodecyl sulphate
SDS-PAGE	Sodium dodecyl sulphate- polyacrylamide gel electrophoresis
SEM	Standard error of the mean
SENSOR	Sentinel Event Notification System for Occupational Risks
Ser	Serine
SMI34	Monoclonal antibody recognising phosphorylated NFH
Ta51	Monoclonal antibody recognising phosphorylated NFH
TBS	Tris-buffered saline
TCP	3,5,6-Trichloro-2-pyridinol
TEMED	N,N,N,N-Tetramethylethylene diamine
TMB	3,3',5,5'-Tetramethylbenzidine
TOCP	Tri-o-cresyl-phosphate
Tyr	Tyrosine
UK	United Kingdom
US	United States
USA	United States of America
UV	Ultra violet
v/v	volume/volume
w/v	weight/volume
WHO	World Health Organisation
βIII-tubulin	Monoclonal antibody recognising β-tubulin
µm	Micron
µM	Micro molar

Publication and scientific communication arising from this thesis

Publications:

1. Sindi, R. A, et al., The effects of a sub-lethal neurite inhibitory concentration of chlorpyrifos and chlorpyrifos oxon on cytoskeletal protiens in differentiating mouse N2a neuroblastoma cells. Conference paper, June 2013.

2. Ramya Sindi, Wayne Harris, Gordon Arnott, Chris Lloyd Mills, and Alan Hargreaves. The effects of a sub-lethal neurite inhibitory concentration of chlorpyrifos and chlorpyrifos oxon on cytoskeletal protiens in differentiating mouse N2a neuroblastoma cells. (Manuscript sent).

Scientific meetings:

1. The toxicity effects of sub-lethal concentration of chlorpyrifos and chlorpyrifos oxon on cytoskeletal proteins in differentiating mouse N2a neuroblastoma cells (Oral presentation).
   East Midlands Universities Postgraduate Research Students Conference, 5th July 2012, University of Nottingham, UK.

2. The toxicity effects of sub-lethal concentration of chlorpyrifos and chlorpyrifos oxon on cytoskeletal proteins in differentiating mouse N2a neuroblastoma cells (Poster).
   6th Saudi Scientific International Conference, 11-14th October 2012, Brunel University, London.

3. The effects of sub-lethal neurite inhibitory concentration of chlorpyrifos and chlorpyrifos oxon on cytoskeletal proteins and cell signalling in differentiating mouse N2a neuroblastoma cells (Oral presentation and poster).

School of Science and Technology Research Conference, 9th May 2013, Nottingham Trent University, Nottingham, UK.

4. The effects of sub-lethal neurite inhibitory concentration of chlorpyrifos and chlorpyrifos oxon on cytoskeletal proteins in differentiating mouse N2a neuroblastoma cells (Poster).
   5th Conference on Advances in Molecular Mechanisms Underlying Neurological Disorders, 23-26th June 2013, University of Bath, UK.

5. The effects of sub-lethal neurite inhibitory concentration of chlorpyrifos and chlorpyrifos oxon on cytoskeletal proteins in differentiating mouse N2a neuroblastoma cells (Poster).
   7th Saudi Students Conference, 1st-2nd February 2014, Edinburgh International Conference Centre, Edinburgh, UK.

6. Sub-lethal exposure to chlorpyrifos and chlorpyrifos oxon induces neurite retraction and neurofilament disruption in pre-differentiated mouse N2a neuroblastoma cells (Poster).
   9th FENS Forum of Neuroscience, 5-9th July 2014, Milan, Italy.

Table of contents

List of Figures

List of Tables

1 Introduction

1.1 Basic aspects of the nervous system

The mammalian central nervous system is composed of two common cell types, neuronal and glial cells. Neurons are one of the essential cells in the nervous system, being responsible for the perception of stimuli, responding to those stimuli and transmitting the cellular signals to other neighbouring neurons or effector cells through synaptic transmission. Neurons are known to be highly polarised cells in that produce axons and dendrites upon differentiation. The morphological features of axons play an important role in neurotransmission and axonal transport (Barres and Barde, 2000). Glial cells are the second common type of cells found in nervous system. Although glial cells are not involved in nervous signal transmission, nor they do not generate axons, these cells provide fundamental homeostatic, nutritional, structural, and defensive support to the neurons (Barone et al., 2000). Glial cells in the central nervous system are composed of a heterogeneous array of cell types of different origin. These include, microglia, which are derived from the immune system. Microglia act as specialised brain macrophages that clean up cellular debris and dead neurons after apoptosis (Compston et al., 1997). The other glial cells are known as astrocytes and oligodendrocytes, which are mainly developed after neurogenesis. Both cells types can be found in differentiating neural stem cell cultures (Compston et al., 1997, Rice and Barone, 2000).

In the adult brain, the ultimate function of astrocytes is to maintain the ionic and trophic balance of the neurons and extracellular environment. Astrocytes also provide guidance for axons and assembly of synapses during brain development, and play crucial roles in neuronal proliferation, migration and differentiation (Aschner et al., 1999). Additionally, astrocytes help to regulate the formation of the blood-brain barrier and respond to neural injury by secreting neurotrophic factors such as glial-derived neurotrophic factor (GDNF), which have a protective role against neuronal damage (Barres and

Barde, 2000). Oligodendrocytes synthesise the myelin sheath, an insulating membrane around axons that provides axonal support and allows electrical signals to be transmitted along axons more efficiently (Compston et al., 1997). As a consequence, any toxicity in these cells could lead to complications in the development of insulated neurons in mammals (Sachana et al., 2008).

The peripheral nervous system is also composed of two major types of glial cells, Schwann cells and enteric glia. Schwann cells consist of two types, myelinating and non-myelinating cells. The non-myelinating cells providing mechanical and metabolic support for neurons, while the myelinating cells, which have similar structure and function to those of oligodendrocytes, providing an insulating sheath around the axons. Enteric glia are found in the autonomic ganglia of the gut and have an essential role in synaptic transmission (Jessen, 2004).

Development of the nervous system involves a series of sensitive and complex events extending from early embryonic life till adolescence. These processes include neuronal cell proliferation, migration, differentiation, synapse formation, glial cell development, and apoptosis, which are all tightly regulated within a specific time frame. Each developmental process has to be complete in a correct order. This complex structure and function of the developing brain increases its vulnerability and sensitivity to toxic injury by environmental pollutants such as organophosphorous (OPs) insecticides and others toxic insult (Grandjean and Landrigan, 2014). Exposure to OP toxicity can cause disruption in the central nervous system which may result in behavioural changes and neuropsychiatric disorders include learning difficulties, disrupted memory, confusion and fatigue (Lotti and Moretto, 2005). OP neurotoxicity can also have adverse effects on the peripheral nervous system such as weakness in the lower limbs and subsequent paralysis (Elersek and Filipic, 2011).

1.2 Organophosphorous insecticides

Pesticides are mixtures of chemicals that are used globally, predominantly in agriculture to protect crops from insect damage. The consumption of pesticides worldwide is estimated at more than five billion kilograms (kg) annually, amongst which organophosphorus insecticides are the most widely used (Gupta, 2006, FAO, 2013). Some of these commonly used OPs include parathion, malathion, methyl parathion, chlorpyrifos, diazinon, dichlorvos, and phosmet. OPs are used in many medical, residential and industrial settings (e.g. lubricants, solvents and fire retardants) but their main uses are as agricultural insecticides (Hargreaves, 2012). Each year, four billion kg of OP insecticides, such as chlorpyrifos, are applied in agricultural fields in different parts of the world, but only small amounts of these target pests, while the remainder pollutes the environment (Gavrilescu et al., 2015).

In Europe, several products, including baby food and processed food are contaminated with more than 250 different OP chemicals. In addition, approximately 50% fruits of European origin, as well as vegetables and cereals have been reported to contain residues of OP agents (EC, 2005). Another study from the USA has also reported that around 11 million kg of OP compounds (primarily chlorpyrifos, diazinon and malathion) were used in the production of agricultural crops in 1995 alone. Residential and commercial properties also consumed a large quantity of insecticidal OP compounds (6 to 9 million kg) in the same year (Aspelin, 1997).

This widespread use of OP compounds and the underlying adverse effects are pose potential risks to public health. Exposure to these insecticides not only affects agricultural workers who deal closely with OPs, but also the general population. Several epidemiological studies have shown that the majority of consumers are repeatedly exposed to low concentrations of OP compounds throughout the environment and food sources, which over long-term may cause chronic damage to the nervous system (Mearns et al., 1994, Stephens et al., 1995). The increased rate of acute pesticide poisoning in humans due to high exposure to OPs is another major public health concern. Globally, around three

million people endure unintentional acute pesticide poisoning and 346,000 deaths per year are reported (WHO, 2008). The World Health Organisation (WHO) also reported that two million cases of intentional (suicidal) pesticide poisoning occurred each year and around 370,000 people each year die from this worldwide (Gunnell et al., 2007). According to a surveillance finding from the US Sentinel Event Notification System for Occupational Risks (SENSOR) pesticides program, OP insecticides were responsible for nearly 50% of acute pesticide related illnesses (Calvert et al., 2004). In the UK and other western countries, the incidence of acute pesticide poisoning related deaths is relatively low (Jamal, 1995). However, the rate in developing countries is estimated to be significantly higher, more than 300,000 deaths/year. This is mainly due to the wider use of OP pesticides, lack of strict regulations, and poor knowledge of safety procedures by people at risk in developing countries (Carlton et al., 2004, WHO, 2008).

The widespread use of OP compounds together with the emerging concerns over their potential impacts on public health has lead to the imposition of restrictions or bans on their uses by the regulatory authorities of some developed countries. For example, in 2000 the Environmental Protection Agency (EPA) in the USA had completely banned the domestic use of chlorpyrifos (CPF), which is one of the highly toxic OPs and the main focus of this thesis (EPA, 2000). Two years later, the United Kingdom Advisory Committee on Pesticides (ACP) raised concerns regarding the potential toxicity of CPF and its impact on food safety and public health (ACP, 2002). As a result of these concerns, all household uses of CPF have been stopped and the use of this pesticide restricted to agricultural application only in certain countries (Colborn, 2006). Despite these restrictions, CPF remains a popular pesticide and is still in use in many developing countries (Salyha, 2010).

1.3 Chlorpyrifos

CPF is one of the most extensively used OP pesticides worldwide. It was first synthesised and manufactured commercially by the Dow Elanco Company in 1965. CPF has a potent biocide activity to control insects in agricultural fields, gardens and homes (Cox, 1994). Since then it has been widely distributed into the world market under several brand names, including Empire, Eradex, Scout, Brodan, Dursban, Lorsban, Reldan and others (Salyha, 2010). Around 850 commercial CPF products were registered for use in the USA in 1997 according to the EPA (EPA, 1999). The use of CPF is still authorised in more than 50 countries worldwide, such as Australia, France, Japan, US, Canada, UK, Spain, Italy, New Zealand and other developed countries (Salyha, 2010).

CPF is used in a wide variety of applications. For example, in the home, CPF is used to control insect pests such as mosquitos, cockroaches, flies, fleas and lice. CPF products are also applied directly to sheep and turkeys, animal sites, farm buildings, storage bins, and on lawns and golf courses. In agricultural settings, CPF is used over several major crops in the world for protection. Some of these crops include vegetables, fruits, corn, tree nuts, soybeans, citrus fruit and wheat (Eaton et al., 2008, Salyha, 2010). According to the National Centre for Food and Agriculture Policy in the USA (2000), around 1.4 million kg of CPF were applied every year in the home and garden market (NCFAP, 2000). In 2011, the annual usage of CPF was estimated at approximately 20 million kg in China alone (Agronews, 2013).

1.3.1 Chemical structure and physical properties

Chlorpyrifos (O,O-diethyl O-3,5,6-trichloropyridin-2-yl phosphorothioate, O,O-diethyl O-3,5,6-trichloro-2-pyridyl phosphorothionate, chlorpyrifos-ethyl) is a colourless to white crystalline solid with a strong mercaptan-like odour (Figure 1.1). CPF is used as the active ingredient in many chemical formulations, which are available in a variety of forms, such as granules, capsules, powder, suspensions, emulsifiable concentrates and gel-based products (Wauchope et al.,

1992). CPF has a lipophilic nature, which is poorly soluble in water but it can dissolve in most organic solvents. Thus, prior to its application into animals or on crops, CPF is usually mixed with solvents such as benzene, acetone, diethyl ether, xylene, carbon disulphide and methanol (Wauchope et al., 1992, Eaton et al., 2008).

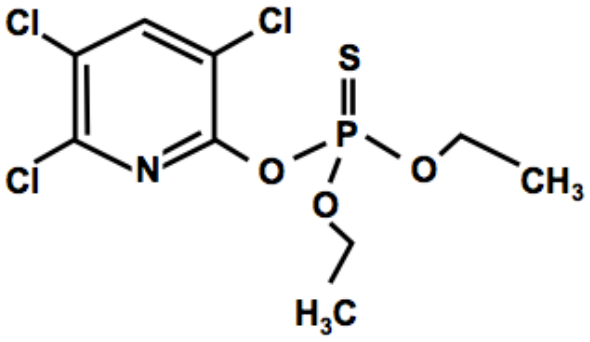

Figure 1.1. Chemical structure of chloryrifos.

1.3.2 Chlorpyrifos routes of exposure

CPF can be rapidly absorbed through skin, oral mucosa, and airways, upon dermal contact, ingestion, or inhalation (Munoz-Quezada et al., 2012). Humans and animals are exposed to CPF through breathing polluted air, inhaling dust, contact during preparation or application of OPs in the workplace, and eating and drinking of contaminated food and water (WHO, 2001).

A major route of CPF dispersion is the indoor application of pesticides and other types of insect treatment. In the US, poison control centres received more than 22,000 cases of CPF exposure between 1985 and 1992 (EPA, 1994). Additionally, surveys of hundreds of US homes have indicated the significant presence of CPF residues in dust samples collected from different US states including Florida, Indiana and Seattle. Recently, several reports have highlighted the detection of CPF in indoor air, floor dust and carpets (Roinestad et al., 1993).

Occupational exposure is another source of CPF poisoning. CPF exposure is quite common among agricultural workers and their family members, sheep

dippers, farmers and pesticide sprayers. However, people and children living in homes on or near a farm that applies OP insecticides are still at risk of exposure to these compounds (Gupta, 2006, Munoz-Quezada et al., 2012). Treatment of workplaces with insecticides for termites or other insect could expose the employees to lethal doses of CPF. Between 1985 and 1992, more than 1300 cases of workplace exposure to CPF were reported to the US poison control centre (EPA, 1994). A recent prospective cohort study was carried out to evaluate the level of occupational exposure on workers involved in CPF manufacture. The outcome of this study showed a significant increase in the level of CPF metabolites in urine samples (Albers et al., 2004). These figures raise a major concern about the implanted guidelines regarding occupational exposure to CPF.

Another prime route of exposure to CPF is the consumption of contaminated water and air. Groundwater contamination with CPF residues was reported in nine US states (EPA, 1992). Similarly, surface water contamination with CPF was measured in South Africa and Spain (Thoma and Nicholson, 1989). Moreover, air contamination with CPF at the application sites was noted. For example, assessment of air samples taken from approximately 1 meter above cornfield showed that one-half of the applied CPF was vaporised and contaminated the air for more than 25 days (Whang et al., 1992). In addition, CPF can be carried out and transferred into the atmosphere from the application site. Zabik and Seiber (1993) detected CPF contamination in air samples collected about 24 kilometres from the application site (Zabik and Seiber, 1993).

After CPF is applied in the environment, it is rapidly absorbed via all routes of exposure (oral, inhalation, dermal). As CPF is a lipophilic compound, it readily crosses biological membranes including the placenta and the blood brain barrier. It enters the bloodstream and distributes into tissues at concentrations that are able to induce neural damage by inhibiting acetylcholinesterase (AChE), one of the key enzymes in the nervous system (Timchalk et al., 2002). In humans, OP half-lives are relatively short (minute to hours) as they undergo rapid hepatic metabolism (mainly through conjugation and esterase-mediated hydrolysis) and excretion through urine, faeces, and breath (Casarett et al., 2001).

1.3.3 Chlorpyrifos biotransformation

After CPF enters the body, it is metabolically converted into its oxygen form chlorpyrifos oxon (CPO), in which the sulphur group is replaced by oxygen. This biotransformation reaction is carried out primarily by the cytochrome P450 (CYP)-dependent monooxygenase system, which mainly exists in the liver (Costa, 2006). CPF can also be converted into CPO directly by brain microsomal CYP450, although at a 100-fold lower rate (Chambers and Chambers, 1989). CPO, in turn, is well absorbed, and exerts toxic effects in animals and humans, as it is a much more potent AChE inhibitor than the parent compound (Lotti, 2001). In the liver, CPO undergoes further hydrolysis to form less toxic products, such as diethylphosphate (DEP) and 3,5,6-trichloro-2-pyridinol (TCP) by A-esterases such as paraoxonase PON1 (Costa, 2006). In addition to CPO bioactivation, CPF is oxidized via CYP450 to diethylthiophosphate (DETP) and TCP (Figure 1.2). These metabolites are then detoxified and filtered through the kidneys and excreted in the urine (Eaton et al., 2008).

The biotransformation of CPF is mainly mediated by CYP450, which is present in humans in several isoforms. It has been shown that CYP2B6 and CYP3A4 are the most effective enzymes in the formation of CPO, while CYP2C19 is the most important isoform for TCP production (Croom et al., 2010). The polymorphic nature of CYPs in humans results in variation in CYP isoform expression which in turn explains the variation in individuals' susceptibility to OP poisoning (Buratti et al., 2007). In addition to the CYP enzymes, the detoxification of CPO to TCP and DEP metabolites also involves plasma A-esterases such as paraoxonase 1 (PON1). Several *in vivo* studies have shown that low levels of this enzyme can increase the susceptibility of humans and animals to OP neurotoxicity (Costa et al., 2013).

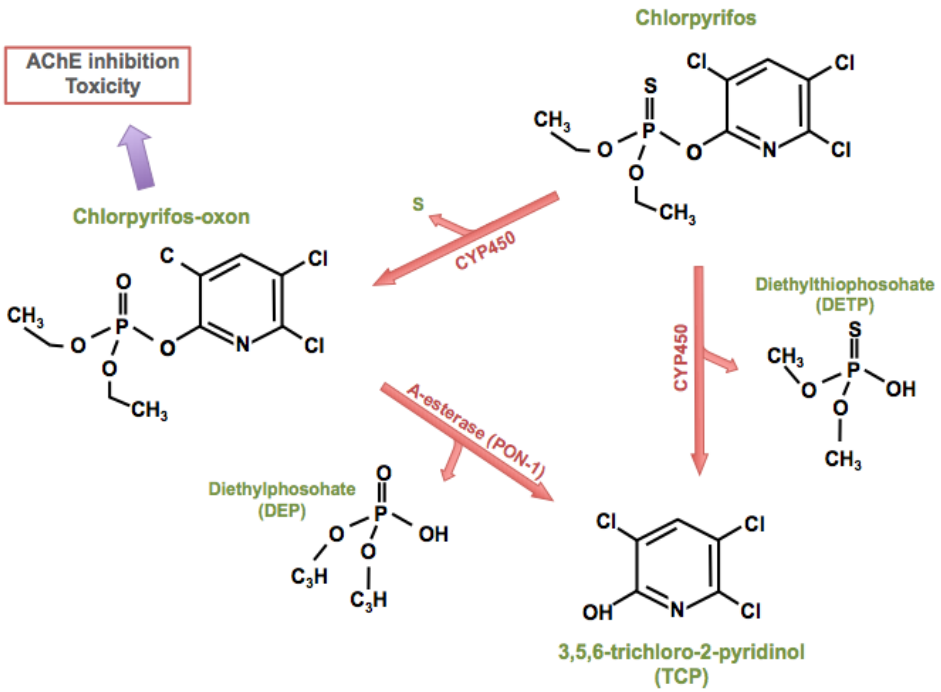

Figure 1.2. Metabolic bioactivation of chlorpyrifos.

1.3.4 Chlorpyrifos toxicity mechanism

The principle mechanism of CPF toxicity involves its ability to interact with and inhibit the AChE enzyme, which is the key enzyme in the nervous system that terminates neurotransmission at central and peripheral cholinergic synapses (Campbell et al., 1997, Steevens and Benson, 1999). The persistent inhibition of AChE activity causes decreased degradation of neurotransmitter acetylcholine (ACh) into choline and acetate, and subsequent accumulation of ACh in the synaptic cleft. ACh binds to two types of postsynaptic receptors; the muscarinic and nicotinic receptors. Muscarinic receptors consist of five subtypes (M1-M5) G-protein coupled receptors, while nicotinic receptors are ligand-gated ion channels in structure (Tata et al., 2014). Details of each subtypes and location are summarised in table 1.1. Binding of ACh to its receptors plays an important role in transmitting electrical information through postsynaptic muscarinic and nicotinic receptors from, to and within the brain and spinal cord. Excess accumulation of ACh can lead consequently to cholinergic overstimulation with various clinical symptoms according to the site at which ACh accumulates (Eaton et al., 2008, Flaskos, 2012) (Figure 1.3).

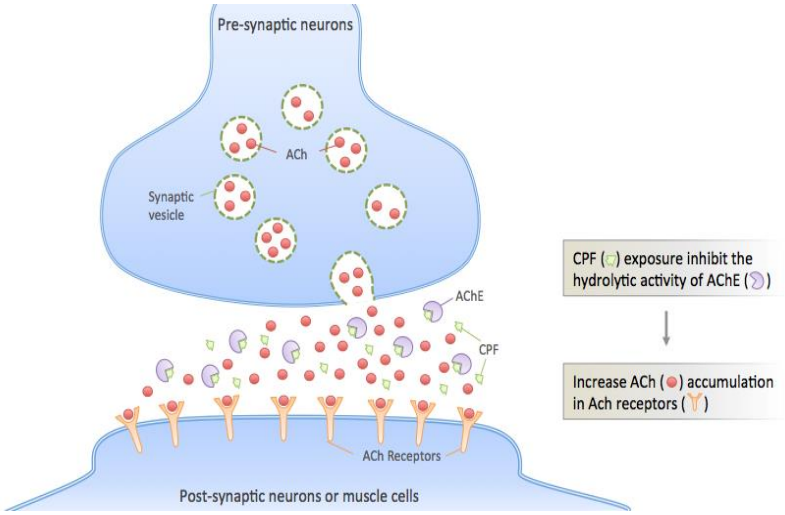

Figure 1.3. Chlorpyrifos effect on AChE

Table 1.1. Acetylcholine receptors, subtypes and location.

ACh receptors	Subtypes	Location
Nicotinic receptors	N1 or Nm	Neuromuscular junction
	N2 or Nn	Autonomic ganglia, central nervous system
Muscarininc receptors	M1	Cortex and hippocampus regions of the brain
	M2	Heart, brain, spinal cord, exocrine gland
	M3	Exocrine glands and smooth muscles
	M4	Central nervous system
	M5	Central nervous system

At the molecular interaction level, only CPO, which has a P=O moiety is a potent inhibitor of AChE, whereas CPF with its P=S moiety lacks this inhibitory effect. For CPF to become a potent inhibitor of AChE, it undergoes bioactivation in the liver to form CPO, which is the main cause of acute toxicity in mammals (Richardson, 1995, Bjorling-Poulsen et al., 2008, Eaton et al., 2008). When CPO binds to the active site of AChE, a covalent bond is formed between the phosphate group of the OP compound and the hydroxyl group of the serine within the active site of AChE. This bond is stable and usually persists for hours or weeks depending on the OP involved (Karalliedde, 1999). The organophosphorylation of AChE by CPO leads to the inhibition of its normal function in degrading the major neurotransmitter acetylcholine (ACh) at the cholinergic nerve endings in the central and peripheral nervous system (Koelle, 1992).

After inhibition by many OP compounds, reactivation of AChE usually occurs by spontaneous hydrolysis of the AChE-OP bond within several hours (Abou-Donia and Lapadula, 1990). However, when AChE is inhibited by CPO, the AChE-CPO complex subsequently undergoes an "ageing" mechanism where it loses one of the two alkoxy labile groups (R_1, R_2) by a non-enzymatic hydrolysis process. When the enzyme-inhibitor conjugate has aged, inhibition of AChE is considered to be irreversible as the enzyme becomes more resistant to reactivation, permanently inhibited and its restoration can occur only by synthesis of new enzyme molecules (Abou-Donia and Lapadula, 1990, Karalliedde, 1999). Inhibition of AChE causes a build up of ACh at cholinergic synapses, which presents all over the body and, consequently, hyperactivation of both nicotinic and muscarinic cholinergic receptors (Abou-Donia, 2003, Elersek and Filipic, 2011).

The resultant clinical manifestations of CPF poisoning can be distinguished into four main categories. These include acute cholinergic syndrome, intermediate syndrome, delayed neuropathy and other chronic neurological disorders. The development of a specific neurological syndrome depends on several factors, including extent and time of exposure, the chemical nature of the compound, and the onset and clinical symptoms (Abou-Donia, 2003).

1.4 Chlorpyrifos associated neurotoxicity

1.4.1 Acute cholinergic syndrome

Excess accumulation of ACh at the synapses of the peripheral nerves after AChE inhibition leads to hyperstimulation of the cholinergic (nicotinic and muscarinic) recepetors in the central and peripheral nervous systems (Abou-Donia, 2003). The resulting "cholinergic syndrome" is the main mechanism underlying CPF intoxication, which is characterised by a variety of clinical symptoms depending on the site of ACh accumulation. When a toxic dose of CPF is inhaled, ingested or absorbed via dermal contact, excess ACh binds to muscarinic receptors. As a result several muscarinic effects may develop, including hypersalivation, increased sweating and lacrimation, bronchoconstriction, bronchorrhoea, hypotension, increased gastrointesinal motility, abdominal cramps, vomiting, diarrhoea, miosis, visual disorders and lowered heart beat (Elersek and Filipic, 2011).

Acute cholinergic syndrome develops very rapidly within a few minutes to several hours from CPF exposure although sometimes it can appear up to one day after (Eaton et al., 2008, Hargreaves, 2012). During this phase, the nicotinic receptors are stimulated causing hypertension, uncontrolled muscle contractions and susequent paralysis (Singh and Sharma, 2000, Elersek and Filipic, 2011). Clegg and van Gemert (1999) reported that severe inhibition of AChE by more than 70% of normal levels can lead to the well characterised symptoms of cholinergic crisis (Clegg and van Gemert, 1999a). In humans, severe exposure to such OPs results in the accumulation of excessive ACh at neuromuscular junctions, leading to the development of neurotoxic effects such as neuromuscular paralysis (i.e. neuromuscular block) throughout the body (Lauder and Schambra, 1999, Costa, 2006, Gupta, 2006). Death can occur within a very short time, and this is usually as a result of a paralysis of the respiratory muscles followed by respiratory failure and/or cardiac arrest (Eaton et al., 2008, Flaskos, 2012, Hargreaves, 2012). Central nervous system symptoms may also arise following severe CPF intoxication. These include, headache, insomnia, spasms, confusion, speaking disorders, coma, ataxia, convulsion and blurred vision

(Clegg and van Gemert, 1999b, Lotti and Moretto, 2005, Elersek and Filipic, 2011).

In 1997, the EPA reported more than 17,000 cases of people affected by acute CPF poisoning between 1993 and 1996 (EPA, 1997). In the US alone, 2,593 incidents of acute CPF poisoning were reported among school children between 1998 and 2002 (Alarcon et al., 2005). According to a recent EPA report, CPF was found to be involved in more than 300 cases of acute toxicity between 2002 and 2011 (EPA, 2013).

Treatment of acute CPF toxicity has two main purposes, to block muscarinic receptors and to reactivate AChE activity. The first aim can be achieved by administering atropine, which serves as cholinergic muscarinic antagonist, and thus, accumulation of ACh on muscarinic receptors is prevented. In order to reactivate the AChE enzyme, a specific antidote, such as the oxime, pralidoxime is administered (Thiermann et al., 1999, Eaton et al., 2008, Eddleston et al., 2008). However, oximes are unable to reactivate the inhibited AChE once the AChE-CPO complex has undergone aging (Eaton et al., 2008). Another potential treatment for CPF intoxication is the use of anticonvulsant drugs such as diazepam, which is used to relieve anxiety and convulsions caused by acute poisoning following CPF exposure (Thiermann et al., 1999, Eaton et al., 2008, Eddleston et al., 2008).

1.4.2 Intermediate syndrome

Another neurotoxic effect associated with CPF exposure is known as intermediate syndrome. Senanayake and Karalliedde (1987) defined it as an intermediate syndrome because it occurred after the acute cholinergic syndrome but before organophosphate-induced delayed neuropathy (OPIDN) (Senanayake and Karalliedde, 1987). In general, it was reported that approximately 20% of people developed manifestations of intermediate syndrome following exposure to OP insecticides (Karalliedde, 2006). The clinical features of intermediate syndrome are usually initiated by respiratory insufficiency, followed by weakness in respiratory, neck and proximal limb muscles (Eaton et al., 2008).

These symptoms usually occur within 24 to 96 h after acute CPF poisoning (Yang and Deng, 2007). For example, a typical case of intermediate syndrome was described in a 16-month old child who developed respiratory arrest and flaccid paralysis 27 h after CPF ingestion (Mattingly et al., 2003).

Although, the precise mechanism that underlies intermediate syndrome remains unclear, a number of proposed mechanisms have been reported. These include, prolonged inhibition of AChE, damage to muscle cells (myopathy), down regulation of ACh receptors and failure of ACh release at neuromuscular junctions (Yang and Deng, 2007, Abdollahi and Karami-Mohajeri, 2012).

The clinical signs of intermediate syndrome, such as severe respiratory muscle weakness, can be addressed by mechanical ventilation and monitoring of respiratory functions. Other manifestations can be treated by administration of oximes. In animal studies, oximes were found to prevent myopathy if administered immediately following CPF exposure. However, when oximes were not used within two hours of CPF poisoning they had no effect (Karalliedde, 2006).

1.4.3 Organophosphate-induced delayed neuropathy (OPIDN)

CPF poisoning can also cause a delayed peripheral neuropathy known as OPIDN. This neurological disorder is a rare neuropathic condition resulting from single or repeated exposure to CPF and other OP insecticides. OPIDN is well characterised by delayed onset of ataxia followed by degeneration in the distal part of long axons and large peripheral nerves with a subsequent degeneration of the myelin sheath in both central and peripheral nervous systems (Abou-Donia and Lapadula, 1990). Abou-Donia (1981) first described OPIDN as an irreversible demyelination syndrome, which was caused by a ‘dying back’ degeneration of the long myelinated nerve axons of the nervous system (Abou-Donia, 1981). Further investigations found that this degeneration was associated with axonal swellings containing aggregates of cytoskeletal protein (Abou-Donia and Lapadula, 1990).

The clinical effects of OPIDN after CPF exposure are typically manifested following recognised cholinergic toxicity and intermediate syndrome. However, there can be a latent period of 6 to 14 days between CPF exposure and the clinical onset of OPIDN (Abou-Donia, 2003, Eaton et al., 2008, Jokanovic et al., 2011). In humans, the early signs of developing OPIDN following exposure to CPF include vomiting and diarrhoea. After the latency period, this is followed by the development of progressive weakness of the lower limbs leading to a neuropathic condition called steppage gait, which involves both foot drop and pointing down together with toes, which drag along the floor during walking. In later stages, limb weakness may also extend to the hands and arms causing abnormal balance and reflex deterioration of certain limbs, and eventually a flaccid paralysis in severe cases. After several weeks, this paralysis may progress into spastic paralysis in which the muscles are affected by prolonged spasms as a result of nerve damage (Abou-Donia, 1981, Abou-Donia and Lapadula, 1990, Abou-Donia, 1993a, Jokanovic et al., 2011). Patients with nerve impairment may recover gradually following rehabilitation. However, the effects of OPIDN usually persist for many years even after rehabilitation, as regeneration of peripheral nerve function is not always reversible (Abou-Donia, 1981, Abou-Donia, 2003, Jokanovic et al., 2011).

The pathology and symptoms of OPIDN have been investigated in numerous animal models (Richardson et al., 1993). Of all animals that have been selected to study OPIDN, hens are the preferred model due to their sensitivity and development of clinical effects that resemble to a large extent those observed in humans (Abou-Donia, 1981, Honorato de Oliveira et al., 2002). In addition, treatment of hens with OP agents via dermal or oral administration and then screening the clinical symptoms of OPIDN is considered to be a relatively easy process, with a lack of complicated tests (Abou-Donia, 1981). Experiments with hens demonstrated that inhibition of neuropathy target esterase (NTE), a membrane associated enzyme of unknown function in neurons, was the primary cellular target of OP mediated neuropathy, and this was the first proposed mechanism involved in OPIDN (Johnson, 1969, Zech and Chemnitius, 1987).

Using hens as experimental models, it was suggested that CPF was able to induce OPIDN if more than 50% of NTE activity was inhibited (Johnson, 1990,

Lotti, 1991). The previous animal studies were in agreement with CPF-induced OPIDN cases in humans, which are mainly based on accidental exposure to CPF (Eaton et al., 2008). For instance, Osterloh *et al*. (1983) demonstrated low levels of plasma cholinesterase and NTE activity in a patient who had ingested CPF. In that case, the patient also showed minimal acute cholinergic syndrome, but coma, cardiac arrhythmia and death ensued 30 hours after poisoning (Osterloh et al., 1983). Moreover, Lotti and colleague (1986) followed up on a male patient who had been accidentally poisoned by oral CPF (< 300 mg/kg) and developed a mild axonal neuropathy after 43 days. In this study, the authors concluded that CPF was able to induce OPIDN, which was associated with a lower level of NTE inhibition than that required in animals (Lotti et al., 1986).

Previous studies on hens also revealed that the onset of clinical symptoms of OPIDN occurred following two main steps. The first one involves inhibition of the enzymatic activity of NTE by phosphorylation, which significantly decreases the hydrolysis of the enzyme (Glynn, 2000). Aging of phosphorylated NTE then follows and OPIDN is initiated. The process of NTE aging occurs when an OP with a negatively charged group covalently binds to the NTE active site serine residue. By aging of NTE, the activity of the enzyme becomes permanently inhibited and OPIDN occurs (Johnson, 1990, Glynn, 2000). Johnson (1969) and Du Toit *et al* (1981) demonstrated that inhibition of NTE in the spinal cord leads to a spinal syndrome only, but not neuropathy. However, to develop an axonopathy such as OPIDN, NTE aging is required (Johnson, 1969, du Toit et al., 1981). NTE inhibition and aging are then followed by several alterations in peripheral nerves. These include degeneration of long axons, myelin sheath loss, proliferation of Schwann cells and accumulation of macrophage in nerves (Singh and Sharma, 2000). Therefore, only OPs that are able to inhibit as well as age the enzymatic activity of NTE can induce OPIDN.

It has been found that the inhibition and ageing of NTE may not represent the only critical early event in the pathogenesis of OPIDN. A number of studies have demonstrated a series of other chemical mechanisms that may be involved in this delayed neurodegenerative condition. These include the disruption of protein kinases that mediate phosphorylation of cytoskeletal proteins of microtubule and

neurofilament networks (Abou-Donia, 2003). In addition, activation of calcium activated neutral protease (CANP) occurs, which promotes axonal degeneration following exposure to OP mediated neuropathy (Emerick et al., 2012). Furthermore, increased intracellular free calcium (Ca^{2+}) levels and phosphorylation of calcium/calmodulin-dependent protein kinase II (Ca^{2+}/CaM kinase II) were also found to occur prior to the onset of clinical signs of OPIDN. In this context, an earlier study by Suwita et al. (1986) has shown that increased activity of calcium/calmodulin protein kinase II was related to phosphorylation of microtubule and neurofilament networks in the brain and spinal cord of hens treated with other OPs such as tri-o-cresyl-phosphate (TOCP), which was administered orally in a single neuropathic dose (Suwita et al., 1986). These findings suggest that alterations in the phosphorylation status of cytoskeletal proteins, destabilisation of microtubules and subsequent axonal degeneration are common biochemical events associated with OPIDN development (Abou-Donia, 1993a, Gupta and Abou-Donia, 1998, Suwita et al., 1986).

The clinical effects of OPIDN can be prevented by administration of NTE inhibitors such as carbamates, sulphonates, and phosphinates, which can inhibit the NTE enzyme without causing aging (Glynn, 2000). Despite having similar effects on NTE activity to OPs, studies have shown that pre-dosing with such agents can protect against the toxic effects of CPF. The basis of this protection is that these agents form a complex with AChE, thus preventing its interaction with CPF (Johnson, 1975, Johnson, 1982). Johnson and Lauwerys (1969) showed that the pre-treatment of chickens with these agents protected them from developing OPIDN when they were subsequently exposed to a neuropathic OP (Johnson and Lauwerys, 1969). However, these agents could potentially initiate the neuropathy-inducing activity of OPs, as Lotti (2000) demonstrated several toxic axonopathies associated with exposure to carbamate and phosphinate compounds (Lotti, 2000).

1.4.4 Other chronic neurological conditions associated with CPF exposure

In addition to the above described classical neurological syndromes, CPF and certain other OPs are capable of causing a number of persistent, long lasting, chronic neurobehavioral and neuropsychiatric disorders. These deficits are collectively named chronic OP induced neuropsychiatric disorder (COPIND), and are observed following acute single dose or repeated subchronic exposure to CPF (Sanchez-Santed et al., 2004). COPIND is characterised by behavioural changes, such as drowsiness, confusion, anorexia, lethargy, anxiety, emotional lability, depression, insomnia, fatigue and irritability (Salvi et al., 2003). Similar symptoms of COPIND have been observed in agricultural workers accidentally exposed to a single dose of CPF, who demonstrated impaired cognitive functions, abnormalities in neuropsychological tests as well as memory and attention deficit (Savage et al., 1988, Rosenstock et al., 1991, Steenland et al., 1994).

Previous studies have described a variety of neurological changes in adults following long term use of OPs. Stephens *et al* (1995) studied farm worker performance after repeated exposure to OPs. They showed relatively slow speed of information processing in neurobehavioural tests, impaired attention, memory problems and greater susceptibility to psychiatric disorders (Stephens et al., 1995). Fiedler and colleagues (1997) found dystonic reactions and schizophrenia amongst people exposed to large doses of CPF for long periods (Fiedler et al., 1997). In addition, exposure to low levels of the same compound was found to induce neurobehavioural effects. For instance, high levels of anxiety were observed in insecticide sprayers but not in farmers (Levin et al., 1976). Impaired cognitive function of weaning rats was also reported after their exposure to sub-acute doses of CPF (Jett et al., 2001).

The impact of CPF insecticides causing cognitive deficits was also investigated in children. Several epidemiological studies have demonstrated that children and adolescents who work as pesticide applicators in agricultural fields such as cotton crops, have significantly more neurological symptoms and lower

neurobehavioural performance compared to non-OP workers (Rohlman et al., 2001, Rohlman et al., 2005, Abdel Rasoul et al., 2008). These findings further confirm the previously highlighted association between the period and duration of applying CPF in agriculture and the extent of cognitive and developmental disorders. However, the precise neurological mechanisms underlying the clinical symptoms of COPIND in humans remain poorly understood (Kamel et al., 2003, Rohlman et al., 2007).

1.5 Developmental neurotoxicity of chlorpyrifos

During gestational development and early childhood, CPF and its metabolite CPO can cause severe brain deficits, abnormalities and permanent impairment, even if the exposure occurs at lower concentration than those required to produce clinical signs of acute neurotoxicity in adults (Grandjean and Landrigan, 2006). In humans, exposure to CPF during early brain development has been linked to several neurodevelopmental disorders in children, including attention deficit hyperactivity disorder (ADHD), autism, learning disabilities, and other emotional and behavioural problems. Such deficits may have considerable impacts on health and the economy (Grandjean and Landrigan, 2006, Engel et al., 2011, Rauh et al., 2012). About one in six children are diagnosed with developmental disorders worldwide (Schettler, 2001). Neurobehavioral problems affect up to 15% of all births (Grandjean and Landrigan, 2014). Children with these deficits may show early onset lifelong damage or delayed effects that appear after a period of time. The severity of the neurodevelopmental effects is varied and may not be clinically obvious. For that reason it can only be assessed in individuals by special applications such as intelligence quotient (IQ) testing (Flaskos and Sachana, 2011). In animals, several *in vivo* studies found that exposure to CPF during critical periods of brain development causes a variety of behavioural abnormalities in developing mice and rats. The neurodevelopmental effects include changes in locomotor skills and cognitive performance (Icenogle et al., 2004, Ricceri et al., 2006).

Developmental neurotoxicity of CPF can occur during the prenatal or postnatal period. Prenatal exposure to CPF occurs through the placental barrier from the exposed mother to the foetus or embryo. Postnatal exposure can be direct via the normal routes of CPF administration, for instance dermal absorption, ingestion or inhalation, or through an indirect exposure such as breastfeeding (Grandjean and Landrigan, 2006).

Previous studies have shown that the developing brain is more susceptible than the mature brain to injury caused by the acute toxicity of CPF (Pope et al., 1991, Pope and Chakraborti, 1992, Whitney et al., 1995). For example, Zheng and colleagues (2000) found that the LD_{50} of CPF in 1-week-old rats is 10-fold lower than that in adult rats (Zheng et al., 2000). Similar differences were also observed between the maximum tolerated dose of CPF in 1 day old rats and 6 to 9 day old animals (Whitney et al., 1995).

The higher susceptibility of the nervous system to toxic agents during foetal life or the early postnatal period compared to that of the adult is due to a number of reasons. Firstly, the developing brain in embryos and infants is more sensitive than that of the mature nervous system in adults (Grandjean and Landrigan, 2006, Flaskos and Sachana, 2011). The second reason is related to the fact that the foetus is not completely protected against toxic compounds by the blood-placenta barrier. Since CPF is a lipophilic compound with low molecular weight, it can easily cross through the placental barrier to the foetal circulation, thus affecting the developing nervous system (Andersen et al., 2000). It has been found that OPs can rapidly cross the placenta and accumulate in umbilical cord blood at higher concentrations than those normally found in maternal blood (Sakamoto et al., 2004). Whyatt and Barr (2000) also demonstrated high levels of CPF metabolites in faecal samples of newborn children of exposed mothers (Whyatt and Barr, 2001).

Another main factor that increases the susceptibility of the foetus and young children to OP neurotoxicity is that the blood brain barrier is not fully developed until 6 months after birth, so it cannot prevent the transfer of some toxic chemicals from the maternal blood to the foetal or infant brain in early life

(Costa et al., 2004). Furthermore, exposure to CPF during prenatal and neonatal life was found to be capable of disrupting the stability and integrity of the blood-brain barrier (Yang et al., 2001, Parran et al., 2005).

Differences in pharmacokinetic aspects such as drug absorption and metabolism following OP exposure, between the young and adults could also account for the vulnerability of the developing brain to developmental neurotoxicity (Flaskos and Sachana, 2011). In this context, CPF absorption in foetal brain is higher than that observed in the maternal brain. This is mainly because of the late development of epidermis keratinization and the thinner skin layers in the human foetus compared to infant and adults, which leads to greater toxin absorption via skin, lung and intestinal mucosa (Kearns et al., 2003, Vidair, 2004). By contrast, biotransformation of CPF is lower in neonates compared to the adult. This is due to the decreased levels of detoxifying enzymes in the liver and other tissues of developing organisms, which leads to increased concentrations of oxon metabolite. For example, the activity and amounts of A-esterase PON1, which is the major plasma enzyme that hydrolyses CPO to less toxic metabolites in humans and mice, is 4-fold lower in developing organisms than in adults (Karanth and Pope, 2000, Vidair, 2004). Karanth and Pope (2000) demonstrated that A-esterase PON1 activity is lower in neonatal rats than in adult rats (12-, 5-, 8-fold lower in plasma, liver, and lung A-esterase PON1, respectively) treated with 1 mM CPO (Karanth and Pope, 2000). Moser et al. (1998) provided more evidence of the age-related differences in the activity of A-esterase PON1 in animals. In that study, it has been found that the activity of plasma PON1 in 1 day old rat is 20-fold lower than that in adult rat following 1 mM CPO exposure (Moser et al., 1998). In humans, a 13-fold variability in PON1 status has been observed (Davies et al., 1996). Furlong et al. (2006) predicted a range of 131 to 164-fold variability in CPO sensitivity among 130 pregnant women farmworkers and their newborns in the Latina cohort based on their PON1 status (Furlong et al., 2006). Therefore, the variation in PON1 level explains the higher susceptibly observed among mothers and newborns to CPO exposure. This finding clarifies the observation of severe CPO effects in some cases where mother and her newborn share a low level of PON1 (Furlong et al., 2006).

Brain developmental processes involve a sequence of events including neural cell proliferation, migration, differentiation, axonogenesis/neurite outgrowth, synaptogenesis, gliogenesis and apoptosis, which start from embryonic life and continue to late adolescence. Animals and humans share the same developmental order. However, the developmental stage at which each of these processes occurs is different between humans and animals (Flaskos and Sachana, 2011, Grandjean and Landrigan, 2014). For example, synaptogenesis and gliogenesis occur during pregnancy in humans, whereas these neurodevelopmental processes start after birth in rats. Disruption at each event of neurodevelopment provides a window of susceptibility to CPF toxicity (Rice and Barone, 2000). Therefore, CPF mediated developmental neurotoxicity is mainly dependent on the developmental stage at which the exposure occurs. The timing at which the exposure to CPF occurs has greater impact in determining the affected regions and function (Flaskos and Sachana, 2011).

A number of experimental reports have demonstrated the ability of CPF and CPO to interfere with the normal development of the nervous system, which may in turn lead to developmental neurotoxicity. Interference by CPF and CPO in the developmental process of neurite outgrowth in neuronal and glial cells and the involved cytoskeletal proteins are the main focus of this thesis, which will discussed in the following part of this chapter.

1.5.1 Neurite outgrowth as a morphological target of CPF-induced developmental neurotoxicity

Neurite outgrowth is an *in vitro* morphological marker of neural cell differentiation. It involves a series of complex events that occur during brain development, including differentiation of precursor cells into a terminal phenotype of neuronal cells, initiation and growth of sheet-like extensions (lamellipodia) and their condensation into minor processes, development of short dendrites and long axons with the guidance of the growth cone, and finally formation of the synapse (Craig and Banker, 1994b). Normal outgrowth of neurites is a critical process in the developing brain and nervous system as it

forms the basis of neuronal connectivity (Radio and Mundy, 2008). Disruption at any stage of this developmental pattern by a toxic agent would impair the neuronal differentiation process leading to developmental neurotoxicity, which has been linked to several neurobehavioral and neurodevelopmental disorders in humans (Webb et al., 2001, Ramakers, 2002).

The ability of CPF and CPO to induce developmental neurotoxicity by interfering with neurite outgrowth in the developing nervous system has been studied in a number of animal and cellular models. For instance, Slotkin et al. (2006) have shown that treatment of neonatal rats with CPF at 1 mg/kg daily dose (subcutaneously injected for four days) inhibits neurite outgrowth as indicated by decreased levels of choline acetyltransferase (ChAT) activity, a cholinergic neuronal marker. The previous study also reported that the effect of CPF towards neurite outgrowth was not associated with an impact on animal survival and caused only 20% reduction in the activity of AChE, which is below the 70% inhibition level that have been shown to induce acute cholinergic symptoms (Slotkin et al., 2006). In this *in vivo* study, neurite outgrowth was evaluated biochemically by measuring the activity of ChAT (membrane protein) and its ratio to total cell protein. As the neural cell contains a single nucleus, measurement of DNA content reflect the numbers of cells. Thus, cell packaging density was assessed by measuring DNA concentration. As the neurites expand and developed into axon and dendrites, it requires contribution of membrane proteins and other cellular proteins. Therefore, the amount of total protein in response to cell differentiation was measured (Slotkin et al., 2006).

The impact of CPF and CPO on neurite outgrowth has also been investigated in *in vitro* studies using different glial and neuronal cell culture models. In most of these reports, OP-induced effects on neurite outgrowth have been evaluated morphometrically by microscopy, following histological or immunostaining techniques, using high-resolution cameras and either manual counting or specific neurite outgrowth analysis software. For instance, a significant inhibition (by 38%) in neurite outgrowth, but not cell viability, in differentiated rat PC12 pheochromocytoma cells was detected after 24 h exposure to 3 µM CPF and 3 nM CPO. The observed CPF-induced effect on neurite outgrowth was detected in the absence of AChE inhibition. However, the CPO effect on neurite

outgrowth was associated with 90% inhibition of AChE activity (Das and Barone, 1999). In addition, CPF, at a non-cytotoxic concentration of 3 µM, impaired neurite outgrowth significantly in cultures of differentiating mouse N2a neuroblastoma cells after 4 or 8 h treatment with a lack of observed effect on AChE activity (Sachana et al., 2001). In the same cell line, CPO, at non-cytotoxic concentrations of 5 and 10 µM was found to impair axon outgrowth in differentiating N2a cells after 4 and 24 h exposure, although in this study there was an acute level of inhibition of AChE (>70% of control levels) which persisted for 24 h (Flaskos et al., 2011). The ability of CPF and CPO to alter the neuronal morphogenesis in the previous *in vitro* studies was seen at relatively high doses of CPF or at CPO concentrations causing acute levels of AChE inhibition. However, a number of studies demonstrated that both compounds are also able to inhibit neurite outgrowth at much lower concentrations without AChE inhibition (Howard et al., 2005, Yang et al., 2008).

Howard et al. (2005) showed that CPF and CPO at lower doses (0.001 µM and 0.01 nM, respectively) than those required to reduce the enzymatic activity of AChE or cell viability, inhibited the axonal and dendritic outgrowth in primary cultures of superior cervical ganglia (SCG) rat embryonic neurons after 24 h treatment (Howard et al., 2005). Under the same exposure conditions, CPF and CPO also interfered with axon outgrowth in embryonic cultures of dorsal root ganglia (Yang et al., 2008). At sub-cytotoxic concentrations (1-10 µM) CPF and CPO were also found to inhibit the extensions outgrowth in rat C6 glioma cells after 24 h of inducing cell differentiation and this effect was not associated with reduced AChE activity (Sachana et al., 2008). These findings demonstrated that neurite outgrowth can be more sensitive than the enzymatic activity of AChE to the toxic effects of CPF and CPO in these cell models. Since the reported alterations in neuronal morphogenesis occurred in both the absence and presence of changes in AChE activity, it is likely that inhibition of AChE is not in the main cause of the inhibition of neurite outgrowth by CPF and CPO. These findings suggest that additional non-cholinergic targets are involved in the developmental toxicity of CPF and CPO. These targets will be discussed in the next section to provide a better understanding as to how their disruption might inhibit neurite outgrowth.

1.5.2 Cellular proteins as molecular target of CPF-induced developmental neurotoxicity

Although CPF exerts poisoning effects due to the CPO mediated inhibition of AChE activity, several other cellular proteins have been proposed as targets for the neurotoxicity of CPF and CPO, including those involved in cytoskeletal architecture, cell signalling pathways and growth associated protein.

1.5.2.1 Cytoskeleton

The neuronal cytoskeleton plays fundamental roles in controlling the developmental processes of the nervous system. These include cell proliferation, migration, differentiation, morphogenesis, neurite outgrowth, elongation of axons, branching of dendrites, steering of growth cones and apoptosis (Hargreaves, 1997, Flaskos, 2014). Disruption of cytoskeletal proteins results in serious damage in these phases of neurodevelopment (Flaskos, 2014). The neuronal cytoskeleton is fibrous network of proteins, which is composed of three main classes of filamentous proteins, microtubules (MTs), intermediate filaments (IFs) and microfilaments (MFs). These components of cytoskeletal proteins have an important role in the regulation of axon growth and stability and thus, they represent potential neurotoxicity targets (Hargreaves, 1997).

1.5.2.1.1 Microtubules

Microtubules (MTs) have important roles in neuron growth and physiology, being implicated in the regulation of neuronal morphology, intracellular transport, and outgrowth of axons and dendrites (Cambray-Deakin, 1991a, Ginzburg, 1991, Lodish et al., 2000a). MTs are straight, hollow cylinders formed by a ring of thirteen protofilaments that are built by the assembly of two tubulin heterodimers, α- and β-tubulin subunits, and MT associated proteins (MAPs) (Cleveland, 1993a, Hargreaves, 1997).

MTs represent the largest type of cytoskeletal structure, with an average external diameter of ~ 25 nm and an internal diameter of ~ 14 nm (Figure 1.4) (Tilney et al., 1973). In mammalian cells, MTs originate from a specific regions called the

centrosomes or microtubule organising centres (MTOCs). MTs are organised in a polar fashion, where the centrosome-attached end is the "minus end", while the other is called the "plus end" (Figure 1.4). Each end has its own growth rate, for example, the plus end grows fast, unlike the minus end which known as the slow growing end (Heidemann et al., 1981b). During cell division and movement, MTs undergo several rearrangements (polymerisation - depolymerisation) that are fuelled by the enzymatic hydrolysis of guanosine triphosphate (GTP), with the plus end extending towards the extremities of the cell (Lodish et al., 2000a). The development of elongating neurons largely depends on the orientation of MTs (Bamburg et al., 1986, Julien and Mushynski, 1998). For instance, in neural cells, the plus end of MTs extends towards the axon tip and the minus end is oriented at the MTOC of the axon. In contrast, in dendrites, the polarity of MTs is mixed, with both ends being distal to the cell body. In non neuronal cells such as glia, the minus end is associated with MTOCs. Each MTOC has the ability to nucleate and organise MTs by polymerising the tubulin subunits (Lodish et al., 2000a).

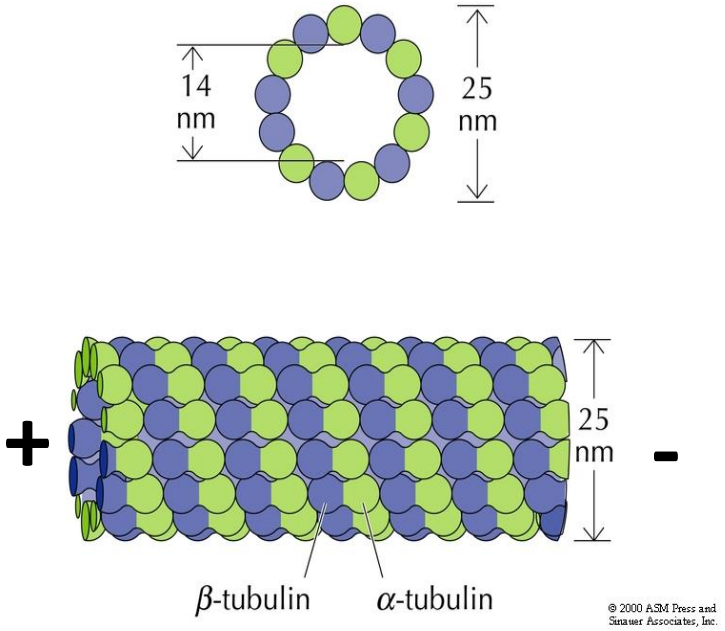

Figure 1.4. Microtubule structure and composition. A schematic diagram of a MT showing the structure of 13 protofilaments packed together to form the cylindrical wall in cross section and a side view of a short section of a microtubule with the tubulin polypeptides aligned into rows (Lodish, 2000).

The main component of MTs is tubulin, which has α- and β- subunits. However, there are other subunits of tubulin such as ϒ-tubulin, which is not present in MTs but has an important role in MT nucleation and polar orientation (Martin et al., 1997). Each α- and β-tubulin subunit has a molecular weight of approximately 50 kDa. They consist of several isoforms encoded by a number of genes (Tischfield and Engle, 2010). Both α- and β-tubulin isoforms have an important role during nervous system development. For instance, class III β-tubulin isotype (βIII-tubulin) is almost exclusively distributed in neuronal cells and has an essential role in cell differentiation and neurite outgrowth. In addition, βIII-tubulin is one of earliest cytoskeletal protein to be expressed during neurodevelopment (Easter et al., 1993).

Tubulin binds a variety of MAPs due to its strongly acidic carboxyl terminal domain (Cleveland, 1993a, Hargreaves, 1997). The carboxyl terminal of tubulin subunits contains an acidic region of 40 amino acids. This peptide sequence is believed to harbour the target region of calcium binding, phosphorylation sites (serine residues) and binding sites of MT-stabilising proteins, such as MAPs (Table 1. 2) (Luduena, 1993). Several post-translational modifications are also involved in the regulation of tubulin polymer formation. The most common modifications include acetylation of α-tubulin at lysine at position 40 (Lys40), detyrosination/tyrosination of α-subunits by the removal/addition of tyrosine (Tyr) residues at the C-terminal. Other post-translational modifications include phosphorylation of β-subunits at a serine residue at position 172 (Ser172) and polyglutamylation of β-tubulin subunits at multiple glutamate residues (Luduena, 1993, Fourest-Lieuvin et al., 2006) (Table 1.2). Such modifications may affect MT stability and locations (Janke and Kneussel, 2010).

Table 1.2. Major microtubule cytoskeletal proteins of the nervous system (adapted from (Kirkpatric and Brady, 1999) .

Protein	Expression pattern and distribution	Post-translational modification
α-tubulin	In all cells, but some isoforms preferentially expressed in brain	Acetylation, Tyrosination, Polyglutamylation
β-tubulin	In all cells, but some isoforms preferentially expressed in brain	Phosphorylation, Polyglutamylation
γ-tubulin	In MTOC of all cells	Phosphorylation
MAP 1a	Appears late, widely distributed	Phosphorylation
MAP 1b	Appears early, then declines; enriched in axons	Phosphorylation
MAP 2a	High molecular weight; expressed in dendrites in mature neurons	Phosphorylation
MAP 2b	High molecular weight; expressed in dendrites	Phosphorylation
MAP 2c	Low molecular weight; expressed in dendrites in developing neurons	Phosphorylation
Tau	Enriched in axons	Phosphorylation

The assembly and stability of MTs is strongly dependent upon MAPs, which regulate the dynamics of tubulin heterodimers (Lodish et al., 2000b, Lodish et al., 2000a). For instance MAPs stimulate MT assembly and are involved in the interaction with IF and actin filaments (Cleveland, 1993b). The main MAPs family members that are known to be important during central nervous system development include MAP 1, MAP 2, tau and stathmin. Their main function during neuronal development is to maintain the stabilisation of the growth cones, and the dynamics of axonal and dendritic MTs (Schoenfeld and Obar, 1994). Other groups of MAPs such as, kinesin and dynein can also function as motor

proteins (ATPases) by driving the intracellular transport of organelles and proteins from the cell body to the extending axons and synapses (Vallee and Bloom, 1991).

MAPs 1 and 2 are composed of three different phosphoproteins each (MAP 1a, 1b, 1c, MAP 2a, 2b, 2c), which can be distinguished according to their molecular weights (Olmsted, 1986). While MAP 1 and MAP 2 are expressed in neuronal cell bodies and dendrites, tau is found primarily in axons (Table 1.2). Tau is also considered as an axonal marker and tau abnormalities are strongly related to the pathophysiology of neurodegenerative diseases, such as Alzheimer's disease (Kolarova et al., 2012).

The role of MTs in organising axonal growth and development is well established. As developing neurites extend, MTs begin to be assembled and to be modulated by posttranslational modifications of tubulin (Cambray-Deakin, 1991a). In this process, MAPs play essential roles, helping to maintain structure, orientation, and function of MTs (Heidemann et al., 1981a, Mandell and Banker, 1995, Craig and Banker, 1994a). Given the important roles of MTs in neuron growth and functions, it is not surprising that MT alterations or disruption of MT protein phosphorylation by toxic agents lead to interference with brain development and may be involved in the pathophysiological mechanisms of several neurodegenerative diseases (Millecamps and Julien, 2013).

The ability of CPF and CPO to cause developmental neurotoxicity via disruption of the microtubule cytoskeleton has been demonstrated in a number of previous studies. For instance, exposure of differentiating rat C6 glioma cells to sub-cytotoxic neurite inhibitory doses (1-10 μM) of CPF and CPO were found to be associated with reduced protein levels of MAP 1b and α-tubulin (Sachana et al., 2008). Furthermore, Abou-Donia (1993) demonstrated that hens exposed to OP exhibited increased phosphorylation of tubulin and MAPs (Abou-Donia, 1993b). In addition, CPO at doses range from 0.1 to 10 μM was shown to induce alterations in MT and MAP ultrastructure in cultured rat brain slices (Prendergast et al., 2007). Therefore, MTs may serve as useful biomarkers of CPF-induced neurodegeneration.

1.5.2.1.2 Intermediate filaments

Intermediate filaments (IFs) are an important component of the eukaryotic cytoskeleton, and are usually identified in cellular studies as markers for neural cell differentiation. IFs are slightly smaller and more biochemically stable than MTs. Thus, they provide structural support for many different cell types including neurons (Omary et al., 2006). All IF proteins contain a conserved α-helical rod domain, flanked by a hypervariable amino-terminal head domain and a carboxy-terminal tail (Figure 1.5). Since the central rod domain contains 310 amino acid residues, which are highly homologous amongst the main IF types, the variations in amino acid sequence of the two end domains determine the difference in the molecular weight and molecular interactions of all IF subunits (Cooper, 2000). IFs are initially constructed from two polypeptide chains wound together in a parallel fashion to form a coiled-coil dimer, two of which then form a staggered tetramer (consisting of two antiparallel dimers), leading to the subsequent formation of octamers, protofilaments and eventually large complex IFs that contain 16 to 32 polypeptides (Figure 1.6) (Lodish et al., 2000b).

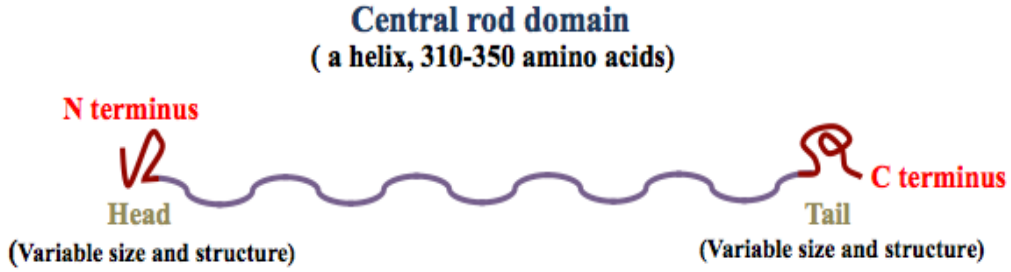

Figure 1.5. Structure of intermediate filament protein subunits. The diagram shows the generalized structure of an IF protein monomer, which contains an α-helical rod domain composed of around 310 amino acid residues, an amino-terminal head domain and the carboxy-terminal domain at the tail.

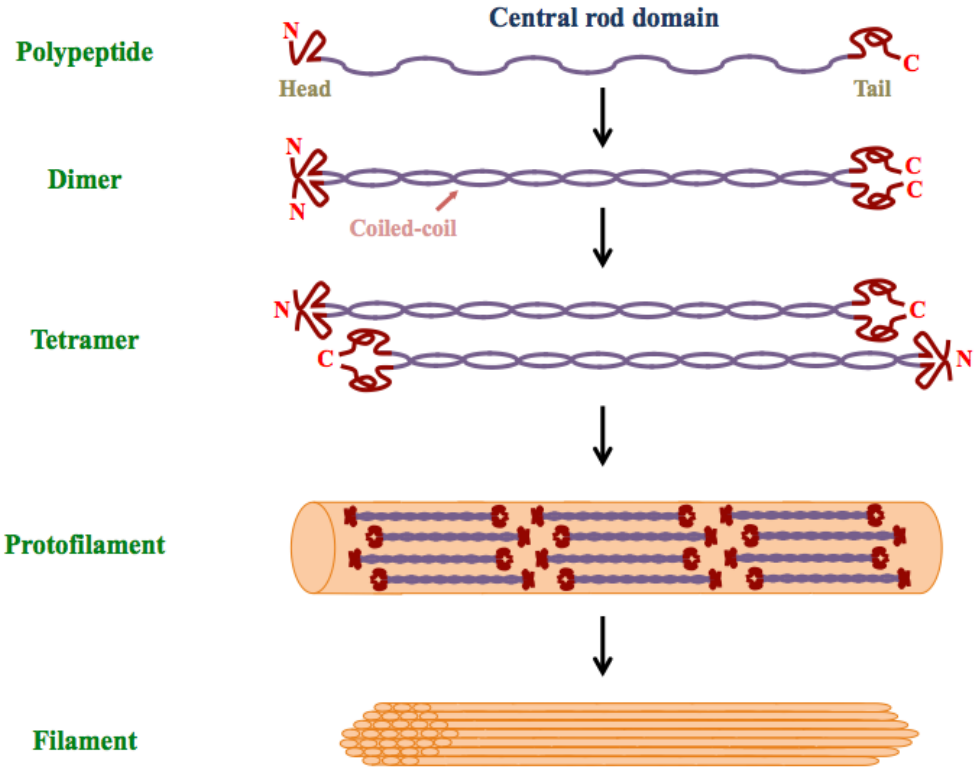

Figure 1.6. Assembly of intermediate filaments. A schematic diagram showing that IFs are assembled from two polypeptide chains wound together to form a parallel coiled-coil dimer. Dimers are staggered in an antiparallel fashion to form tetramers, octamers, protofilaments and eventually large complex IFs that contain 16 to 32 polypeptides.

Although there are more than 50 different IF proteins, which have been classified into six main groups based on their amino acid sequence homology, two classes of IFs that are specific to the nervous system are the focus of this dissertation. These include neurofilament (NF) proteins and glial fibrillary acidic protein (GFAP), which are mainly expressed in neuronal and astroglial cells, respectively (Cooper and Hausman, 2000).

NFs are composed of three polypeptides chains termed neurofilament heavy (NFH), medium (NFM) and light (NFL) chains, which are categorised according to their molecular weights of approximately 200, 145 and 70 kDa, respectively (Ackerley et al., 2003). In mammals, these triplet proteins are found in mature neurons but are highly expressed in axons. NFs provide support during axon

extension and also play major roles in the complex series of interactions that regulate axonal growth and development (Lee and Cleveland, 1996). NFs share a similar structure to all other IF proteins in which each NF subunits contain head, central rod and tail domains. The central rod domain that comprises 310 amino acids plays an important role in NF polymerisation, whereas the tail domains of NFH and NFM are important in the formation of fine lateral projections (Yuan et al., 2012). The central rod domain of each NF is co-assembled with other NF subtypes to form a filament with 10 nm in diameter. NFL forms the central core of this filament, while NFM and NFH subunits are situated on its surface forming radial projections that interconnect NFs with other cytoskeletal elements (Rao et al., 2003). Therefore, cross bridges between NF extensions of the tail domains and other organelles in the cytoplasm stabilise the axonal outgrowth (Hirokawa et al., 1984).

The axonal cytoskeleton contains MTs, NFs and microfilaments (MFs) that are assembled in ordered networks of filaments interconnected by cross-bridges. Newly synthesised NFs are transported into the axonal space in a slow non-diffuse manner and then rapidly incorporated into the axonal cytoskeleton. The process of NF assembly and transport is launched within the neuronal cell body and continues as they are transported into and along the axons by axonal transport (Black and Lasek, 1980).

During NF assembly, NFs undergo several post translational modifications which involve phosphorylation of the carboxyl terminal domains. Phosphorylation of NFs is crucial for the regulation of their axonal stability and transport, assembly and disassembly in the cell (Williamson et al., 1996). Additionally, it plays an important role in regulating the interactions between NFs themselves and the interaction of NFs with MTs (Hisanaga and Hirokawa, 1989, Hisanaga et al., 1991). It has been demonstrated that increased NFH phosphorylation is directly related to an increase in the spacing between NF subunits and axonal diameter (Hirokawa et al., 1984). Moreover, aberrantly phosphorylated NFs accumulate in neuronal cell bodies and can be found in axon from patients with neurodegenerative diseases such as Alzheimer's and Parkinson's disease (Rudrabhatla et al., 2011). Abnormal NF aggregation is also a common histological hallmark of OP poisoning (Jensen et al., 1992).

Phosphorylation of NF subunits can occur at the carboxyl terminal domains, which contain multiple Lysine-Serine-Proline (KSP) region or phosphorylation sites. NFH and NFM are known to have the highest number of phosphorylatable sites compared to NFL, which is less phosphorylated (Perrot and Eyer, 2009). This is due to the extreme length of the tail domain of NFH and NFM and the presence of large numbers of KSP repeats compared to NFL (Yuan et al., 2012). It has been demonstrated that NFs can also be phosphorylated at the amino head domain. However, the phosphorylation sites in the latter are less abundant than those at the carboxyl domains (Sihag et al., 2007). Phosphoarylation of NFH and NFM begins after their synthesis in the cell body and continues along their transport into the axon towards the synapses (Nixon et al., 1982).

Phosphorylation of the tail domain of NFH and NFM is regulated by different protein kinases and phosphatases. Protein kinases are sets of several enzymes that have the ability to phosphorylate proteins by adding a phosphate group to them, such as mitogen activated protein kinases/extracellular-signal-regulated kinase 1/2 (MAPKs/ERK1/2) (further details in section 1.4.2.2) (Veeranna et al., 1998). Phosphatases are a group of enzymes that removes a phosphate group from a protein such as protein phosphatase 1 and 2A (PP2A and PP1) (Strack et al., 1997). In patients with Alzheimer's disease, NF phosphorylation was associated with activation status of ERK1/2 and decreased levels of PP1 and PP2A (Gong et al., 1993, Veeranna et al., 2004). The mechanisms underlying the NF phosphorylation mediated by kinases and phosphatases are not completely understood.

Data from previous studies showed that exposure of differentiating N2a cells to sub-cytotoxic neurite outgrowth inhibitory levels of CPF (3 µM) caused a significant reduction in the level of total NFH (Sachana et al., 2001). In addition, the densitometric analysis of western blots in a study by Flaskos *et al.* (2011) reported that neurite inhibitory effects of CPO were associated with reduced levels of total NFH in a concentration dependent manner in N2a cells (Flaskos et al., 2011). However, phosphorylated levels of NFH were unaffected by CPO. The observed alteration of NFH was further confirmed by the aggregation localised in cell bodies (Flaskos et al., 2011). Other OPs have been also shown to affect the NF network in different ways. Hargreaves et al. (2006) showed that

sub-cytotoxic neurite inhibitory concentration of phenyl saligenin phosphate (PSP) were associated with reduced levels of total NFH following 4 and 24 h exposure in differentiating N2a cells. A transient increase in NFH phosphorylation after 4 h exposure and a subsequent decrease after 24 h were also seen together with aggregates in the cell bodies in PSP-treated cells (Hargreaves et al., 2006). In the same cell line, inhibition of axon outgrowth was found to be accompanied with reduced levels of total and phosphorylated NFH in cells treated with trio-ortho-cresyl phosphate (TOCP) for 24 h (Fowler et al., 2001). However, increased expression of NFH phosphorylation without significant changes in total NFH were detected in differentiating N2a cells exposed to sub-cytotoxic concentrations of diazinon oxon (DZO) for 24 h (Sidiropoulou et al., 2009a). In an animal study, increased phosphorylation status of NFH has been found in the spinal cord of hens treated with TOCP (Suwita et al., 1986) and PSP (Jortner et al., 1999). This alteration in NFH suggests that these OP compounds including CPF and CPO have the ability of to interfere with molecular expression of axonal cytoskeleton proteins and the arrangement of cytoskeletal networks within the cell (Flaskos et al., 2007, Harris et al., 2009a).

GFAP is the major IF protein found in mature astrocytes of the nervous system. GFAP can also be found in other types of cells such as the glial cell of the digestive system, and the non-myelinating Schwann cells in the peripheral nervous system, which have similar function to those of astrocytes (Yang and Wang, 2015). GFAP has an important role in modulating the shape and motility of astrocytes by providing structural support for their processes (Eng et al., 2000). Astrocytes can be activated in response to neuronal damage, brain injury, genetic disorder or neuronal toxicity in a process called reactive astrocytosis or astrogliosis. Increased astro-glial cells number and levels of GFAP expression were found to be the main characteristics of astrocytes' reaction to OP intoxication (O'Callaghan, 1988). During reactive astrogliosis, GFAP is responsible for the formation and extension of astrocytic processes. Earlier studies showed that generation of GFAP-deficient-mice was associated with neurological or behavioural abnormalities, abnormal myelination, and reduced myelin thickness in the spinal cord (Gomi et al., 1995, Liedtke et al., 1996). Other studies detected increased levels of GFAP in brains of humans suffering

from neurodegenerative conditions such as Alzheimer and Parkinson's disease (Zhang et al., 2014). These data suggest that GFAP could be a useful protein marker of neurological pathophysiology (Liu et al., 2012).

During brain development, increased expression of GFAP is an indication of glial differentiation from neural precursor cells into astrocytes, which usually reaches a peak at the second and third postnatal week. Thus, GFAP has also been recognised as a biomarker for astrocyte differentiation (Bramanti et al., 2010). Since glial development continues into adolescence, effects on developing glia during postnatal development due to CPF and CPO exposure could contribute to developmental neurotoxicity. Garcia et al. (2002) showed that subcutaneous administration of CPF for 4 days to developing rats at the peak of gliogenesis and glial differentiation results in decreased GFAP levels (Garcia et al., 2002). Similar findings were also observed in cultures of differentiating rat C6 glioma cells, when treated with sub-cytotoxic concentrations (1-10 μM) of DZO for 24 h. The decreased GFAP expression level obtained in the previous study is indicative of OP direct injury on astro-glial cells (Sidiropoulou et al., 2009b).

1.5.2.1.3 Microfilaments

Microfilaments (MFs) are another class of cytoskeletal network; they are composed of actin protein with a molecular weight of approximately 43 kDa. MFs are formed by polymerisation of two globular strands of actin monomers (G-actin) twisted around each other like strings of pearls to form F-actin, through the binding of adenosine triphosphate (ATP) (Theriot, 1994, Hargreaves, 1997). Thus, F-actin is formed by the addition of G-actin monomers at the positive end of F-actin (Hargreaves, 1997). Actin is found in all glial and neuronal cells and enriched in presynaptic terminals, dendritic processes and growth cones (Kuczmarski and Rosenbaum, 1979). Actin filaments are relatively thin and short in length in all regions of the neuron. However, MFs are more prominent and much longer in the axonal branching lamellipodia and particularly in the filopodia of the growth cone (Pak et al., 2008, Lowery and Van Vactor, 2009). The growth cone is a highly motile structure that explores the extracellular

environment, determines the direction of growth, and then guides the extension of the axon in that direction. The main morphological elements of growth cones are lamellipodia and filopodia, which are sheet-like and finger-like protrusions, respectively. They are rapidly formed and later disappear from the terminal tip. Such movements reflect rapid, controlled rearrangement of MFs, which is thought to be involved in the control of axonal path finding (Cooper, 2011).

During neuronal development, actin filaments are dynamic and undergo rapid assembly-disassembly cycles that enable the filopodia to extend towards and retract from the growth direction (Cooper and Hausman, 2000). The bundles of MFs in growth cone projections together with the associated actin network are thought to be involved in growth cone movement, myelination and cell migration (Sobue, 1993). MF dynamics occur through the incorporation and release of (i.e. the exchange) of actin monomers (G-actin) at the ends of the polymer (Zhang et al., 2005). This process is regulated by ATP hydrolysis and the interaction with actin binding protein such as growth associated protein-43 (GAP-43) and actin depolymerizing factor (ADF)/cofilin (McGough and Chiu, 1999). It has been proposed that disturbing MF regulation may be one additional target of OPs. In this context, Harris et al. (2009) found increased levels of cofilin in N2a cells induced to differentiate for 24 h in the presence of 10 µM diazinon (DZ). The observed alterations in the levels of cofilin might suggest a disruption in the MF dynamic and polymerization as well as organization of MF network (Harris et al., 2009b). Changes in this actin-binding protein could also disrupt the ability of cofilin to regulate growth cone motility and neurite outgrowth (Endo et al., 2003).

Other studies hypothesised that GAP-43 is another protein that plays an important role in the regulation of neurite outgrowth (Skene, 1989, Pekiner et al., 1996). GAP-43 is found prominently in the growth cones and elongating axons in the neurons (Das et al., 2004). During neurodevelopment, GAP-43 regulates the formation of growth cones, interferes with the development of axons, and is involved in the plasticity of the synapse (Benowitz and Routtenberg, 1997). It has been demonstrated that GAP-43 synthesis is elevated during axonal outgrowth (Skene, 1989, Pekiner et al., 1996), and thus, inhibition of neurite

outgrowth could be reflected by altered expression level of GAP-43 (Das et al., 2004).

Exposure of differentiating N2a cells to neurite inhibitory concentrtaions of CPF, CPO and other OPs have been associated with reduced levels of GAP-43 (Fowler et al., 2001, Sachana et al., 2001, Sachana et al., 2003, Sachana et al., 2005, Sidiropoulou et al., 2009a, Flaskos et al., 2011). The findings of the previous studies indicated that disturbance in the levels of GAP-43 synthesis might possibly affect the transport of this protein to axon and dendrites from the cell body. Thus, GAP-43 could be a common molecular marker of OPs-induced neurite outgrowth inhibition (Sachana et al., 2005).

1.5.2.2 Cell signalling pathway involved in neurite outgrowth

The complex developmental processes of the nervous system are dependent on precisely controlled activation or inactivation of several signal transduction pathways (Bertrand et al., 2002). Mitogen activated protein kinases (MAPKs) are key signalling pathways that functionally regulate neural cell proliferation, differentiation, mitosis, survival and apoptosis (Perron and Bixby, 1999). MAPKs are serine/threonine kinases, which activated by extracellular stimuli such as OP exposure, osmotic stress or heat shock (Widmann et al., 1999). MAPK activation is dependent on a series of phosphorylation events at both threonine and tyrosine residues, whereas MAPK inactivation is mediated by a number of phosphatases that have the ability to hydrolyse the phosphate group and reduce the MAPK activity (Shaw and Filbert, 2009).

In mammals, MAPK pathway is consists of three main signalling modules include the extracellular-signal regulated kinases (ERK1/2), the stress-activated protein kinases p38, and the JUN N-terminal kinases (JNK) (Chang and Karin, 2001). Each MAPK signalling group is composed of three acting kinases: a MAPK, a MAPK kinase (MAPKK) and a MAPK kinase kinase (MAPKKK). MAPKKKs are phosphorylated and activated by MAPKK, which in turn phosphorylate and activate MAPKs (Figure 1.7). MAPKKKs activation occurs

through phosphorylation of Ser/Thr residues and/or interaction with small G-protein such as Ras in response to extracellular stimuli (Cargnello and Roux, 2011).

The two MAPK pathways p38 and JNK activation have been linked to apoptotic cell death (Wang et al., 1998). They are responsive to cellular stress that could be induced by stress stimuli such as, inflammatory cytokines or heat shock. In the signalling cascades of JNK and p38, each MAPKK can be activated by multiple MAPKKKs for instance, MEK3 and MEK6 activates the p38 pathway whereas MEK4 and MEK7 activate the JNK pathway (Figure 1.7) (Robinson and Cobb, 1997).

ERK1/2 are among the most extensively studied kinases of the MAPK pathway and the MAPKs of interest in this thesis. ERK1 was first cloned in 1990s and consider one of the well characterised MAPK in mammals (Boulton et al., 1991). It was initially found to be phosphorylated at tyrosine and threonine residues in response to growth factors (Cooper et al., 1982). ERK1/2 have similar amino acid identity and are highly expressed in neurons in the mature nervous system (Boulton et al., 1990). The ERK pathway is controlled by mitogen activated extracellular receptors and growth factors that stimulate neural cell proliferation and differentiation, and is suppressed in many events leading to apoptosis (Jin et al., 2002).

ERK1/2 are activated by several growth factors such as nerve growth factor (NGF), and epidermal growth factor (EGF) (Boulton et al., 1991). Additionally, ERK1/2 are activated by cytokine receptors, osmotic stress, microtubule disorganisation, and G protein-coupled receptors such as kinase suppressor of Ras (KSR) (Raman et al., 2007). However, the main route of activation of ERK1/2 mainly occurs by cell surface receptor, such as tyrosine kinase receptors. In the ERK1/2 signalling cascade, the growth factor receptor-bound protein (Grb) links the tyrosine kinase receptor to guanine nucleotide exchange factors, such as son of sevenless (SOS), which are proteins that can activate the small GTPases. Then, the signal is transduced to the small GTP binding protein (Ras), activating Raf, which then acts as a MAPKKK. This, in turn, activates

MEK1/2 which acts as MAPKK, which finally activates the terminal ERK1/2 as MAPK (Figure 1.7) (Johnson and Lapadat, 2002).

ERK1/2 can phosphorylate many neuronal proteins, such as NFH and other substrates (Shaul and Seger, 2007). In a previous study by Veeranna et al. (1998) it has been found ERK1/2 are capable of phosphorylating all types of KSP repeats in the C-terminal tail domains of NFH and NFM in rat brain. In the same study, it has also been demonstrated that inhibition of the ERK1/2 by MEK inhibitor (PD98059) caused a decrease in neurite length in primary culture of rat hippocampal cells (Veeranna et al., 1998). This implies that ERK1/2 may regulate the axonal cytoskeletal proteins involved in neurite outgrowth.

Numerous *in vitro* studies have demonstrated the effect of CPF exposure on cell signalling cascades. Caughlan and colleagues (2004) showed that CPF at sub-cholinergic levels induced apoptosis in rat cortical neurons by the activation of ERK1/2, JNK and p38 MAPK pathways. The authors also found that embryonic neuronal cells were more sensitive than postnatal cells, which indicate that CPF is able to disrupt the activities of MAPK families involved in neuronal cell development and survival (Caughlan et al., 2004). Consistent with this finding, increased activation of ERK1/2 was also observed in primary cultures of human astrocytes following CPF exposure (Mense et al., 2006). Moreover, in human neuroblastoma SH-SY5Y cells, CPF caused induction of JNK and p38 MAPK activation (Ki et al., 2013).

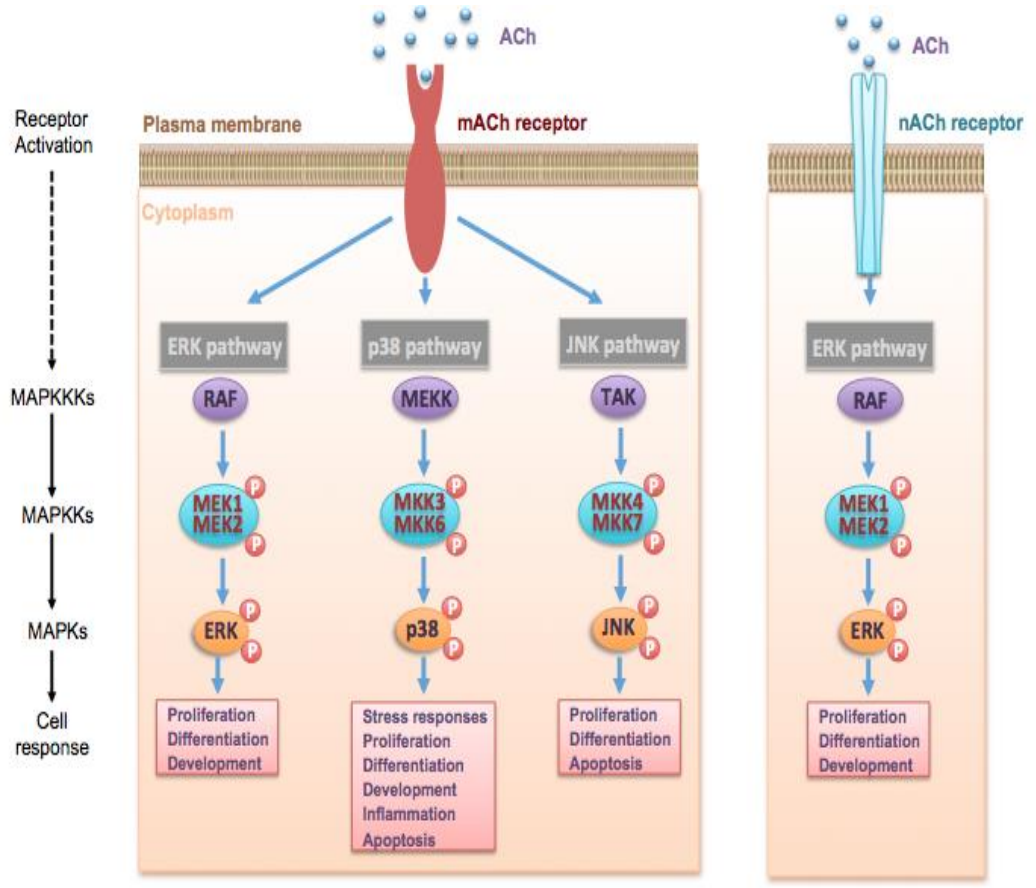

Figure 1.7. Schematic diagram of the MAPK signalling pathways. The general mitogen-activated protein kinase (MAPK) signalling cascade includes the activation of a MAPK kinase kinase (MAPKKK), which then activates a MAPK kinase (MAPKK), which activates the terminal MAPK. MAPK pathways consists of three main signalling modules include the extracellular-signal regulated kinases (ERK1/2), the stress-activated protein kinases p38, and the JUN N-terminal kinases (JNK). In the MAPK/ERK pathway, the exposure to CPF and the binding of ACh to muscarinic and nicotinic ACh receptors activates the small GTP binding proteins Ras activates Raf, which acts as a MAPKKK. This in turn, activates MEK1/2, which acts as a MAPKK, which finally activates the terminal ERK1/2 as MAPK. ERK1/2 are linked to cell development, while activation of p38 and JNK has been linked to cell apoptosis. In the signalling cascades of JNK and p38, each MAPKK can be activated by multiple MAPKKKs; for instance, MEK3/6 activates p38 pathway, whereas MEK4/7 activates the JNK pathway.

1.6 The use of *in vitro* mammalian cell models for assessment of CPF neurotoxicity

The high ethical and economic impact, together with complex and time consuming processes associated with animal experiments for neurological purposes have prompted investigators to identify alternative methods that could be used for assessing both physiological and pathological processes. Hence, *in vitro* models provide invaluable assets and a simplified tool for studying the neurotoxicity of OP pesticides at both cellular and molecular levels (Silva et al., 2006). The use of *in vitro* cell culture models for neurotoxicity assessment has some intrinsic limitations, such as diminished metabolic capability, lack of cell to cell interaction (e.g. between neurons and glial cells), and partial involvement of pharmacokinetic factors, which may not accurately determine the effective *in vivo* levels (Rice and Barone, 2000, Flaskos, 2012). However, these culture systems have many important advantages that make them appropriate approach in this project.

First, mammalian cell lines have the ability to reproduce large numbers of homogenous cells by simple preparation. Second, they are easy to grow, store and maintain for an extended periods of time (Radio and Mundy, 2008, Flaskos, 2012). Additionally, they enable the testing of CPF and CPO at different concentrations on neuronal and glial cells, separately. Moreover, they also permit the detection of cellular alterations as well as characterisation of molecular changes during a specific neurodevelopmental phase, such as neurite outgrowth. Furthermore, the differentiated neuronal cells that express the main morphological features of neurites including axons and dendrites make it possible to control the timing and onset of development and adjust the research method to the needs of the study (Banker and Goslin, 1998). This advantage has made numerous cell lines suitable models for high throughput screening. Neural stem cells derived from humans also provide the potential benefit of predicting the neurotoxicity of CPF and CPO in a more physiologically relevant cellular system. However, there is a lack of published work to show that stem cells derived from humans are able to predict human developmental neurotoxicity any

better than cell lines derived from rodents (Radio and Mundy, 2008). The two mammalian cell lines used in this thesis to investigate the developmental neurotoxicity of CPF and CPO are further described below.

1.6.1 Mouse N2a neuroblastoma cell line

The N2a cell line has been widely used as a model for the study of OP toxicity on neuronal differentiation and neurite outgrowth (Henschler et al., 1992, Flaskos et al., 1998, Sachana et al., 2001, Sachana et al., 2003, Sachana et al., 2005, Hargreaves et al., 2006, Sidiropoulou et al., 2009a, Flaskos et al., 2011, Sachana et al., 2014). N2a cells were derived from the mouse C1300 tumor (neuroblastoma) and can differentiate into a neuron-like morphology that expresses AChE and many neuronal markers, including adrenergic and cholinergic markers (Klebe and Ruddle, 1969). In mitotic conditions, N2a cells grow as round neuroblasts. N2a cells are differentiated by removal of serum and the addition of dibutyryl cyclic 3', 5'-monophosphate (dbcAMP) in serum free medium. Serum withdrawal results in non-dividing differentiating cells that extend neurites with morphological characteristics of neurons, while dbcAMP promotes N2a cell differentiation by mimicking the action of cAMP. Once N2a cells are differentiated, they undergo several morphological changes. The most prominent change involves the formation of axon-like processes and dendrites, which is accompanied by the increased perikaryon and nucleus size (Haffke and Seeds, 1975). The neurites produced by N2a cells are rich in cytoskeletal proteins such as NFs and MTs (Schubert et al., 1969).

One drawback of the N2a model is that axons and dendrites generated from this cell line may not replicate some of the complex characteristics of neurites observed in original primary neurons (Radio and Mundy, 2008). However, the ability of N2a cells to express NFs, MTs and AChE together with their commercial availability makes them an attractive model for screening CPF neurotoxicity on neurite outgrowth in this study.

1.6.2 Human neural stem cells (ReNcell CX)

ReNcell CX is human neural progenitor cell line, which was isolated by the ReNeuron Group (Guildford, Surrey, UK). The cell line is available commercially (Merck Millipore) and has the ability for self-renewal and to produce a co-culture of neurons and glial cell types including oligodendrocytes and astrocytes (Seaberg and van der Kooy, 2003). ReNcell CX cells were derived from the cortical region of a 14-week gestation human foetal brain, which has a normal male karyotype. This cell line has been immortalized by retroviral transduction of the c-myc oncogene to produce unlimited clonal human neural stem cells (Donato et al., 2007, Kornblum, 2007). ReNcell CX cell morphology is that of typically round neurospheres in their undifferentiated state when grown in uncoated tissue culture flasks. However, when cultured as a monolayer on laminin coated surfaces in the presence of growth factors, the cell line maintains its normal diploid karyotype even after prolonged passage (Jakel et al., 2004). After removing mitogenic growth factors from the culture medium, neural progenitor stem cells migrate from the neurospheres onto a laminin coated surface, extracellular matrix (ECM) coating protein, and can be differentiated into a mixed population of three main cell types of the nervous system, including neurons, oligodendrocytes and astrocytes (Kornblum, 2007). These differentiated cells are identical to those detected in the human nervous system. In addition, unlike the N2a cell line, the axons and dendrites elaborated from differentiated neuronal stem cells have the same complexity of original neurons (Bal-Price et al., 2008, Radio and Mundy, 2008). Therefore, using the neural progenitor ReNcell CX cell line in the current thesis has enabled us to investigate the effects of CPF and its metabolite on cell differentiation in a more human relevant model.

1.7 Aims of the thesis

There is considerable evidence that CPF insecticide and its oxon form CPO can inhibit the outgrowth of extensions and disrupt the levels of cytoskeletal proteins in differentiating neural cell lines. It is, however, known that the toxicity may depend on the developmental stage at which exposure occurs. The majority of previous *in vitro* studies have involved the administration of OPs at the same point of induction of cell differentiation. However, little was known about the effects of OPs on cells that have been committed to differentiation and have already elaborated neurites. Such a study was performed in the current work in order to make an original contribution to knowledge, as the toxic effects of these OPs were to be examined at developmental points other than those reported in previous work.

Earlier studies by research colleagues had shown that exposing differentiating mouse N2a neuroblastoma cells to a sub-lethal concentration of CPF inhibited the outgrowth of axons (Sachana et al., 2001). By replicating the same culture conditions of the previous study, the aims of this thesis were to:

1. Investigate the effects of a neurite inhibitory concentration of CPF and CPO on cell viability, AChE and neurite retraction in pre-differentiated N2a cells over a range of time points.
2. Relate the effects on neurite maintenance to the levels of expression and activities of cytoskeletal and associated regulatory proteins in pre-differentiated N2a cells using quantitative Western blotting.
3. Evaluate the sensitivity of different parameters of neurite outgrowth (e.g. average cell number, average neurite number, average and maximum neurite length, mean processes and branches per cell) and the underlying effects on cytoskeletal proteins following exposure to range concentrations of both OPs by high content analysis and cell ELISA.
4. Apply the same high throughput approaches to test the effects of both compounds in a human neural progenitor stem cell model using human ReNcell CX stem cells that form a co-culture of neuronal and glial cells.

2 Materials and methods

2.1 Materials

2.1.1 Reagents

All reagents used in the laboratory were of the highest grade and purchased from Sigma-Aldrich Chemical Company, Poole, UK, unless otherwise specified. They are listed in tables 2.1 and 2.2.

Table 2.1. List of cell culture reagents

Reagents	Code	Supplier
Dulbecco's Modified Eagles Medium (DMEM) with 4.5g/L glucose and 2mM L-glutamine	BE12-614F	Lonza, UK
Penicillin/streptomycin (Penicillin 5,000 units/ml, Streptomycin 5,000 units/ml)	DE17-603E	
Foetal bovine serum (FBS) South American origin	FB-1001	Biosera
3-(4,5-dimethylthiazol-2-yl)-2,5 diphenyltetrazolium bromide (MTT)	M2128	Sigma-Aldrich
N^6,2'-O-Dibutyryladenosine 3',5'-cyclic monophosphate sodium salt (dbcAMP)	D0627	
Dimethylsulphoxide (DMSO) sterile-filtered hybridoma tested	D2650	
Trypan blue solution 0.4% (w/v)	T8154	
Laminin from Engelbreth-Holm-Swarm murine sarcoma basement membrane	L2020	
L-glutamine		Gibco, Life Technologies USA
StemPro® Accutase® cell dissociation reagent	A11105-01	

StemPro® Neural supplement	A10508-01	
KnockOut™ DMEM/F-12 (1X)	12660-012	
Neurobasal® -A medium, no L-glutamine, L-glutamic acid or aspartic acid	10888-022	
Recombinant human EGF (10 µg)	1380077C	
Recombinant human FGFb (10 µg)	1424760B	

Table 2.2. List of other reagents and materials.

Reagents	Code	Supplier
3MM chromatography paper	CJF240090	Fisher Scientific
3,3',5,5'-Tetramethylbenzidine (TMB)	T0440	Sigma-Aldrich
3-(4,5-dimethylthiazol-2-yl)-2,5 diphenyltetrazolium bromide (MTT)	M2128	
5, 5 Dithiobis 2-nitrobenzoic acid (DTNB)	D8130	
5-Carboxy fluorescein diacetate N-succinimidyl ester (CFSE) fluorescent cell staining dye	87444	
AccuGel 29:1 acrylamide (40% (w/v) acrylamide/bisacrylamide 29:1)	EC852	Geneflow
Acetone	121403/0031	Fisher Scientific
Acetylthiocholine iodide (ATCh)	A5751	Sigma-Aldrich
Amersham Protran 0.2 µm pore size nitrocellulose membrane	10600001	General Electric
Ammonium persulphate (APS)	A3678	Sigma-Aldrich
Bicinchoninic acid (BCA)	23223	
Blueye prestained protein ladder (Approx. 0.1-0.4 mg/ml of proteins in buffer (20 mM Tris-phosphate pH 7.5, 2% w/v SDS, 0.2 mM dithiothreitol, 3.6 M urea and 15% (v/v) glycerol)	PM007-0500	GeneDirex
Bovine serum albumin (BSA)	A1302	Melford

Bromophenol blue	18030	Fluka
Copper (II) phthalocyanine	C2284	Sigma-Aldrich
Dimethylsulphoxide (DMSO)	CHE1854	Fisher Scientific
Enhanced chemiluminescence reagent (ECL)	ME157124	Thermo Scientific
Ethanol	101076H	Fisher Scientific
Glacial acetic acid	200.580-7	
Glycerol 10% (v/v)	15892001C	ACROS organics
Hydrochloric acid	H1000PB17	Fisher Scientific
Hydrogen peroxide (H_2O_2)	H1009	Sigma-Aldrich
Iodoacetamide	1149	
Methanol	M400/17	Fisher Scientific
β-Mercaptoethanol	M3148	Sigma-Aldrich
Mineral oil	EC2324558	
N,N,N,N-tetramethylethylene diamine (TEMED)	EC503	National diagnostic
Paraformaldehyde 4% (w/v)	HT501128	Sigma-Aldrich
p-Nitrophenyl phosphate liquid substrate system	SLBC2208V	
Protogel® resolving buffer (4x) (1.5 M Tris-HCl buffer pH 8.8, 0.4% (w/v) SDS)	EC892	Geneflow
Protogel® stacking buffer (4x) (0.5 M Tris-HCl buffer pH 6.8, 0.4% (w/v) SDS)	EC893	
Sodium acetate	S2889	Sigma-Aldrich
Sodium azide	S2002	Fisher Scientific
Sodium chloride	B22297	Sigma-Aldrich
Sodium dodecyl sulphate (SDS)	18299	Melford
Sodium hydroxide (NaOH)	1823	Sigma-Aldrich
Sodium phosphate dibasic	94046	Fisher Scientific
Sodium phosphate monobasic	71505	

Sulphuric acid (H_2SO_4)	339741	Sigma-Aldrich
Tris (hydroxymethyl) aminomethane	C22561	
Triton X-100	T8787	
Tween 20	P1379	
Urea	U6504	
VectaShield® mounting medium for fluorescence containing 4',6-diamidino-2-phenylindole (DAPI)	H1400	Vector Laboratories Ltd

2.1.2 Cell culture plastic-ware

All sterile cell culture plastic ware were supplied by Scientific Laboratory Supplies (Nottingham, UK). Cryotube vials (Nunc brand products), were purchased from Merck Ltd. Leicester, UK. Disposable Haemocytometer C-Chip slides, were supplied by Labtech International Ltd, UK. Eight-well 15µ-slides for live cell analysis (IbiTreat), were purchased from Thistle Scientific, UK. Ninety six-well plates (NUNC-immuno plate), were purchased from Thermo Scientific, UK.

2.1.3 Test compounds

Chlorpyrifos and chlorpyrifos oxon (purity 97.6%) from Chem Service Inc. (West Chester, PA, USA), were supplied by Greyhound Chromatography (Birkenhead, UK).

2.1.4 Cell lines

2.1.4.1 Mouse N2a neuroblastoma cells

Neuro 2A (N2a) is a neuroblastoma line derived from mouse neural crest. N2a is a well-established cell line and has widely been used to study neuronal differentiation, axonal outgrowth and cell signalling pathways (Ostrea et al., 2002). It also has the ability to differentiate into neurons within a few days. It

was purchased from American Type Culture Collection (ATCC® - product no. CCL-131™, Middlesex, UK).

2.1.4.2 Human ReNcell CX

ReNcell CX human neural progenitor cell line was derived from cortical brain tissue of a 14-week gestating human foetus following normal terminations and in accordance with nationally UK approved ethical and legal guidelines. It was purchased from Merck Millipore (MILLIPORE® - catalogue no. SCC007, UK).

2.2 Methods

2.2.1 Mouse N2a neuroblastoma cells

2.2.1.1 N2a cell maintenance

Mouse N2a cells were grown and maintained as a monolayer in DMEM containing 4.5g/L glucose and 2 mM L-glutamine, and supplemented with 10% (v/v) FBS, penicillin (100 units/ml) and streptomycin (100 units/ml). Cells were incubated at 37°C in a humidified atmosphere of 95% air /5% CO_2.

Cells were passaged or sub-cultured when growth reached 70-80% confluence (i.e. every 3-5 days). On reaching 80% confluence, the cell cultures were either used to seed monolayers on cell culture plates for assays, T75 flasks for Western blot analysis or passaged to maintain the cell line.

2.2.1.2 N2a cell restoration from liquid nitrogen storage

When it was needed to perform experiments, a vial of frozen cells was removed from liquid nitrogen storage and thawed quickly by incubation in a 37^{o}C water bath for 2 min. The outside of the vial was sterilised with 70% (v/v) ethanol. The contents were diluted with 1 ml of pre warmed fresh growth medium and then rapidly transferred into a Sterlin tube containing 9 ml of pre warmed fresh growth medium. The Sterlin tube was then centrifuged at 300 g for 5 min and the

supernatant was decanted to remove any residual cryopreservation medium (DMEM containing 5% (v/v) DMSO as a cryopreservation agent). The resultant cell pellet was resuspended in 1 ml of pre warmed growth medium and mixed gently by slow pipetting up and down before being transferred into a T25 flask containing 10 ml of fresh growth medium. Cells were allowed to recover for 24 h at 37^{o}C in a humidified atmosphere of 95% air/5% CO_2, after which the medium was changed. They were then cultured until the growth reached 60-80% confluence. Upon reaching 80% confluence, cells were passaged and transferred into T75 flasks and cultured until ready for experimental use.

2.2.1.3 N2a cell culture

To passage the cell cultures, half of the growth medium was carefully poured off the flask into a waste beaker without disturbing the attached cell monolayer. Cells were mechanically removed from the flask surface using a sterile Pasteur pipette to detach the cells by aspirating growth medium and squirting it out on the monolayer surface of the cell culture flask. Cell suspensions were then transferred into Sterilin tubes and harvested by centrifugation at 300 g at room temperature for 5 min. The supernatant was carefully discarded and the resultant pellet was resuspended in 1 ml of growth medium by passing the cell suspension several times through a 1000 µl Gilson pipette to break up the pellet. Using a Pasteur pipette, three to four drops of cell suspension were placed in a T75 flask containing 40 ml of fresh growth medium. In the case of T25 flasks, one to two drops were transferred in 10 ml of growth medium. Cells were incubated at 37°C in a humidified atmosphere of 95% air/5% CO_2 and kept until the monolayer became 80% confluent. Only cells that had not yet reached passage number 20 were used in differentiation experiments because later passages are more susceptible to genetic drift.

2.2.2 Human neural ReNcell CX stem cells

2.2.2.1 Preparation of coated cell culture ware

All tissue culture flasks, plates or other plastic ware that were used to culture ReNcell CX cells were coated with laminin for 24 h before the day that cells needed to be seeded. Laminin is an ECM protein, which supports and enhances neural progenitor stem cell adhesion, proliferation, differentiation and neurite elongation (Flanagan et al., 2006). For coating, 1mg/ml laminin from Engelbreth-Holm-Swarm murine sarcoma basement membrane (Sigma–Aldrich) was thawed at room temperature before use. Laminin was diluted to 20 μg/ml final concentration in Neurobasal® medium (Gibco) that contained no L-glutamine, L-glutamic acid, or aspartic acid. Laminin solution was added to cover the surface of the required tissue culture vessel. A five ml volume of this solution was used to coat a T75 flask and 2 ml volume for a T25 flask. Coated flasks were incubated at 37°C in a 5% CO_2 incubator for at least 4 h if these flasks were going to be used on the same day that cells needed to be passaged; otherwise, coated flasks were stored at 4°C for 24 h or until needed. Just before using a coated flask for culturing ReNcell CX cells, the laminin solution was aspirated and flasks rinsed once with sterile PBS.

2.2.2.2 Preparation of ReNcell CX maintenance medium

ReNcell CX cells were maintained in KnockOut™ DMEM: nutrient mixture F-12 (DMEM/F-12) low osmolality medium without HEPES buffer. The medium (500 ml) was supplemented with recombinant human epidermal growth factor (EGF) (20 ng/ml; Gibco), basic fibroblast growth factor (FGFb) (20 ng/ml; Gibco), StemPro® neural supplement (2% by volume; Gibco), L-glutamine (0.5 mM), penicillin (100 units/ml) and streptomycin (100 units/ml).

2.2.2.3 ReNcell CX cell restoration from liquid nitrogen storage

Cells were thawed from the liquid nitrogen when a coated laminin flask was ready to be used. A vial of ReNcell CX cells was removed from the liquid nitrogen storage and incubated in a 37°C water bath for 1 or 2 min until it

completely thawed. The outside of the vial was wiped with 70% ethanol to sterilise and the cells were transferred into a Sterilin tube using a 2 ml sterile pipette. After the cells had been transferred into the tube, 9 ml of maintenance medium (pre warmed to 37^{o}C) were immediately added drop by drop to avoid osmotic shock that may result in decreased cell viability. The cell suspension was gently mixed by slow pipetting up and down with 1000 µl Gilson pipette and centrifuged at 300 g for 5 min. Following centrifugation, the supernatant was decanted completely to remove any residual cryopreservation medium (KnockOut™ DMEM/F-12 medium containing 5% (v/v) DMSO), and the resultant pellet was resuspended in 1 ml of pre warmed maintenance medium. The cell suspension was then plated onto a laminin coated T75 flask containing 10 ml of fresh maintenance medium. Cells were allowed to recover for 24 h in a humidified atmosphere of 95% air/5% CO_2 until the cells were approximately 80% confluent and the medium was changed every 48 h. Upon reaching 80% confluence, cells were passaged or cryopreserved for later use.

2.2.2.4 Culturing of ReNcell CX cells

ReNcell CX cells were passaged or subcultured by carefully removing the maintenance medium from the coated flask and rinsing the detached monolayers with pre warmed PBS. After that, the PBS was aspirated and 1-2 ml of accutase (Gibco) were applied according to the size of flask (1 ml for T25 and 2 ml for T75 flasks) to dissociate the cells. Accutase was pre warmed at room temperature before use. Flasks were then immediately incubated for 2 min in a 37°C incubator and the flask was gently tapped as cell detachment was monitored using a microscope. Without removing the accutase, fresh KnockOut™ DMEM/F-12 maintenance medium was added in the proportion of twice the volume of accutase to stop its activity, and the cell suspension was transferred into a Sterilin tube and centrifuged for 5 min at 300 × g at room temperature. The resultant pellet was resuspended in 1 ml of maintenance medium by pipetting gently back and forth to break up the pellet. Using a Pasteur pipette, three to four drops of cell suspension were placed in a laminin coated T25 flask containing 5 ml of maintenance medium. Cells were incubated at 37°C in a humidified atmosphere of 95% air/5% CO_2 and monitored until they reached

70-80% confluence. For all experiments conducted in this study, ReNcell CX cells lower than passage 15 were used to reduce the possibility of changing cell features.

2.2.3 Seeding and counting of cells for experiments

To seed the cells, cell monolayers were grown to reach 60-80% confluence, then detached and harvested by centrifugation at 300 g for 5 min as described in sections 2.2.1.3 and 2.2.2.4. Cell pellets were resuspended in 1 ml of growth medium. Cell dilutions were then prepared and cells were counted either manually using a haemocytometer, or automatically using an automated cell counter.

2.2.3.1 Manual cell counting

Cell counting using a haemocytometer was firstly developed for the quantitation of blood cells but then became a common and effective tool for counting a variety of other cell types. However, it can be a time consuming operation and may result in poor counting due to low sample concentration or device misuse.

Manual cell counting was used initially for N2a cells only. To seed the cells and count them manually, a 1 in 20 dilution of N2a cell suspension was prepared by mixing 10 µl of N2a cell suspension with 190 µl of fresh growth medium in an Eppendorf tube. A volume of 10 µl of cell dilution was loaded into the chamber of a disposable haemocytometer (Labtech International Ltd, UK) (0.1 mm depth under the coverslip) where cells in five squares (four corners and one centre) of 1 mm^2 each were counted at 100× magnification. Since each square is 1×1 mm and the depth is 0.1 mm, the volume correction factor for the haemocytometer is 10^4. The average cell number per ml was calculated according to the following calculations:

Cells/ml = average count per square × dilution factor × 10^4

Total cells = cells/ml × total original volume of cell suspension from which the sample was taken.

N2a cells were then seeded in new flasks/plates to yield a cell density of 50,000 cells/ml medium and allowed to recover before treatments for 24 h at 37^{o}C in a humidified atmosphere of 95% air/ 5% CO_2 (Table 2.3).

2.2.3.2 Automated cell counting

Over recent years, automated cell counting has become the robust alternative process to manual haemocytometer cell counting as it can provide a total cell count in a fraction of the time. In addition to the rapid performance, automated cell counting produces an accurate, reproducible result and assesses cell viability in a single step. A TC20 automated cell counter (BioRad, USA) was used in this study. The device utilised already prepared TC20 Trypan blue dye, which was composed of 0.4% Trypan blue (w/v) in 0.81% (w/v) sodium chloride and 0.06% (w/v) potassium phosphate dibasic solution. Trypan blue is a vital stain that differentiates between live and dead cells. The principle of this dye is based on the blue acid dye chromophores which react and are taken up by the internal region of dead (non-viable) cells through a damaged membrane, whereas live (viable) cells do not take up this dye.

For this, 10 µl of cell suspension were added to10 µl of Trypan blue solution in a test tube. The tube was thoroughly mixed by pipetting and left to stand for 4 min to allow for cells to be exposed to the stain. A volume of 10 µl of this mixture was then loaded by pipette tip into a chamber of the counting slide. The slide was inserted into the slide slot of the TC20 cell counter and cell counting was automatically initiated as soon as the cell counter detected the presence of the slide and Trypan blue dye. When Trypan blue was detected in a sample, the result was adjusted to account for the 1 to 1 cell dilution. For example, a 1×10^6 cells/ml mixed 1 to 1 with Trypan blue was at a concentration of 5×10^5 cells/ml. The TC20 takes the dilution into account and multiplies results by 2. The result was reported on the monitor as the estimated concentration of the undiluted sample: 1×10^6 cells/ml. The percentage of live cells also appears on the count screen. Once the cell counter completed the cell count, the slide was removed from the slide slot and screen returned to home mode ready for another slide.

Cell counts per ml were used to determine the volume necessary to seed the cells at a required cell density in growth medium. Cell density of 50,000 cells/ml was used to plate out mouse N2a cells and 100,000 cells/ml was used for ReNcell CX cells (Table 2.3). Flasks were then incubated at 37^{o}C in a humidified atmosphere of 95% air/5% CO_2 for 24 h to allow for cell recovery.

Table 2.3. Loading cell density for experiments with N2a and ReNcell CX cells.

Type of cell culture ware	N2a		ReNcell CX	
	Loading volume	Total cells number	Loading volume	Total cells number
T75 flask	40 ml/flask	2,000,000	10 ml/flask	1,000,000
T25 flask	10 ml/flask	500,000	5 ml/flask	500,000
8 well slide	300 µl/well	15,000	200 µl/well	20,000
24 well plate	500 µl/well	25,000	300 µl/well	30,000
96 well plate	200 µl/well	10,000	200 µl/well	20,000

2.2.4 Induction of cell differentiation

Prior to the induction of N2a or ReNcell CX cell differentiation, mitotic cell monolayers were detached at 70-80% confluence and harvested by centrifugation as previously described in sections 2.2.1.3 and 2.2.2.4. Cell pellets were resuspended in 1 ml of DMEM (N2a) or KnockOut™ DMEM/F-12 medium (ReNcell CX) and cell density was plated out at 50,000 cell/ml for N2a or 100,000 cells/ml for ReNcell CX according to the required size of flask. Each cell type was maintained at 37^{o}C in a humidified atmosphere of 95% air/5% CO_2 for 24 h to allow for cell recovery. The growth medium was then carefully removed by aspiration from the edge of the culture-ware to avoid disturbing the attached cells. ReNcell CX differentiation was initiated by replacing the maintenance culture medium with mitogen free medium. The Removal of growth factors EGF and FGFb from the maintenance culture medium induces ReNcell CX cells differentiate by stopping cell proliferation. N2a cell differentiation was induced by replacing growth medium with serum free medium (i.e. growth medium minus FBS) containing 0.3 mM dibutyryl cyclic adenosine

monophosphate (dbcAMP). The addition of dbcAMP to serum free medium induces N2a cell differentiation by decreasing cell division and increasing intracellular cAMP, which stimulate the development of axon-like neurites (Prashad and Rosenberg, 1978).

For this, dbcAMP was dissolved in sterile-filtered serum free medium from a stock solution 30 mM. The final concentration of 0.3 mM dbcAMP was given by adding 100 µl of stock solution to 10 ml of serum free medium. Both cell lines were induced to differentiate at 37^{o}C in an atmosphere of 5% CO_2, 95% air for 20 h before being treated with or without the test OP compounds.

2.2.5 Exposure of cells to organophosphate compounds

CPF and CPO were prepared as 200-fold concentrated stock solutions in DMSO and added to the serum free medium immediately before use. Controls cells were treated with serum free medium containing the same concentration of DMSO 0.5% (v/v). Both compounds were dissolved in DMSO as it provides rapid and complete absorption.

Following induction of N2a cell differentiation, serum free medium was removed and replaced with an equal volume of fresh serum free medium containing 0.3 mM dbcAMP and various concentrations of OP compounds (1, 3 and 10 µM final concentrations). Control cells were incubated with the same amount of serum free medium containing 0.3 mM dbcAMP and an appropriate volume of DMSO (final concentration 0.5% v/v). Cells were returned to the CO_2 incubator and exposed to the toxins for a further 2, 4 or 8 h, after which cell pellets or lysates were prepared according to the required assay.

Similarly, ReNcell CX cells were induced to differentiate by withdrawing the growth factors EGF and FGFb from the maintenance medium and again various concentrations of test OP compounds were added to the medium just prior to its addition to the cells. Plates were then incubated at 37^{o}C incubator for the required exposure time.

The 3 μM final concentration of both OP compounds was chosen for initial work on the basis that it was a sub-cytotoxic axon outgrowth inhibitory level towards differentiating N2a cells, as determined by a previous group study (Sachana et al., 2001).

2.2.6 Cryopreservation of cell lines

In order to store and preserve the cells for long term use, cells were stored in liquid nitrogen cryovessel until needed. Briefly, the contents of a T25 flask of confluent cells were detached, harvested and resuspended in 1 ml of freezing medium (DMEM for N2a or knockout DMEM/F-12 medium for ReNcell CX, supplemented with 5% (v/v) DMSO). This cell suspension was placed into 1 ml cryo vials and lagged in tissue paper before being incubated overnight at -80^{o}C for a minimum of 8 h. The cryo vials were then transferred to a liquid nitrogen container (-196^{o}C) and stored until needed.

The two step freezing method is carried out instead of immersing the warm cell sample directly into liquid nitrogen to reduce the effects of forming a gaseous nitrogen layer (Leidenfrost effects), which limits heat transfer (Gottfried et al., 1966).

2.2.7 Cell viability assessment

Measurement of cell viability is considered the cornerstone for the most *in vitro* studies of cellular response to toxic agents. The effects of CPF and CPO on the viability of N2a cells were determined by the MTT (3-(4,5-dimethylthiazol-2-yl)-2,5 diphenyltetrazolium bromide) reduction assay, which was first described by Mosmann (1983). MTT is a colorimetric assay based on the ability of cellular dehydrogenase enzymes (mainly succinate dehydrogenase) from viable cells to cleave the tetrazolium rings of the pale yellow MTT and form purple formazan crystals. These crystals are largely impermeable to the cell membrane resulting in their accumulation within healthy cells. Solubilisation of the crystals by the addition of DMSO results in their liberation, which can be detected using a spectrophotometer. The ability of the cells to reduce MTT provides an indication

of metabolic activity, as the quantified level of the formazan product is directly proportional to the number of surviving cells. This in turn may be interpreted as a measure of cell viability.

The MTT approach is safe, sensitive, easy to perform and provides rapid measurement. Moreover, its reagent yields stable colour and low background absorbance value in the absence of cells. Additionally, there is a linear relationship between MTT absorbance and cell number, which allow for an accurate quantification of changes in cell growth. Therefore, it is widely accepted among toxicity studies and considered as a reliable tool to determine cell viability (Mosmann, 1983).

2.2.7.1 Preparation of buffers and reagents

2.2.7.1.1 Phosphate buffered saline (PBS)

The buffer was prepared in a total volume of 1 L containing 137 mM NaCl, 2.7 mM KCl, 8.1 mM Na_2HPO_4, 2 mM KH_2PO_4 at pH 7.4.

2.2.7.1.2 (3-(4,5-dimethylthiazol-2-yl)-2,5 diphenyltetrazolium bromide) MTT

This was prepared by dissolving 5 mg of MTT per ml of PBS. Aliquots (1 ml) were stored frozen at -20 ºC until required.

2.2.7.2 Assay protocol

Cells were plated out at the required density in Corning 24 well plates and grown for 24 h in growth medium prior to the induction of cell differentiation. Differentiating cells were treated without or with different concentrations of CPF or CPO (1, 3, 10 µM) for 2, 4 or 8 h as described in sections 2.2.1.3, 2.2.3, 2.2.4 and 2.2.5. Thirty minutes prior to the end of the experimental incubation time, a volume of 50 µl MTT was added to each well and cells were incubated at 37^{o}C. After 30 min, serum free medium was then aspirated from the wells and 500 µl

of DMSO were added to each well. Treatment of the cell monolayers with DMSO results in the liberation of blue, water-insoluble formazan crystals. The plate was then agitated to dissolve this product completely. A total of 200 µl of each of the resulting solutions was transferred into a 96-well plate and the absorbance was read at a wavelength of 570 nm using a microplate reader (ASYS Expert 96, Biochrom, UK). The absorbance then expressed as a percentage of MTT reduction for the corresponding control.

2.2.8 Measurement of N2a cell differentiation

Differentiation of N2a cells was assessed using the 5-carboxyfluorescein diacetate N-succinimidyl ester (CFSE) fluorescent cell staining dye. The cell labelling marker has been used in a wide variety of different experimental applications, such as monitoring lymphocytes and bacterial proliferation, cell migration and tracking fibroblast division (Hoefel et al., 2003, Li et al., 2003). In this study, CFSE labelling was used as a new research tool for the detection of the neurotoxic effects of CPF and CPO on N2a cell differentiation.

Visualisation of cells with fluorescent esterase substrate provides an alternative to Coomassie Brilliant Blue (CBB) staining, which has long been utilised in determination of cell differentiation (Flaskos et al., 1998, Flaskos et al., 1999, Sachana et al., 2001, Sachana et al., 2003, Sachana et al., 2005, Hargreaves et al., 2006, Flaskos et al., 2007). The non-fluorescent molecules of the succinimidyl ester pass into viable cells through cell membranes and become converted by intracellular non-specific esterases into fluorescent products. This fluorescein derived from CFSE covalently binds to cellular components and retained inside the cells for several weeks. Once the cells were labelled with this dye, differentiated cells were monitored for the presence of neurites using epifluorescence or confocal microscopy. Not only is CFSE highly specific, stable and more sensitive than CBB, it can also provide a useful marker for visual identification of both fixed and living cells (Garton and Schoenwolf, 1996). Furthermore, CFSE dye can be used for both *in vitro* and *in vivo* experiments (Lyons, 1999). The only drawback of CFSE is that it can be toxic to cells at high

concentration. However, this problem can be eliminated by determining the optimum loading time and concentration of the dye, which does not affect the normal functions of cells and yields a good fluorescent stain (Parish, 1999).

2.2.8.1 Preparation of reagents

2.2.8.1.1 5-carboxyfluorescein diacetate N-succinimidyl ester (CFSE)

This was prepared by dissolving 50 mM CFSE stock into 0.5% (v/v) DMSO to give a total volume of 1 ml.

2.2.8.2 Determination of optimum concentration of CFSE

Working stock concentrations of CFSE were prepared in 0.5% (v/v) DMSO (20 mM, 2 mM, 0.2 mM, 0.02 mM and 0.002 mM). After N2a cells were harvested and resuspended in 1ml of growth medium, they were loaded in a Corning 24 well plate. The plate was incubated at 37°C for 24 h and induced to differentiate for 20 h as previously described in section 2.2.4. The different stock concentrations of CFSE in 0.5% (v/v) DMSO were applied directly to each well at 1 to 200 dilution (5 µl/ml) to give final concentrations of (100 µM, 10 µM, 1 µM, 100 nM, 10 nM) and re-incubated for 10 min at 37°C. Medium including the dye was then removed and the cell monolayer rinsed with fresh pre warmed serum free medium. To check the health status of differentiated cells following exposure to the dye, a MTT reduction assay was performed. The optimal concentration of CFSE was chosen on the basis that this level was not considered to be cytotoxic towards differentiated cells, as determined by MTT reduction assay (see section 2.2.7).

2.2.8.3 Staining of cells with CFSE dye

N2a cells were seeded into an 8-well cell culture slide at an original density of 50,000 cells/ml and induced to differentiate for 20 h as indicated in sections 2.2.1.3, 2.2.3 and 2.2.4. They were then incubated for 10 min with the optimum concentration of CFSE dye (10 µM) in pre warmed sterile PBS, before being incubated for 2, 4 or 8 h in the presence and absence of 1, 3 or 10 µM CPF or

CPO at 37°C. After the required length of toxin exposure, cells were fixed for 15 min at room temperature in pre warmed 4% (w/v) paraformaldehyde followed by three 10-min washes in PBS. Cells were then mounted under glass cover slips using VectaShield® mounting medium for fluorescence and viewed using an Olympus DP71 epifluorescence microscope. CFSE was excited with 488 nm fluorescein isothiocyanate (FITC) laser-line and emitted in green. From each well, five random fields were selected giving a total cell count of 200-300 cells/well. In each well, the total number of axon-like processes, which are defined as extensions greater than two cell body diameters in length with an extension foot (Keilbaugh et al., 1991), were recorded and the mean number of axon-like processes per 100 cells was calculated (Flaskos et al., 1998).

2.2.9 Acetylcholinesterase activity assay

Measurement of AChE activity is routinely evaluated in cultured cell lines that are used to model the mechanisms associated with OP neurotoxicity in *in vitro* studies (Flaskos et al., 1994). Inhibition of the enzymatic activity of AChE by OPs is one of the proposed mechanisms underlying the effects on neurite outgrowth. The screening assay is extremely sensitive and suitable for the detection of the enzymatic activity of AChE in a small number of cells (Ellman et al., 1961). The activity of AChE enzyme in cells exposed to OP compounds was measured in a spectrophotometric assay developed by Ellman and colleagues in (1961). The method is based on the production of thiocholine by the action of AChE on acetylthiocholine, which forms a yellow coloured product with 5,5'-dithiobis(2-nitrobenzoic acid) (DTNB). This colour intensity can be measured at 412 nm and it is proportional to the enzyme activity in the sample.

$$\text{Acetylthiocholine} \xrightarrow{\text{AChE}} \text{thiocholine + acetic acid}$$

$$\text{Thiocholine} \xrightarrow{\text{+DTNB}} \text{yellow product}$$

2.2.9.1 Preparation of reagents

2.2.9.1.1 Acetylthiocholine iodide (ATCh)

The substrate was prepared in a total volume of 20 ml containing 1.25mM ATCh and 200mM sodium phosphate buffer at pH 7.4 and kept on ice until required.

2.2.9.1.2 5,5-dithiobis (2-nitrobenzoic acid) (DTNB)

This reagent was freshly prepared in a total volume of 20 ml containing 1.25 mM DNTB and 200 mM sodium phosphate buffer at pH 7.4 and kept on ice until required.

2.2.9.1.3 Sodium phosphate buffer

The buffer was prepared in a total volume of 200 ml containing 200 mM sodium phosphate (monobasic) and 200 mM sodium phosphate (dibasic) at pH7.4.

2.2.9.2 Assay protocol

Cells were plated out at the required density in T75 or T25 culture flasks and cultured for 24 h prior to the induction of cell differentiation. Differentiating cells were treated with different concentrations of CPF or CPO (1, 3, 10 μM) for the required length of time as described in sections 2.2.1.3, 2.2.3, 2.2.4 and 2.2.5. Harvested cells were then, resuspended in 1 ml of ice cold PBS at 4°C and transferred into a micro centrifuge tube. Cells were micro-centrifuged at 10,000 g for 3 min to remove traces of culture medium. PBS was then carefully removed from the micro centrifuge tube and cell pellets were resuspended in 1 ml of ice cold 200 mM sodium phosphate buffer (pH 7.4) containing 0.1% (v/v) Triton X100 at 4°C.

A volume of 100 μl of the cell lysate was transferred into a 96-well plate in 4 replicates. Then, 100 μl of a 1:1 mixture containing ATCh substrate and the colour indicator DTNB were added to each well. The activity of AChE in N2a cells was determined in each sample. Absorbance was immediately measured at

412 nm and recorded at 1 minute intervals for a total of 10 min at 25°C using a microplate reader (ASYS Expert 96, Biochrom, UK). The absorbance in blank wells (with the assay buffer only) was used as a control, and subtracted from the values for those wells with the AChE reactions. As the absorbance background was increasing with time, the absorbance intensity value of the blank wells was subtracted for each data point.

The amount of protein was determined in the remaining cell extract by the bicinchoninic acid (BCA) assay as described in section 2.2.11. BSA protein standards were prepared in a range of 0-2 mg/ml in the same assay buffer (sodium phosphate buffer) as that used to lyse the cell pellets (Table 2.5). AChE data were plotted as absorbance at 412 nm vs. time in minutes. Specific activity of AChE (Absorbance change/min/mg protein) was expressed as a percentage of the corresponding control value ± SEM.

2.2.10 Phosphatase assay

The activity of alkaline phosphatase (ALP) was detected using para-Nitrophenyl Phosphate (pNPP) liquid substrate system (Sigma). The assay principle utilises pNPP that turns into a yellow coloured product (maximal absorbance at 405 nm) when hydrolysed by ALP. The rate of colour change is directly proportional to the enzyme activity.

p-nitrophenyl phosphate (pNPP) $\xrightarrow{\text{phosphatase}}$ p -nitrophenol + phosphate

N2a cells were seeded and induced to differentiate in the presence and absence of OPs in T75 culture flasks for 2, 4 or 8 h as described in sections 2.2.1.3, 2.2.3 and 2.2.4. Cells were harvested by centrifugation, resuspended in 1 ml ice-cold PBS (pH 7.4) and transferred into micro centrifuge tubes. All tubes were then centrifuged at 10,000 g for 3 min. The PBS was then removed and cell pellets were kept on ice and resuspended in 300 µl of ice cold TBS containing 0.5% (v/v) Triton X100. Cell pellets were broken down by pipetting and 50 µl of each lysate were transferred into a 96-well microtitre plate in 4 replicates. The

reaction was started when 100 µl of pNPP liquid substrate system were added into each well. The absorbance was then recorded at regular intervals for 30 min at 405 nm at 25°C using a microtitre plate reader (ASYS Expert 96, Biochrom, UK). Protein was estimated in the retained 100 µl of cell lysate by BCA assay, and specific activity (Absorbance change/min/mg protein) was expressed as a percentage of the corresponding control value ± SEM.

2.2.11 Protein determination assay

Total amount of protein in samples was determined using a modified bicinchoninic acid (BCA) protein assay kit from Sigma-Aldrich. The assay is similar to the method of Lowry with minor modifications (Lowry et al., 1951), using bovine serum albumin (BSA) as standard . The principle of the BCA assay relies on the formation of a Cu^{2+} -protein complex under alkaline conditions, followed by reduction of the Cu^{2+} ions from cupric sulphate to Cu^{+} by the peptide bonds in a protein. The molecules of BCA then bind with Cu^{+} forming a purple-blue product, which can be measured at 570 nm by spectrophotometry. The absorbance is proportional to the amount of protein present in the sample.

Using a BCA assay kit from Sigma-Aldrich, the BCA working reagent was prepared by mixing 50 parts of BCA reagent A (1% (w/v) bicinchoninic acid sodium salt, 2% (w/v) sodium carbonate, 0.16% (w/v) sodium tartrate and 0.95% (w/v) sodium bicarbonate in 0.1 M sodium hydroxide at pH 11.5) with 1 part of reagent B (4% (w/v) copper (II) sulphate pentahydrate). A light green solution was obtained. The amount of reagents needed was dependent on the number of used wells as indicated in (Table 2.4).

Table 2.4. BCA working reagent preparation.

Number of wells to be used in a 96-well plate assay	Amount of reagent A (ml)	Amount of reagent B (µl)
40	8	160
80	16	320
96	19	380

To produce a standard curve, serial dilutions of BCA standards ranging from 0 to 2 mg/ml were prepared from a 2 mg/ml BSA stock solution in the same buffer that was used in preparing the cell lysates. The serial dilutions of BCA were prepared in 2 ml micro centrifuge tube as indicated in Table 2.5, and vortex mixed. The assay was performed in a 96-well plate, where 25 µl of standards or protein sample were mixed with 200 µl of BCA working reagent and incubated for 30 min at 37°C in an LEEC incubator (LSC 2933). Absorbance was then read at 570 nm and protein concentration of each sample was determined from the average of triplicates using the linear correlation obtained from the BSA standard curve.

Table 2.5. Preparation of BSA protein standards for protein determination.

Volume of 2 mg/ml BSA (µl)	Volume of assay buffer (µl)	Final concentration of BSA (mg/ml)
0	1000	0
200	800	0.4
400	600	0.8
600	400	1.2
800	200	1.6
1000	0	2

2.2.12 One dimensional polyacrylamide gel electrophoresis (SDS-PAGE) and Western blotting

2.2.12.1 Preparation of buffers and reagents

2.2.12.1.1 ×4 Laemmli sample buffer

The buffer was prepared in a total volume of 10.2 ml containing 40% (v/v) glycerol, 8% (w/v) SDS, 20% (v/v) β-mercaptoethanol, 0.01% (w/v) Bromophenol blue and 0.1 M Tris HCl, at pH 6.8.

2.2.12.1.2 10% (w/v) Ammonium persulphate (APS)

This was prepared by dissolving 5 mg of APS into 50 µl of dH_2O.

2.2.12.1.3 Running buffer

The buffer was prepared in a total volume of 1 L containing 25.6 mM Tris-base, 192 mM glycine and 0.1% (w/v) SDS at pH 8.3.

2.2.12.1.4 Transfer buffer

The buffer was prepared in a total volume of 1 L containing 48 mM Tris-base, 39 mM glycine, 0.037% (w/v) SDS and 20% (v/v) methanol.

2.2.12.1.5 Tris-buffered saline (TBS)

The buffer was prepared in a total volume of 1 L containing 10 mM Tris and 140 mM NaCl at pH 7.4.

2.2.12.1.6 Bovine serum albumin (BSA)

The blocking buffer was prepared in TBS containing 3% (w/v) BSA and 0.01% (w/v) sodium azide.

2.2.12.2 Preparation of N2a cell lysates for SDS-PAGE

N2a cells were plated out at a density of 50,000 cells/ml in T75 flasks (2 million cells/T75 flask) and differentiated for 20 h before being treated with OP compounds for 2, 4 or 8 h as described in sections 2.2.1.3, 2.2.3 and 2.2.4. After the required period of toxin exposure, serum free medium was carefully removed from the flasks and cell monolayers were rinsed gently with pre warmed PBS. Intact cell monolayers were then solubilised by boiling in 2 ml of 0.5% (w/v) sodium dodecyl sulphate (SDS) in 18.0 megohm-cm nanopure water (Barnstead™ Nanopure® Diamond™, Life science, UK). Lysates were detached mechanically by cell scraper and transferred to micro centrifuge tubes, boiled for 5 min and then allowed to cool to room temperature for 10-15 min.

DNA was then extracted from each lysate by placing 500 µl of cell lysate into a spin column (Dutscher Scientific, catalogue no. 789068) and centrifuging for few seconds at 10,000 g at room temperature. After centrifugation, the filter with the captured DNA was carefully removed and discarded. The supernatant from the lower chamber was placed into a clean micro centrifuge tube labelled as protein lysate sample minus DNA. This step was repeated few times until the required amount of sample was obtained. The amount of protein presented in each sample was then estimated by BCA assay.

When the protein concentration of cell lysates was very low, the sample was precipitated by ice-cold acetone. In brief, 9 parts of ice cold acetone were added to 1 part of protein sample in a micro centrifuge tube, vortex mixed and incubated at −20 °C overnight. The tubes were then centrifuged at maximum speed of 10,000 g for 20 min at 4°C to pellet the precipitated protein. The acetone was then carefully decanted from the tube and discarded properly in non-chlorinated waste bottles, and the remaining protein pellets were left to air-dry at room temperature for 30 min. After complete acetone evaporation, pellets were resuspended with 100 µl of 0.5% (w/v) SDS in TBS and mixed thoroughly by a 100µl Gilson pipette to dissolve the protein. BCA assay was performed again to estimate the amount of protein presented in each sample. Once the protein concentration had been determined, samples were prepared for SDS polyacrylamide gel electrophoresis (SDS-PAGE) by mixing 150 µl of each cell lysate with 50 µl of ×4 Laemmli sample buffer and boiled for 5 min prior to loading.

2.2.12.3 SDS-PAGE assay

The resultant proteins from cell lysates were subsequently separated according to their molecular weight using SDS-PAGE.

2.2.12.3.1 Preparation of resolving gels

Based on the molecular weight of the investigated proteins, a 10% (w/v)

acrylamide resolving gel was prepared in all the experiments (Table 2.6). The resolving gel is also called separating gel, which separates the proteins by size. A Bio-Rad mini-PROTEAN III™ electrophoresis chamber was used. Spacers, combs and two glass plates of 1.5 mm thickness were washed and wiped thoroughly with 70% (v/v) ethanol prior to assembly. One foam pad was placed in the casting apparatus and glass plates were assembled evenly into the plate holders. Once the plates were mounted on the casting stands, it was first filled with water and allowed to stand for 5 min to check for any leakage and the water was then removed before being replaced with the gel mixtures. The 10% (w/v) acrylamide resolving gel mixture was prepared according to the number of gels that were going to be used, as indicated in Table 2.6. Acrylamide polymerisation was then initiated by the addition of the volumes indicated of 10% (w/v) APS and TEMED, after which the mixture was swirled gently. Then 8 ml of resolving gel mixture were transferred into each cast to allow sufficient space for a stacking gel to be added later. Distilled water was carefully overlaid on the top layer of the freshly poured gel mixture to create a smooth interface and prevent any gel shrinkage. The gel mix was allowed to polymerise at room temperature for approximately 30 to 40 min.

Table 2.6. Preparation of 10% (w/v) acrylamide resolving gel.

10% (w/v) acrylamide resolving gel reagents	Volume (for 2 gels)
Accu gel 29:1 40% (w/v) acrylamide:bisacrylamide (29:1)	5.0 ml
Protogel® Resolving buffer (1.5 M Tris-HCl buffer pH 8.8, 0.4% (w/v) SDS)	5.0 ml
Distilled water	9.78 ml
10% (w/v) Ammonium persulphate (APS)	200 µl
TEMED	40 µl
Total volume	20 ml

2.2.12.3.2 Preparation of stacking gel

The required amount of 4% (w/v) polyacrylamide stacking gel was prepared and polymerised by the presence of 10% APS and TEMED as indicated in Table 2.7. The stacking gel solution was mixed gently and poured onto the polymerised resolving gel after removing the top layer of distilled water. The stacking gel is used because it allows proteins entry and accumulation at the interface of the resolving gel. After filling the chamber with stacking gel solution, a comb of the correct thickness was immediately inserted into the unpolymerised gel mixture to create the wells into which the samples would be loaded. The gel mixture was then allowed to polymerise for 30 min at room temperature. After this, the comb was carefully removed and wells were rinsed by flushing with running buffer using a 1000 µl Gilson pipette before loading the samples.

Table 2.7. Preparation of 4% (w/v) acrylamide stacking gel.

4% (w/v) acrylamide stacking gel reagents	Volume (for 2 gels)
Accu gel 29:1 (40% (w/v) acrylamide:bisacrylamide (29:1))	1.0 ml
Protogel® stacking buffer (0.5 M Tris-HCl buffer pH 6.8, 0.4% (w/v) SDS)	2.5 ml
Distilled water	6.4 ml
10% APS	100 µl
TEMED	20 µl
Total volume	10 ml

2.2.12.3.3 Preparation of protein samples for loading

Equal amounts of cell protein, as estimated by BCA assay, were loaded into the gel to ensure even protein loading. A Blueye prestained protein ladder (2 µl) was loaded along with the protein samples to allow estimation of molecular weight. The Blueye prestained protein ladder (GeneDirex, UK) used in this study is a three colour protein standard with 12 prestained proteins, in which molecular weights range from 10 to 245 kDa).

2.2.12.3.4 Separation of proteins in cell lysates by gel electrophoresis

To separate the proteins, gels were placed vertically in the electrophoresis chamber and filled with running buffer. Electrophoresis was run initially at 50 volts using a Bio-Rad power pac 300 for 10 min. This voltage was used first to organise the samples in the stacking gel. After that, the voltage was increased to 150 volts and electrophoresis allowed to continue until the dye front reached the base of the gel plates. As the dye reached the end of the gel, the voltage was switched off. Gels were carefully removed to avoid damaging the glass plates or the gel.

2.2.12.4 Western blotting

On completion of the separation of proteins by SDS-PAGE, the gels were mechanically removed from the plates and the stacking gels were cut off. The remaining resolving gel, which contained the separated proteins, was electrophoretically transferred onto nitrocellulose membrane filters by wet blotting (Towbin et al., 1979).

Briefly, gels to be blotted, nitrocellulose membranes (0.45 μM pore size) (Hybond C, Amersham) and 3 MM filter papers (Whatman® filter paper, from Sigma-Aldrich) were soaked in transfer buffer for 5 min. The presence of methanol in the transfer buffer is necessary to remove any non-protein-bound SDS and to enhance the adsorption of protein to the nitrocellulose membrane. Filter papers and membranes were carefully cut to the same size as the gel to avoid wastage.

A transfer sandwich was then physically built on the side of the transfer cassette facing the anode (+) starting with a wet sponge and followed by three wetted filter papers, nitrocellulose membrane, the gel, three additional wetted filter papers and finally a second sponge. Any wrinkles, folds or air bubbles between the different layers of the sandwich were avoided by rolling a glass rod lightly across the components. Bubbles were removed as they can cause blank spots on the membrane where no protein transfer occurs. This assembled sandwich was

then securely fixed in the transfer cassette and immersed in the blotting chamber (Mini Trans-Blot® Electrophoretic Transfer cell; Bio-Rad) containing transfer buffer. A voltage of 30 volts was applied overnight at room temperature.

2.2.12.5 Immunoprobing of nitrocellulose blots

The resultant Western blots were blocked with 3% (w/v) BSA in TBS (BSA/TBS), containing 0.01% (w/v) sodium azide as a preservative. Blocking is essential to inhibit non-specific binding between protein and the membrane. For this, blots were placed on a shaker (Heidolph Unimax 1010) and agitated slowly with the blocking solution for at least 1 h at room temperature. Following the blocking step, blots were incubated with appropriate dilutions of primary antibodies made in BSA/TBS at 4°C overnight (Table 2.8). Blots were then washed to remove excess primary antibody that can cause high background using 0.05% (v/v) Tween-20 in TBS detergent solution (TBS/Tween). This wash was performed six times (10 min/wash) with constant agitation at room temperature. After washing, blots were probed with horseradish peroxidase (HRP)-conjugated secondary antibodies for 2 h at room temperature (Table 2.9). Following 6 further washes with TBS/Tween, the unbound secondary antibodies were removed from the membrane and antibody reactivity was visualized with enhanced chemiluminescence (ECL) reagents (Thermo Scientific, USA) in a G:BOX imager dark system (Syngene, Cambridge, UK). The ECL reagents were allowed to equilibrate at room temperature before an equal volume of ECL reagent A and B were mixed freshly and applied on the membrane to detect the band of interest. A densitometric analysis of antibody reactivity was then performed, where band densities on images of developed blots were determined using Advanced Image Data Analysis (AIDA) software (version 4.03) (Raytest GmbH, Straubenhardt, Germany). Using this software, each individual band was superimposed over the region of interest and a peak profile was constructed. An arbitrary value of the area beneath the peak, which represents the antibody reactivity, was then obtained. All band densities were measured and corrected for background, then normalised to band densities for B512 reactivity, which was used as internal control. Data are expressed as a percentage of the average value of the peak area compared to its corresponding control ± SEM.

Table 2.8. List of monoclonal and polyclonal primary antibodies used in Western blotting.

Primary antibody	Clone	Dilution	Species	Approx. molecular weight of target (kDa)	Code	Supplier
Cytoskeletal proteins						
Anti-phospho neurofilament H	Ta51	1:1000	Rat	200	MAB5448	Chemicon International
Anti-neurofilament 200 (phos and non phos)	N52	1:250	Mouse	200	N0142	Sigma-Aldrich
Anti-growth associated protein-43 (GAP-43)	GAP-7B10	1:1000	Mouse	43	G9264	
Anti-α-tubulin	B512	1:2000	Mouse	55	T6074	
Anti-βIII-tubulin	2G10	1:1000	Mouse	55	T8578	
Anti-tubulin polyglutamylated	B3	1:1000	Mouse	55	T9822	
Anti-acetylated tubulin	611B1	1:1000	Mouse	55	T6793	
Anti-tyrosine tubulin	TUB-1A2	1:1000	Mouse	55	T9028	
Anti-MAP-1B	H130	1:1000	Rabbit	200	B1904	Santa Cruz Biotechnology
Anti-MAP-2	H300	1:1000	Rabbit	200-140	J1805	
Cell signalling proteins						
Anti-total ERK1/2	K-23	1:1000	Rabbit	44-42	D1906	Santa Cruz Biotechnology
Anti-phosphorylated ERK1/2	E-4	1:500	Mouse	44-42	sc-7383	
Heat shock proteins						
Anti-HSP90	AC16	1:1000	Mouse	90	H1775	Sigma-Aldrich
Anti-HSP70	BRM22	1:1000	Mouse	70	H5147	

Anti-HSP60	LK2	1:1000	Mouse	60	H3524	

Table 2.9. List of secondary antibodies used in Western blotting.

Secondary Antibody	Type	Dilution	Code	Supplier
Anti-mouse IgG	HRP	1:1000	A9044	Sigma-Aldrich
Anti-rabbit IgG	HRP	1:1000	A6154	
Anti-goat IgG (H+L)	HRP	1:1000	805-035-180	Jackson Immuno Research
Anti-rat IgG	HRP	1:1000	P0450	DAKO-Cytomation

2.2.13 Indirect immunofluorescence

Indirect immunofluorescence staining is a technique that relies on using fluorescently-labeled antibodies to detect specific target antigens in two steps. First, cells are stained with unconjugated primary antibody that binds to the antigen. Then a fluorescent-conjugated secondary antibody is used to detect the primary antibody (Odell and Cook, 2013). The fluorescent dye allows visualisation and study of the intracellular distribution of neurofilament and microtubule proteins by utilising an epifluorescence or confocal microscope.

Initially, N2a cells were plated at a density of 50,000 cells/ml on an 8-well cell culture chamber slide (NUNC, Thermo Scientific) in a total volume of 300 µl of growth medium per well. Cells were induced to differentiate for 20 h before being treated in the presence and absence of 3 µM CPF or CPO for 2, 4 or 8 h at 37°C as mentioned in sections 2.2.1.3, 2.2.3 and 2.2.4. After the required time of toxin exposure, the medium was aspirated from each well and cells were fixed to retain the shape and locations of all cellular proteins using 500 µl/well of pre warmed 4% (w/v) paraformaldehyde (Sigma-Aldrich, UK) for 15 min at room temperature. Cells were then washed three times with 300 µl/well of ice cold PBS (2 min/rinse). Cell membrane permeabilisation was then performed by

incubating the cells for 15 min at room temperature in 0.05% (v/v) Tween-20 in PBS. This detergent solution created small holes in the membrane, which allowed the antibody to access the cytoplasm. Following three further rinses with PBS, non-specific binding was prevented by blocking the fixed cells with 500 µl of BSA/TBS per well for 1 h at room temperature. After blocking, cells were incubated with 200 µl/well of primary antibodies (diluted 1 in 500 in BSA/TBS) against NFH (N52), phosphorylated NFH (SMI34) and tubulin (B512) overnight at 4°C and washed three times with TBS/Tween to remove unbound primary antibodies. The cells were then incubated for 1 h at room temperature with Alexa Fluor® anti-IgG secondary antibody diluted 1/500 in BSA/TBS blocking buffer (Table 2.10). After 3 further washes in TBS/Tween, the chamber partitions and mounting silicon were carefully removed from the slide. For mounting, anti-fade mountant (VectaShield® mounting medium for fluorescence; Vector Laboratories Ltd., Peterborough, UK) containing 4',6-diamidino-2-phenylindole (DAPI) counterstain for nuclei visualization was applied to the exposed cell monolayers after careful aspiration of excess TBS. A glass cover slip was then placed in position and air bubbles were carefully removed by gentle pressure. A layer of clear nail polish was then applied around the extreme edges of the cover slip to fix it in place. Finally, the slide was viewed using an Olympus DP71 epifluorescence microscope system, which equipped with an argon/krypton laser (FITC: Excitation 493/ Emission 528; DAPI: Excitation 360/ Emission 460). Cell images were acquired using Cell^F software. Negative control was included in this experiment by incubating non OP-treated cells with the secondary antibody only to confirm the specificity of the primary antibody.

Table 2.10. Secondary antibodies used in indirect immunofluorescence staining.

IF Secondary antibody	Target species	Dilution	Code	Supplier
Alexa Fluor® 568 IgG	Rabbit	1:500	A21069	Invitrogen
Alexa Fluor® 488 IgG (H+L)	Mouse	1:500	A21204	

2.2.14 Live cell imaging

The real time changes in cell morphology following OP toxin exposure were determined by CFSE fluorescent dye and monitored using a Leica TCS SP5 confocal laser scanning microscope with epifluorescence optics and in an environmental chamber. In this experiment, live N2a cells were labelled by CFSE. Since CFSE fluorescent dye is dependent on the activity of esterase, only live cells are labelled.

N2a cells were plated out at a density of 50,000 cells/ml (10,000 cells/well) in a black clear 96-well treated plate (BD Bioscience, USA) and incubated overnight at 37 °C to allow for the cells to adhere to the bottom of the plate. After 24 h of cell recovery, cells were differentiated for 20 h as indicated in sections 2.2.1.3, 2.2.3 and 2.2.4. After the induction of differentiation, cells were incubated for 10 min with 10 μM CFSE dye in pre-warmed sterile PBS at 37 °C. After CFSE labelling, PBS was replaced by serum free medium including 0.3 mM dbcAMP, and the plate was transported directly to a Leica TCS SP5 confocal laser scanning microscope. This system is equipped with true confocal scanner and five spectrophotometer channels. The N2a cells were incubated in an environmental chamber, which controlled the temperature at 37^{o}C in a humidified atmosphere of 95% air/5% CO_2 Following incubation, Leica application suite advanced fluorescence lite (LAS AF) was configured for fluorescence by setting the laser intensity to 25%. The live cell images were acquired using (xyzt) scanning mode, a frame size of 512 x 512 pixels, a scanning speed at 400Hz, a pixel size of 785 x 785 nm and image size of 387.5 x 20 μm. The fluorophore was then selected from the beam path window and CFSE was excited with 488 nm fluorescein isothiocyanate (FITC) laser-line and emitted in green. Once the laser had been activated, non-treated live cells were first observed in order to create a time zero measurement before the addition of toxins. After that, a 3 μM concentration of CPF or CPO was added to each treatment well (see section 2.2.5) and the same positions were viewed every 30 min for an interval of 8 h exposure time. The scanned images were shown at maximum intensity Z-projections of 25 slices of 1 micron thickness. After collecting a stack of optical sections (Z-series), the sample was reconstructed in

three dimensions, then rotated or tilted to view cells that would otherwise be obscured. The fixed images were then manipulated using LAS AF lite and some neurites were detected and labelled. A time-lapse imaging in one focal plane was then obtained and a play back movie was prepared using Windows Movie Maker software.

2.2.15 Cell ELISA

The levels of and post translational modifications to cytoskeletal proteins in both N2a and RenCell CX cell cultures were further determined and quantified using a cell-based enzyme linked immunosorbent assay (ELISA) technique, based on the approach of Schmuck and Ahr (1997) but with modifications (Schmuck and Ahr, 1997). The immunoassay uses an enzyme linked to an antibody as a marker for the detection of a specific antigen in a wet sample. This subsequent reaction forms a yellow colour product, which can be measured at 405 nm by spectrophotometer. The intensity of the colour change is proportional to the protein or antigen present in the sample.

2.2.15.1 Preparation of buffer and reagents

2.2.15.1.1 100 mM Sodium acetate buffer

The buffer was prepared by dissolving 8.2 g of sodium acetate in 900 ml of distilled water at pH 6. The final volume made up to 1 L with distilled water.

2.2.15.1.2 5 M Sulphuric acid (H_2SO_4)

50 ml of H_2SO_4 were added to 200 ml of distilled water.

2.2.15.1.3 3,3,5,5'-Tetramethylbenzidine (TMB)

A total of 10 mg of TMB was dissolved in 1 ml of DMSO (stock). The developing substrate was prepared using TMB and 3% (v/v) hydrogen peroxide (H_2O_2) in 100 mM sodium acetate buffer at pH 6.

2.2.15.1.4 3% (v/v) Hydrogen peroxide (H_2O_2)

A volume of 10 µl of 30% (v/v) H_2O_2 (stock) was added to 90 µl of distilled water.

2.2.15.1.5 Developing buffer

The developing substrate was prepared by the addition of 150 µl of TMB and 30 µl of 3% (v/v) H_2O_2 into 20 ml of 100 mM sodium acetate pH 6.

2.2.15.2 Assay protocol

The assay was performed in a sterile flat bottom 96-well plate (Sarstedt, USA). Cells were plated out at the density of 50,000 cells/ml for N2a and 100,000 cells/ml for ReNcell CX in a total volume of 200 µl growth medium per well in four replicates and incubated overnight at 37°C in 5% CO_2. After 24 h recovery, cells were differentiated before being treated with or without OP test compounds at different concentrations 1, 3, and 10 µM in fresh differentiation medium for 2 or 8 h as indicated in sections 2.2.1.3, 2.2.2.4, 2.2.3, 2.2.4 and 2.2.5. On termination of toxin exposure, serum free medium was aspirated from each well and cell monolayers were fixed by pre warmed 4% (w/v) paraformaldehyde (Sigma-Aldrich, UK) (200 µl/well) for 10 min at room temperature. Fixative was then removed and the plate was washed twice with 200 µl/well of ice cold TBS (2 min/wash). Cells were then incubated in permeabilisation buffer (0.5% (v/v) Tween-20 in TBS) for 15 min at room temperature after which they were rinsed twice with TBS. A volume of 300 µl/well of BSA/TBS (blocking buffer) was then applied and the plate was covered and incubated overnight at 4°C. The blocking buffer was then removed and 100 µl/well of primary antibodies diluted 1 to 1000 in blocking solution were added and incubated overnight at 4°C (Table 2.11).

After removing the primary antibodies, wells were washed again twice with TBS/Tween, followed by 2 h incubation in 200 µl/well of diluted HRP conjugated secondary antibodies (1:2000 dilution) at room temperature (Table

2.12). After the secondary antibodies had been removed from the plate, two final washes with TBS/Tween 20 were applied for 2 min each and then wash solution was removed completely from wells by turning the plate upside down and tapping gently on a paper towel to remove traces of wash buffer. The reaction was started by the addition of 100 µl of developing substrate buffer into each well. After 5 min incubation at room temperature, a blue colour product was developed which was then stopped by adding 100 µl of 5 N sulphuric acid. Absorbance was measured spectrophometrically using a micro plate reader (ASYS Expert 96, Biochrom, UK) at 405 nm. Results were expressed as antibody binding in treated cells as a percentage of that in untreated controls (set as 100%) ± SEM. The background level was estimated by omitting the primary antibodies. The specificity of antibody was confirmed by non OP-treated cells incubated with the secondary antibody only.

Table 2.11. List of primary antibodies used in cell ELISA.

Primary Antibody	Clone or batch	Dilution	Species	Code	Supplier
Anti- neurofilament 200 (phos and non phos)	N52	1:1000	Mouse	N0142	Sigma-Aldrich
Anti- phospho neurofilament H (1)	Ta51	1:1000	Rat	MAB5448	Chemicon®
Anti- phospho neurofilament H (2)	SMI34	1:1000	Rabbit	14814302	Covance
Anti- α tubulin	B512	1:1000	Mouse	T6074	Sigma-Aldrich
Anti- total ERK1/2	K-23	1:1000	Rabbit	D1906	Santa Cruz Biotechnology
Anti- phosphorylated ERK1/2	E-4	1:1000	Mouse	Sc-7383	
Anti- βIII tubulin	2G10	1:1000	Mouse	T8578	Sigma-Aldrich
Anti- glial fibrillary acidic protein (GFAP)	GA5	1:1000	Mouse	G3893	

Table 2.12. List of secondary antibodies used in cell ELISA.

Secondary Antibody	Type	Dilution	Code	Supplier
Anti- rabbit IgG	HRP	1:2000	A6154	Sigma-Aldrich
Anti- mouse IgG	HRP	1:2000	A9044	
Anti- rat IgG	HRP	1:2000	P0450	DAKO-Cytomation

2.2.16 High-throughput analysis

In the later stages of the project, the cytotoxic effects of CPF and CPO on neurite outgrowth of N2a and ReNcell CX cells were further determined using the ImageXpress Micro Widefield High Content Analysis System (Molecular Devices, USA). This technique permits rapid assessment of the effects of a wide range of chemicals at different concentrations on multiple parameters of neurite outgrowth. The screening system integrates an inverted epifluorescence microscope combined with automated image acquisition and analysis software to quantify different subcellular measurements of neurite outgrowth such as, cell count, neurite count, neurite length and cell body area (Smith and Eisenstein, 2005, Dragunow, 2008).

Typically, cells were plated out at the density of 50,000 cells/ml for N2a and 100,000 cells/ml for ReNcell CX cells in 8-well Ibidi µ-slides. The cells were grown for 24 h in growth medium prior to the induction of cell differentiation for 20 h. Differentiating cells were then treated without or with different concentrations of CPF or CPO (1, 3 and 10 µM) for 2 or 8 h at 37°C as previously described in sections 2.2.1.3, 2.2.3, 2.2.4 and 2.2.5. Following OP exposure, cells were fixed for 10 min using 500 µl of pre warmed 4% (w/v) paraformaldehyde (Sigma-Aldrich, UK) at 37°C. After fixing, cells were washed three times with 300 µl/well of ice cold TBS (2 min/rinse) and cell membranes were permeabilised using 0.5% (v/v) Tween-20 in TBS for 15 min at room temperature. Following three further rinses with TBS, cells were blocked in BSA/TBS (500 µl/well) overnight at 4°C. After blocking, fixed cell monolayers were incubated with 200 µl of primary antibodies. For N2a cells, anti-α-tubulin (clone B512) and anti- pNFH (SMI34 and Ta51) antibodies were used. For ReNcell CX cells, anti-neuronal marker (βIII tubulin and Ta51) and anti-astro-glial marker (GFAP) antibodies were used. All primary antibodies were diluted 1:1000 in BSA/TBS and added to each well, after which the fixed monolayers were then incubated overnight at 4°C. Unbound primary antibodies were removed by three washes in 200 µl of TBS/Tween for 5 min. Conjugated secondary antibodies, Alexa Fluor® 488 goat anti-mouse or Alexa Fluor® 568 goat anti-rabbit immunoglobulins (both diluted 1:500 in BSA/TBS) (Invitrogen),

were added to each well for 1 h at room temperature. Three further washes were then applied using 300 µl of TBS/Tween, five min each. Cell nuclei were labelled with DAPI counterstain for 1 min, followed by a further TBS wash. In the final wash slides were filled with TBS containing 0.01% (w/v) sodium azide as a preservative and stored at 4°C prior to image acquisition and analysis. Negative control was included in this experiment by incubating non OP-treated cells with the secondary antibody only to confirm the specificity of the primary antibody.

Ibidi µ-slides were then loaded into an ImageXpress Micro Widefield High Content Screening System plate holder for automated image acquisition and analysis. The system uses a widefield automated microscope capable of fluorescence, transmitted light and phase-contrast imaging of fixed-cell assays. The system was set to automatically focus and record images from four different sites in each individual well. The size of each well is 9.4 × 9.4 mm, and acquired image is 741.6 × 587.6 µm. Fluorescence images were produced using multiple emission filter and matched laser excitation filters for two different channels, (DAPI) for nuclei (ex= 377/50 nm, em= 447/60 nm) and (FITC) for cell body and neurites (ex= 482/35 nm, em=536/40 nm). Images were acquired using a Nikon 10x objective lens and 1.4 megapixel cooled CCD camera, with a stand-alone illuminator (Lambda LS) connected to the system, which involves a 175W Xenon-arc lamp, lamp housing, cold mirror and power supply (Sutter Instrument, USA). The 10x objective lens was used in order to acquire all neurites in one field of view, thus enabling more reliable analysis of neurite outgrowth.

The acquired images were then segmented by multi-coloured tracing masks on neurites and cell bodies. Segmentation masks were generated using the MetaXpress imaging and analysis software (version 5.1.0.46; Molecular devices, USA), where each neurite segment is given the same coloured mask as that of their parent neuronal cell bodies. The segmentation images were then analysed by the neurite outgrowth module integrated within the MetaXpress imaging and analysis software, using neurite outgrowth configuration setting to measure a number of morphological parameters including average number of cells/field, average cell body area/field, neurite length/cell, mean processes/cell, mean

branches/cell, percentage of cells with significant outgrowth and average intensity of staining within the positive cells. Particles from each image were identified as cells if valid nuclei width between 5 to 10 µm had been detected and cell body width ranged from 15 to 20 µm. Outgrowth was recorded as significant when minimum cell outgrowth was more than 10 µm (approximately half a cell body diameter in length). The measurement ranges for cell bodies and outgrowths were determined in preliminary studies using untreated cells from multiple cultures to develop settings to exclude non-cellular particles from the analysis. Using a 10x objective, four fields/well from four independent experiments were acquired for the analysis of at least 200 cells/well. The cellular results obtained by the analysis software were then transferred to a GraphPad Prism spreadsheet and results were plotted as mean ± SEM. Each OP treatment was compared to its corresponding control.

2.2.17 Statistical analysis

All sets of data were based on a minimum of 4 separate experiments and expressed as mean ± standard error of the mean (SEM). The analysis was conducted using GraphPad Prism (version 6.0f) (GraphPad software, California, USA), a statistics and scientific 2D graphing software. Average values for each treatment were compared to the corresponding controls or other treatment group by one-way or two-way analyses of variance (ANOVA). The analysis was followed by a Tukey post hoc test, which takes into account multiple comparisons, with 95% confidence interval. Results were considered to be significantly different when $p < 0.05$.

3 Effects of chlorpyrifos and chlorpyrifos oxon on neurite outgrowth in pre-differentiated mouse N2a neuroblastoma cells

3.1 Introduction

To this day, CPF remains one of the most extensively used OP insecticides worldwide. Despite the strict bans on its household applications, CPF is still widely used on corn and fruits crops, posing high risks to farm workers, applicators, families and children living in close proximity to agricultural areas where this OP is applied (EPA, 2015). Exposure to CPF can cause acute neurotoxicity symptoms as a result of the inhibition of AChE activity in central and peripheral cholinergic synapses. This inhibition prevents the breakdown of the neurotransmitter ACh, which plays major roles both in neurotransmission and in the developmental process of the brain (Barr and Angerer, 2006). As a result, increased ACh accumulation in the synaptic cleft and consequent over stimulation of muscarinic and nicotinic receptors lead to convulsions, neuromuscular block and respiratory failure (Costa, 2006, Flaskos, 2012).

The metabolic activation of CPF to CPO is known to be the main causative event behind most cases of acute neurotoxicity induced by OPs in adults (Richardson, 1995). This is due to the fact that CPO is much more potent than CPF at inhibiting the activity of AChE (Monnet-Tschudi et al., 2000). However, there is a large amount of epidemiological evidence demonstrating that both CPF and CPO are also capable of inducing developmental neurotoxicity in developing organisms through their interference with developmental processes in the nervous system, such as neurite outgrowth (Campbell et al., 1997, Crumpton et al., 2000, Flaskos, 2012). Several *in vitro* and *in vivo* experimental studies have shown that the toxic action of CPF and CPO on the developing brain is not limited to hyper activation of the cholinergic system, but that it involves other potential targets (Slotkin, 2004). For example, CPF and CPO were found to interfere with the unique developmental process of the brain and the nervous

system by causing several morphological changes in the formation of neurites. These neurites have an essential role in axonal plasticity (Andrieux et al., 2002, Wall, 2005). Clinical signs of neurological syndromes associated with CPF and CPO induced neurotoxicity may arise as a consequence of its effects on axon production, especially in the developing brain in children.

To investigate the impact of OPs on neurite outgrowth in neural cell culture systems, several experimental protocols have been implemented. The majority of previous studies share a common differentiation condition, in which cells are treated with OPs at the same time as induction of cell differentiation (Sachana et al., 2008, Flaskos et al., 2011). This method, known as co-differentiation exposure, can be used to evaluate the ability of OP to inhibit the outgrowth of neurites. However, little work has been done regarding the impact of OPs on cells that have been committed to differentiation and have already formed neurites, a treatment referred to as post-differentiation exposure. Since the mechanisms involved in OP-induced neurotoxicity may vary depending on the differentiation condition used, Sachana and colleagues adopted the post-differentiation exposure strategy to evaluate the effects of CPF on the mouse N2a neuroblastoma cell line (Sachana et al., 2001, Sachana et al., 2005).

Initially, the neuronal cells were allowed to differentiate for 20 h by the removal of serum and in the presence of 0.3 mM dbcAMP to exhibit a network of axons and dendrites, and then treated with or without 3 µM of CPF for 4 and 8 h (Sachana et al., 2001). Work by Sachana *et al* showed that this non- cytotoxic concentration of CPF caused a significant reduction in the number of axon-like processes in pre-differentiated N2a cells by 50% compared to non-CPF treated controls following 4 and 8 h exposure (Sachana et al., 2001, Sachana et al., 2005). The results obtained from these studies not only demonstrated the ability of CPF to inhibit neurite outgrowth but also its capability to cause a retraction of pre-formed neurites.

Although the strategy conducted at such a developmental stage by Sachana *et al* (2001, 2005) was the least investigated among the literature, it provides valuable information regarding the toxic effect of OP toxins on the outgrowth of pre-

formed neurites. Since only the effects of CPF were investigated on differentiated N2a cells with pre-formed axons, it was of interest to know whether a similar concentration of CPO acts in the same manner as CPF on neurite outgrowth produced in this cellular system. Additionally, it was important to elucidate whether the neurotoxic actions of both OPs on cell morphology were associated with AChE inhibition. Previously, reduced activity of AChE was observed in N2a cells exposed to 1-10 µM CPO for up to 24 h from the point of induction of cell differentiation (Flaskos et al., 2011). However, it was suggested that AChE inhibition was not directly related to neurite inhibitory effects of CPO.

By applying post-differentiation exposure conditions, the aim of the current study was to compare the effects of CPO to that seen with CPF towards pre-differentiated N2a cells. Therefore, both compounds at a concentration of 3 µM were investigated in parallel with respect to their ability to interfere with the outgrowth of neurites produced from differentiated N2a cells following 2, 4 and 8 h exposure. To achieve this aim, a range of experimental techniques such as MTT reduction assay, CFSE fluorescence cell staining and live cell imaging were used in this study. A further aim was to determine whether the morphological effects on axon-like neurites were related to the acute toxicity target (AChE) using enzymatic activity assay.

3.2 Results

3.2.1 Effects of CPF and CPO on the viability of pre-differentiated N2a cells

Mouse N2a neuroblastoma cells were induced to differentiate by serum withdrawal and the addition of 0.3 mM dbcAMP for 20 h before being treated without (0.5% v/v DMSO control) or with 3 µM CPF or CPO for 2, 4 and 8 h. To examine the viability of pre-differentiated N2a cells after being exposed to both OPs, MTT reduction assays were performed as described in section 2.2.7. The results demonstrated in figure 3.1 show no effect on the reduction of MTT by pre-differentiated N2a cells when compared to its corresponding control after 2, 4, and 8 h exposure to 3 µM CPF or CPO.

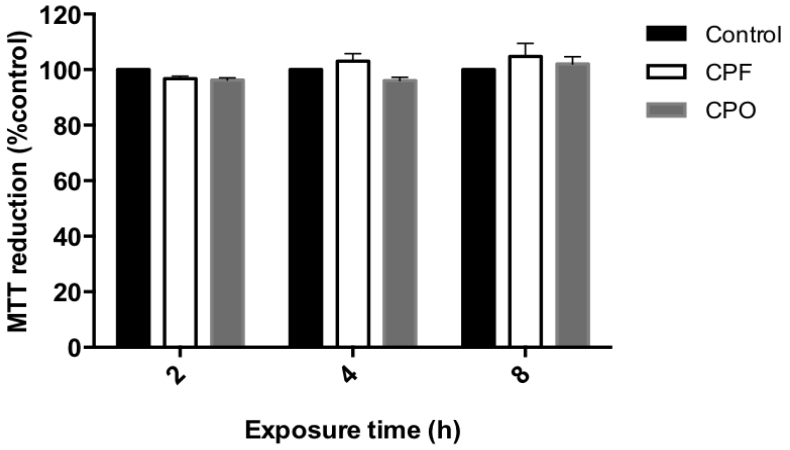

Figure 3.1. Effects of 3 µM concentration of CPF and CPO on pre-differentiated N2a cell viability. After 20 h of differentiation, N2a cells were treated without (0.5% v/v DMSO control) or with 3 µM CPF or CPO for 2, 4 and 8 h and the levels of MTT reduction were measured to evaluate cell viability. Results are expressed as a mean percentage of the corresponding untreated control at each time point ± SEM from four separate experiments. Statistical significance of data was analysed using one way ANOVA. When SEM bar is not apparent, this means that error is smaller than the symbol size.

3.2.2 The optimal concentration of CFSE fluorescent dye

N2a cell differentiation was assessed in cells stained with CFSE fluorescent dye. Since high concentrations of CFSE can be toxic to cells and lead to impairment in cell division, the appropriate concentration of the dye to be used was determined based on its effects on MTT reduction. Various concentrations of CFSE ranging between 10 nM and 100 µM were tested for their ability to inhibit the MTT reduction assay (explained in section 2.2.8.2).

In figure 3.2, it can be seen that there was no significant decrease in MTT reduction in pre-differentiated N2a cells incubated with 10 nM to 100 µM CFSE compared to control (no CFSE). On the basis of this result, 10 µM CFSE was considered to be non-cytotoxic towards N2a cells and was chosen to be the optimal concentration for staining the pre-differentiated N2a cells in this study.

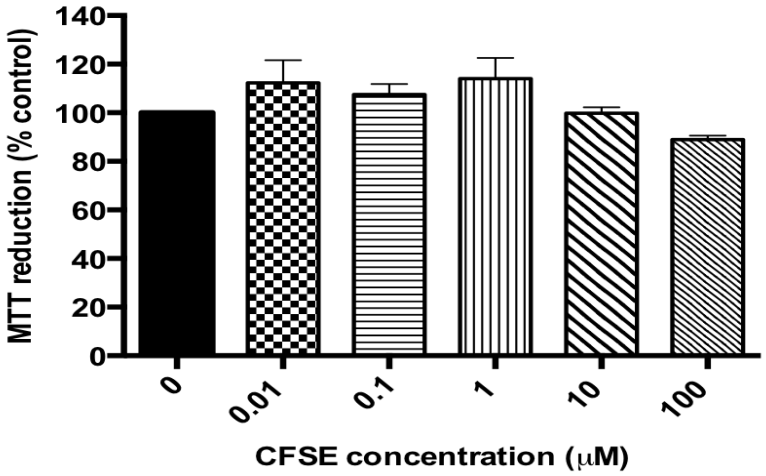

Figure 3.2. Effects of CFSE on MTT reduction in pre-differentiated N2a cells. After 20 h of induction cell differentiation, N2a cells were labelled with different concentration of CFSE and the levels of MTT reduction were measured to evaluate cell viability. Results are expressed as a mean percentage of the corresponding untreated control ± SEM from four separate experiments. Statistical significance of data was analysed using one way ANOVA. When SEM bar is not apparent, this means that error is smaller than the symbol size.

3.2.3 Effects of CPF and CPO on cell morphology and neurite outgrowth in pre-differentiated N2a cells

The previous work by Sachana et al (2001) showed that CPF at a sub-cytotoxic concentration of 3 µM had the ability to induce retraction of approximately 50% of axon-like processes formed by differentiated N2a cells following 8 h of exposure, as determined by CBB staining (Sachana et al., 2001). However, the effects of CPO on the morphology of pre-differentiated N2a cells and neurite outgrowth had not been previously tested. In order to achieve comparable results to the previous work with CPF, pre-differentiated live N2a cells were stained directly with 10 µM CFSE dye, exposed to OPs for 2, 4 and 8 h, then fixed. The cells were then viewed by using an Olympus DP71 epifluorescence microscope (see section 2.2.8.3). At each time point, fluorescence images of non OP-treated controls and treated cells were taken (Figure 3.3), and the total number of axon-like neurites was recorded (Figure 3.4).

The fluorescence images in figure 3.3 show that pre-differentiated N2a cells in the absence of both OP had typical neuronal cell morphology of round cell bodies with long extending axons-like processes. After exposure to 3 µM CPF and CPO, a retraction of long axons was apparent compared to control cells. However, this alteration in neurite outgrowth was more pronounced in CPO-treated cells compared to CPF and control at each time point. As the exposure time to both OPs increased, the reduction in neurite outgrowth also increased compared to the non-treated controls at each time point.

These findings were further confirmed by quantitative analysis of the effects of both OPs on neurite outgrowth formed by pre-differentiated N2a cells (Figure 3.4), which indicated a time-dependent reduction in the outgrowth of axon-like processes following exposure to 3 µM CPF or CPO compared to the non OP-treated controls. Both CPF and CPO at a concentration of 3 µM were able to induce a significant reduction in the number of axons per 100 cells compared to their corresponding controls at each time point in pre-differentiated N2a cells ($p < 0.0001$). Additionally, a significant difference on the inhibition of axon

outgrowth was also observed when the CPF treatment was compared to CPO at each time point ($p = 0.005$) (Figure 3.4).

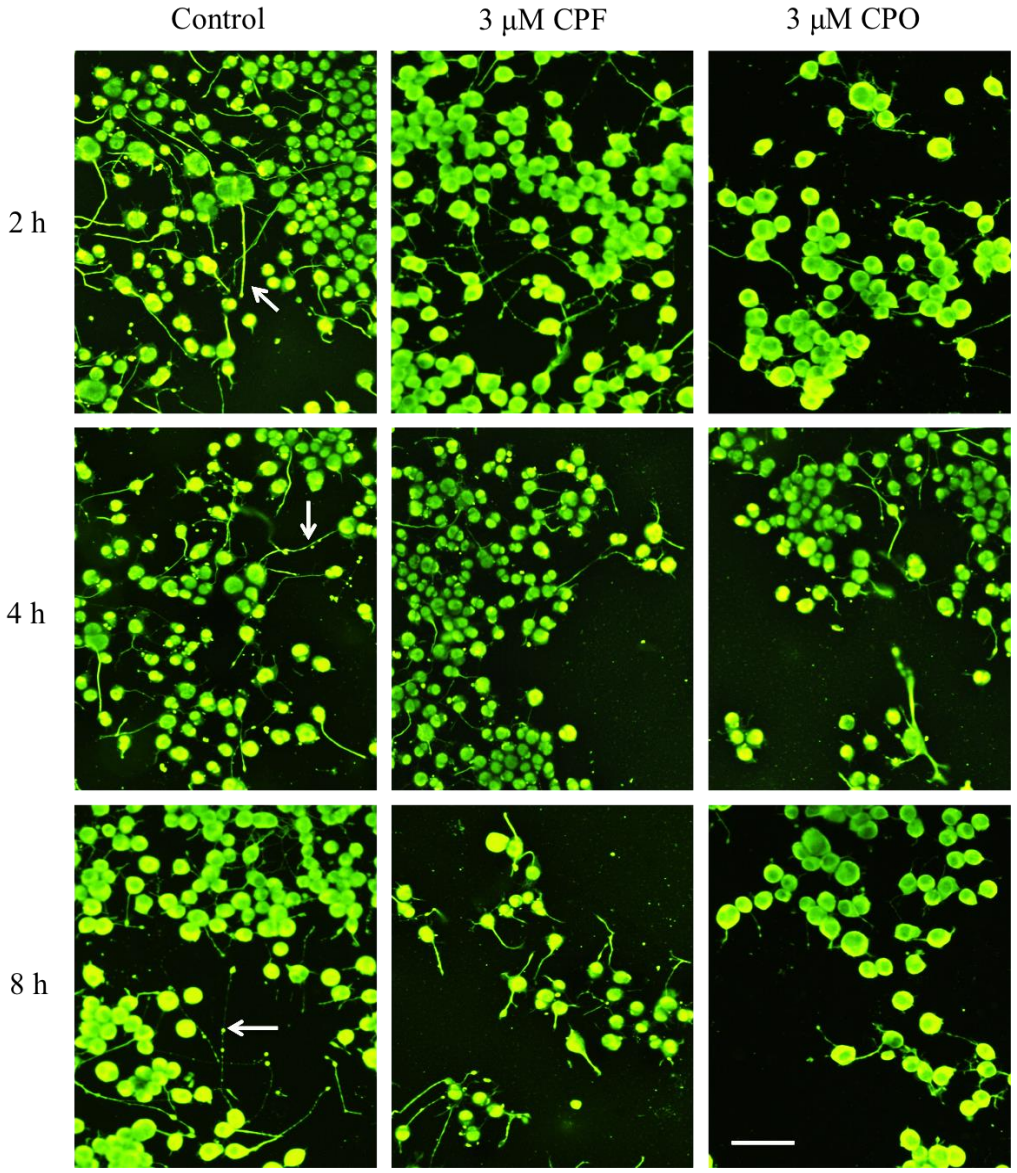

Figure 3.3. Effects of 3 µM concentration of CPF and CPO on the morphology of pre-differentiated N2a cells. Displayed are representative fluorescence images of N2a cells induced to differentiate for 20 h prior to being incubated in the absence (Control) or presence of 3 µM CPF or 3 µM CPO for 2, 4 and 8 h. Cells were stained with CFSE and fixed. Arrows show typical axon-like processes detected in non-OP treated controls. Scale bar represents 50 µm. .

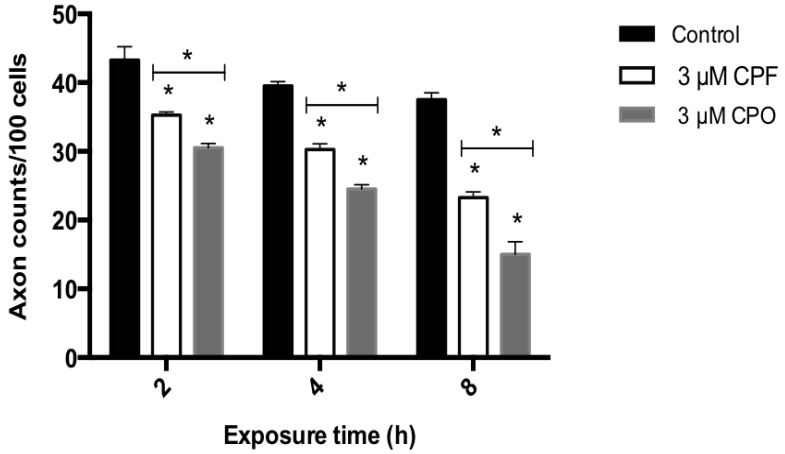

Figure 3.4. Quantitative analysis of the effects of CPF and CPO on neurite outgrowth. N2a cells were induced to differentiate for 20 h, labelled with CFSE then incubated with or without 3 µM CPF or CPO for 2, 4, and 8 h. Data are expressed as mean number of axon-like processes per 100 cells ± SEM for four independent experiments. Asterisks indicate where OP treated cell values were significantly different from the corresponding control ($p < 0.0001$). Bars with asterisks indicate significant differences between CPF and CPO treatments at each time point ($p = 0.005$).

3.2.4 The real time effects of CPF and CPO on axon stability in pre-differentiated N2a cells

In order to determine the time scale of the morphological changes reported in the previous section, the real time changes induced by CPF and CPO on axon outgrowth in pre-differentiated N2a cells were further studied using a live cell imaging approach, as described in section 2.2.14. The first images of control and OP-treated cell panel were taken at minute 20, whereas subsequent images were recorded at 1 h intervals for a period of 8 h from the point of toxin addition. Neurites were labelled by arrows and numbers to track the changes over time. Time-lapse videos of control and OP-treated cells were also prepared from a sequence of images at 30 min time intervals and are provided on a CD accompanying this thesis.

As indicated in figure 3.5, there was no observed retraction of neurites in non OP-treated controls. Following exposure to 3 µM CPF or CPO, neurite length was shown to be highly affected over time compared to non OP-treated controls (Figure 3.6 and 3.7). Approximately 25% of neurites retracted within the first 2 to 4 h after treatment with both OPs, suggesting that some of these changes were occurring at a very early stage. At 8 h treatment with CPO, the images showed some cell vesiculation. However, no other alterations in cell morphology were detected, such as changes in cell body shape or size in both controls and treated cells (Figure 3.5 and 3.7).

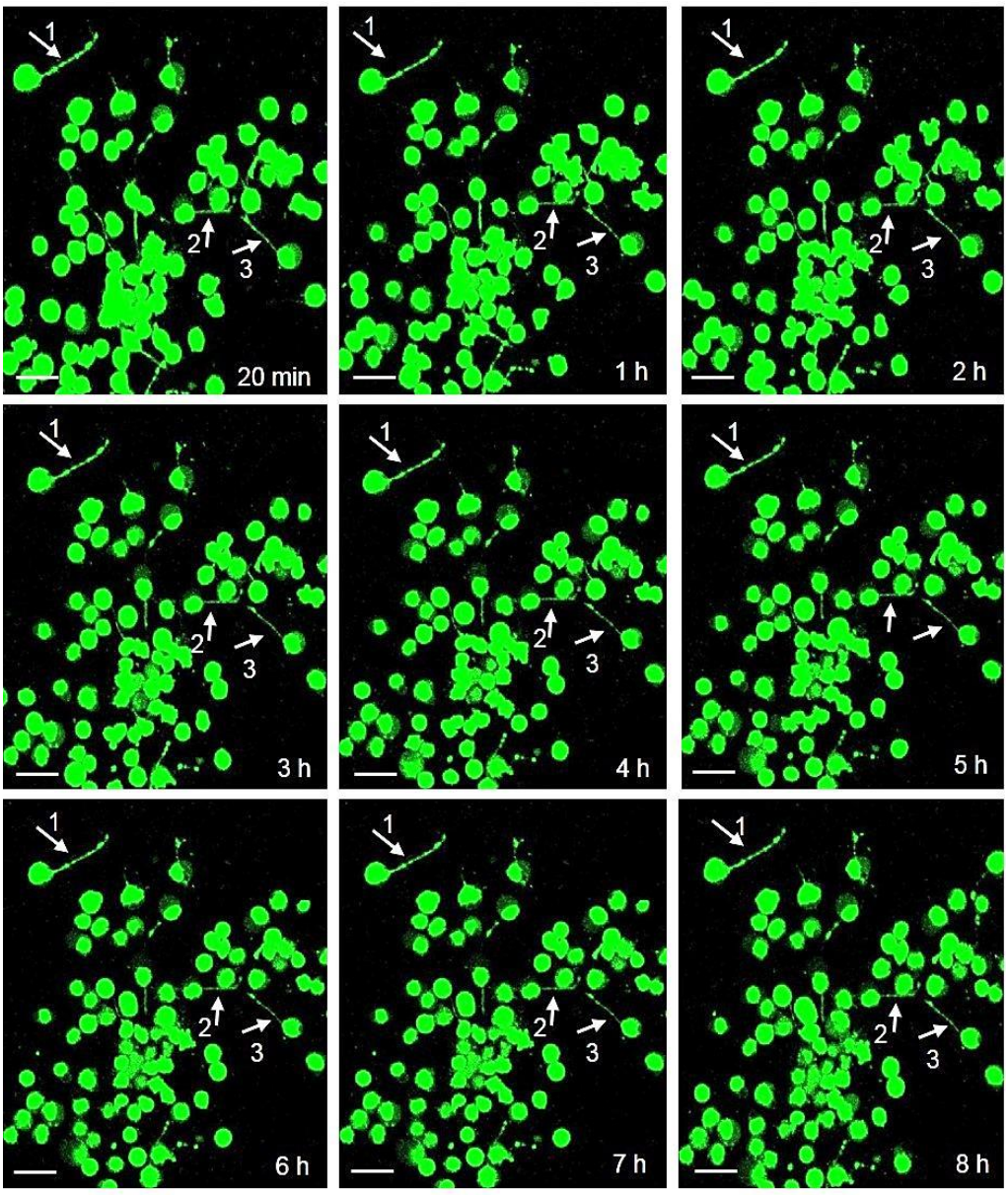

Figure 3.5. The real time measurements of neurites in pre-differentiated N2a cells determined by live cell imaging. N2a cells were induced to differentiate for 20 h, stained with CFSE then incubated for further 8 h in the absence of OP to monitor the real time changes in cell morphology. Shown are digital images of a representative field of view for the non OP-treated control. The first image was taken at minute 20. Subsequent images were taken 1 h intervals, using a Leica TCS SP5 confocal laser scanning microscope with epifluorescence optics. Arrows-labelled 1-3 show typical neurites in pre-differentiated N2a cells (untreated control). Scale bar represents 50 µm.

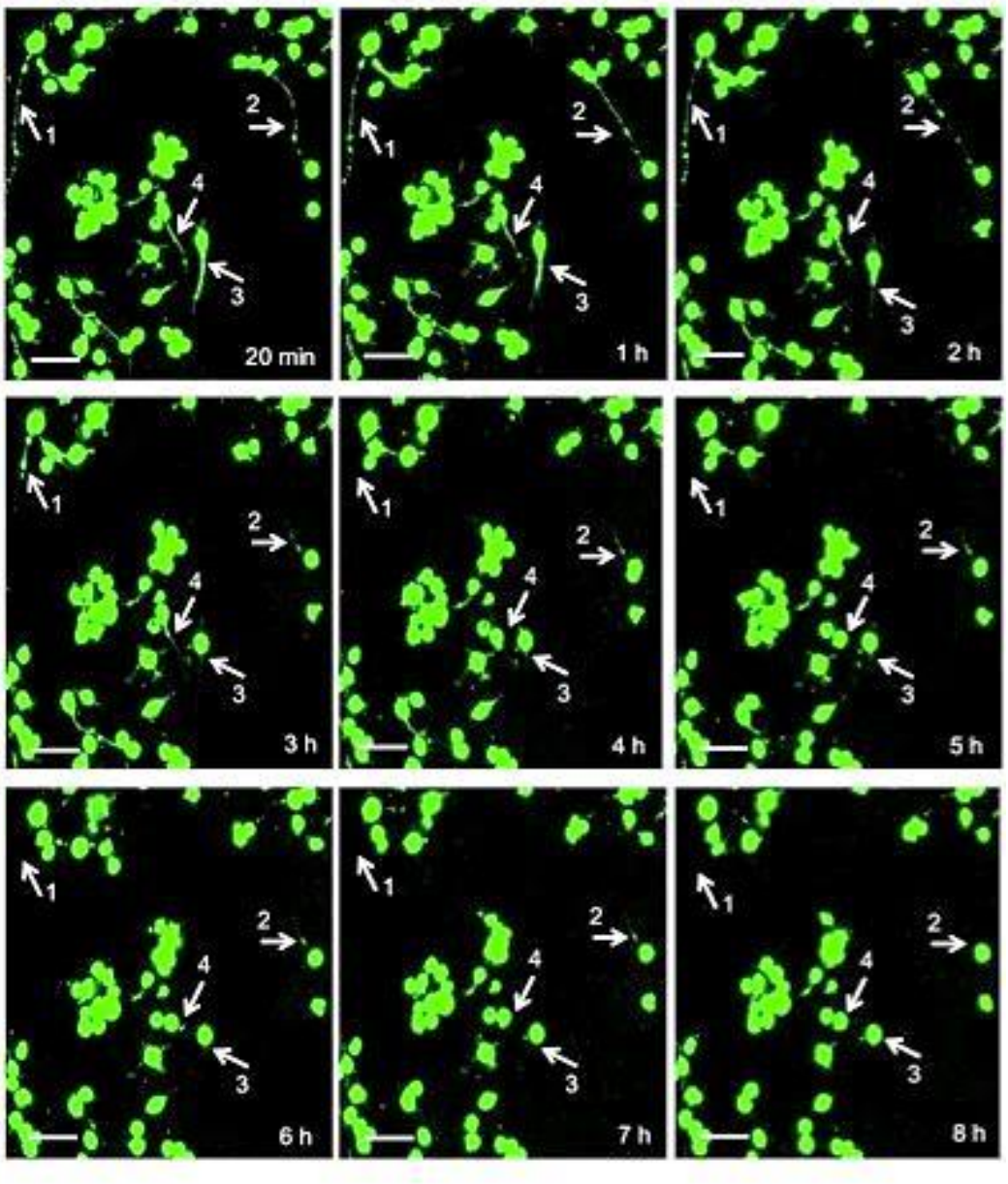

Figure 3.6. The real time effects of CPF on pre-differentiated N2a cells determined by live cell imaging. N2a cells were induced to differentiate for 20 h, stained with CFSE then incubated for further 8 h in the presence of 3 µM CPF. The real time changes in cell morphology following OP exposure were recorded for a period of 8 h. Shown are digital images of a representative field of CPF treated cells. The first image was taken at minute 20. Subsequent images were taken 1 h intervals, using a Leica TCS SP5 confocal laser scanning microscope with epifluorescence optics. Arrows labelled 1-4 show retracting neurites detected in pre-differentiated N2a cells treated with CPF for 8 h. Scale bar represents 50 µm.

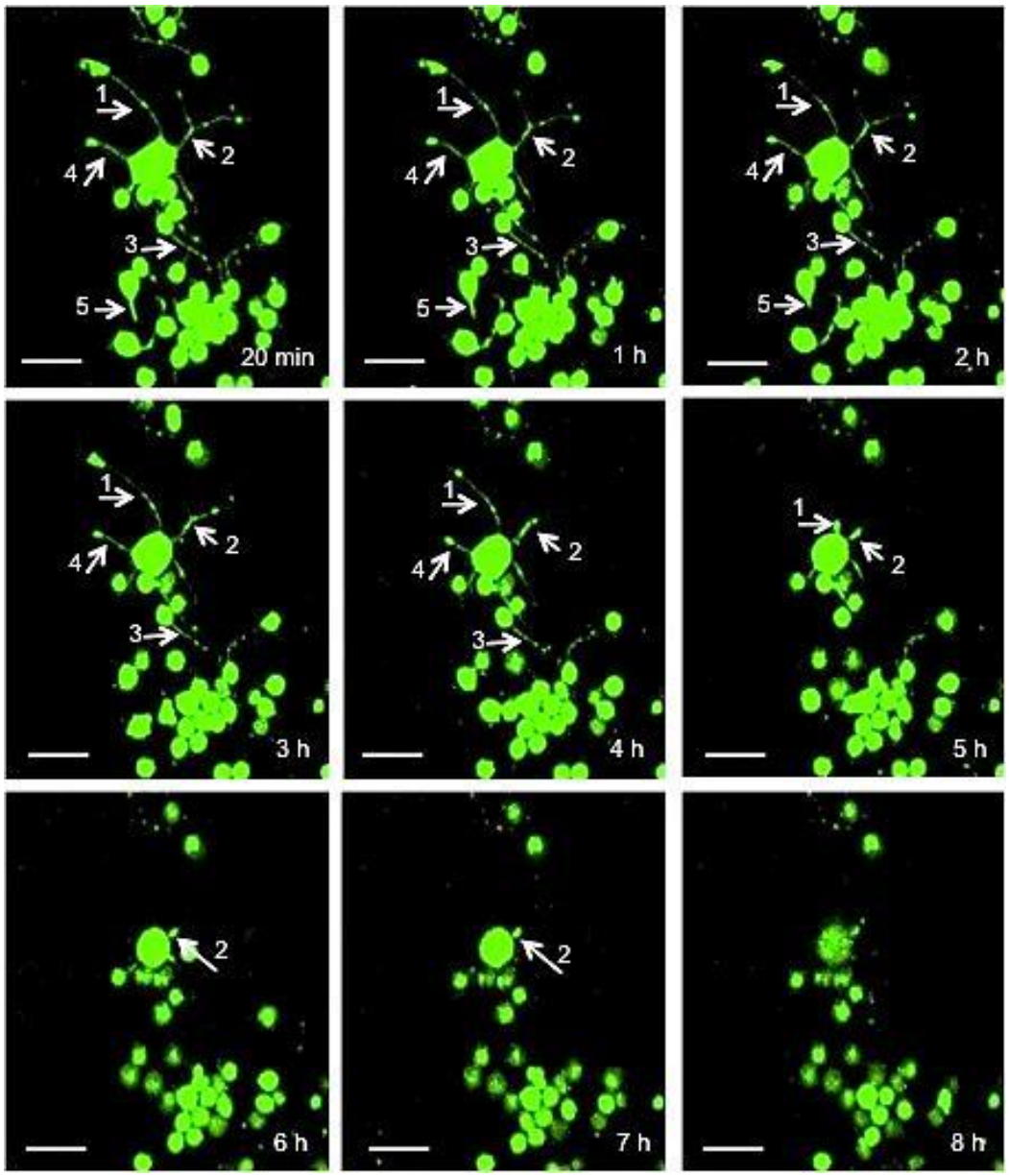

Figure 3.7. The real time effects of CPO on pre-differentiated N2a cells determined by live cell imaging. N2a cells were induced to differentiate for 20 h, stained with CFSE then incubated for further 8 h in the presence of 3 µM CPO. The real time changes in cell morphology following OP exposure were recorded for a period of 8 h. Shown are digital images of a representative field of CPO treated cells. The first image was taken at minute 20. Subsequent images were taken 1 h intervals, using a Leica TCS SP5 confocal laser scanning microscope with epifluorescence optics. Arrows labelled 1-5 show retracting neurites detected in pre-differentiated N2a cells treated with CPO for 8 h. Scale bar represents 50 µm.

3.2.5 Effects of CPF and CPO exposure on AChE activity of pre-differentiated N2a cells

To determine whether the observed morphological changes in the outgrowth of neurites in pre-differentiated N2a cells could be related to the effect on the acute toxicity target (AChE), the impact of 3 µM CPF and CPO on the activity of AChE was assessed in parallel, as explained in section 2.2.9.

After 2, 4, and 8 h exposure of pre-differentiated N2a cells to CPO, a sustained significant reduction (> 70%) in the specific activity of AChE was observed compared to the non OP-treated control ($p < 0.0001$) (Figure 3.8). However, CPF-treated cells showed little or no effect on AChE activity compared to the untreated control at all exposure time points.

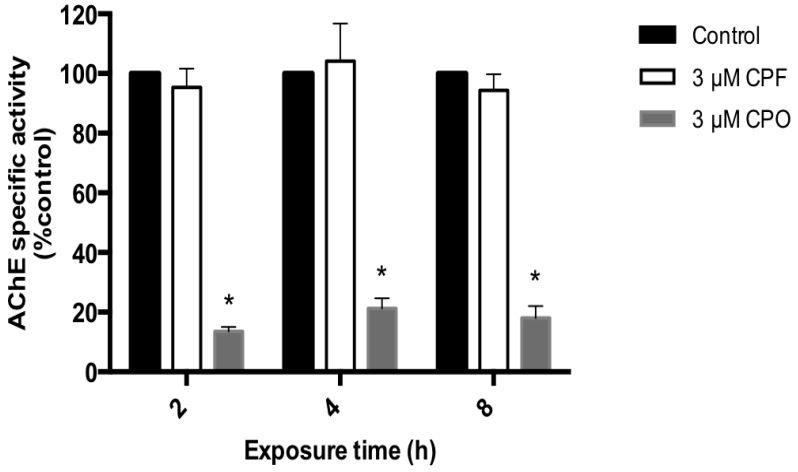

Figure 3.8. Effects of 3 µM CPF and CPO on AChE activity in pre-differentiated N2a cells. Mouse N2a cells were induced to differentiate for 20 h before being incubated with or without 3 µM CPF and CPO for 2, 4, and 8 h, after which the activity of AChE was measured. Enzyme specific activity (Absorbance change/min/mg protein) is expressed as a percentage of the corresponding control value ± SEM from four independent experiments. Asterisks indicate statistically significant changes compared to the non OP-treated control values at each time point ($p < 0.0001$).

3.3 Discussion

The non-cytotoxic effect observed towards pre-differentiated N2a cells incubated with 10 µM CFSE suggested that this concentration is optimal for cell staining in this study. The data presented on neurite outgrowth in CFSE-labelled cells demonstrated that both CPF and CPO caused neurite retraction when pre-differentiated N2a cells were exposed for 2, 4, and 8 h. Although inhibition of neurite outgrowth from N2a cells has been previously investigated following CPF exposure (Sachana et al., 2001), and other OPs such as leptophos, phenyl saligenin phosphate (PSP), diazinon and CPO (Sachana et al., 2003, Hargreaves et al., 2006, Harris et al., 2009b, Flaskos et al., 2011) using CBB staining, this is the first time that CFSE was used to measure the development and maintenance of neurites by N2a cells. The current data showed that CFSE provided comparable results to CBB, which has been widely used to study the effects of OPs on neurite outgrowth previously. In addition, CFSE is highly specific, stable and more sensitive than CBB. Another major advantage of CFSE, is that it can be used as a useful marker for visual identification of both fixed and living cells (Garton and Schoenwolf, 1996). Therefore, CFSE labelling provides a novel and reliable approach to assess cell differentiation and neurite outgrowth as an alternative to CBB.

The observed retraction of neurites induced by CPF in cultured N2a cells under post-differentiation conditions is in good agreement with that noted in the same culture system using a similar concentration of CPF under both post and co-differentiation conditions (Sachana et al., 2001). In addition, the current study revealed for the first time the potential ability of CPO to induce neurite retraction in pre-differentiated N2a cells, an effect which appears to be even stronger than that of CPF. The fact that CPO was found to be more potent in reducing the length of axon-like neurites compared to its parent compound in the current work is in agreement with a number of previous studies. In pre-differentiated rat PC12 pheochromocytoma cells, CPO at a concentration of 1 nM was 1000-times more potent in reducing the neurite outgrowth than 1 µM CPF following 24 h exposure (Das and Barone, 1999). Under co-differentiation conditions, CPO at the much lower concentration of 0.001 nM also showed greater ability than CPF

(0.001 µM) to reduce axonal length in primary cultures of sympathetic and sensory neurons derived from embryonic rat after 24 h (Howard et al., 2005, Yang et al., 2008).

The inability of either compound to affect MTT reduction after 2, 4 and 8 h of exposure suggested that the 3 µM concentration used in this study was sub-cytotoxic towards pre-differentiated N2a cells. Hence, it is likely that alterations in neurite outgrowth were not due to cell death, but were a genuine cellular response to OP exposure. This finding is consistent with previous studies, which employed similar concentrations of CPF and other OPs such as diazinon and diazinon oxon and found no significant effects on the viability of differentiating N2a cells when exposed for periods of up to 24 h (Sachana et al., 2003, Sachana et al., 2005, Flaskos et al., 2007, Sidiropoulou et al., 2009a).

The rapid collapse of neurites observed using live cell imaging further confirms the neurite inhibitory effect of CPF and CPO towards pre-differentiated N2a cells. All neurites, irrespective of initial size, exhibited reduced lengths within 2 h of exposure to both compounds. However, cell body shape and size were found to be relatively unaffected following OP exposure for the same time periods. This finding suggests that the retraction of pre-formed axons in N2a cells, which is initiated at an early time point following exposure to 3 µM CPF and CPO, is the first visible sign of the effects of both compounds on neurite outgrowth.

The significant reduction in the specific activity of AChE observed at all time-points following CPO exposure is in line with a previous study by Flaskos et al. (2011). They demonstrated sustained inhibition of AChE in N2a cells after CPO exposure from the point of induction of cell differentiation for 4 or 24 h (Flaskos et al., 2011). A reduced activity of AChE was also noted in N2a cells exposed for 4 h from the point of induction of differentiation to the OP diazinon oxon, although in that case no significant effect on enzyme activity was observed after 24 h (Sidiropoulou et al., 2009a). However, it is unlikely that inhibition of AChE alone could account for the observed changes in the outgrowth of neurites in N2a cells, as CPF (as would be expected) had little effect on AChE in the current work. A number of *in vivo* (Slotkin et al., 2006) and *in vitro* (Das and Barone,

1999, Fowler et al., 2001, Howard et al., 2005) studies suggest that OPs that are weak inhibitors of AChE can also induce marked impairment in the development of neurites. In this respect, the OP trio-ortho-cresyl phosphate significantly inhibited the development of axon-like processes in N2a cells (Fowler et al., 2001). However, it is only a weak inhibitor of AChE (Lock and Johnson, 1990). Therefore, inhibition of AChE enzymatic activity by CPF or CPO is unlikely to be the main cause of retraction of axon-like neurites in pre- differentiated N2a cells, although neurite outgrowth data in the current study are consistent with the possibility that it may contribute to the severity of the effects.

As previously discussed, the post differentiation conditions may reflect a model of developmental toxicity. The concentration of 3 µM CPF and CPO was chosen due to its proven ability to induce a reduction by 50% in both neurite outgrowth and in the number of pre-formed neurites in differentiating N2a cells without affecting cell viability. CPO-induced morphological and biochemical impacts were also observed *in vivo* in the developing organism following administration of similar OP concentrations to those employed in this study. Using meconium analysis (used to estimate the foetal exposure to environmental toxicants), about 22.8 µM CPF has been detected in meconium samples of new-born children (Ostrea et al., 2002) and low micromolar levels of oxon metabolites are attainable in the developing human foetus (Flaskos, 2012). Therefore, the applied OP concentration in this study has clinical relevance to human developmental neurotoxicity.

With regard to the possible transfer of the oxon form from the maternal tissue to the foetus, oxon metabolites have higher water solubility compared to their respective parent compounds (Sogorb and Vilanova, 2010). This would affect their ability to enter the foetus via the lipid membranes of the placenta. The detection of significant cholinesterase inhibition in the mammalian foetus following *in vivo* exposure of pregnant animals to organophosphorothionate pesticides suggests that foetal exposure to CPO can occur (Gupta, 1995). The foetus is thought to be primarily exposed to the parent compound, but may also encounter oxon metabolite in the maternal tissues. The relatively low expression of CYP2B6 (a key enzyme in the process of oxon formation in humans) in

human placenta suggest that the placenta does not make a major contribution to oxon formation (Pelkonen et al., 2006, Foxenberg et al., 2007, Croom et al., 2010). Although CYP2B6 is present at low levels in the human foetus compared to later stages of development (Croom et al., 2010), paraoxonase 1 (PON 1), which is responsible for hydrolysing and detoxifying the oxon forms of certain OPs such as CPO, is also relatively low at this stage (Costa, 2006). This could allow some oxon formation and/or accumulation in foetal tissue. Additionally, reduced levels of serum PON1 due to genetic polymorphisms in the *PON1* gene is found to be associated with increased susceptibility to the toxic effect of the oxon metabolite (Costa, 2006).

The observed dying back of axons in this pre-differentiated N2a cell model could also reflect what it might occur following OP toxicity in adults. It is highly likely that such a concentration of CPO (3 µM), which caused severe inhibition in AChE levels to more than 70% would be lethal to the foetus (Heilmair et al., 2008). However, there are numerous case studies of patients who have survived such levels of cholinesterase inhibition with the help of pharmacological intervention, such as adrenaline and/or oxime administration, only to develop delayed neuropathy. For example, a 19 year old male who ingested a large dose of CPF and was hospitalised suffering from cholinergic crisis. After he was treated with atropine and pralidoxime, the patient recovered partially from neurological symptoms (Nand et al., 2007). Administration of this combined treatment has an important role in reversing the respiratory muscles weakness or paralysis, and other parasympathetic effects associated with OP poisoning (Tush and Anstead, 1997). However, after 24 h of CPF exposure, he developed respiratory paralysis and required mechanical ventilation for 16 days. Weeks later, he had progressive signs of OPIDN, such as deficits in the lower limbs and muscular atrophy (Nand et al., 2007). Thus, survivors of acute cholinergic crisis can be affected by a delayed neuropathy involving dying back of axons in peripheral/central neurons (Clegg and van Gemert, 1999a, Nand et al., 2007, Thivakaran et al., 2012). Indeed, it has been shown that CPF administered at acute levels in animal models can lead to OPIDN (Gupta, 2006). Therefore the morphological changes in neurite outgrowth following CPO exposure have potential clinical relevance in terms of delayed neuropathy.

From the results presented in this chapter, it can be concluded that exposing pre-differentiated N2a cells to a sub-cytotoxic concentration of CPF and CPO causes neurite retraction. The findings also demonstrate that CPO exerts more potent effects compared to those of CPF on neurite outgrowth and AChE. However, the morphological effects on axon-like neurites are not completely dependent on the inhibition of AChE. They could be associated with other non-cholinergic targets, which will be investigated in depth at the molecular level in the next chapter.

4 Effects of chlorpyrifos and chlorpyrifos oxon on cytoskeletal and associated regulatory proteins in pre-differentiated N2a cells

4.1 Introduction

The previous chapter demonstrated that sub-cytotoxic concentration of 3 µM CPF and CPO had the capacity to induce the retraction of axon-like neurites in pre-differentiated N2a cells. Since the observed morphological alterations in neurite outgrowth were not directly related to the inhibition of the enzymatic activity of AChE, it was of interest to investigate whether the retraction of axon-like processes was associated with altered expression and activities of cytoskeletal and associated regulatory proteins in pre-differentiated N2a cells.

The neuronal cytoskeleton, and in particular the microtubule and neurofilament networks play an important role in neurite development and stability (Cambray-Deakin, 1991b). Impairment of neurite outgrowth following exposure to OPs has been linked with disruption of the expression levels of cytoskeletal proteins (Fowler et al., 1997, Flaskos et al., 1998, Sachana et al., 2001, Sachana et al., 2003, Sachana et al., 2005, Hargreaves et al., 2006, Flaskos et al., 2007, Flaskos et al., 2011, Sachana et al., 2014). Earlier reports evaluated the effects of CPF on a number of cytoskeletal and associated regulatory proteins in N2a cells under different differentiation and exposure conditions (Sachana et al., 2001, Sachana et al., 2005). N2a cells treated with CPF showed increased levels of HSP-70 under co-differentiation exposure conditions, whereas no observed effects were found on HSP-70 levels in pre-differentiated cells (Sachana et al., 2001). Additionally, Sachana and colleagues (2005) showed reduced levels of GAP-43 in pre-differentiated N2a cells treated with CPF. However, when N2a cells were exposed to CPF at the point of induction of cell differentiation, it had no impact on GAP-43 expression (Sachana et al., 2005). The findings of these studies suggest that the effects of CPF on these proteins depend to some extent on the differentiation stage of the cells.

With regard to CPO, Flaskos and colleagues (2011) investigated the CPO-related effects on cytoskeletal proteins in N2a cells using co-differentiation experimental protocols. Data obtained from that work showed reduced levels of GAP-43 and NFH in differentiating N2a cells following CPO exposure for 24 h (Flaskos et al., 2011). The effects of CPO on cytoskeletal proteins in pre-differentiated N2a cells have not been determined in post-differentiation experiments, and there is a lack of quantitative data in the case of CPF.

The aim of this chapter was to assess the impacts of sub-cytotoxic concentrations of both CPF and CPO on cytoskeletal and associated regulatory proteins in pre-differentiated N2a cells following 2, 4 and 8 h exposure. The study focused on the effects of both OPs on the levels of specific microtubule, neurofilament and heat shock proteins, which were determined using quantitative Western blotting. Subsequently, alterations in the activation status of MAP kinase ERK 1/2 and the enzymatic activity of phosphatase were investigated to relate them to any changes observed in NFH phosphorylation. Additionally, disruption of the intracellular distribution of microtubule and neurofilament networks was analysed using indirect immunofluorescence staining. This work was done in order to relate the alterations in neurite outgrowth observed in the chapter three to the levels of expression and activities of cytoskeletal and associated regulatory proteins in pre-differentiated N2a cells.

4.2 Results

4.2.1 Effects of CPF and CPO on the expression levels of microtubule proteins

The molecular changes underlying the morphological effects of 3 µM CPF and CPO on neurite outgrowth in pre-differentiated N2a cells were studied further by quantitative Western blotting. For immunoblotting, Western blots of lysates of pre-differentiated N2a cells exposed to 3 µM CPF or CPO for 2, 4, and 8 h were probed with antibodies against a range of microtubule proteins. These included antibodies to MAP-1B, MAP-2, acetylated and tyrosinated α-tubulin, polyglutamylated tubulin and βIII tubulin, as described in section 2.2.12 and table 2.12.

As indicated in figure 4.1 and table 4.1, the reactivity of anti-α-tubulin showed no significant changes following exposure of cells to both CPF and CPO at any time point. Therefore, the band densities for all proteins were normalised to that for α-tubulin (using monoclonal antibody clone B512), which was used as internal control. Similarly, there were no significant effects on the cross reactivity of lysates of pre-differentiated N2a cells with antibodies that recognise MAP-1B, MAP-2, acetylated, tyrosinated and polyglutamylated forms of α-tubulin and βIII-tubulin following exposure to both CPF and CPO at all time-points compared to control.

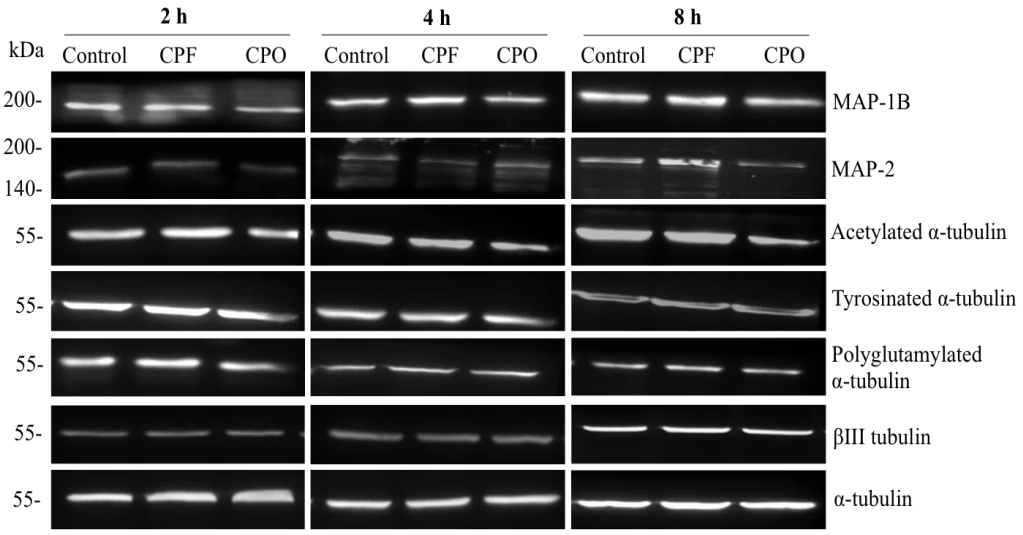

Figure 4.1. Detection of microtubule proteins on Western blots of pre-differentiated N2a cell lysates. N2a cells were induced to differentiate for 20 h prior to treatment with 3 µM CPF or 3 µM CPO, or without OP (Control) for 2, 4, and 8 h. The N2a cell lysates were then subjected to SDS-PAGE and Western blotting as described in Materials and methods. Shown are typical blots probed with antibodies against MAP-1B, MAP-2, βIII-tubulin, acetylated, tyrosinated and polyglutamylated α-tubulin, followed by HRP-conjugated secondary antibodies and developed by ECL reagents. Blots probed with anti-α-tubulin were used as internal control.

Table 4.1. Densitometric analysis of Western blots probed with antibodies to microtubule proteins. Western blots probed with antibodies that recognise MAP-1B, MAP-2, βIII-tubulin, acetylated, tyrosinated and polyglutamylated α-tubulin. The antibody reactivity was then visualized with ECL reagents as described in Materials and methods. Densitometric peak areas were quantified using AIDA software and values are expressed as a percentage of the corresponding time point control ± SEM for four separate experiments. Band densities for all proteins were normalised to blots probed with anti-α-tubulin. Asterisks indicate significant differences compared to the corresponding untreated control.

Antigens	**Incubation time (h)**	**Densitometric peak area (% control ± SEM)**	
		3 µM CPF	**3 µM CPO**
MAP-1B	2	98 ± 4	96±8
	4	106 ± 8	112±13
	8	85 ± 10	89±11
MAP-2	2	101±5	98±5
	4	100±4	105±5
	8	111±13	89±15
Acetylated tubulin	2	102±2	103±4
	4	103±4	123±19
	8	125±11	102±13
Tyrosinated tubulin	2	103±4	102±2
	4	102±1	105±7
	8	112±5	110±10
Polyglutamylated tubulin	2	94±6	95±5
	4	102±7	89±11
	8	88±18	87±16
βIII tubulin	2	107±12	96±5
	4	99±5	104±11
	8	99±6	94±10
Total α-tubulin	2	107±8	96±7
	4	102±4	109±7
	8	103±6	106±7

4.2.2 Effects of CPF and CPO on the expression levels of neurofilament and growth-associated proteins

As indicated in figure 4.2 and table 4.2, a transient significant reduction was observed in the levels of antibody reactivity with GAP-43 on blots of lysates (using monoclonal antibody clone GAP7B10) after 4 h exposure of cells to CPF ($p < 0.004$), and CPO ($p < 0.002$). However, GAP-43 reactivity was unaffected following exposure to both OPs at the earlier time point (2 h) and seemed to recover following 8 h exposure. Reactivity of cell lysates with anti-total NFH antibody (clone N52) was similar to the corresponding control at all time-points. In contrast, reactivity with anti-pNFH (clone Ta51) was considerably higher than the reactivity level of lysates from non OP-treated controls following 2 h exposure to both CPF ($p < 0.02$), and CPO ($p < 0.0006$). This increase in the levels of pNFH at 2 h was then followed by a significant decline in comparison to control values after 8 h exposure to both CPF ($p < 0.004$) and CPO ($p < 0.0002$).

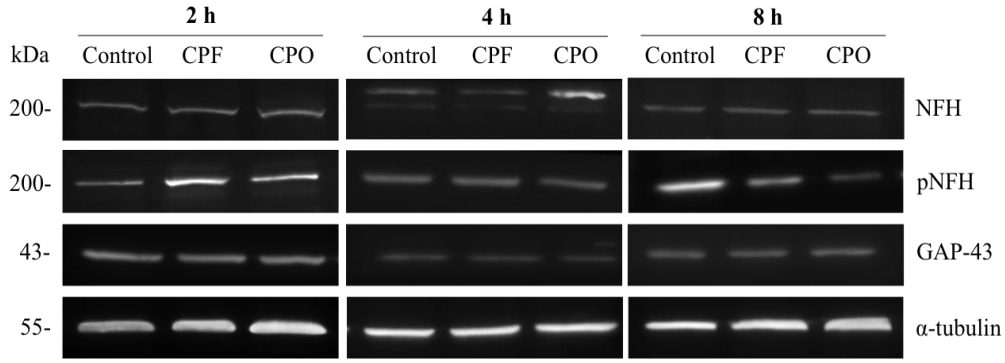

Figure 4.2. Detection of neurofilaments and growth associated proteins on Western blots of pre-differentiated N2a cell lysates. N2a cells were induced to differentiate for 20 h before treatment with or without 3 µM CPF or CPO for 2, 4, and 8 h. N2a cell lysates were then subjected to SDS-PAGE and Western blotting as described in Materials and methods. Shown are typical blots probed with antibodies to NFH, pNFH and GAP-43 followed by HRP-conjugated secondary antibodies and developed by ECL reagents. Blots probed with anti-α-tubulin were used as internal control.

Table 4.2. Densitometric analysis of Western blots probed with antibodies to neurofilaments and growth associated proteins. Western blots of cell lysates were probed with antibodies that recognise NFH, pNFH and GAP-43, followed by visualisation of antibody reactivity with ECL reagents as described in Materials and methods. Densitometric peak areas were quantified using AIDA software and values are expressed as a percentage of the corresponding time point control ± SEM for four separate experiments. Band densities for all proteins were normalised to blots probed with anti-α-tubulin. Asterisks indicate values that were statistically significant from their corresponding non OP-treated control; *$p < 0.02$, **$p < 0.004$, ***$p < 0.002$, ▲$p < 0.0002$, ■$p < 0.0006$.

Antigens	Incubation time (h)	Densitometric peak area (% control ± SEM)	
		3µM CPF	3µM CPO
NFH	2	107 ± 9	101 ± 8
	4	102 ± 18	81 ± 22
	8	120 ± 12	105 ± 16
pNFH	2	214 ± 16*	444 ± 90■
	4	84 ± 7	93 ± 12
	8	36 ± 13**	30 ± 7▲
GAP-43	2	107 ± 12	96 ± 5
	4	75 ± 10**	60 ± 10***
	8	106 ± 11	117 ± 17

In order to confirm the observed alteration in the phosphorylation status of NFH, the phosphorylation ratio was calculated (pNFH:NFH) at all time-points. As can be seen in table 4.3, there was a significant increase in the phosphorylation ratio following exposure to both CPF and CPO ($p < 0.01$) for 2 h. Although the level returned to normal at the 4 h time point, it showed a significant reduction to 29% and 27% of normal levels with CPF and CPO treatment for 8 h, respectively ($p < 0.001$).

Table 4.3. The phosphorylation ratio of the change in pNFH:NFH following OP exposure over time. Band intensities of pNFH relative to control were calculated as a ratio to that of NFH. A value of 1 represents normal level of phosphorylation of NFH. Asterisks indicate changes that were statistically significant compared to normal levels; *$p < 0.01$, **$p < 0.001$.

Phosphorylation ratio	Incubation time (h)	3µM CPF	3µM CPO
pNFH:NFH	2	2.02 ± 0.23*	4.19 ± 0.80*
	4	1.03 ± 0.21	1.53 ± 0.22
	8	0.29 ± 0.08**	0.27 ± 0.03**

4.2.3 Effects of CPF and CPO on the expression levels of heat shock proteins

In order to determine whether altered levels of HSPs could be indicative of cellular injury induced by OP exposure, the effects of both CPF and CPO on the expression levels of three families of HSPs (HSP-90, HSP-70 and HSP-60) were investigated by quantitative Western blotting, as described in section 2.2.12.

As illustrated in figure 4.3 and table 4.4, the densitometric analysis of probed Western blots of pre-differentiated N2a cell lysates treated with 3 µM CPO for 4 h revealed transient significant reduction in the levels of HSP-90 compared to controls ($p < 0.003$). However, reactivity with HSP-90 antibody was unaffected at the earlier time point (2 h) and seemed to recover following 8 h exposure to CPO.

Although exposure of lysates of pre-differentiated N2a cells treated with CPO for 4 h had reduced levels of the HSP-70 and HSP-60, the effects were not statistically significant at that time point, nor at 2 or 8 h. In CPF-treated cells, no significant change in reactivity levels was detected with all three anti-HSP antibodies at all time-points.

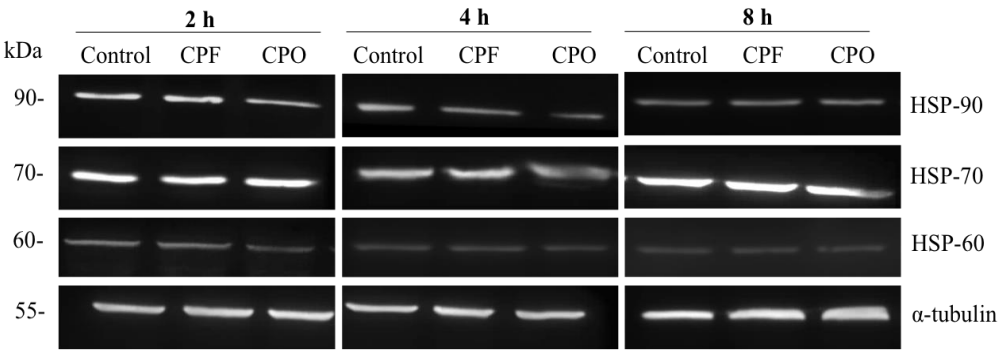

Figure 4.3. Detection of heat shock proteins on Western blots of pre-differentiated N2a cell lysates. N2a cells were induced to differentiate for 20 h before treatment with or without 3 µM CPF or CPO for 2, 4, and 8 h. N2a cell lysates were then subjected to SDS-PAGE and Western blotting as described in Materials and methods. Shown are typical blots probed with monoclonal antibodies to HSP-90 (clone AC16), HSP-70 (clone BRM22) and HSP-60 (clone LK2) followed by HRP-conjugated secondary antibodies and developed by ECL reagents. Blots probed with anti-α-tubulin were used as internal control.

Table 4.4. Densitometric analysis of Western blots probed with antibodies to heat shock proteins. Western blots of cell lysates were probed with antibodies that recognise HSP-90, HSP-70 and HSP-60, after which antibody reactivity was visualised with ECL reagents, as described in Materials and methods. Densitometric peak areas were quantified using AIDA software and values are expressed as a percentage of the corresponding time point control ± SEM for four separate experiments. Band densities for all proteins were normalised to blots probed with anti-α-tubulin. Asterisks indicate values that were statistically significant changes from their corresponding non OP-treated control; *$p < 0.003$.

Antigens	Incubation time (h)	Densitometric peak area (% control ± SEM)	
		3µM CPF	3µM CPO
HSP-90	2	97 ± 4	96 ± 7
	4	101 ± 8	77 ± 3*
	8	97 ± 4	94 ± 2
HSP-70	2	95 ± 6	96 ± 5
	4	92 ± 5	90 ± 11
	8	109 ± 6	106 ± 9
HSP-60	2	102 ± 3	97 ± 3
	4	106 ± 6	89 ± 5
	8	100 ± 12	90 ± 26

4.2.4 Effects of CPF and CPO on activation status of MAP kinase ERK1/2

Further analyses were performed to determine whether the altered levels of reactivity of lysates with antibody to pNFH could be attributed to changes in the activation status of MAP kinase ERK 1/2, which is known to be a convergence point of signalling pathways involved in neurite outgrowth and to play an important role in the phosphorylation of NFH (Veeranna et al., 1998, Perron and Bixby, 1999).

As indicated in figure 4.4 and table 4.5, data from Western blotting analyses using anti-total ERK antibody showed no significant changes in reactivity levels with lysates from pre-differentiated N2a cells treated with either CPF or CPO compared to non OP-treated controls at any time-point. In contrast, anti-pERK antibodies showed increased reactivity compared to the corresponding control at all time-points but the changes were only statistically significant at the early time point (2 h). The data in table 4.6, showed that there was a significant increase in the phosphorylation ratio following exposure to both CPF and CPO ($p < 0.05$) at 2 h exposure.

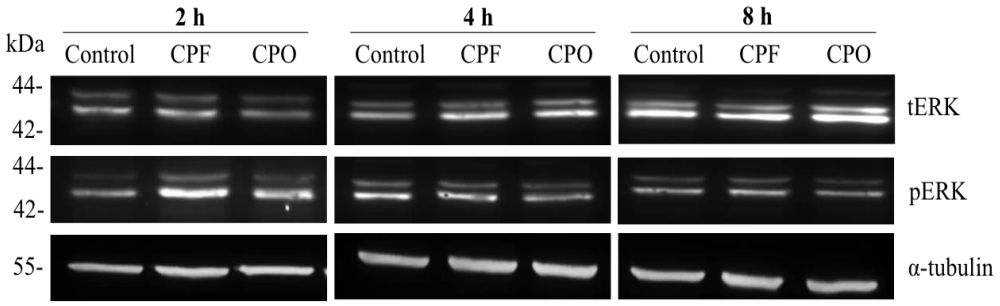

Figure 4.4. Detection of the activation status of MAP kinase ERK 1/2 on Western blots of lysates from pre-differentiated N2a cells. N2a cells were induced to differentiate for 20 h before treatment with or without 3 µM CPF or CPO for 2, 4, and 8 h. N2a cell lysates were then subjected to SDS-PAGE and Western blotting as described in Materials and methods. Shown are typical blots probed with antibodies to total ERK (K-23) and phosphorylated ERK (E-4) followed by HRP-conjugated secondary antibodies and developed by ECL reagents. Blots probed with anti-α-tubulin were used as internal control.

Table 4.5. Densitometric analysis of Western blots probed with antibodies to MAP kinase ERK1/2. Western blots of cell lysates were probed with antibodies that recognise total ERK and phosphorylated ERK, after which antibody reactivity was visualised with ECL reagents, as described in Materials and methods. Densitometric peak areas were quantified using AIDA software and values are expressed as a percentage of the corresponding time point control ± SEM for four separate experiments. Band densities for all proteins were normalised to blots probed with anti-α-tubulin Asterisks indicate values that showed statistically significant differences from their corresponding non OP-treated control; *p < 0.02, **p < 0.001.

Antigens	Incubation time (h)	Densitometric peak area (% control ± S.E.M.)	
		3µM CPF	3µM CPO
Total ERK	2	106 ± 7	95 ± 11
	4	111 ± 14	115 ± 20
	8	107 ± 7	107 ± 8
pERK	2	147 ± 21*	128 ± 6**
	4	149 ± 33	142 ± 34
	8	113 ± 15	91 ± 2

Table 4.6. The phosphorylation ratio of the change in pERK:total ERK following OP exposure over time. Band intensities of pERK relative to control were calculated as a ratio to that of total ERK. A value of 1 represents normal level of phosphorylation of ERK. Asterisks indicate changes that were statistically significant compared to normal levels; *p < 0.05.

Phosphorylation ratio	Incubation time (h)	3µM CPF	3µM CPO
pERK: tERK	2	1.3 ± 0.02*	1.3 ± 0.02*
	4	1.3 ± 0.21	1.2 ± 0.22
	8	1.0 ± 0.08	0.8 ± 0.03

4.2.5 Effects of CPF and CPO on phosphatase activity in pre-differentiated N2a cells

Since there was a clear relationship between the early changes in reactivity of antibodies against pNFH and pERK in OP-treated cell lysates at 2 h, further experiments were carried out to detect the possible cause for the subsequently significant reductions in NFH phosphorylation following 8 h exposure. For this, phosphatase activity was detected using the pNPP liquid substrate system with lysates prepared from cells incubated with or without OPs under the same post differentiation exposure conditions, as described in section 2.2.10.

As demonstrated in figure 4.5, there was an observed increase relative to the controls in the level of phosphatase activity in pre-differentiated N2a cell lysates treated with either CPF or CPO for 2 and 8 h. However, this effect appeared to be statistically significant only at 8 h exposure ($p < 0.002$) when analysed by two-way ANOVA. At 4 h treatment, no noticeable changes in phosphatase activity were detected in OP-treated cells compared to untreated control.

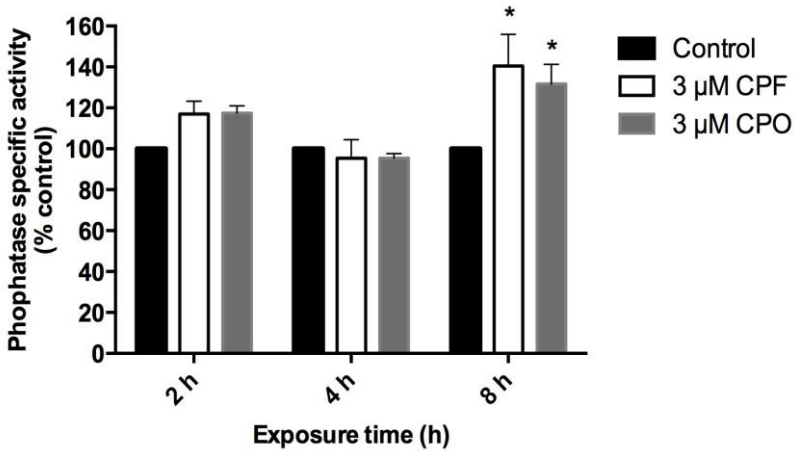

Figure 4.5. Effects of CPF and CPO on phosphatase activity in pre-differentiated N2a cells. Mouse N2a cells were induced to differentiate for 20 h before being incubated with or without 3 µM CPF or CPO for 2, 4, and 8 h, after which the activity of phosphatase was measured as described in Materials and methods. Enzyme specific activity is expressed as percentage of the corresponding control value ± SEM from four separate experiments. Asterisks in the 8 h treatment indicate changes that are statistically significantly different from the non OP-treated corresponding control ($p < 0.002$).

4.2.6 Effects of CPF and CPO on the intracellular distribution of cytoskeletal proteins

Since 3 μM CPF and CPO were able to cause retraction of pre-formed neurites and interfere with the expression levels of cytoskeletal proteins, it was of interest to determine whether they were also capable of disrupting the intracellular distribution of neuronal cytoskeleton proteins. The neurotoxic effects of both OPs on microtubule and neurofilament protein distribution were studied by indirect immunofluorescence staining of pre-differentiated N2a cells following 2 and 8 h exposure. As previously explained in section 2.2.13, pre-differentiated N2a cells were stained with antibodies against total NFH (clone N52), pNFH (clone SMI34) and βIII-tubulin (clone 2G10).

As shown in figures 4.6 and 4.7, anti-βIII-tubulin antibody demonstrated intense staining in neurites and cell bodies of treated and non OP-treated cells at both exposure time points. In the case of anti-total NFH, it can be seen that there was relatively strong staining of axons in control cells, as shown by horizontal arrows, but weak neurite staining was observed in CPF and CPO treated cells at both 2 and 8 h exposure. The staining intensity of anti-pNFH in axons was similar to that of anti-total NFH in non OP-treated controls. However, much less neurite staining was observed and more aggregates were detected in cell bodies (vertical arrows) with anti-pNFH in OP treated cells at both time-points.

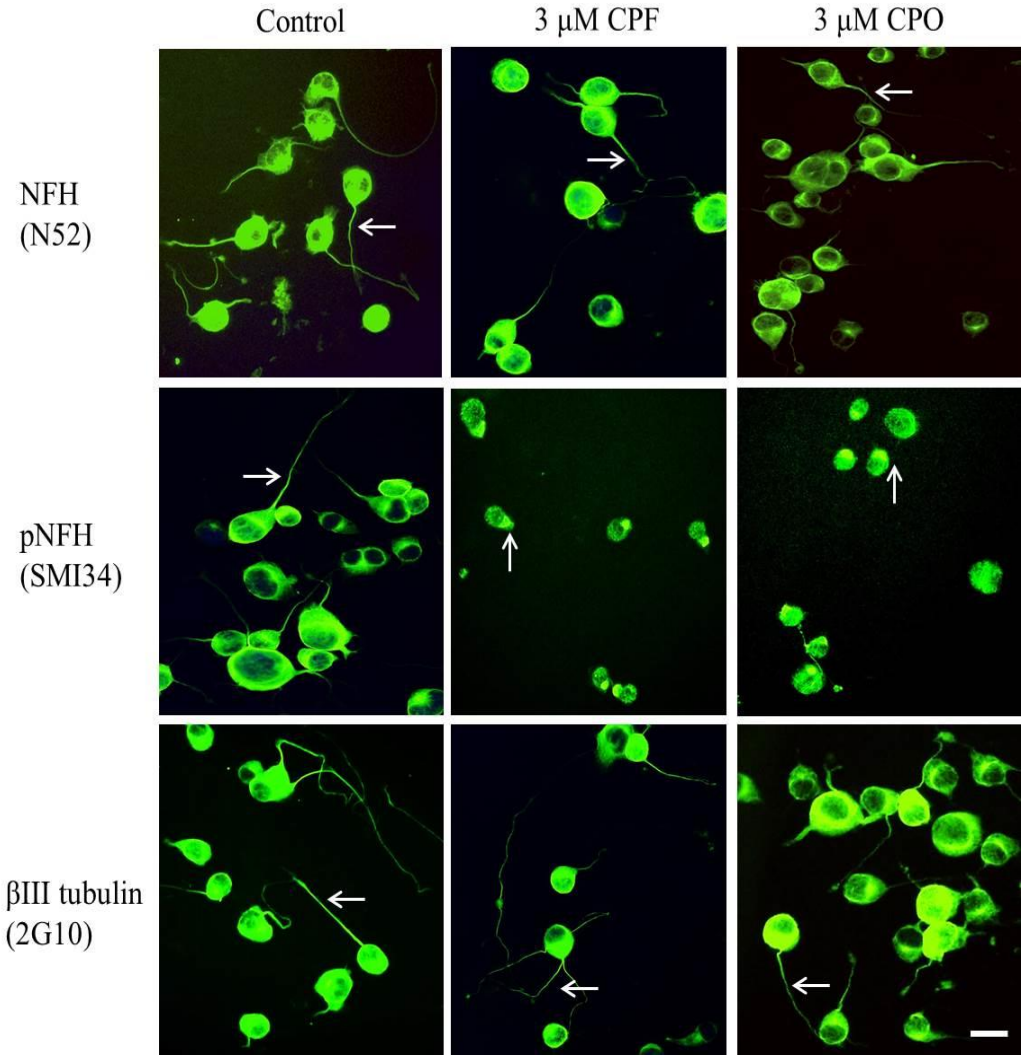

Figure 4.6. Effects of 2 h exposure to CPF and CPO on the intracellular distribution of cytoskeletal proteins in pre-differentiated N2a cells. Following 20 h of cell differentiation, N2a cells were treated without (control) or with 3 µM CPF or CPO for 2 h. N2a cells were then fixed and stained by indirect immunofluorescence as described in Materials and methods. Shown are digital images of non OP-treated controls and cells exposed to 3 µM CPF or CPO stained with anti-total NFH (N52), anti-pNFH (SMI34) and anti-βIII-tubulin (2G10). Horizontal arrows highlight typical axon-like neurites and vertical arrows indicate the presence of aggregates in cell bodies. Scale bar represents 30 µM.

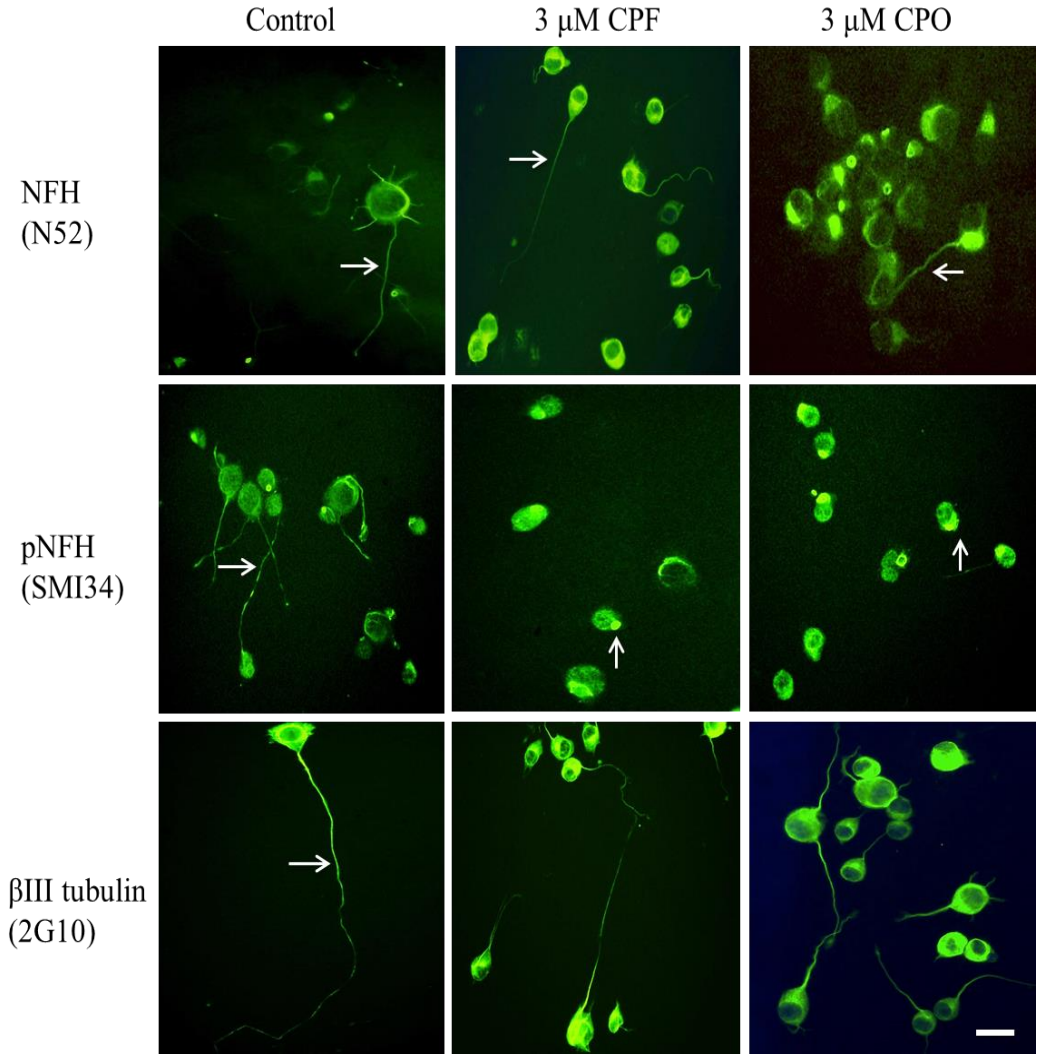

Figure 4.7. Effects of 8 h exposure to CPF and CPO on the intracellular distribution of cytoskeletal proteins in pre-differentiated N2a cells. Following 20 h of cell differentiation, N2a cells were treated without (control) or with 3 µM CPF or CPO for 2 h, after which, cells were fixed and stained by indirect immunofluorescence as described in Materials and methods. Shown are digital images of non OP-treated controls and cells exposed to 3 µM CPF or CPO stained with anti-total NFH (N52), anti-pNFH (SMI34) and anti-βIII-tubulin (2G10). Horizontal arrows highlight typical axon-like neurites and vertical arrows indicate the presence of aggregates in cell bodies. Scale bar represents 30 µM.

4.3 Discussion

The neurite retraction observed in pre-differentiated N2a cells following exposure to a sub-cytotoxic neurite inhibitory concentration of CPF and CPO indicated that these effects were not related to AChE inhibition (Chapter three). The aim of this chapter was to reveal whether retraction of neurite outgrowth was associated with disruption of cytoskeletal and associated regulatory proteins and whether the effects on these non-cholinergic targets could underlie the morphological changes in neurite outgrowth produced from pre-differentiated N2a cells.

Microtubule proteins such as tubulin and MAPs are mainly involved in neuronal cell differentiation and neurite development (Cambray-Deakin, 1991b). The fact that densitometric analysis in the current study revealed a lack of detectable changes in the reactivity of N2a cell lysates with antibodies against α-tubulin, tubulin posttranslational modifications, βIII-tubulin and MAPs following treatment with CPF and CPO together with the lack of effect in indirect immunofluorescence staining with anti-tubulin, suggested that the levels of microtubule proteins were unaffected under our experimental conditions. Similar findings were observed in previous studies, which found that the same concentration of CPF and CPO had no effect on the levels of α-tubulin when applied to pre-differentiated N2a cells (Sachana et al., 2005) or at the point of induction of cell differentiation (Flaskos et al., 2011). Unchanged levels of α-tubulin have also been observed following exposure to other OPs such as PSP, diazinon and the pyrethroid cypermethrin (Hargreaves et al., 2006, Flaskos et al., 2007). The previous data together with the current findings suggest that the microtubule network is not a primary target of these OPs.

Neurofilaments, in particular NFH, play a key role in regulating axon growth and stability (Williamson et al., 1996) and are increasingly expressed and phosphorylated as axons develop (Lee and Cleveland, 1994, Veeranna et al., 1998). The importance of NFH phosphorylation is that it regulates the transport of neurofilaments within axons, which plays an essential role in axonal growth and stability (Shaw, 1991, Sihag et al., 2007). Extensive phosphorylation of NFH

results in a slower rate of axonal transport (Yuan et al., 2006). Thus, it was of interest to determine whether neurite retraction could be reflected at the molecular level by altered levels of phosphorylation of NFH. The observed increase in the reactivity of antibodies against pNFH and the calculated phosphorylation ratios in OP-treated cell lysates at 2 h and the following decline at 8 h exposure, together with the lack of statistically significant effects of OPs on the reactivity of antibodies that recognise total NFH at all time-points are consistent with an early transient hyperphosphorylation followed by a reduced phosphorylation state of NFH, with no overall effect on the total levels of NFH protein. The transient increase in NFH phosphorylation in pre-differentiated N2a cells treated with CPF and CPO mirrored the effect of other OPs such as phenyl saligenin phosphate (PSP) and trio-ortho-cresyl phosphate (TOCP) in N2a cells under co-differentiation conditions (Fowler et al., 2001, Hargreaves et al., 2006). In animal studies, altered phosphorylation status of NFH has also been found in the spinal cord of hens treated with TOCP (Suwita et al., 1986) and PSP (Jortner et al., 1999). Taken together, these findings suggest that several OPs may be able to disrupt the phosphorylation status of NFH.

The data for CPF are in agreement with the study of Sachana et al. (2001), which revealed little or no effect on the levels of NFH from N2a cells following exposure to CPF under similar post differentiation conditions (Sachana et al., 2001). However, in a study by Flaskos et al. (2011), where CPO was added to N2a cells at the same time as induction of differentiation, immunoblot analysis indicated significant reduction in NFH protein but the level of NFH phosphorylation remained close to the control values (Flaskos et al., 2011), suggesting that the effect of CPO observed in the current work was specific for pre-differentiated cells. Thus, the toxicity response appears to be related to the developmental stage of cell differentiation at which the exposure to OPs occurs, although the possibility that the longer exposure time (24 h) in the latter study may have affected the outcome cannot be discounted.

Results obtained from immunoblot analysis using monoclonal antibody GAP7B10, which recognises GAP-43, suggested that CPF and CPO induced a transient reduction in GAP-43 after 4 h exposure. GAP-43 is a cytoskeleton

membrane linker that is highly expressed in the growth cones and extending axons in neuronal cells (Skene, 1989, Das et al., 2004). During neurodevelopment, GAP-43 regulates the formation of growth cones, and modulates the development and stability of axons (Meiri et al., 1986, Benowitz and Routtenberg, 1997, Meiri et al., 1998). It has been demonstrated that GAP-43 synthesis is elevated during axonal outgrowth (Skene, 1989, Pekiner et al., 1996) and thus, inhibition of neurite outgrowth could be associated with altered expression level of GAP-43 (Das et al., 2004). Since reduced levels of GAP-43 in the current study occurred in parallel with the collapse in axon outgrowth observed by live cell imaging following exposure of pre-differentiated N2a cells to CPF and CPO (chapter three), it could also have contributed to the detachment of the growth cones. This finding is consistent with previous studies, which showed reduced levels of GAP-43 in pre-differentiated N2a cells exposed to similar concentration of CPF and other OPs (i.e. CPF-methyl) for 4 h (Sachana et al., 2005) and in N2a cells induced to differentiate for 24 h in the presence of CPO (Flaskos et al., 2011). However, this is the first time that reduced level of GAP-43 was observed under post-differentiation exposure conditions for CPO.

The decreased levels of GAP-43 were also associated with impaired axon outgrowth in N2a cells treated for 4-24 h from the point of induction of differentiation with different OPs such as TOCP, leptophos, diazinon and the carbamate ester carbaryl (Fowler et al., 2001, Sachana et al., 2003, Harris et al., 2009b). Taken together, the current and previous findings suggest that reduced levels of GAP-43 can be considered as a common molecular marker for the neurite inhibitory effects caused by these OPs. Interestingly, the observed recovery in the level of GAP-43 at 8 h after its significant reduction in 4 h time point suggested the ability of the expression of this protein to recover to equal levels to that of controls. The transient reduction in the levels of GAP-43 may further suggest that this could be due to changes in proteolytic degradation and/or gene expression, which was then subsequently recovered by increase synthesis.

The chaperone role played by HSPs is important in maintaining the integrity of neuronal proteins against abnormal protein folding, which may also be related to

their protective role against apoptosis induced by OP toxicity (Hartl and Hayer-Hartl, 2002, Bukau et al., 2006). Elevated levels of these proteins were detected in brains affected by neurodegenerative disease (Hamos et al., 1991, Anthony et al., 2003). In addition, it has been demonstrated that increased levels of HSP-70 could provide a potential marker of toxic injury in mammalian brain (Gonzalez et al., 1989). In the current study, the lack of detectable changes in the expression levels of HSP-70 in CPF and CPO-treated cells at all exposure time points is compatible with an earlier study conducted under similar experimental and differentiation conditions, which also showed no effect on the levels of HSP-70 in CPF-treated pre-differentiated N2a cells (Sachana et al., 2001). The observation that CPO had no effects on the levels of HSP-70 in the current study indicated that CPO is acting in a similar manner as CPF with respect to this HSP under the post-differentiation exposure conditions used. However, under co-differentiation exposure conditions, raised levels of HSP-70 compared to control were detected in N2a cells following exposure to 3 μM CPF for 4 and 8 h (Sachana et al., 2001), and diazinon oxon (1 to 10 μM) for 24 h (Sidiropoulou et al., 2009a). Interestingly, reduced levels of HSP-70 were found in N2a cells exposed for 24 h to 10 μM diazinon under co-differentiation conditions (Flaskos et al., 2007). Taken together, these findings suggest that, with respect to HSP expression, the effects of CPF and CPO could involve distinct mechanisms that are dependent on the developmental stage at which exposure occurs.

HSP-60 is a mitochondrial stress protein, which is mainly found in the mitochondria (Anthony et al., 2003). The current study showed that the levels of HSP-60 were not altered in pre-differentiated N2a cells exposed to 3 μM CPF and CPO compared to non OP-treated controls. Previously, increased immunoreactivity of HSP-60 in brain epithelial cells was detected in patients with Alzheimer's disease compared to normal subjects, which indicated that mitochondrial damage was associated with this neurodegenerative condition (Anthony et al., 2003). However, the lack of noticeable differences on the expression of HSP-60 presented in this study suggested that mitochondrial stress proteins were not a major target for CPF and CPO toxicity in pre-differentiated N2a cells under our experimental conditions.

HSP-90 is another chaperone protein that is found abundantly in the cytosol and highly expressed in mammalian brain cells (Gupta et al., 2010). HSP-90 binds to cytoskeletal proteins such as tubulin and actin, and is thought to have a role in stabilising the neuronal cytoskeleton (Csermely, 2001). It also interacts with protein kinases that are important in regulating the cell death and survival (Sreedhar et al., 2004). Under stress conditions such as pesticide exposure, HSP-90 with the assistance of HSP-70 plays an important role in degradation of misfolded, damaged or denatured proteins (Gupta et al., 2010). The transient reduction observed in levels of HSP-90 in CPO-treated cells but not CPF-treated cells in the current study could reflect the ability of CPO to disrupt the functions of HSP-90, as it has been reported that decreased levels of HSP-90 could affect many cellular processes and increase the mortality of mammalian cells upon thermal stress (Bansal et al., 1991, Gopinath et al., 2014).

On the other hand, the lack of alterations in the expression of HSP-90 in CPF-treated cells is inconsistent with previous work, in which a much lower concentration of CPF (50-200 nM) induced synthesis of HSP-90 in undifferentiated rat pheochromocytoma PC12 neuronal cells following 24 h exposure (Bagchi et al., 1996). This discrepancy could be explained by several experimental differences in the cell lines, differentiation conditions, sub-cytotoxic OP concentrations, and/or exposure times used. With respect to the latter, the shorter exposure time in the current study, may not have been sufficient for the threshold levels required to induce expression of HSP-90 to be reached. It is important to mention that the total cellular HSP content was measured this study. It would be beneficial for future work to measure these proteins in the cytosolic and mitochondrial fractions separately after OP exposure.

The observed alterations in NFH phosphorylation were consistent with the possible disruption of cell signalling pathways involved in cytoskeletal regulation. In the current study, it was important to relate these changes to the activation status of the MAP kinase ERK 1/2, since it known as a convergence point for cell signalling pathways involved in neuronal cell differentiation (Perron and Bixby, 1999). This protein kinase is activated in N2a cells following

induction of cell differentiation by serum withdrawal (Hargreaves et al., 2006) and such activation is required for the development of neurites (Singleton et al. 2000; Lopez-Maderuelo et al. 2001). Moreover, it is known to be important in the phosphorylation of NFH (Perron and Bixby, 1999). In the current study, the increase in reactivity of anti-pERK and the calculated phosphorylation ratios with a lack of detectable changes in anti-total ERK reactivity after 2 h exposure to both compounds suggested that OP treatment lead to increased activation of ERK, which may account for the changes in NFH phosphorylation at that time point. However, the lack of significant changes in anti-pERK in OP-treated cells compared to the control after 4 and 8 h exposure suggested that the OP-induced activation was short-lived. The finding of the current study, with respect to the activation status of the MAP kinase ERK1/2, is compatible with a previous study conducted under co-differentiation conditions, which also showed transient increased reactivity of anti-pERK but not anti-total ERK in N2a cells exposed to PSP for 4 h (Hargreaves et al., 2006). These data together suggest that several OPs are capable of inducing transient changes in ERK activation that might disrupt NFH phosphorylation in treated cells.

Interestingly, the data obtained from the measurement of phosphatase activity were consistent with the possibility that increased phosphatase activity could account for the observed reduction in NFH phosphorylation at the later time point. Previously, it has been reported that protein phosphatase 2A from both rat spinal cord and rabbit skeletal muscle can reduce the phosphorylation of NFH following hyperphosphorylation by cyclin-dependent kinase-5 (cdk5) in neurodegenerative disease (Veeranna et al., 1995). In addition, reduced levels of protein phosphatase 2A and other phosphatases were found to be associated with altered NFH phosphorylation in protein aggregates found in Alzheimer's disease (Vogelsberg-Ragaglia et al., 2001) and amyotrophic lateral sclerosis brain (Kesavapany et al., 2007). Therefore, protein phosphatase 2A might be one potential NF-associated phosphatase involved in the reduced phosphorylation of NFH following 8 h exposure to both CPF and CPO. However, further investigation is needed to identify specific phosphatases involved in the regulation of NFH phosphorylation in OP treated cells.

Indirect immunofluorescence findings further confirmed the idea that both compounds used in the current study can impair neurite development and interfere with the expression levels of cytoskeletal proteins. The relatively strong staining of axon-like neurites for total NFH in control cells, and in cell body-located aggregates with weaker staining of the axon-like neurites that remained in OP-treated cells, may reflect disruption of the neurofilament network in treated cells. This was even more apparent from changes in the staining pattern with anti-p-NFH from clear axonal staining in the control cells to mainly aggregates in the cell bodies of treated cells suggested that the phosphorylated NFH was more highly affected by CPF and CPO treatment at both time points (2 and 8 h). This disruption in the intracellular distribution of neurofilaments is consistent with that observed in previous studies, in which cells were induced to differentiate for 24 h in the presence and absence of sub-lethal neurite inhibitory concentrations of PSP (Hargreaves et al., 2006), diazinon (Flaskos et al., 2007) and CPO (Flaskos et al., 2011).

On the other hand, strong staining patterns with β-tubulin antibody obtained by indirect immunofluorescence further confirm the observation of the densitometric analysis which revealed no changes in the reactivity of pre-differentiated N2a cell lysates with antibodies against β-tubulin following treatment with 3 μM concentration of either compound. The similar distribution of tubulin in cell bodies and neurites of treated and non-treated cells indicated no major disruption of the microtubule network, suggesting that microtubules are not the main target for OP pesticides in pre-differentiated N2a cells.

In summary, the results presented in this chapter suggest that OP-induced neurite retraction in pre-differentiated N2a cells is associated with early transient increases in NFH phosphorylation, which is then followed by a decline at 8 h, and a transient reduction in GAP-43 but that the level of total NFH and microtubules was unaffected. Increased activation of the ERK1/2 MAP kinase signalling pathway accounts for the observed alterations in pNFH at 2 h, whereas increased levels of phosphatase activity mediate the dephosphorylation at 8 h. Although neither compound was able to affect the levels of HSP-70 and HSP-60, CPO seemed to cause a transient inhibition in levels of HSP-90. These findings

together demonstrate that, at a molecular level, sub-cytotoxic concentrations of CPO induce a similar pattern of effects to those of CPF in pre-differentiated N2a cells with respect to the levels and intracellular distribution of cytoskeletal proteins and on the levels of growth associated proteins, activation status of ERK1/2 and phosphatase activity.

5 Development of medium to high throughput assays of organophosphate toxicity in pre-differentiated N2a cells

5.1 Introduction

Neurite outgrowth is one of the main morphological features of neurodevelopment, and has been investigated in numerous *in vitro* studies. Extension of neurites (axons and dendrites) during brain development is a crucial factor that determines neuronal connectivity (Radio et al., 2008). Thus, disruption of this critical cellular process as a result of OP exposure could lead to neurodegenerative effects in developing organisms (Rice and Barone, 2000, Costa, 2006, Grandjean and Landrigan, 2006). As neurite outgrowth *in vitro* exhibits many of the morphological and molecular changes that occur in axon outgrowth during nerve regeneration *in vivo*, neurotoxin-induced changes in this phenomenon may also reflect the ability of xenobiotics to cause axon retraction and/or inhibit nerve regeneration in adult animals (Burgoyne, 1991, Berger-Sweeney and Hohmann, 1997).

The neurotoxic effects of CPF and CPO on neurite outgrowth in pre-differentiated N2a cells observed in chapter three were assessed using manual laboratory techniques, by which the number of axon-like processes was quantified per 100 cells following CFSE staining. Although this method demonstrated the ability of both compounds to induce changes in the process of neurite outgrowth, the acquisition of microscopic images and the subsequent quantitative analyses were time-consuming and gave information only about neurites that were longer than two cell body diameters in length only (i.e. axon-like). In addition, the assessment of neurite outgrowth was based on a single concentration of both compounds. Although this concentration (3 µM) for CPF was previously demonstrated to induce 50% inhibition in the outgrowth of axon-like processes in pre-differentiated N2a cells without affecting cell viability

(Sachana et al., 2001), it provides no information about the concentration-effect relationship of these OPs on the cellular model.

Therefore, high throughput/high content screening has been developed using fully automated integrated systems for cell imaging and data analysis (Abraham et al., 2004, Smith and Eisenstein, 2005). This advanced technology provides reliable, time efficient and rapid measurements of neurite outgrowth overcoming the common limitations of manual methods used in this study. Additionally, high throughput/high content screening can assess the effects of a wide range of chemicals and neurotoxicants on multiple parameters of neurite outgrowth such as neurite number, neurite length, cell body area and the extent of neurite branching. Changes in each endpoint can be analysed and presented as average or total count per each individual cell in the captured image (Radio and Mundy, 2008). Moreover, high throughput/high content assays can be used with different cellular models in order to compare and characterise the effects of several OPs or other chemicals on neurite outgrowth in multiple cell types (Mundy et al., 2010). Earlier reports have validated the feasibility of this approach for evaluating the neurotoxicity potential of various chemicals on neurite outgrowth in neural cell lines under post- differentiation (Wilson et al., 2014) and co-differentiation exposure conditions (Radio et al., 2008, Radio et al., 2010, Harrill et al., 2011, Harrill and Mundy, 2011).

As previously mentioned, the molecular basis of the OP-induced effects on neurite outgrowth in pre-differentiated N2a cells observed in chapter four were examined using immunoblotting techniques. However, the procedure was time consuming and effects of both OPs on cytoskeletal proteins and their regulatory pathways in pre-differentiated N2a cells was again based on only one concentration of both compounds. In order to provide rapid, quantitative dose-response analysis for the effects of CPF and CPO at different time points, a medium to high throughput method such as cell ELISA was developed as part of the current study. This idea was first described by Schmuck and Ahr (1997), who showed that cells can be differentiated in the presence and absence of OPs and the levels of neurite enriched cytoskeletal proteins can be determined by the aid of cell ELISA (Schmuck and Ahr, 1997). Some of the advantages of this

technique when used as an alternative to Western blotting approach used in the previous chapter is the ability to apply several concentrations of both CPF and CPO simultaneously on a single microtitre plate and thus, reducing the amount of reagents, materials, costs and processing time.

The key aims of this chapter were to develop medium to high throughput assays in order to examine the effects of multiple concentrations of CPF and CPO at different time points on neurite outgrowth, cytoskeletal proteins and their regulatory pathways in pre-differentiated N2a cells in a rapid quantitative analysis. This would, in turn, validate the previous findings obtained from analysis of CFSE staining and antibody reactivity with Western blots of cell lysates treated with a single concentration (3 µM) of both compounds, and help to determine the concentration dependence of the response.

5.2 Results

5.2.1 Development of high throughput assays of neurite outgrowth

To quantitatively analyse multiple parameters of neurite outgrowth in pre-differentiated N2a cells following CPF and CPO treatment, cells were fixed and stained by indirect immunofluorescence with antibodies against α-tubulin (clone B512) and pNFH (clones Ta51 and SMI34). Monoclonal antibody B512 was expected to stain microtubules in axons, dendrites and cell bodies, whereas the anti-pNFH antibodies were expected to preferentially stain mainly neurofilaments in axons of neuronal cells. These particular antibodies were used because they are neurite-enriched cytoskeletal proteins and thus, allowing for the OP-induced effects on multiple parameters of neurite outgrowth in pre-differentiated N2a cells to be investigated. Images of stained monolayers were acquired using the ImageXpress Micro Widefield High Content Screening System and neurite outgrowth analysis was performed using MetaXpress imaging and analysis software, as described in section 2.2.16.

Figure 5.1 demonstrates the segmentation of acquired images obtained by high throughput assays used in this part of the current study. All representative images shown are from non OP-treated controls stained with B512, Ta51 and SMI34. Image acquisition was performed using two wavelengths; FITC to detect cell body and neurites (green) and DAPI to identify nucleus of all cells in a field (blue). The resultant merged images showed staining distribution of FITC and DAPI within each neuronal cell. Image segmentation was then performed using MetaXpress imaging and analysis software and displayed as multicoloured masks tracing the neurites and cell bodies in the acquired image. For accurate image segmentation, the analysis settings of the integrated neurite outgrowth application module were optimised and configured to catch maximum relevant detail with minimal background noise. The following parameters of neurite outgrowth were chosen for the analysis and measurements were provided in mathematical algorithms:

- Average number of cells/field (total number of neural cell bodies averaged by the number of fields)
- Average cell body area/field (total area of cell bodies in square micron averaged by the number of fields)
- Average number of neurites (total number of neurites produced from the cell bodies averaged by the number of fields)
- Maximum neurite length/cell (the length in microns of the longest neurite from the neuronal cell body to an extreme segment per cell)
- Average neurite length/cell (the total length in microns of all significant outgrowths averaged by the number of cells)
- Mean processes/cell (average number of neurites longer than 10 µm/cell).
- Mean branches/cell (average number of branches originating from neurites produced by each cell)
- Significant outgrowth (neurites longer than 10 µm in length)
- Percentage of cells with significant outgrowth (cells with at least one neurite > 10 µm in length).

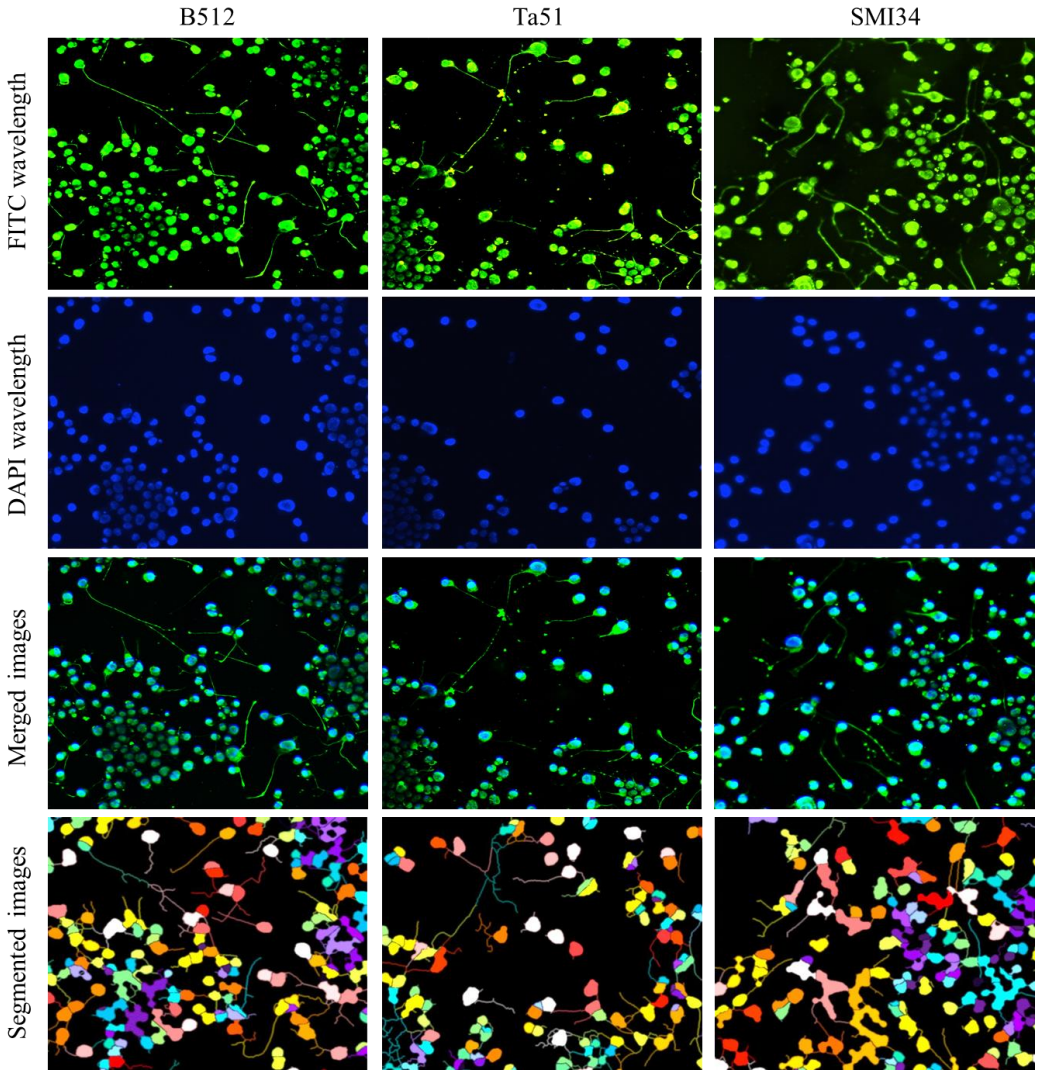

Figure 5.1. Segmentation of stained pre-differentiated N2a cells using high throughput screening assays. Cells were fixed and stained with antibodies recognising α-tubulin (B512) and pNFH (Ta51 and SMI34) followed by Alexa Fluor® conjugated anti-IgG secondary antibodies. All Images shown are from non OP-treated controls from a single field of view. Acquired images were obtained using ImageXpress Micro system (10x objective) with two wavelengths; FITC for cell body and neurites detection and DAPI for nucleus counting. Segmented images with multicoloured tracing masks on neurites and cell bodies were generated using the Neurite Outgrowth Module within the MetaXpress imaging and analysis software for monitoring different parameters of neurite outgrowth.

5.2.2 Monitoring multi-parameters of neurite outgrowth in pre-differentiated N2a cells

The concentration-range (1, 3, 10 µM) effects of CPF and CPO on neurite outgrowth in pre-differentiated N2a cells were investigated following 2 and 8 h exposure using high throughput assay. Data of multi-parametric analysis of neurite outgrowth obtained by quantitation of B512 and pNFH (clone Ta51) staining are shown in this chapter. Confirmatory data using another anti-pNFH antibody (clone SMI34) are displayed in appendix (Figure 8.1-8.4). The current study focused on the effects of CPF and CPO at 2 and 8 h time points because most alterations in neurite outgrowth and associated protein changes were observed at these two exposure times in earlier chapters.

Figure 5.2 shows the high throughput data for cell number and cell body area obtained by analysis of B512 and Ta51 staining at 2 and 8 h exposure. The presented data show that all concentrations of CPF and CPO had no effects on the average neuronal cell number/field after 2 and 8 h exposure compared to the untreated controls (Figure 5.2A1-A4). Similarly, both B512 and Ta51 staining showed no effects on the measurements of cell body area/field of pre-differentiated N2a cells following 2 h exposure to both OPs (Figure 5.2B1 and B2). After 8 h treatment, staining with both antibodies showed slight but not significant decreases in the average cell body area/field following exposure to 1 and 3 µM CPF and CPO compared to non OP-treated control (Figure 5.2B3 and B4). However, the highest concentration (10 µM) of both OPs significantly reduced this parameter as indicated with B512 ($p < 0.01$) and Ta51 ($p < 0.0001$) staining (Figure 5.2B3 and B4).

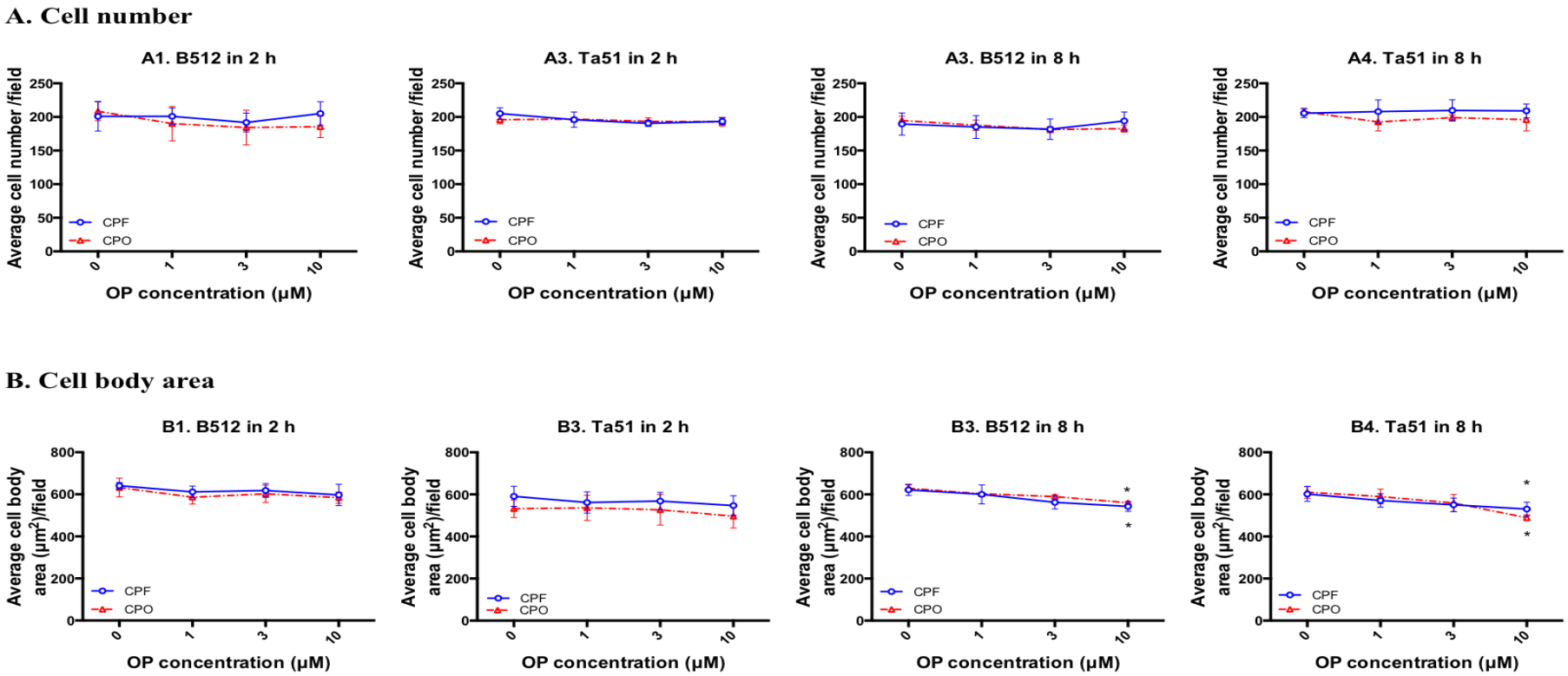

Figure 5.2. Effects of CPF and CPO on cell number and cell body area in pre-differentiated N2a cells as assessed by high throughput assays. Cell were then fixed and stained with B512 and Ta51, after which data were acquired using the ImageXpress Micro system and the cell number and cell body area were measured using MetaXpress imaging and analysis software. Data show dose-related effects of both CPF and CPO on the average cell number/field (A) and the average cell body area (μm^2)/field (B) with B512 and Ta51 staining at 2 h and 8 h. High throughput data are represented as mean values ± SEM from four independent experiments. Data were analysed using two-way ANOVA. The CPF effects are presented as blue solid lines with circles; the CPO effects are presented as red dashed lines with triangles. Asterisks indicate changes that are statistically different from the non OP-treated controls with B512 (*$p < 0.01$) and Ta51 (*$p < 0.0001$) staining. When SEM bars are not apparent, this means that error is smaller than the symbol size.

The effects of multiple concentrations of CPF and CPO on the average number of neurites/field and the percentage of cells with significant outgrowth (neurites > 10 µm in length) are shown in figure 5.3. As indicated in figure 5.3A1-A4, no effects were observed on the average neurite number/field in cells treated with 1 µM CPF and CPO, but significant decreases ($p < 0.001$) were detected with B512 and Ta51 staining at 3 and 10 µM of both compounds at both time points. Following 2 h exposure, the quantitative analysis of both stains for the average number of neurites/field in pre-differentiated N2a cells showed that the treatment of 3 µM CPF and CPO caused 13% and 18% decline, respectively, compared to the corresponding non OP-treated control (Figure 5.3A1 and A2). In addition, exposing the cells to a higher concentration of 10 µM reduced the average neurite number/field to 30% with CPF and 40% with CPO using both stains (Figure 5.3A1 and A2).

When pre-differentiated N2a cells were exposed to both OPs for 8 h, the reduction in the average neurite number/field detected by Ta51 staining was greater than those obtained with B512 (Figure 5.3A3 and A4). The quantitative analysis of B512 staining for the average number of neurites/field in pre-differentiated N2a cells showed that 3 and 10 µM CPO resulted in 30% and 36% decline, respectively (Figure 5.3A3). However, Ta51 analysis demonstrated 33% and 55% fall in the average number of axon-like neurite compared to the non OP-treated controls at 3 and 10 µM CPO, respectively (Figure 5.3A4).

Figure 5.3B illustrates the number of cells with neurites length above 10 µm (i.e significant outgrowth) as quantified by B512 and Ta51 staining following OP treatment for 2 and 8 h. Quantitation of B512 staining showed lack of detectable changes on the number of cells with significant outgrowth in pre-differentiated N2a cells treated with multiple concentrations of CPF and CPO for 2 and 8 h (Figure 5.3B1 and B3). In contrast, Ta51 staining showed dose and time-dependent decreases in this parameter in OP-treated cells at both time points. The observed reduction in the number of cells with long neurites was statistically significant at 3 and 10 µM CPF and CPO in compare to the non OP-treated controls ($p < 0.05$). The reduction in number of cells with significant outgrowth

was greater at 8 than at 2 h for CPO at both 3 and 10 μM concentrations (Figure 5.3B2 and B4).

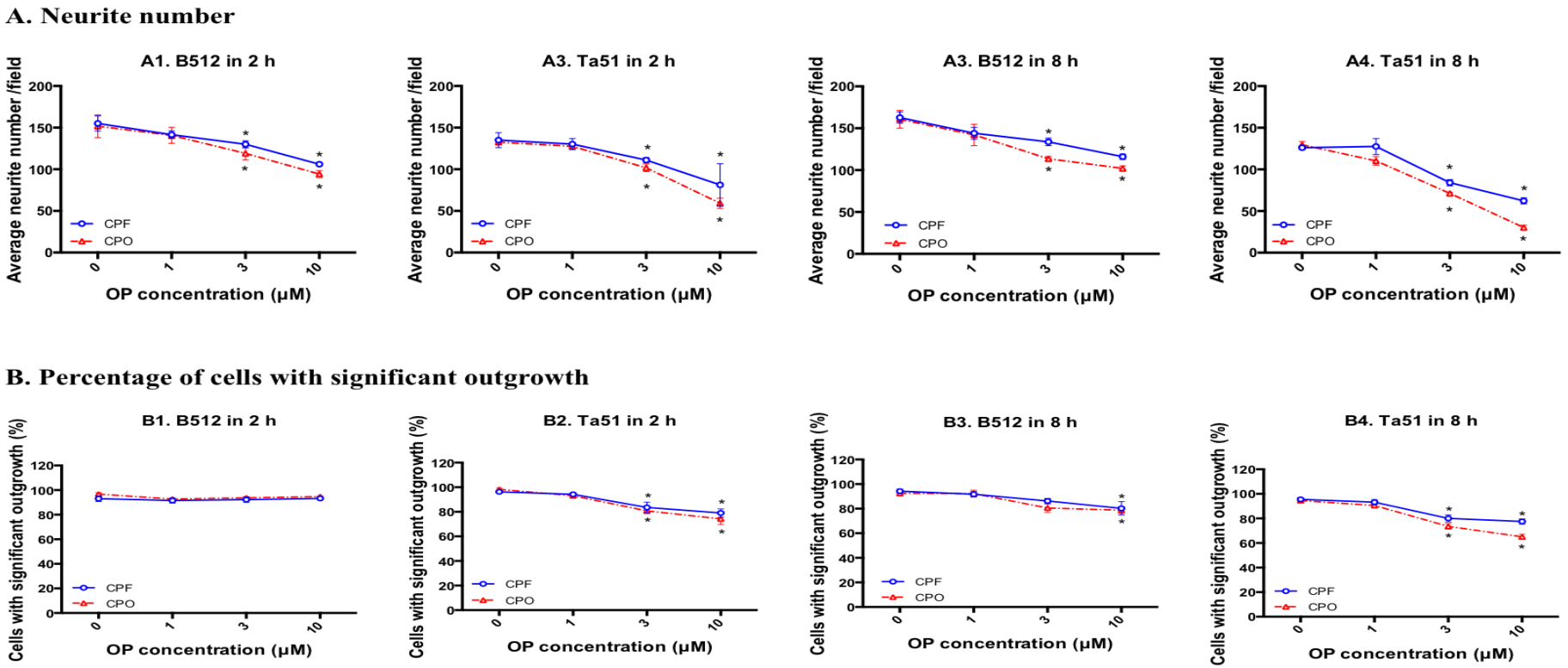

Figure 5.3. Effects of CPF and CPO on neurite number and percentage of cells with significant outgrowth in pre-differentiated N2a cells as assessed by high throughput analysis. Cells were stained with B512 and Ta51, after which data were acquired using ImageXpress Micro system and measured using MetaXpress imaging and analysis software. Data show dose-related effects of both CPF and CPO on the average neurite number/field (A) and the percentage of cells with significant outgrowth (B) at 2 and 8 h with B512 and Ta51 staining. Data are presented as mean values ± SEM from four independent experiments for both time points. Data were analysed using two-way ANOVA. The CPF effects are presented as blue solid lines with circles; the CPO effects are presented as red dashed lines with triangles. Asterisks indicate changes that are statistically different from the non OP-treated controls ($p < 0.05$). When SEM bars are not apparent, this means that error is smaller than the symbol size.

Further parameters of neurite outgrowth such as the maximum and average neurite length per neuronal cell were also assessed using high throughput assays. Following 2 and 8 h exposure, there was a dose-dependent decrease in both parameters of neurite outgrowth in OP-treated cells compared to the non OP-treated controls. A significant dose-related reduction ($p < 0.05$) was observed at two concentrations (3 and 10 µM) of both CPF and CPO (Figure 5.4A and B).

With regard to the measurement of maximum neurite length per neuronal cell, Ta51 staining was more sensitive in detecting long neurites than B512 staining (Figure 5.4A1-A4). It can be seen that the maximum neurite length/cell in non OP-treated controls obtained by B512 stain ranged from 30 to 37 µm, whereas, those measured with Ta51 stain were 46 to 58 µm. Figure 5.4A1 and A3 shows the quantitative analyses of B512 for the dose-related effects of both CPF and CPO on maximum neurite length/cell; CPF exposure for 2 h had no significant effects on this parameter at all concentrations (Figure 5.4A1). However, 8 h exposure to 10 µM CPF significantly decreased the maximum length of B512-positive neurites/cell by 53% compared to the control ($p < 0.0001$) (Figure 5.4A3). On the other hand, Ta51 staining exhibited a dose-dependent decline in the maximum neurite length/cell following CPO treatment for 2 and 8 h. The treatment of pre-differentiated N2a cells with 3 and 10 µM CPO caused a significant reduction in maximum neurite length/cell when compared to the non OP-treated control ($p = 0.005$ at 2 h, and $p < 0.0001$ at 8 h) (Figure 5.4A1 and A3). Figure 5.4A2 and A4 shows the measurements of maximum neurite length/cell obtained by the analysis of Ta51 staining. This indicated that both CPF and CPO at concentrations of 3 and 10 µM were able to induce significant reductions in the maximum length of neurites per cell compared to controls at both time points in pre-differentiated N2a cells ($p < 0.007$ at 2 h; $p < 0.0001$ at 8 h).

As illustrated in figure 5.4B1-B4, both B512 and Ta51 staining generated similar trends for the impacts of multiple concentrations of CPF and CPO on the average neurite length per cell at both time points. Following 2 h exposure of both compounds, both staining showed that the average neurite length per cell measurements were significantly reduced by approximately 25% and 40% at 3

and 10 µM, respectively ($p < 0.0001$) (Figure 5.4B1 and B2). A further reduction in average neurite length per cell was observed following 8 h exposure to CPF and CPO. The treatment of 3 µM of both OPs resulted in 30% decrease ($p < 0.0001$) in this parameter, while a higher concentration of 10 µM significantly reduced the average length of neurites per cell to 45% ($p < 0.0001$) (Figure 5.4B3 and B4).

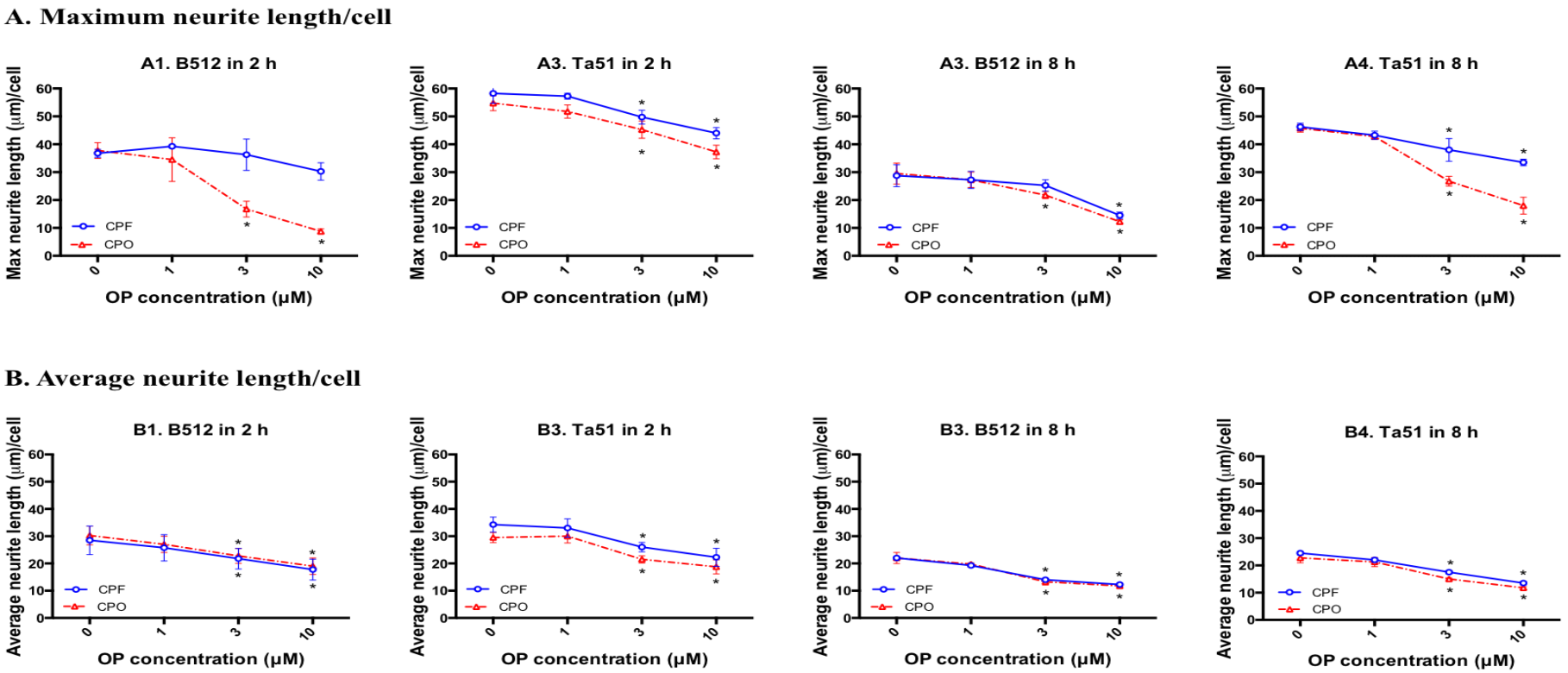

Figure 5.4. Effects of CPF and CPO on maximum and average neurite length/cell in pre-differentiated N2a cells as assessed by high throughput analysis. Cells were stained with B512 and Ta51, after which data were acquired using ImageXpress Micro system and measured using MetaXpress imaging and analysis software. Data show dose-related effects of both CPF and CPO on the maximum neurite length/cell (A) and the average neurite length/cell (B) at 2 and 8 h with B512 and Ta51 staining. Data are presented as mean values ± SEM from four independent experiments for both time points. Data were analysed using two-way ANOVA. The CPF effects are presented as blue solid lines with circles; the CPO effects are presented as red dashed lines with triangles. Asterisks indicate changes that are statistically different from the non OP-treated controls (*$p < 0.05$). When SEM bars are not apparent, this means that error is smaller than the symbol size.

Further parameters of neurite outgrowth such as the mean number of processes and branches per neuronal cell were also assessed using high throughput assay. As demonstrated in figure 5.5A and B, measurements with both B512 and Ta51 staining show that there was a concentration-dependent decline in the number of processes and branches/cell in pre-differentiated N2a cells treated with both CPF and CPO for 2 and 8 h compared to non OP-treated controls. A significant dose-related decrease ($p < 0.01$) was observed at 3 and 10 µM CPF and CPO at both exposure time points. Staining neurites with B512 revealed a higher number of processes and branches/cell than those detected by Ta51 staining.

Similar data on the effects of CPF and CPO on neurite outgrowth parameters were obtained when another anti-pNFH antibody (SMI34) was used (see appendix; Figure 8.1-8.4).

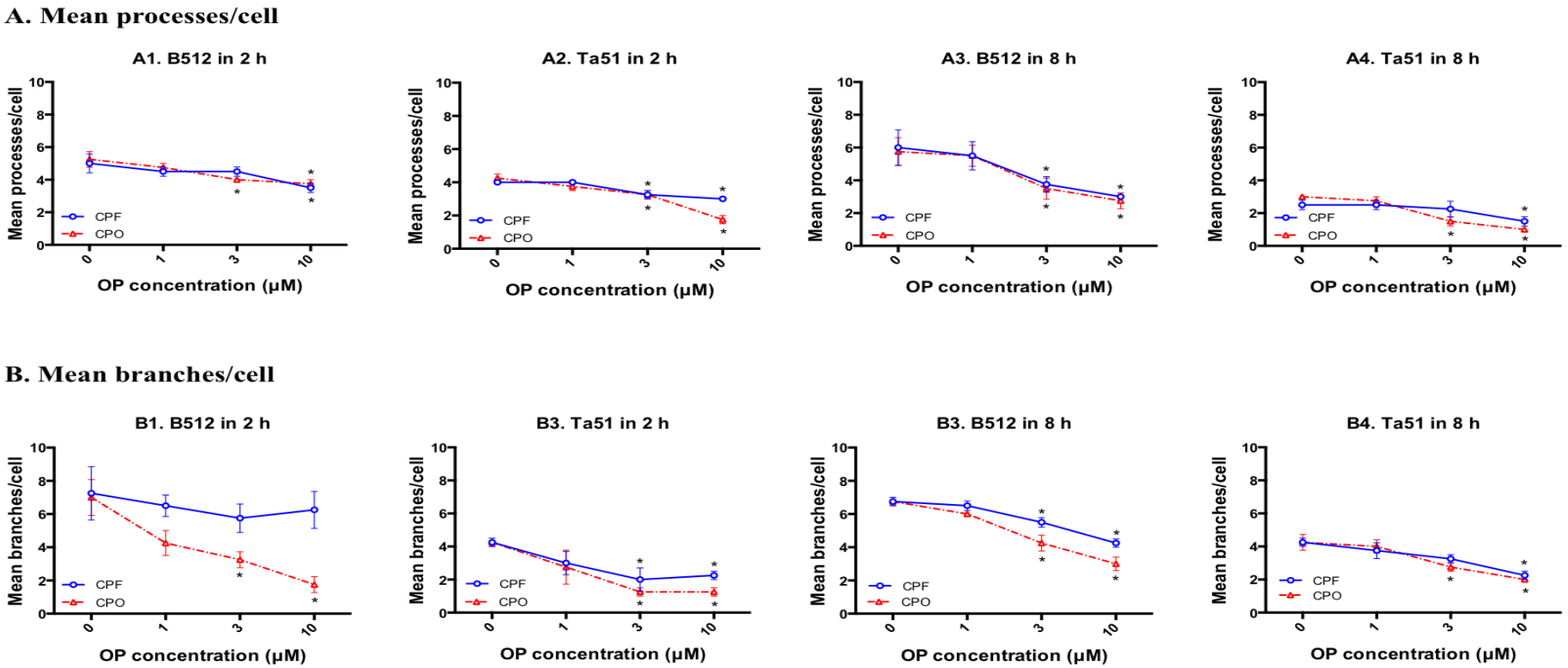

Figure 5.5. Effects of CPF and CPO on the mean number of processes and branches/cell in pre-differentiated N2a cells as assessed by high throughput analysis. Cells were stained with B512 and Ta51, after which data were acquired using ImageXpress Micro system and measured using MetaXpress imaging and analysis software. Data show dose-related effects of both CPF and CPO on the mean processes/cell (A) and the mean branches/cell (B) at 2 and 8 h with B512 and Ta51 staining. Data are presented as mean values ± SEM from four independent experiments for both time points. Data were analysed using two-way ANOVA. The CPF effects are presented as blue solid lines with circles; the CPO effects are presented as red dashed lines with triangles. Asterisks indicate changes that are statistically different from the non OP-treated controls (*$p < 0.05$). When SEM bars are not apparent, this means that error is smaller than the symbol size.

5.2.3 Effects of CPF and CPO on the viability of pre-differentiated N2a cells

To ensure that the 1-10 µM dose-range of CPF and CPO used in this study was non-cytotoxic towards pre-differentiated N2a cells, MTT reduction assays were carried out, as described earlier in section 2.2.7. The results demonstrated in figure 5.6A and B show that all concentrations of CPF and CPO had no effect on the reduction of MTT in OP-treated cells at either time point when compared to their corresponding non OP-treated controls. The results obtained from traditional MTT viability assay was compatible with high throughput data on cell count, which showed that treatment of pre-differentiated N2a cells with 1, 3 and 10 µM CPF and CPO had no inhibitory effects on cell number.

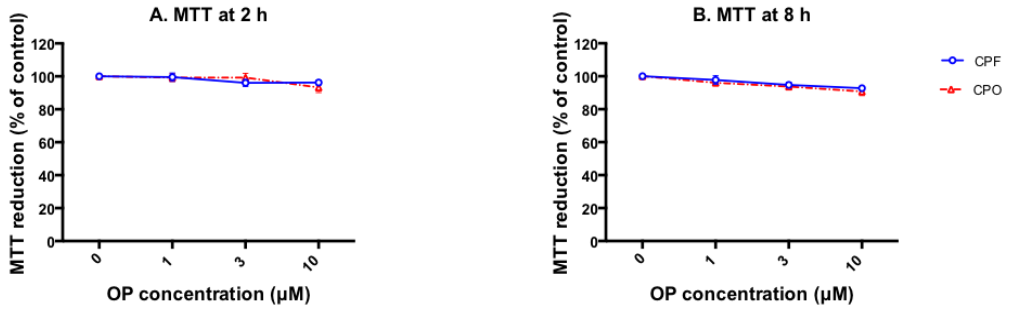

Figure 5.6. Effects of CPF and CPO on MTT reduction in pre-differentiated N2a cells. After 20 h of differentiation, N2a cells were treated without (0.5% v/v DMSO control) or with 1, 3 and 10 µM CPF or CPO for 2 and 8 h. The effects of both OPs on MTT reduction were measured to evaluate cell viability after 2 h (A) and 8 h (B) exposure. Data are expressed as a percentage of the non-OP treated control ± SEM from four separate experiments. Data were analysed using one way ANOVA. The CPF effects are presented as blue solid lines with circles; the CPO effects are presented as red dashed lines with triangles. The lack of asterisks reflect the fact that no statistically significant changes were found in MTT reduction in OP-treated cells compared to the untreated controls at both time points. When SEM bars are not apparent, this means that the error is smaller than the symbol size.

5.2.4 Determination of concentration-response effects of CPF and CPO on cytoskeletal and associated regulatory proteins using cell ELISA

The effects of multiple concentrations of CPF and CPO on cytoskeletal proteins and cell signalling pathway associated with their regulation in neurite outgrowth were further assessed in pre-differentiated N2a cells using cell ELISA technique for rapid quantification. The changes in the binding levels of these proteins using monoclonal antibodies against α-tubulin (clone B512), NFH (clone N52), pNFH (clones Ta51 and SMI34), and ERK1/2 MAP kinase were determined and quantified in controls and OP-treated cells following 2 and 8 h exposure, as described in section 2.2.15. These time points were chosen to focus on conditions under which both OPs induced significant changes in Western blotting analysis of lysates from cells exposed to a single concentration (3 µM) of each compound (Chapter 4).

Quantification of B512 reactivity (which detects total α-tubulin) by cell ELISA showed that it was not affected under any of the exposure conditions tested (Figure 5.7A1 and A2). Similarly, treatment of pre-differentiated N2a cells with all concentrations of both compounds had no effect at either time point on the binding levels of N52 (which recognises total NFH) when compared to controls (Figure 5.7B1 and B2).

Figure 5.7C1-D2 shows data from cell ELISAs using monoclonal antibodies Ta51 and SMI34, which both recognise pNFH. In figure 5.7C1, a dose-dependent increase was seen in the levels of Ta51 binding in pre-differentiated N2a cells treated with both CPF and CPO for 2 h. The elevation in Ta51 levels was statistically significant at 3 and 10 µM concentrations of CPF ($p = 0.007$) and CPO ($p < 0.0001$) compared to that of non OP-treated controls (Figure 5.7C1). After 8 h incubation with 3 and 10 µM CPF and CPO, a significant decline ($p < 0.05$) was observed in the levels of Ta51 binding in OP-treated cells in compare to controls (Figure 5.7C2). A different epitope of pNFH (recognised by SMI34) showed no significant changes in the levels of antibody binding to

pre-differentiated N2a cells exposed to all concentrations of CPF and CPO compared to non OP-treated controls at both time points (Figure 5.7D1 and D2).

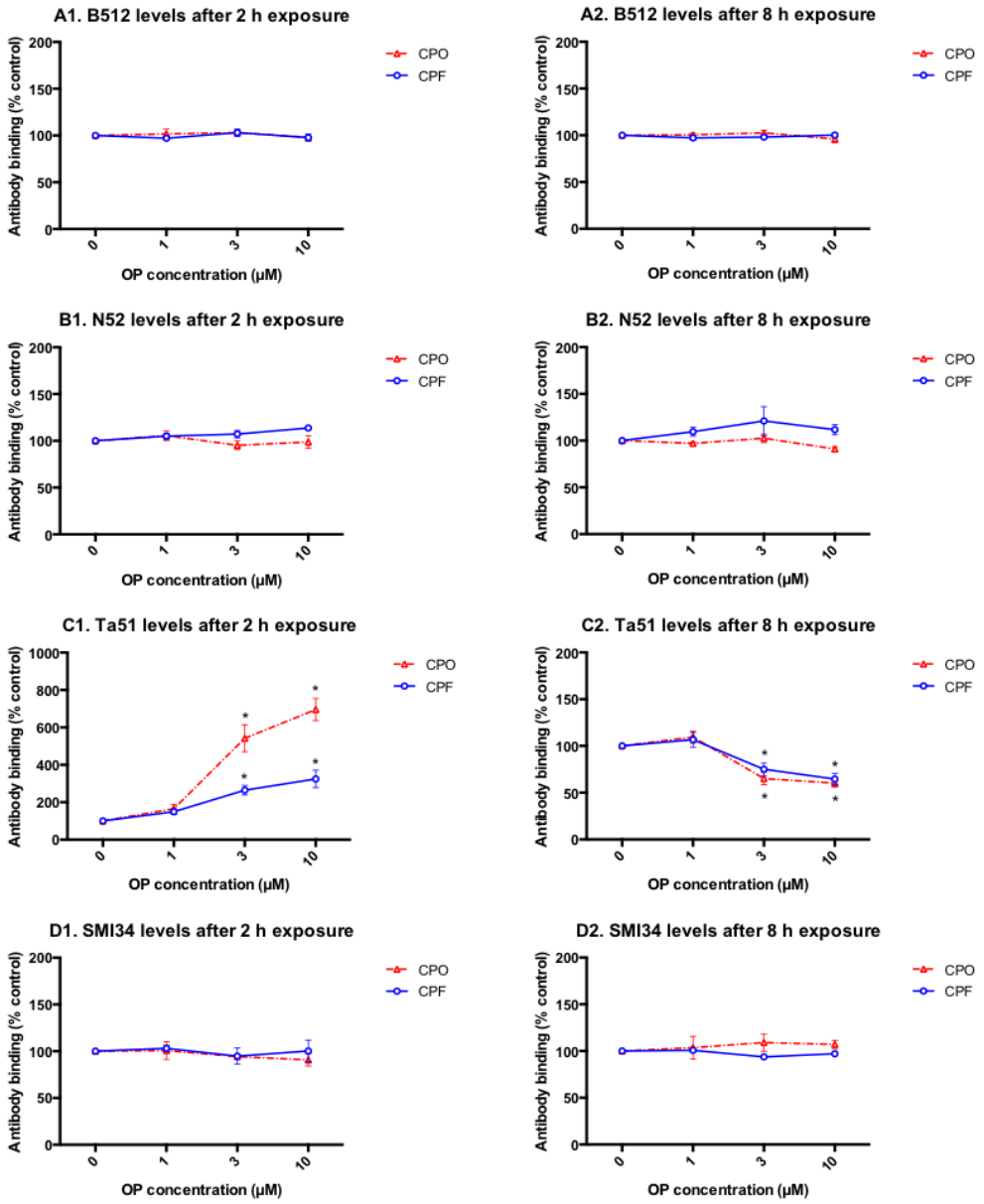

Figure 5.7. Effects of CPF and CPO on cytoskeletal proteins in pre-differentiated N2a cells as determined by cell ELISA. N2a cells were induced to differentiate for 20 h before being incubated without (0) or with 1, 3 and 10 µM concentrations of CPF or CPO for 2 and 8 h. Changes in the binding levels of antibodies that recognise α-tubulin (B512) (panel A), NFH (N52) (panel B) and pNFH (Ta51 in panel C and SMI34 in panel D) were quantified in controls and OP-treated cells following 2 and 8 h exposure using cell ELISA. Data are presented as a percentage of the non OP-treated control ± SEM (from four independent experiments at both time points). Data were analysed using one-way ANOVA. The CPF effects are presented as blue solid lines with circles; the CPO effects are presented as red dashed lines with triangles. Asterisks indicate changes that are statistically different from the non OP-treated controls ($p < 0.05$).

Since there dose-dependent changes were observed in the levels of binding Ta51 antibody to pre-differentiated N2a cells treated with CPF or CPO for 2 and 8 h, it was of interest to investigate whether these alterations in pNFH could be associated with changes in ERK 1/2 MAP kinase activation.

Figure 5.8A1 shows dose-dependent decreases in the binding levels of total ERK (tERK) to pre-differentiated N2a cells following 2 h exposure to both CPF and CPO. However, this reduction was only statistically significant ($p < 0.0001$) at 10 µM concentrations of both compounds when compared to the non OP-treated controls. After 8 h exposure (Figure 5.8A2), treatment of pre-differentiated N2a cells with up to 10 µM of both OPs showed no effects on the binding levels of total ERK.

Figure 5.8B1 and B2 demonstrates the dose-response effects of both CPF and CPO on the levels of anti-phosphorylated ERK (pERK) binding to pre-differentiated N2a cells. Exposure to both compounds for 2 h caused similar concentration-dependent increases in the binding levels of pERK antibody, which was statistically significant at 3 ($p < 0.001$) and 10 µM ($p < 0.0001$) compared to non OP-treated controls (Figure 5.8B1). By contrast, compared to the control, no changes were observed in anti-pERK reactivity with monolayers of pre-differentiated N2a cells exposed to either OP for 8 h (Figure 5.8B2).

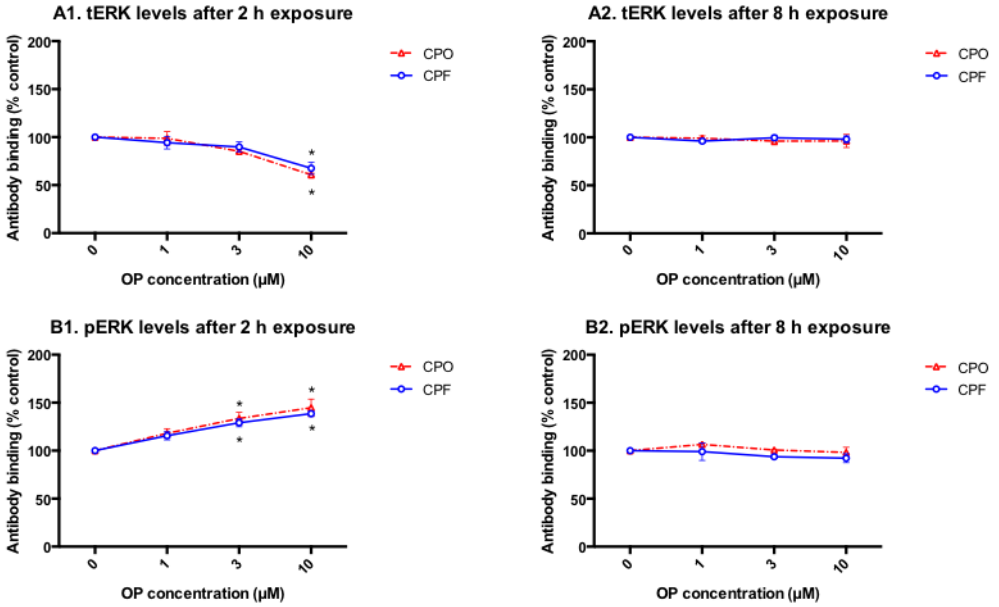

Figure 5.8. Effects of CPF and CPO on the activation status of ERK1/2 MAP kinase on pre-differentiated N2a cells as determined by cell ELISA. N2a cells were induced to differentiate for 20 h before being incubated without (0) or with 1, 3 and 10 µM concentrations of CPF or CPO for 2 and 8 h. Changes in the binding levels of antibodies that recognise total ERK (K-23) (panel A) and phosphorylated ERK (K-4) (panel B) were quantified in controls and OP-treated cells following 2 and 8 h exposure using cell ELISA. Data are presented as a percentage of the non OP-treated control ± SEM (from four independent experiments at both time points). Data were analysed using one-way ANOVA. The CPF effects are presented as blue solid lines with circles; the CPO effects are presented as red dashed lines with triangles. Asterisks indicate changes that are statistically different from the non OP-treated controls ($p < 0.05$). When SEM bars are not apparent, this means that error is smaller than the symbol size.

5.3 Discussion

The main aim of the current chapter was to develop medium to high throughput assays to examine the effects of several doses of CPF and CPO on multiple parameters of neurite outgrowth in pre-differentiated N2a cells over two time points. The amount of data obtained using the high throughput assays represents the sensitivity and feasibility of this technique to detect and quantify OP-induced changes in neurite outgrowth in a pre-differentiated cell model. The use of a fully automated approach in this part of the current study provided rapid analysis for the effects of both OPs on neurite outgrowth compared to the manual approach of measuring neurite outgrowth (CFSE staining) used in chapter three, which gave robust data but was time consuming and gave information restricted to longer neurites only. Additionally, the instrumentation of high throughput analysis validated the data obtained from the use of a single sub-cytotoxic concentration (3 µM) of CPF and CPO at the beginning of this thesis (chapter 3) and in previous work (Sachana et al., 2001, Sachana et al., 2005, Flaskos et al., 2011).

In this study, both anti-α-tubulin (B512) and anti-pNFH (Ta51 and SMI34) staining were utilised in order to compare and evaluate the potential of each marker in detecting the neurotoxic effects of both OPs on neurite outgrowth. B512 staining was expressed in cell bodies and neurites that were both dendrite-like and axon-like, whereas Ta51 and SMI34 staining was more specific for axon-like neurites. As indicated in data of neurite outgrowth parameters obtained by high throughput analysis (Figure 5.2), B512 staining detected more cells and a large cell body area compared to those quantified with Ta51 staining. However, Ta51 was more selective than B512 staining in detecting long neurites. Thus, B512 staining was more effective than Ta51 for the quantitative analysis of cell number and cell body area parameters, while Ta51 was more suitable for axon-like neurite related analysis such as neurite length and number.

The high throughput quantification of pre-differentiated N2a cell number indicated that 1-10 µM CPF and CPO had no significant effect on the average cell number per field at both exposure time points. The data from the automated

high throughput agreed with the dose-response effects of CPF and CPO in MTT reduction assays both in the current study and in previous work in our laboratory (Sachana et al., 2001, Sachana et al., 2005, Flaskos et al., 2011). Thus, findings from both assays confirmed that all concentrations of CPF and CPO used in this study were non-cytotoxic towards pre-differentiated N2a cells after 2 and 8 h exposure. Similarly, measurements of the average cell body area per field, which indicate the circular shape of N2a cell bodies, revealed that both compounds at 1 and 3 µM had no effect on this parameter. However, the automated system detected a reduction in the average cell body area in pre-differentiated N2a cells exposed for 8 h to the highest concentration (10 µM) of both CPF and CPO, which may suggest that treated cells could becoming more compact in shape at that time point.

The quantitative assessment of the average number of neurites per field, maximum and average neurite length per cell, number of processes and branches per cell, and cells with significant outgrowth all indicate that pre-differentiated N2a cells respond to both CPF and CPO in a dose- and time-dependent manner. This suggests that the neurite length and branching decrease as the concentrations of both OPs and the exposure time increase. The observation that these parameters of neurite outgrowth were reduced at concentrations of CPF and CPO that have no effects on cell number and viability confirms the sub-cytotoxic neurite inhibitory effect of both compounds towards pre-differentiated N2a cells.

The analysis of neurite outgrowth using high throughput assays in the current study can provides a valuable comparison between data generated from this automated system and those obtained using manual approaches at the beginning of this thesis. In this context, high throughput measurements of maximum and average neurite length per each neuronal cell corresponds most closely to the determination of axon-like neurites previously measured with the aid of CFSE stain following 3 µM CPF and CPO (Chapter 3). Although automated neurite length measurements were performed in a rapid and more sensitive way compared to the manual gross assessment of long neurites by CFSE staining, both approaches were in a good agreement showing that there was a dose-

dependent decrease in the neurite length and/or long neurite number in pre-differentiated N2a cells treated with both CPF and CPO for 2 and 8 h. The presented data also suggest that both automated and manual assays are suitable for assessing neurite outgrowth number and/or neurite length. However, the former facilitates rapid generation of more complex datasets for multiple compounds, concentrations and parameter measurements.

As axons extend and are guided to their synaptic targets, they form a number of branches, which play an essential role in connecting single neuron with multiple neurons (Hjorth et al., 2014). Utilisation of high throughput assays for neurite outgrowth was sensitive enough to support this study with additional information on neurite branching. Such a parameter could not be achieved previously using the manual measurement approach due to time constraints. In the current study, the data show changes in the actual branching of neurites as another sensitive parameter of neurite outgrowth, which was affected by both OPs in a similar concentration-dependent manner as other measures of neurite outgrowth in pre-differentiated N2a cells at both time points. In humans, alterations in the formation of axonal branches have been reported in brains affected by neurodegenerative diseases (Larner, 1995, Kwon et al., 2006). The observed inhibition in the mean branches per cell might indicate a disruption in cytoskeletal proteins involved in the formation of neurite branches. For instance, increased MAP1B was found to be associated with decreased axonal branching in adult dorsal root ganglia neurons (Bouquet et al., 2004). Altered expression of GAP-43 in response to neurite branching has been also demonstrated in rat hippocampal mossy fibres (Bendotti et al., 1997). Earlier studies also linked the accumulation of actin filaments in axons with the formation of neurite branches in cultured neurons (Gallo, 2006, Ketschek and Gallo, 2010). Therefore, it would be of interest to extend this work to investigate the molecular basis underlying the observed effects of CPF and CPO on neurite branching.

The current study has shown that cell-based ELISA is a rapid and simple method to study the molecular basis of the observed OP-induced effects on neurite outgrowth. Quantification of anti-tubulin and anti-NFH antibody binding in pre-differentiated N2a cells by cell-based ELISA revealed that both CPF and CPO at

neurite inhibitory concentrations (3 and 10 µM) had no effects on the levels of α-tubulin and total NFH at any time point (Figure 5.5A and B). These data suggested that disruption of the expression levels of these proteins was not responsible for the observed inhibition in multiple parameters of neurite outgrowth in pre-differentiated N2a cells. Although these findings are completely compatible with the data presented in chapter four of this thesis in which 3 µM concentration CPF and CPO had no effects on the reactivity of the same antibodies with Western blots of cell lysates, the cell-based ELISA assay demonstrated that even higher concentration (10 µM) of both compounds similarly had no effect.

Inhibition of neurite outgrowth was not associated with significant alterations in α-tubulin, whilst further analysis using anti-pNFH suggested that there may be a change in NFH phosphorylation. In this high throughput part of the study, the employed pNFH antibodies (Ta51 and SMI34), which interact with different phosphorylated epitopes on the c-terminal Lys-Ser-Pro (KSP) repetitive region of NFH, demonstrated different results in the cell ELISA (Shaw, 1991, Lichtenberg-Kraag et al., 1992, Sihag et al., 2007). Using cell-based ELISA, the binding of anti-SMI34 antibody showed that the levels of phosphorylation at the epitope of NFH it recognises were unaffected in pre-differentiated N2a cells after CPF and CPO exposure. However, the binding levels of Ta51 antibody demonstrated a significant increase in NFH phosphorylation at 2 h and a subsequent decrease at 8 h in pre-differentiated N2a cells treated with 3 and 10 µM CPF and CPO. The quantitative changes on cell ELISA for this antibody are consistent with previously observed results (chapter 4) where Western blots probed with Ta51 antibody were used to evaluate the effects of 3 µM concentration of both OPs on pNFH in pre-differentiated N2a cells. These findings suggest that the amount of phosphorylation at the Ta51 epitope changed much more than that at the SMI34 epitope.

The discrepancy between the SMI34 and Ta51 antibodies demonstrated in the cell ELISA may be due to different effects, possibly by different kinases, at different phosphorylation sites on NFH. However, this finding cannot alter the fact that there were detectable alterations in NFH phosphorylation at both time

points as indicated by Ta51 antibody using two different approaches. Although no significant changes in NFH phosphorylation were observed with SMI34 antibody using cell ELISA, the fact that SMI34 antibody revealed decreases in neurite outgrowth parameters in high throughput studies (Appendix; Figure 8.1-8.4) in the same manner as Ta51 strongly suggests that the retraction of axon-like neurites has occurred in OP-treated cultures.

The observed alterations in pNFH together with the lack of effects on total NFH and α-tubulin at both time points suggest that altered phosphorylation state of NFH is dose dependent and represents a specific target for the inhibitory effects of CPF and CPO on neurite outgrowth in pre-differentiated N2a cells. The observed increase in the reactivity of antibody against pNFH at 2 h and the subsequent decline at 8 h exposure to both OPs suggest that the hyperphosphorylation of NFH at early time point is transient and followed by a reduced phosphorylation state of NFH. This disruption in NFH phosphorylation is similar to those found in N2a cells treated with PSP for 24 h under co-differentiation conditions (Hargreaves et al., 2006). Moreover, the reduction in NFH phosphorylation at 8 h is in agreement with a previous study, which showed reduced levels of pNFH in N2a cells induced to differentiate for 24 h in the presence of TOCP (Fowler et al., 2001). These findings together indicate that neurite inhibitory effects of some OPs are associated with their ability to disrupt the NFH phosphorylation.

As NF subunits accumulate in the axon, they become extensively phosphorylated on the c-terminal domain of NFH. Since phosphorylation of NFH has an important role in axon maturity and stability (Sihag et al., 2007), the changes observed in NFH phosphorylation at 2 and 8 h could indicate a transient hyperphosphorylation of NFH causing disruption in the neurofilament networks or a breakdown in their stability and consequently affecting axon stability. It has also been demonstrated that extensive phosphorylation of KSP regions in NFH results in the formation of sidearm projections, which subsequently affect the interactions of NFs with other NFs (Eyer and Leterrier, 1988) and/or other cytoskeletal elements such as MTs (Hisanaga and Hirokawa, 1990). Additionally, phosphorylation of KSP sites found to decrease the rate of slow

axonal transport and increase the axonal diameter (Hirokawa et al., 1984, de Waegh et al., 1992). Of particular interest is the fact that disruption of the phosphorylation status of NFH has been linked with the axonal degeneration that leads to the development of OPIDN following OP exposure (Suwita et al., 1986, Abou-Donia and Lapadula, 1990, Abou-Donia, 1993a). In this context, Suwita et al. (1986) detected increased phosphorylation of NFH in spinal cord neurofilaments isolated from chicken treated with TOCP as an early event in OPIDN pathogenesis (Suwita et al., 1986). Furthermore, Jortner et al. (1999) demonstrated reduced NFH phosphorylation using a different antibody to pNFH (SMI31) in spinal cords of PSP-treated chickens between 4 days of exposure and the appearance of OPIDN lesions such as degeneration of myelinated nerve fibers (Jortner et al., 1999). The fact that altered NFH phosphorylation has also been described *in vivo* for other OP treatment underlines the capability of the pre-differentiated N2a cell model to predict the *in vivo* delayed toxicity following OP exposure. These findings also suggest that several OPs may be able to disrupt the phosphorylation status of NFH.

The observed alterations in NFH phosphorylation confirmed by the data presented in this chapter are consistent with the possible disruption of MAPK signalling pathways. Thus, the effects of both CPF and CPO on the activation of the MAP kinase ERK1/2, one of the MAP kinase family responsible for NFH phosphorylation during neurite outgrowth in healthy neurons, were further investigated in this study. This is due to that fact that ERK1/2 is activated in N2a cells following induction of cell differentiation by serum withdrawal (Hargreaves et al., 2006) and this activation is essential for neurite outgrowth (Singleton et al., 2000, Lopez-Maderuelo et al., 2001). Additionally, activated ERK1/2 is thought to have a role in NFH phosphorylation, by phosphorylating the KSP repeats located in NFH protein (Veeranna et al., 1998). In the current study, 2 h exposure to 3 and 10 µM concentrations of both CPF and CPO was found to increase the levels of anti-pERK antibody with either no detectable change or a slight decrease in the levels of anti-total ERK antibody binding to pre-differentiated N2a cells. These findings suggested that both OP treatments lead to increased activation of ERK, which may explain the observed increase in NFH phosphorylation at the early time point. The lack of significant changes in the

activation of MAP kinase ERK1/2 compared to the control in pre-differentiated N2a cells exposed to the same dose-range CPF and CPO for 8 h indicates that OP-induced activation of ERK was short-lived. The reduced levels of NFH phosphorylation at 8 h with a corresponding decline in the activation ERK 1/2 to control levels at the same time could be due at least partly to a transiently increased activation of ERK 1/2 at 2 h. The fact that increased levels of protein phosphatase activity were found to be associated with decreased NFH phosphorylation in pre-differentiated N2a cells treated with 3 µM concentration of both compounds for 8 h (chapter 4), suggests that increased phosphatase activity could also contribute to the reduced phosphorylation of NFH following 8 h exposure to both CPF and CPO. However, due to a limited supply of phosphatase reagents, the effects of 10 µM CPF and CPO on phosphatase activity at 8 h exposure were not investigated and further work would be needed to identify the specific phosphatases involved in the modulation of NFH phosphorylation in OP-treated cells.

In summary, this chapter demonstrates that high throughput assays can be successfully applied to assess the dose-response effects of CPF and CPO on multiple parameters of neurite outgrowth in pre-differentiated N2a cells. This approach shows that concentration dependent inhibitory effects of both CPF and CPO on neurite number and length, processes and branches occur at concentrations that have no effects on cell number, the latter being in good agreement with the lack of effect on cell viability as determined by MTT reduction. The automated system not only provides rapid analysis but also provides other novel information on neurite outgrowth parameters, not easily detected manually, showing that both compounds inhibit the branching of neurite in a concentration-dependent manner. Consistency with data obtained from MTT reduction and CFSE assays in chapter three, further confirms that manual counting techniques were useful and reliable in detecting the neurite inhibitory neurotoxic effects of both OPs in pre-differentiated N2a cells. The study presented in this chapter also illustrates the value of B512, Ta51 and SMI34 antibodies to detect biomarkers of neurite outgrowth via high throughput assays in the N2a cell model. At a molecular level, the cell-based ELISA developed in this chapter represents a useful alternative and sensitive approach to detect the

dose-response changes in cytoskeletal proteins and associated signalling pathways disrupted by OPs in pre-differentiated N2a cells. Findings from this approach correlate well with Western blot results, showing that neurite outgrowth inhibitory effects of both CPF and CPO are accompanied by significant alterations in the levels of NFH phosphorylation and disruption in the activation status of ERK 1/2. In order to examine whether neurite outgrowth and the cytoskeleton are affected in a similar manner in a more human relevant cell model, the effects of both CPF and CPO on a human neural progenitor cell line are examined in the next chapter. .

6 Testing the effects of chlorpyrifos and chlorpyrifos oxon in a human neural progenitor stem cell model

6.1 Introduction

Although the work presented in this thesis has focused mainly on the toxic effects of CPF and CPO on pre-differentiated N2a cell line of mouse origin, it was also of interest to test the effects of these toxins on cell differentiation in a more human relevant cell model. The benefits of using neural progenitor stem cells derived from human is that measuring neurite outgrowth in a cellular model that more closely resembles the complexity of the human nervous system neurons *in situ*, can be more effective at predicting the chemical-related changes *in vivo* (Radio and Mundy, 2008).

Neural stem cells were first isolated from different regions of embryonic human brain (Vescovi et al., 1999). Recent advances have also led to the isolation of human neural progenitor stem cells from the neocortex region in adult nervous system (Richardson et al., 2006). Since then the human neural progenitor stem cells have become valuable tools for neuroscience research. Evaluating the toxicity of xenobiotics on human neural cells can reduce the level of uncertainty associated with cells derived from animal models (Donato et al., 2007). Earlier research using human neural progenitor stem cells was restricted because of the short life span in culture and the limited capacity to maintain a stable phenotype and genotype across passages (Wright et al., 2006, Donato et al., 2007). Development of immortalised human neural progenitor stem cells using the myc oncogenic transcription factor was highly effective at overcoming these limitations (Dang et al., 1999, Kim, 2004). The ability of these cells to accommodate self-renewal, which generates large numbers of cells, together with their genomic stability is the key advantage of immortalisation using myc technology. These features have facilitated the utilisation of these cells for toxicity screening (Klemm and Schrattenholz, 2004).

An example of such immortalised human neural progenitor stem cell line is the commercially available ReNcell CX cell line (Merck Millipore), which was derived from a 14-week human foetal brain cortex. ReNcell CX cells can differentiate into a mixed population of neurons, astrocytes and oligodendrocytes upon mitogen withdrawal (Donato et al., 2007, Kornblum, 2007). Due to their immortalisation with myc oncogene transduction, these cells have the capacity for self-renewing as they are multipotent, as well as phenotypically and genetically stable (Donato et al., 2007). Thus, ReNcell CX is a useful model for assessing neurotoxicity *in vitro* (Breier et al., 2008). Using high throughput assays, Breier et al. (2008) used ReNcell CX cells in an undifferentiated state to evaluate the effects of chemicals such as lead acetate and methyl mercury chloride on neural stem cell proliferation and viability (Breier et al., 2008). However, chemical-induced changes in neurite outgrowth in differentiated ReNcell CX cells are yet to be investigated. Despite the large number of potential neurotoxicants investigated on ReNcell CX and other human neural progenitor stem cells, to date the effects of CPF and CPO on these cell lines have not been evaluated. Therefore, it was of interest to study the effects of CPF and CPO on a human relevant cell model. It was of further interest to determine whether this human neural progenitor stem cell line, which contains mixture of neuronal and glial cells at early differentiation stage was affected by both compounds in a similar manner as pre-differentiated N2a cells.

To achieve these aims, ReNcell CX cells were utilised as a cell model in the current study. Under post differentiation exposure conditions similar to those applied to N2a cells, cells were exposed to multiple concentrations of CPF and CPO for 2 and 8 h. High throughput screening assays were used to assess the effects of OPs on multiple parameters of neurite outgrowth, and to confirm the expression of mature neural stem cell markers βIII-tubulin, pNFH and GFAP. MTT reduction assays were also used to assess the viability of cells following OP exposure. Additionally, the effects of both compounds on the enzymatic activity of AChE of pre-differentiated ReNcell CX cells were tested at both time points. Finally, cell ELISA assays were carried out to study the molecular mechanism underlying the neurotoxic effects of both CPF and CPO on neurite outgrowth in pre-differentiated ReNcell CX cells.

6.2 Results

6.2.1 Characterisation of differentiated ReNcell CX cells

ReNcell CX cells were induced to differentiate for 20 h before being treated without (0.5% v/v DMSO control) or with 1, 3 and 10 µM CPF or CPO for 2 and 8 h (section 2.2.2). Upon the removal of growth factors from culture medium, ReNcell CX cells are capable of differentiation into a co-culture of neurons, astrocytes and oligodendrocytes (Donato et al., 2007, Kornblum, 2007). To confirm the phenotypes of differentiated ReNcell CX cells, these cells were immunostained with DAPI nuclear counterstain, anti-βIII- tubulin, anti-pNFH (clone Ta51) and anti-GFAP primary antibodies. These antibodies were chosen because βIII-tubulin and pNFH are neuronal-specific markers, which stain the neuronal cell body and neurites (axon and/or dendrites) effectively. GFAP was also selected as it is highly expressed by astrocytes and is considered as a useful marker of astroglial neurotoxicity (Harry et al., 1998). Utilising high throughput screening, the expression of neuronal and glial-specific markers was examined and viewed prior commencing the analysis of neurite outgrowth (section 2.2.16).

Figure 6.1 demonstrated representative images of pre-differentiated ReNcell CX cells. Following 20 h of induction of cell differentiation, ReNcell CX cells were successfully differentiated into subpopulations of developing neuronal and glial cells as indicated by their ability to express neuronal markers βIII-tubulin (Figure 6.1A) and pNFH (Figure 6.1B), and the astroglial-marker GFAP (Figure 6.1C). Pre-differentiated ReNcell CX cells were positive for all neural cell markers.

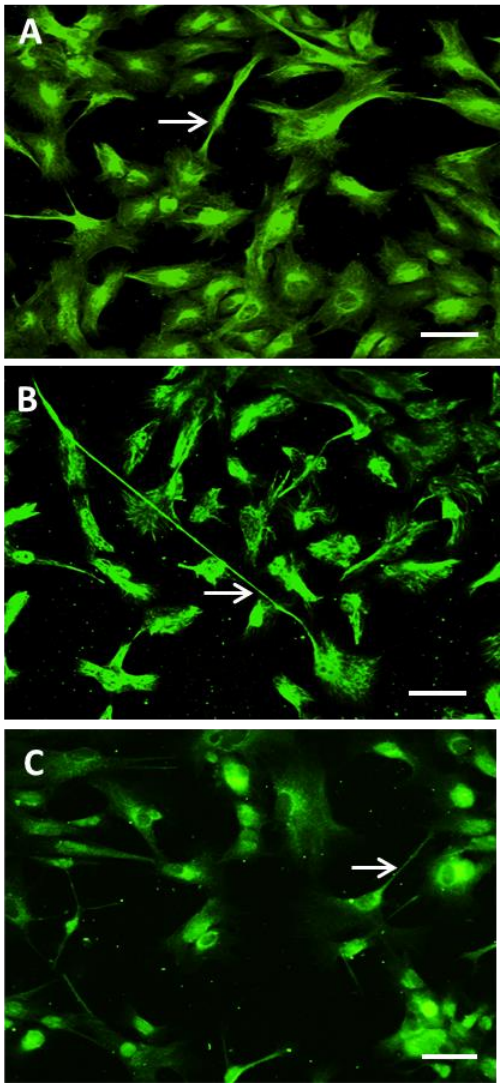

Figure 6.1. Characterisation of differentiated ReNcell CX cell line. Cells were induced to differentiate for 20 h by mitogen removal before being fixed and stained with antibodies recognising the neuronal markers βIII-tubulin (A) and pNFH (B), and the glial marker GFAP (C) followed by Alexa Fluor® 488 conjugated anti-IgG secondary antibodies. The representative images shown are from untreated control cells from a single field of view, with FITC excitation wavelength for neurites and cell bodies (green). Images were acquired using ImageXpress Micro Widefield High Content Screening system and captured using a 10x objective lens and Nikon camera system. Arrows show typical axon-like processes detected in neuronal cells (A and B) and astrocyte extensions (C) in pre-differentiated ReNcell CX cells. Scale bar represents 100 µm.

6.2.2 Effects of CPF and CPO on multiple parameters of neurite outgrowth in pre-differentiated ReNcell CX cells

Using high throughput analysis, the effects of CPF and CPO were assessed over a concentration range of 1-10 µM on multi-parameters of neurite outgrowth in pre-differentiated ReNcell CX cells after 2 and 8 h exposure. The parameters used to determine the effects of both compounds on ReNcell CX cells were similar to those applied in N2a cells experiments, which included cell number, cell body area, neurite number, percentages of cells with significant outgrowth, maximum and average neurite length and mean processes/cell. Additionally, the average intensity of βIII-tubulin, pNFH and GFAP staining within neurites and cell bodies of each antibody-positive cell were evaluated by high throughput assay, as described in section 2.2.16.

Figure 6.2 demonstrates the segmentation of acquired images obtained by high throughput assay employed in this part of the current study. All representative images shown are from untreated control ReNcell CX cells from a single field of view. Image acquisition was performed using two wavelengths; FITC to detect cell body and neurites (green) and DAPI to identify the nucleus of all cells in a field (blue). The resultant merged images showed staining distribution of FITC and DAPI within each cell type. Image segmentation was then performed using MetaXpress offline analysis software and displayed as multicoloured masks tracing the neurites and cell bodies in the acquired image. It can be seen that the staining patterns of antibodies to βIII-tubulin, pNFH and GFAP were accurately detected allowing for the OP-induced effects on multiple parameters of neurite outgrowth in pre-differentiated ReNcell CX cells to be evaluated.

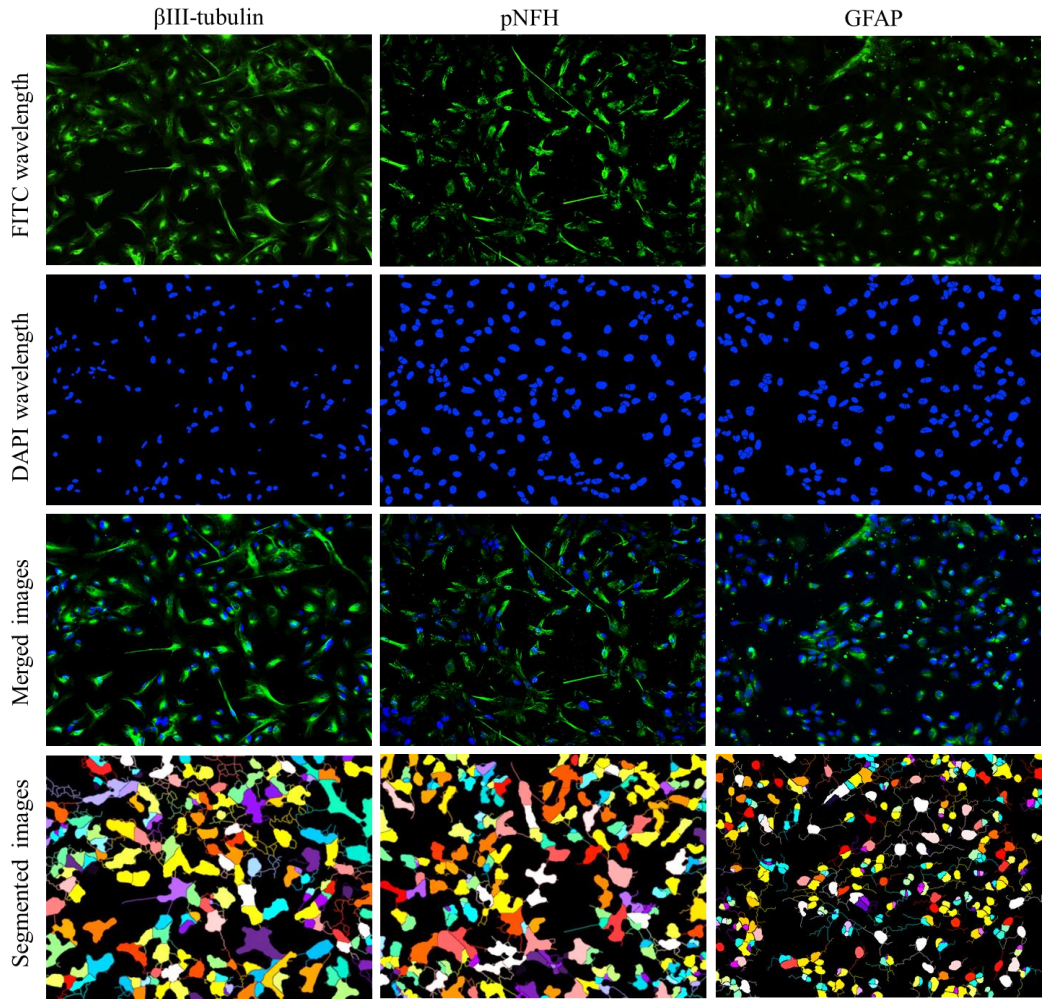

Figure 6.2. Segmentation of stained pre-differentiated ReNcell CX cells using high throughput screening assay. Cells were induced to differentiate for 20 h before being incubated with or without 1, 3 and 10 µM CPF or CPO for 2 and 8 h. Cells were fixed and stained with antibodies recognising the neuronal marker βIII-tubulin and pNFH, and the glial marker GFAP followed by Alexa Fluor® conjugated anti-IgG secondary antibodies. All Images shown were from untreated controls from a single field of view. Acquired images were obtained using ImageXpress Micro system (10x objective) with two wavelengths; FITC for detecting cell bodies and neurites and DAPI for nucleus counting. Segmented images with multicoloured tracing masks on neurites and cell bodies were generated using the Neurite Outgrowth Module within the MetaXpress analysis software for monitoring different parameters of neurite outgrowth including cell number, cell body area and outgrowth length for each identified cell.

Figure 6.3 shows the dose-related effects of CPF and CPO following 2 and 8 h exposure on the average cell number/field and the average cell body area/field in pre-differentiated ReNcell CX cells. The presented high throughput data show that all concentrations of CPF and CPO had no effects on either the average number of both neuronal and glial cells/field or on the average area of cell bodies/field after 2 and 8 h exposure compared to untreated controls, as indicated by the analysis of anti-βIII-tubulin, anti-pNFH and anti-GFAP staining (Figure 6.3A and B).

The average number of non OP-treated neuronal cells/field after 20 h differentiation was between 295 and 271 cells as detected with βIII-tubulin marker and between 225 and 200 cells with Ta51 staining (Figure 6.3A1-A2, A4-A5). The average count of differentiated glial cells ranged between 303 to 246 cells/field in controls, as indicated by anti-GFAP staining (Figure 6.3A3 and A6). Exposure of pre-differentiated ReNcell CX cells to CPF and CPO at all doses had no significant effect on the average number of neuronal or glial cells/field compared to the non OP-treated controls (Figure 6.3A).

Figure 6.3B displays the high throughput measurement of the average cell body area/filed in both neuronal and glial cell populations. It can be seen that the average neuronal cell body area/field is greater than glial cell body area, as indicated by antibody staining of βIII-tubulin and GFAP markers, respectively. The average neuronal cell body area/field measured with Ta51 staining was smaller than that obtained by βIII-tubulin. This is probably due to the fact that Ta51 preferentially stains axons. The data also demonstrated that CPF and CPO at all concentrations had no effect on this parameter following 2 and 8 h exposure compared to non OP-treated controls.

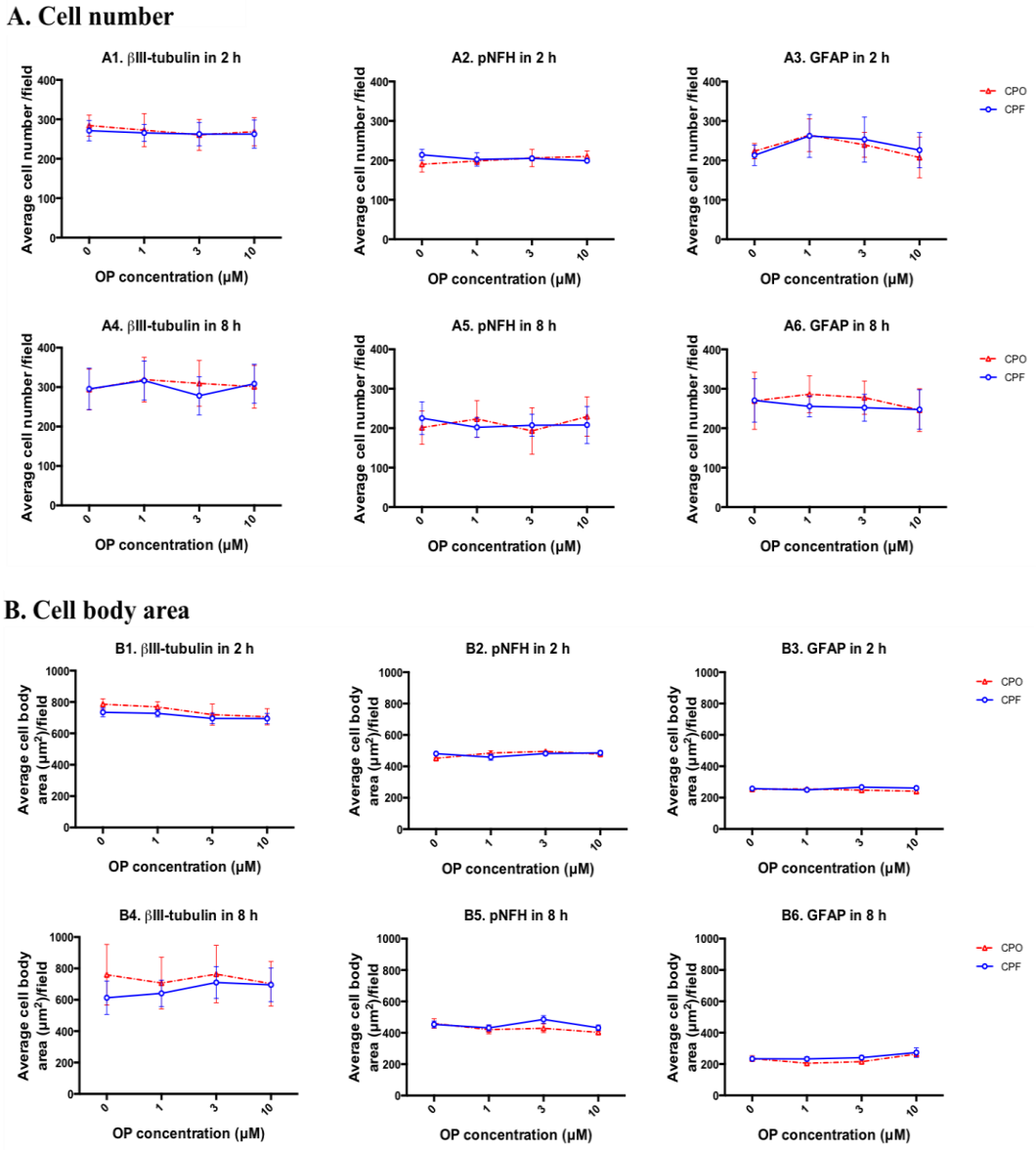

Figure 6.3. Effects of CPF and CPO on cell number and cell body area of pre-differentiated ReNcells CX cells as assessed by high throughput assay. Cells were fixed and stained with antibodies recognising the neuronal markers βIII-tubulin and pNFH, and the glial marker GFAP followed by Alexa Fluor® 488 conjugated anti-IgG secondary antibodies. OP-induced effects on multiple parameters of neurite outgrowth were measured using MetaXpress imaging and analysis software. Data show the dose-related effects of both CPF and CPO on the average cell number/field (A), and the average cells body area/field (B) with βIII-tubulin, pNFH and GFAP staining. The CPF effects are presented as blue solid lines with circles; the CPO effects are presented as red dashed lines with triangles. Data are represented as mean values ± SEM from four independent experiments. Both sets of data were analysed using two-way ANOVA. When SEM bars are not apparent, this means that error is smaller than the symbol size

Specific parameters of neurite outgrowth such as the average number of neurites/field and the percentage of cells with significant outgrowth (cells with neurites longer than 10 µm in length) were also obtained using high throughput assay (Figure 6.4). As demonstrated in figure 6.4A, the data of the average number of neurites/field (dendrites and axons-like processes) suggest that, while the number of neuronal and glial cells/field was unaffected, the average number of neurites in both cells/field was significantly ($p < 0.05$) decreased in OP-treated cells after 8 h exposure compared to controls.

In neuronal cells, the average number of neurites/field (dendrites and axons) in untreated control ranged between 40 and 25 neurites/field as obtained with βIII-tubulin marker (Figure 6.4A1 and A4). The quantitative analysis of Ta51 showed that at least 18 of the detected neurites were axon-like processes in the controls (Figure 6.4A2 and A5). In glial cells, GFAP staining demonstrated 18 to 17 glial-extensions in the non OP-treated controls (Figure 6.4A3 and A6).

Exposure of pre-differentiated ReNcell CX cells to all concentrations of CPF and CPO for 2 h had no effect on the average number of neurites/field generated from neuronal or glial cells when compared to the untreated control (Figure 6.4.A1, A2 and A3). After 8 h treatment, no change was observed in the average number of neurites/field in cells treated with 1 and 3 µM CPF and 1 µM CPO compared to the non OP-treated control as indicated with βIII-tubulin staining. However, the same staining detected a significant ($p < 0.005$) reduction in the average neurite number/field by 24% and 42% in cell treated with 10 µM CPF and CPO, respectively compared to the untreated control (Figure 6.4A4).

As indicated in figure 6.4A5, pNFH staining showed no effects on the average number of axon-like processes/field following 8 h treatment with 1 µM CPF and CPO. However, significant decreases ($p < 0.05$) in the average number of axon-like processes/field were detected with Ta51 staining at 3 and 10 µM concentrations of both compounds after 8 h exposure. The quantitative analysis of Ta51 staining showed that 8 h treatment with 3 µM CPF and CPO caused 20% and 29% decline, respectively compared to the non OP-treated control. In addition, exposing the cells to 10 µM of both compounds for 8 h reduced the

number of axon-like processes/field to 35% with CPF and 52% with CPO when compared to non OP-treated control (Figure 6.4A5).

The quantitative analysis of GFAP presented in figure 6.4A6 showed that CPF and CPO exposure for 8 h cause a significant ($p < 0.01$), concentration-dependent reduction in the number of glial-extensions/field in pre-differentiated ReNcell CX cells compared to the non OP-treated control. At concentrations of 3 and 10 µM CPF, a fall in the average glial-extensions number/field was observed of 26% and 39%, respectively, compared to non OP-treated controls. The average number of glial extensions/field was further reduced compared to non OP-treated controls by 34% and 55% in cells treated with 3 and 10 µM CPO, respectively ($p < 0.05$) (Figure 6.4A6).

Quantification of cells with outgrowths greater than 10 µm in length showed that CPF and CPO are capable of inducing neurite retraction (Figure 6.4B). In the non OP-treated control, βIII-tubulin staining showed 65% to 70% of neuronal cells with significant outgrowth (outgrowth length >10 µm) including dendrites and axon-like processes. However, only 40% of neuronal cells contain axon-like processes as indicated with Ta51 staining. After 2 h exposure to both compounds, the percentage of βIII-tubulin-positive neuronal cells with outgrowth greater than 10 µm fell significantly ($p < 0.05$) by 8% and 16% of control value at 3 and 10 µM, respectively (Figure 6.4B1). This percentage was further significantly ($p < 0.05$) reduced by 15% and 23% of control value following 8 h treatment with 3 and 10 µM concentrations of both compounds, respectively (Figure 6.4B4). The quantitative analysis of Ta51 staining demonstrated that CPF and CPO induced a significant, dose-dependent decrease in the number of neuronal cells with axon-like processes in cultures of pre-differentiated ReNcell CX cells, although the observed reduction after 2 h exposure to both compounds was similar to that detected at 8 h. As indicated in figure 6.4B2 and B5, no effect was observed in the percentages of cells with significant outgrowth after exposure to 1 µM CPF. However, CPF at 3 and 10 µM caused significant ($p < 0.05$) reduction by 24% and 33% of untreated control value, respectively. Similarly, exposure to CPO at 1, 3 and 10 µM resulted in 12%, 25% and 39% inhibition, respectively ($p < 0.05$) (Figure 6.4B2 and B5).

The quantitative analysis of GFAP staining in figure 6.4B3 and B6 showed that CPO at all doses and CPF at 3 and 10µM had the ability to interfere with the length of glial cell extensions in cultures of pre-differentiated ReNcell CX cells. As indicated in figure 6.4B3, exposure to 10 µM CPF and CPO significantly ($p < 0.0001$) reduced the percentage of glial cells with extensions > 10µm by 23% and 40%, respectively compared to the non OP-treated control at 2 h. Increasing the exposure time to 8 h, resulted in 44% and 50% decrease in the percentage of glial cells with significant extensions compared to untreated controls (Figure 6.4B6).

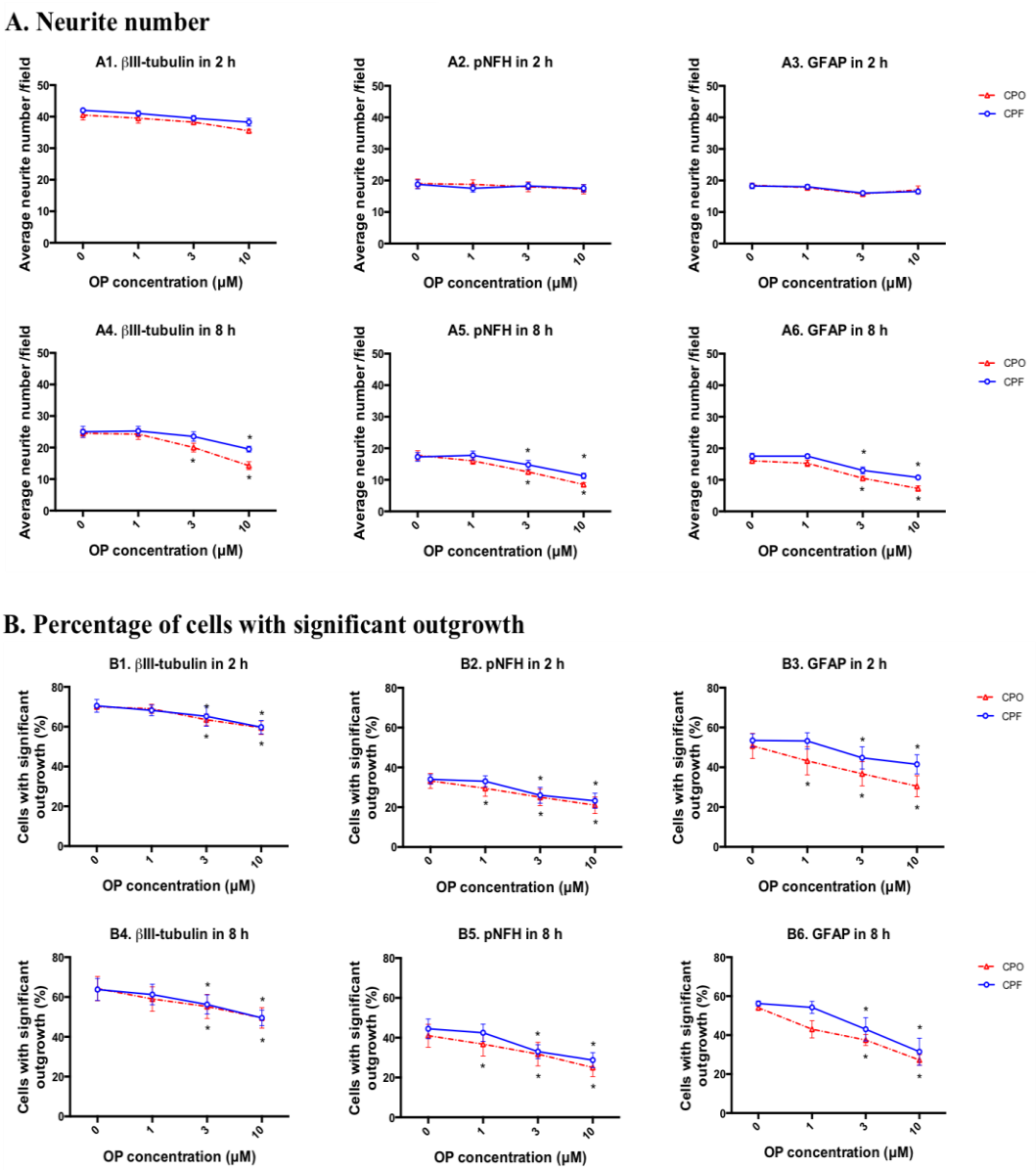

Figure 6.4. Effects of CPF and CPO on neurite number and percentage of cells with significant outgrowth in pre-differentiated ReNcells CX cells as assessed by high throughput assay. Cells were fixed and stained with antibodies recognising the neuronal markers βIII-tubulin and pNFH, and the glial marker GFAP followed by Alexa Fluor® 488 conjugated anti-IgG secondary antibodies. OP-induced effects on multiple parameters of neurite outgrowth were measured using MetaXpress imaging and analysis software. Data show the dose-related effects of both CPF and CPO on the average neurite number/field (A), and the number of cells with significant outgrowth (%) (B) with βIII-tubulin, pNFH and GFAP staining. The CPF effects are presented as blue solid lines with circles; the CPO effects are presented as red dashed lines with triangles. Data are represented as mean values ± SEM from four independent experiments. Both sets of data were analysed using two-way ANOVA. Asterisks demonstrate changes that are statistically different from the non OP-treated controls (*$p < 0.05$). When SEM bars are not apparent, this means that error is smaller than the symbol size.

High throughput analysis further revealed the maximum length of neurites per each neuronal and glial cell after 20 h of differentiation. With βIII-tubulin staining, the maximum length of neurites in non OP-treated control ranged between 10 to 14 µm (Figure 6.5A1 and A4), whereas the maximum length of Ta51-positive-neurites was 22 µm (Figure 6.5A2 and A5). In GFAP positive cells, the maximum length of glial extensions ranged between 17-22 µm in untreated controls (Figure 6.5A3 and A6).

As illustrated in figure 6.5A, there was a significant dose and time-dependent reduction in the maximum neurite length per cell for both neurons and glia in cultures of pre-differentiated ReNcell CX cells following CPF and CPO exposure for 2 and 8 h. The analysis of βIII-tubulin staining demonstrated that after 2 h treatment, the maximum length of neurites per neuronal cell was significantly reduced by approximately 16% and 33% at 3 and 10 µM CPF, respectively, and by 18% and 28% at 3 and 10 CPO, respectively ($p < 0.0001$) (Figure 6.5A1). A greater reduction in the maximum neurite length per neuronal cell was observed following 8 h exposure to CPF and CPO. Treatment with 3 and 10 µM CPF resulted in 20% and 39% decrease, respectively ($p < 0.0001$), while CPO exposure at 3 and 10 µM concentrations caused 33% and 49% decline, respectively ($p < 0.0001$) (Figure 6.5A4). However, both compounds at 1 µM had no significant effects upon this parameter at either time points (Figure 6.5A1 and A4).

Similar effects of CPF and CPO on the maximum length of Ta51-positive (axon-like) neurites was also observed. At concentrations of 1, 3 and 10 µM, CPO was found to induce a significant inhibitory effect on the maximum length of axons/neuronal cells in pre-differentiated ReNcell CX cells after both 2 and 8 h exposure, with 10 µM CPO causing 39% and 43% reduction, respectively ($p < 0.0001$) compared to the non OP-treated control (Figure 6.5A2 and A5). Although CPF at 1 µM had no effect on the maximum length of such neurites after 2 and 8 h exposure, concentrations of 3 and 10 µM caused significant reductions of 11% ($p < 0.05$) and 20% ($p < 0.0001$) compared to controls at both time points (Figure 6.5A2 and A5).

Measurements of glial cells extension length were also obtained using high throughput with the aid of GFAP staining. As demonstrated in figure 6.5A3 and A6, the maximum length of astrocyte extensions/cell ranged between 17 to 22 µm in untreated controls. Exposure of pre-differentiated ReNcell CX cells to CPF and CPO for 2 and 8 h caused a significant ($p < 0.05$), dose- and time-dependent decrease in the maximum neurite length per glial cell compared to non OP-treated controls (Figure 6.5A3 and A6). The data in figure 6.5A3 indicated that 2 h exposure to CPF at 1 and 3 µM, and CPO at 1 µM concentrations caused a slight but not significant reduction in the maximum neurite length/cell compared to the untreated controls. However, a significant ($p < 0.05$) decline was observed at 10 µM CPF (24% decrease), 3 and 10 µM CPO (28% and 36% decline, respectively) compared to the maximum neurite length/cell in the non OP-treated controls (Figure 6.5A3).

Figure 6.5A6 show that, after 8 h treatment, the maximum neurite length/glial cell was further decreased compared to untreated controls, with 3 and 10 µM CPF causing 20% and 27% reduction, respectively. In addition, it can be seen that all concentrations of CPO (1, 3 and 10 µM) significantly ($p < 0.0001$) reduced the length of GFAP-positive extension outgrowth by 13%, 29% and 42%, respectively compared to the non OP-treated control (Figure 6.5A6).

The data in figure 6.5B demonstrated that both compounds significantly ($p < 0.05$) decreased the average neurite length per cell in pre-differentiated ReNcell CX cells in a similar manner as the maximum neurite length per cell at both time points. With βIII-tubulin staining, the average length of neurites/cell in non OP-treated control ranged between 8 to 5 µm (Figure 6.5B1 and B4). After 2 h treatment, this parameter was significantly reduced by approximately 12.5% and 25% at 3 and 10 µM CPF, respectively and by 20%, 36% and 47% at 1, 3 and 10 CPO, respectively ($p <0.05$) (Figure 6.5B1). However, no effect was observed on the average neurite length per cell after 2 h exposure with 1 µM CPF (Figure 6.5B1). A greater reduction in the average neurite length per neuronal cell was observed following 8 h exposure to CPF and CPO. Treatment with 10 µM CPF resulted in 41% decrease ($p < 0.001$), while CPO exposure at 3 and 10 µM concentrations caused 36% and 50% decline ($p < 0.0001$), respectively compared

to the non OP-treated controls (Figure 6.5B4). However, both compounds at 1 µM and CPF at 3 µM had no significant effects upon this parameter at 8 h exposure (Figure 6.5B4).

The analysis of Ta51 staining demonstrated that CPF at 1 and 3 µM had no effects on the average length of neurites per neuronal cell after 2 h exposure (Figure 6.5B2). However, this parameter was significantly reduced by approximately 20% at 10 µM CPF ($p < 0.01$), and by 14% ($p < 0.02$), 24% ($p < 0.001$), and 38% ($p < 0.0001$) at 1, 3 and 10 CPO, respectively compared to the non OP-treated control (Figure 6.5B2). After 8 h treatment, the average length of neurites per neuronal cell was significantly decreased by approximately 17% and 37.5% at 3 and 10 µM CPF, respectively, and by 26%, 38% and 47% at 1, 3 and 10 CPO, respectively ($p < 0.0001$) (Figure 6.5B5). However, no significant change was observed on the average neurite length per cell after 8 h exposure with 1 µM CPF (Figure 6.5B5).

Figure 6.5B3 and B6 show that the average length of astrocyte extensions/cell ranged between 10 to 12 µm in the non OP-treated controls. Exposure of pre-differentiated ReNcell CX cells to CPF and CPO for 2 and 8 h caused a significant ($p < 0.05$), concentration-dependent decrease in the average neurite length per glial cell compared to the non OP-treated controls. As indicated in figure 6.5B3, CPF exposure at 3 and 10 µM concentrations significantly ($p < 0.0001$) reduced this parameter by 16% and 27%, respectively compared to the non OP-treated control at 2 h. In addition, exposure of cells to all concentrations of CPO (1, 3 and 10 µM) significantly ($p < 0.0001$) decreased the average length of GFAP-positive neurite by 12.5%, 25% and 35%, respectively compared to the non OP-treated control at the same time point (Figure 6.5B3). Similar levels of reduction in the average neurite length per neuronal cell were also observed following CPF and CPO exposure for 8 h (Figure 6.5B6). Treatment with 3 and 10 µM CPF resulted in 11% and 29% decrease ($p < 0.01$), respectively, while CPO exposure at 1, 3 and 10 µM concentrations caused 9%, 25.5%, and 40% decline ($p < 0.01$), respectively compared to the non OP-treated controls (Figure 6.5B6). However, CPF at 1 µM had no significant effects upon this parameter at both time points (Figure 6.5B3 and B6).

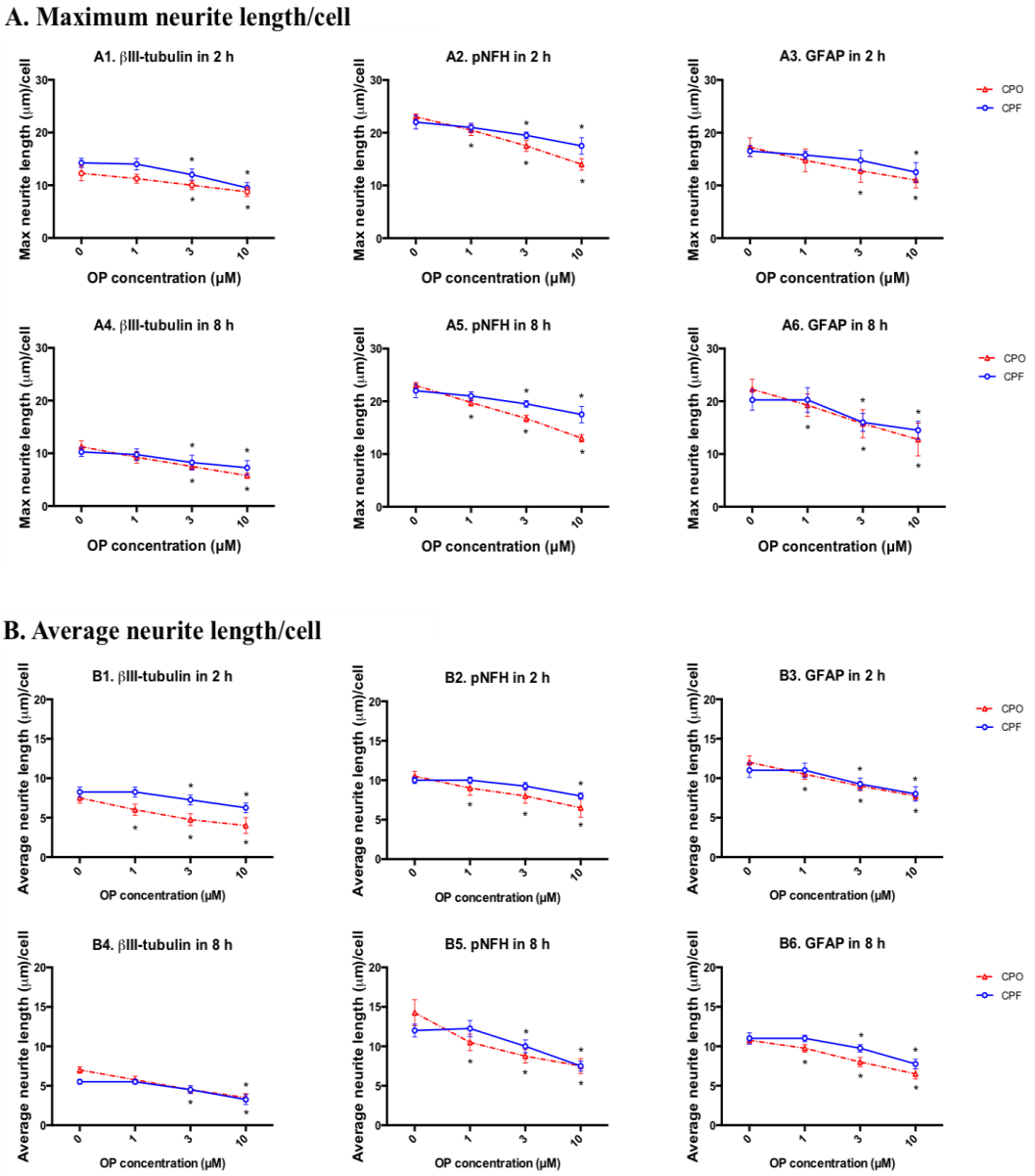

Figure 6.5. Effects of CPF and CPO on the maximum and average neurite length per cell in pre-differentiated ReNcells CX cells as assessed by high throughput assay. Cells were fixed and stained with antibodies recognising the neuronal markers βIII-tubulin and pNFH, and the glial marker GFAP followed by Alexa Fluor® 488 conjugated anti-IgG secondary antibodies. OP-induced effects on multiple parameters of neurite outgrowth were measured using MetaXpress imaging and analysis software. Data show dose-related effects of both CPF and CPO on maximum neurite length/cell (A), and average neurite length/cell (B) with βIII-tubulin, pNFH and GFAP staining. The CPF effects are presented as blue solid lines with circles; the CPO effects are presented as red dashed lines with triangles. Data are represented as mean values ± SEM from four independent experiments. Both sets of data were analysed using two-way ANOVA. Asterisks indicate changes that are statistically different from the non OP-treated controls (*$p < 0.05$). When SEM bars are not apparent, this means that error is smaller than the symbol size.

The impacts of multiple concentrations of CPF and CPO on the mean number of processes per cell were also evaluated using high throughput analysis. As indicated in figure 6.6A, staining of pre-differentiated ReNcell CX cells with βIII-tubulin, pNFH and GFAP showed that there were no overall changes on this parameter of neurite outgrowth following exposure to all doses of CPF and CPO for 2 or 8 h. Approximately 3 processes/cell were detected with anti-βIII-tubulin. However, only one per cell was detected by Ta51 staining. This observation indicates that there were more dendrites than axons, which is a typical characteristic of differentiated neuronal cells. GFAP staining detected one extension per glial cell, which remained the same after 2 and 8 h exposure to both OPs.

Data in figure 6.6B1 and B4 show that there was no significant change in the average intensity of βIII-tubulin staining within neuronal cells after CPF and CPO treatment for 2 and 8 h compared to untreated controls. The data in figure 6.6B3 and B6 demonstrate that the average intensity of GFAP staining within glial cells was slightly but not significantly increased after both OP treatment for 2 and 8 h compared to control. By contrast, a dose-dependent decrease in the average intensity of Ta51 within neuronal cells was observed in OP-treated cells following 2 and 8 h exposure compared to untreated control (Figure 6.6B2 and B5). After 2 h exposure to both compounds, this reduction was statistically significant ($p < 0.0001$) at 3 and 10 µM causing 18% and 28% decline, respectively compared to untreated control (Figure 6.6B2). Further reduction was also observed in the average intensity of Ta51 staining after 8 h, which was significant ($p < 0.0001$) at 3 and 10 µM CPF (11% and 19.5%, respectively) and 1, 3, 10 µM CPO causing 8.5%, 19% and 28% decrease, respectively (Figure 6.6B5).

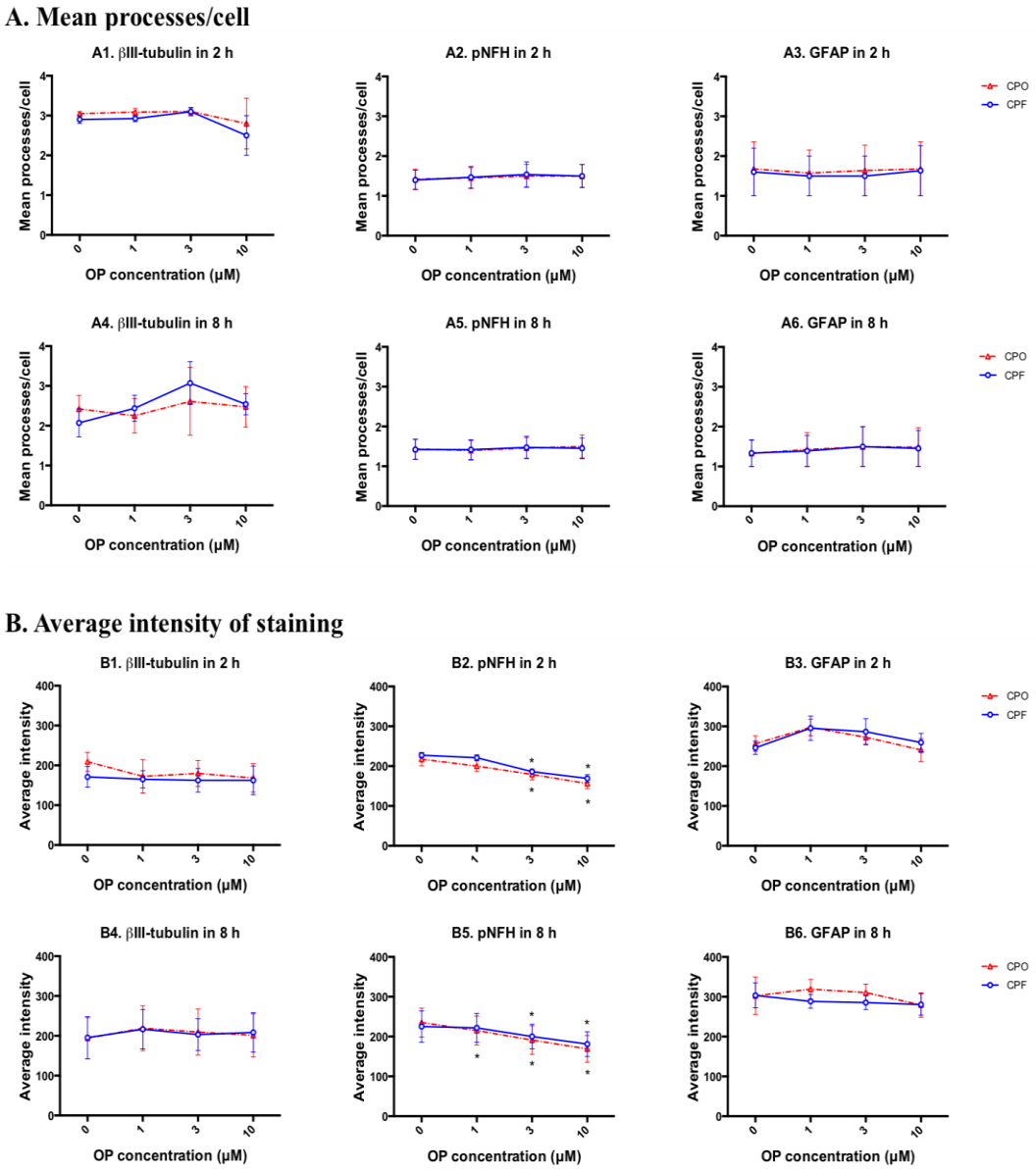

Figure 6.6. Effects of CPF and CPO on the mean number of processes per cell and staining intensity in pre-differentiated ReNcells CX cells as assessed by high throughput assay. Cells were fixed and stained with antibodies recognising the neuronal markers βIII-tubulin and pNFH, and the glial marker GFAP followed by Alexa Fluor® 488 conjugated anti-IgG secondary antibodies. OP-induced effects on multiple parameters of neurite outgrowth were measured using MetaXpress imaging and analysis software. Data show dose-related effects of both CPF and CPO on mean processes/cell (A), and average staining intensity (B) with βIII-tubulin, pNFH and GFAP staining. The CPF effects are presented as blue solid lines with circles; the CPO effects are presented as red dashed lines with triangles. Data are represented as mean values ± SEM from four independent experiments. Both sets of data were analysed using two-way ANOVA. Asterisks indicate changes that are statistically different from the non OP-treated controls (*$p < 0.0001$). When SEM bars are not apparent; it means that the error is smaller than the symbol size.

6.2.3 Effects of CPF and CPO on the viability of pre-differentiated ReNcell CX cells

To examine the viability of pre-differentiated ReNcell CX cells after being exposed to both OPs, MTT reduction assays were performed, as described in section 2.2.7. Figure 6.7 shows the concentration-related effects of CPF and CPO after 2 and 8 h exposure in pre-differentiated ReNcell CX cells. The data indicated that all concentrations of CPF and CPO tested had no significant effect on MTT reduction in pre-differentiated ReNcell CX cells when compared to the untreated controls at both time points (Figure 6.7A and B).

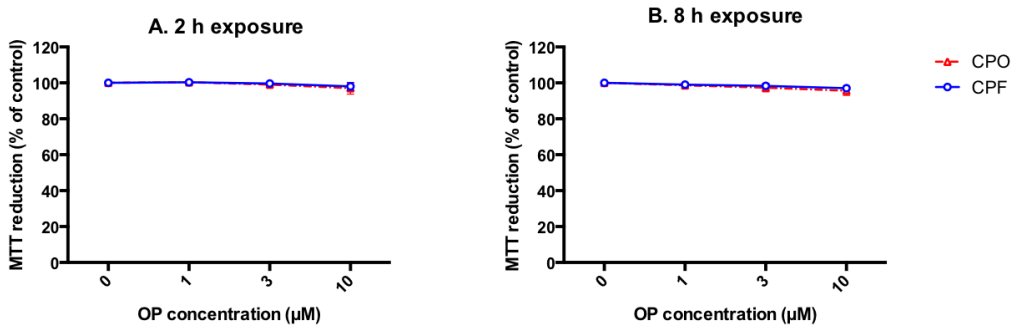

Figure 6.7. Effects of CPF and CPO on MTT reduction in pre-differentiated ReNcell CX cell. After 20 h of differentiation, ReNcell CX cells were treated without (0.5% v/v DMSO control) or with 1, 3 and 10 µM CPF or CPO for 2 and 8 h. The effects of both compounds on MTT reduction were measured to evaluate cell viability after 2 h (A) and 8 h (B) exposure. Data are expressed as a percentage of the non-OP treated control ± SEM from four separate experiments. Data were analysed using one way ANOVA. The CPF effects are presented as blue solid lines with circles; the CPO effects are presented as red dashed lines with triangles. The lack of asterisks reflect the fact that no statistically significant changes were found in MTT reduction in OP-treated cells compared to the untreated controls at both time points. When SEM bars are not apparent, this means that the error is smaller than the symbol size.

6.2.4 Effects of CPF and CPO exposure on AChE activity in pre-differentiated ReNcell CX cells

To determine whether the observed morphological changes in pre-differentiated ReNcell CX cells could be related to an effect on the acute toxicity target AChE, the impact of CPF and CPO on the activity of AChE was assessed, as explained in section 2.2.9.

After 2 and 8 h exposure, it can be seen that CPF at 1 and 3 µM had no significant effect on AChE activity of pre-differentiated ReNcell CX cells compared to non OP-treated controls (Figure 6.8A and B). In contrast, CPF at higher concentration (10 µM) significantly decreased the specific activity of AChE of pre-differentiated RenCell CX cells by 24% and 20% following 2 and 8 h exposure, respectively compared to the control value ($p = 0.01$). Exposure of pre-differentiated ReNcell CX cells to CPO was also found to cause a considerable dose-dependent inhibition in the AChE activity, with 1, 3, and 10 µM causing 47%, 58.5%, and 67% reduction after 2 h and 35.5%, 50%, and 62.5% inhibition after 8 h exposure compared to the untreated controls ($p < 0.0001$). As expected, CPO was found to be more potent in inhibiting the AChE activity compared to CPF, with an IC_{50} value (concentration that caused 50% inhibition in AChE) of approximately 1-2 µM at 2 and 8 h exposure.

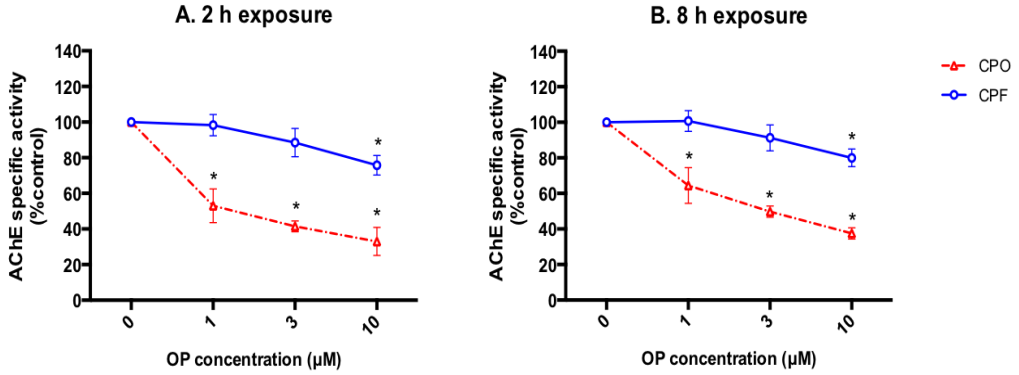

Figure 6.8. Effects of CPF and CPO on AChE activity in pre-differentiated ReNcell CX cells. Cells were induced to differentiate for 20 h before being incubated without (0) or with or 1, 3 and 10 µM concentration of CPF and CPO for 2 and 8 h, after which, AChE activity was measured. Enzyme specific activity is expressed as a percentage of the absorbance change/mg protein/min value of the corresponding control ± SEM from four separate experiments. The CPF effects are presented as blue solid lines with circles; the CPO effects are presented as red dashed lines with triangle. Asterisks indicate statistically significant changes compared to the corresponding non OP-treated controls (*p = 0.01 with CPF) (*p < 0.0001 with CPO).

6.2.5 Effects of CPF and CPO on cytoskeletal proteins and associated cell signaling pathways in pre-differentiated ReNcell CX cells

The neurotoxic effects of CPF and CPO on neurite outgrowth parameters in pre-differentiated ReNcell CX were further studied by evaluating the molecular changes in cytoskeletal proteins and developmentally related cell signalling pathways. Cell ELISAs were employed to determine and quantify OP-induced changes in the binding of antibodies recognising total βIII-tubulin (clone 2G10), GFAP (clone GA5), pNFH (clone Ta51), total NFH (clone N52), total ERK (K-23) and pERK (clone E-4) after 2 and 8 h exposure, as described in section 2.2.15. Results with anti-GFAP antibody were omitted from this study as poor absorbance values were detected in untreated controls. The very low values were considered unreliable to perform accurate qualitative analysis for the effects of CPF and CPO on GFAP protein.

As demonstrated in figure 6.9A and C, there were no significant changes in antibody binding to βIII-tubulin and total NFH in pre-differentiated ReNcell CX cells treated with all three concentrations of CPF or CPO at 2 and 8 h compared to the non OP-treated controls. In contrast to the unchanged levels of total NFH reactivity, the binding level of pNFH was significantly decreased in OP-treated cells compared to the untreated control (Figure 6.9B1 and B2; $p < 0.05$). After 2 h treatment, it was demonstrated that 1 µM CPF and CPO had no effect on the binding level of pNFH compared to the level in the non OP-treated control. However, both compounds at 3 and 10 µM caused a significant decline in NFH phosphorylation levels compared to the non OP-treated control at 2 h exposure (Figure 6.9B1). The 8 h exposure of pre-differentiated ReNcell CX cells to all concentrations of CPO and 3 and 10 µM CPF was also found to cause a significant reduction in pNFH levels compared to the level in untreated control (Figure 6.9B2). However, no significant change was observed on the levels of pNFH compared to non OP-treated control after 8 h exposure with 1 µM CPF (Figure 6.9B2).

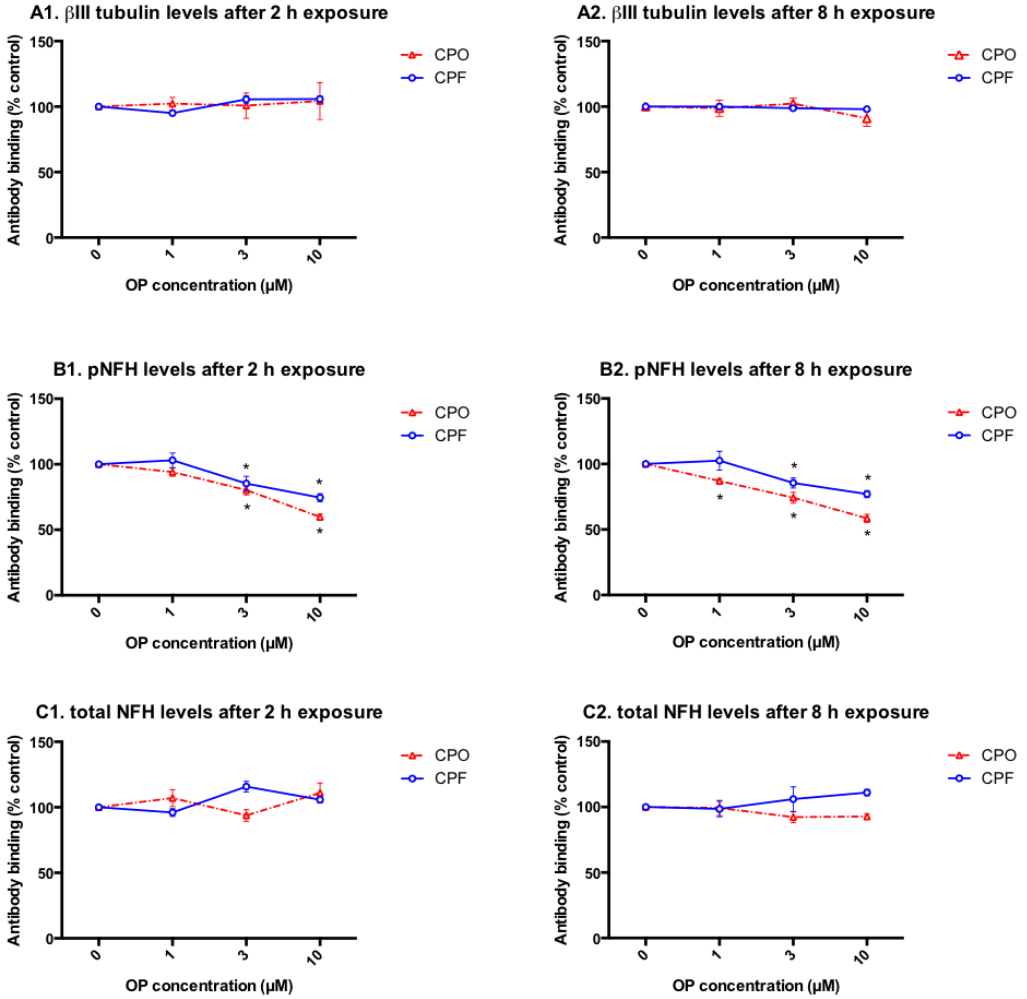

Figure 6.9. Effects of CPF and CPO on cytoskeletal proteins in pre-differentiated ReNcell CX cells as determined by cell ELISA. Cells were induced to differentiate for 20 h before being incubated without (0) or with 1, 3 and 10 μM concentrations of CPF or CPO for 2 and 8 h. Changes in the binding levels of antibodies recognising βIII-tubulin (panel A), pNFH (panel B) and total NFH (panel C) were quantified in fixed monolayers using cell ELISA. Data are presented as a percentage of the non OP-treated control ± SEM from four independent experiments at both time points. Data were analysed using one way ANOVA. The CPF effects are presented as blue solid lines with circles; the CPO effects are presented as red dashed lines with triangles. Asterisks indicate changes that are statistically different from the non OP-treated controls ($p < 0.05$). When SEM bars are not apparent, this means that the error is smaller than the symbol size.

With regard to the effects of OPs on the ERK1/2 MAP kinase signalling transduction pathway, it can be seen that dose-range CPF and CPO had no effect on the binding of antibodies recognising total ERK nor pERK in pre-differentiated ReNcell CX cells treated for 2 or 8 h (Figure 6.10A and B).

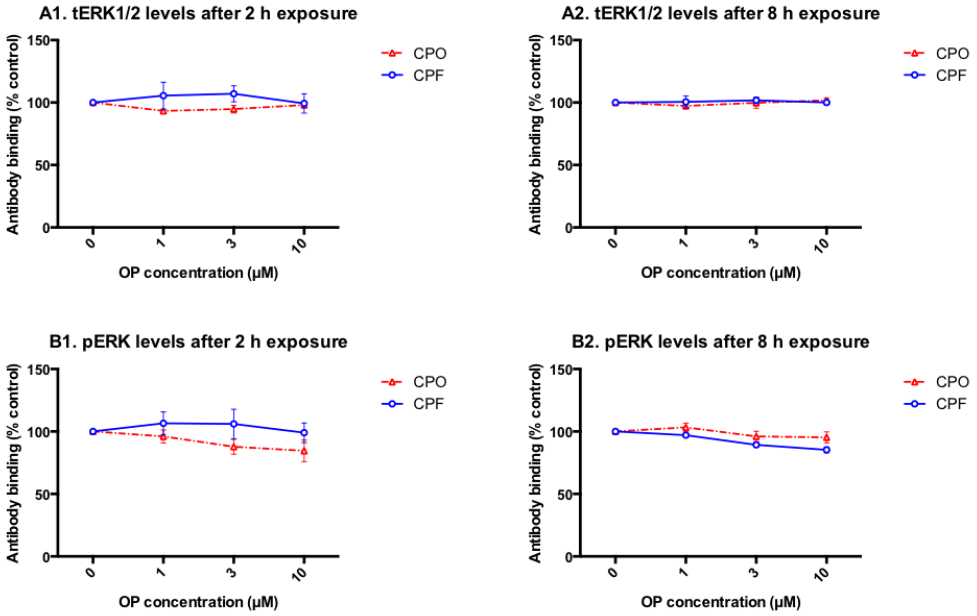

Figure 6.10. Effects of CPF and CPO on the activation status of ERK1/2 MAP kinase in pre-differentiated ReNcell CX cells as determined by cell ELISA. Cells were induced to differentiate for 20 h before being incubated without (0) or with 1, 3 and 10 µM concentrations of CPF or CPO for 2 and 8 h. Changes in the binding levels of antibodies recognising total ERK (K-23) (panel A) and phosphorylated ERK (K-4) (panel B) were quantified in controls and OP-treated cells using cell ELISA. Data are presented as a percentage of the non OP-treated control ± SEM from four independent experiments at both time points. Data were analysed using one way ANOVA. The CPF effects are presented as blue solid lines with circles; the CPO effects are presented as red dashed lines with triangles.When SEM bars are not apparent, this means that the error is smaller than the symbol size.

6.3 Discussion

The utilisation of human neural stem cells for neurotoxicity screening has been demonstrated in a number of earlier studies (Breier et al., 2008, Mundy et al., 2010, Krug et al., 2013, Wilson et al., 2014). The majority of these reports used undifferentiated human-derived neural progenitor cells (Breier et al., 2008) or differentiated human-derived neuronal cells only (Wilson et al., 2014). In contrast, the current study utilised human ReNcell CX cells, which differentiate into a co-culture of neuronal and glial cells providing a more relevant model of the central nervous system. Simulating the same differentiation conditions and OP exposure as the N2a cell model (Chapters 3, 4 and 5), the current work provided novel information to the literature in terms of the effects of CPF and CPO on pre-formed neurites in ReNcell CX cells.

The current study indicated that ReNcell CX cells were successfully differentiated into a mixed population of neuronal and glial cells, which exhibited extensive developing neurite network upon 20 h of growth factor removal. The characterisation of pre-differentiated ReNcell CX cell morphology was confirmed by the expression of βIII-tubulin, pNFH and GFAP neural cell markers using high throughput assay. Induction of ReNcell CX cells differentiation by mitogen withdrawal is in agreement with previous studies, which identified the neuronal and glial cell population using βIII-tubulin and GFAP as biomarkers (Donato et al., 2007).

The high throughput data presented in this study showed that both CPF and CPO at all concentrations had no effect on the average cell number or cell body area of neuronal and glial cells per field following 2 and 8 h of exposure. This result was further supported by MTT reduction assay, which clearly showed that the dose-range used of both compounds had no effect on pre-differentiated ReNcell CX cell viability at both time points. The observed lack of both compounds on cell number, cell body area and viability suggested that the range of CPF and CPO concentrations employed, as for N2a experiments, was sub-cytotoxic towards pre-differentiated ReNcell CX cells and that impacts on neurite

outgrowth was a direct response to their neurotoxicity rather than a consequence of cytotoxicity.

The concentration-dependent reduction in neurite length in pre-differentiated ReNcell CX cells induced by treatment with sub-cytotoxic concentrations of both CPF and CPO was seen as early as 2 and 8 h after exposure. The observed changes in maximum and average neurite length, and number of neurites via analysis of antibody reactivity with βIII-tubulin, pNFH and GFAP suggested that both compounds caused a significant and rapid retraction of dendrites, axon-like processes and extensions in neuronal and glial cells in this co-culture system. This possibility was further confirmed by the observation that there were fewer cells with significant outgrowth under the same conditions. Collectively, high-throughput analysis indicated that exposure to sub-cytotoxic concentrations of both compounds has the ability to induce a retraction of neurites in both neuronal and glial cells.

The observed reduction in neurite outgrowth in pre-differentiated ReNcell CX cells is consistent with those reported earlier in pre-differentiated N2a cells (Chapter 5) using similar experimental conditions and data analysis techniques. The current finding is also in agreement with the study of Sachana et al. (2001), who found a 50% impairment in the outgrowth of axon-like processes in pre-differentiated N2a cell model following 4 and 8 h exposure to 3 µM CPF (Sachana et al., 2001, Sachana et al., 2005). Additionally, Flaskos et al. (2011) used similar CPO concentrations to those applied in the current study and found that, when added at the point of induction of N2a cell differentiation, CPO reduced the outgrowth of axon-like processes in a dose-dependent manner after 24 h exposure (Flaskos et al., 2011). The demonstrated inhibitory effect of CPF and CPO in glial-extensions were also determined in a previous study by Sachana et al. (2008), in which a similar concentration range of both compounds (1-10 µM) was able to inhibit the extension outgrowth produced from differentiating rat C6 glioma cells after 24 h exposure (Sachana et al., 2008). However, this is the first time that the effect of CPF and CPO towards neurite outgrowth was investigated in a human neural stem cell based model that contains a mixed population of neuronal and glial cells.

The high throughput data analysis also showed that 2 and 8 h exposure to both compounds had no effect on the staining intensity of anti-βIII-tubulin and anti-GFAP, which is consistent with the lack of effect observed on neuronal and glial cell numbers and cell body area. This suggests that there was no change in the synthesis of these antigens or in the way they were distributed in their corresponding cell types. However, the staining intensity with Ta51, which recognises pNFH was reduced in OP-treated cells. Since neuronal cell count and cell body area were unaffected, the reduced intensity of Ta51 staining may have reflected a decrease in pNFH localisation in neurites, which is consistent with the observed reduction in neurite length following CPF and CPO treatment at both time points.

Quantification of OP-induced changes in cytoskeletal proteins obtained by cell ELISA showed unchanged levels of βIII-tubulin in pre-differentiated ReNcell CX cells after CPF and CPO exposure for 2 and 8 h. The lack of an effect on βIII-tubulin level again suggested no overall changes in the synthesis of this neuron specific tubulin isoform. This finding was consistent with high throughput screening data using anti-βIII-tubulin staining which showed no change in neuronal cell number, cell body area or staining intensity in cells incubated with antibody to this isoform. In pre-differentiated N2a cells, the levels of both α and β-tubulin were also found to be unaltered after 2 and 8 h treatment with similar concentrations of CPF and CPO (Chapter 4 and 5). Evidence of unchanged level of α and β-tubulin subunits in pre-differentiated N2a cells and C6 glial cell lines following similar exposure time with CPF and CPO was also demonstrated in a number of previous studies (Sachana et al., 2001, Sachana et al., 2005, Sachana et al., 2008). Moreover, exposure of cells to other OPs such as PSP, diazinon and to the pyrethroid cypermethrin under both co- and post-differentiation exposure conditions were found to have no effect on tubulin levels (Hargreaves et al., 2006, Flaskos et al., 2007).

During neuronal development, α and β-tubulin are the main constituents of MT structure, which have an essential role in cell differentiation and neurite outgrowth (Easter et al., 1993). Reduction in the levels of tubulin subunits after CPF and CPO exposure could indicate a disruption in the MT network due to

reduced subunit and/or polymer levels. Thus, the unchanged levels of α and β-tubulin found in this study together with previous data suggested that CPF and CPO exposure were not associated with tubulin synthesis alterations or MT network disruption.

With regard to NFs, data from cell ELISA's suggest that CPF and CPO exposure reduced the level of pNFH (Ta51 reactivity) with no overall effect on the level of total NFH (N52) after 2 and 8 h exposure. The reduction in the level of Ta51 presumably reflects a decreased phosphorylation status of NFH protein, which is in accordance with the observed retraction of axon-like processes and the lower staining intensity detected with Ta51 staining via high throughput analysis. The observed decline in pNFH together with the lack of effects on total NFH and βIII-tubulin at both time points suggested that decreased phosphorylation state of NFH is a specific target for the inhibitory effects of CPF and CPO on neurite outgrowth in pre-differentiated ReNcell CX cells. This finding is also consistent with previous studies, which showed reduced levels of pNFH in N2a cells induced to differentiate for 24 h in the presence of TOCP (Fowler et al., 2001) or PSP (Hargreaves et al., 2006). The fact that CPF and CPO decreased the level of NFH phosphorylation in a similar manner as other OPs suggests that several OPs are able to induce a neurite retraction and this effect is associated with reduced levels of pNFH as an early neurotoxic marker.

The observation of decreased levels of NFH phosphorylation in pre-differentiated ReNcell CX cells treated with CPF and CPO is also in agreement with the significant decrease in the reactivity of SMI31 antibody with spinal cord NFH phosphorylation in chickens treated with PSP (Jortner et al., 1999). The altered NFH phosphorylation described *in vivo* for PSP and the subsequent observed degeneration of myelinated nerve fibre indicated early effects in the clinical lesions of OPIDN (Jortner et al., 1999). The fact that altered NFH phosphorylation has also been found *in vivo* for other OP treatments highlights the potential ability of pre-differentiated ReNcell CX cells to predict the *in vivo* delayed toxicity following OP exposure.

As NFs accumulate in the axon, they become extensively phosphorylated on the C-terminal domain of NFH. This phosphorylation of NFH has an important role in axon maturity and stability (Shaw, 1991, Sihag et al., 2007). Thus, the observed sustained reduction in NFH phosphorylation could indicate a change in the NF networks or a breakdown in NF subunit stability and a consequent decrease in axon stability. In addition, the imbalance in the phosphorylation status of NFH could cause disruption in the interactions of NFH side arms with other macromolecules in axons (Nixon and Marotta, 1984, Eyer and Leterrier, 1988, Hisanaga and Hirokawa, 1990).

The lack of CPF and CPO effects on the levels of NFH in pre-differentiated ReNcell CX cells is in agreement with the earlier works on pre-differentiated N2a cells (Chapter 5), which revealed no effect on the levels of NFH in OP-treated cells compared to control at both time points under similar post differentiation exposure conditions. However, treatment of pre-differentiated ReNcell CX cells with CPF and CPO led to a reduction in pNFH at both time points which was not the case in pre-differentiated N2a cells where a rise in pNFH level was initially observed at 2 h followed by a significant decline at 8 h. This could be explained by the fact that N2a cells is a mono-culture cell model while ReNcell CX cells is a co-culture of mixed neuronal and glial cell types which could influence the outcome. For example, glial cells produce and secrete neurotrophins such as glial derived neurotrophic factor (Lin, 1996). In a study by the host laboratory, it was found that conditioned medium from glial cells protected differentiating N2a cells from the neurite inhibitory effects of OPs (Harris et al., 2009a). They also play a role in guiding neurite growth during neural development (Deumens et al., 2004). Another reason that could clarify the observed diversity is the origin of both cells where N2a cells are derived from the mouse C1300 tumour (neuroblastoma) (Klebe and Ruddle, 1969) whereas ReNcell CXs were produced from human foetal cortex (Donato et al., 2007). Different neuronal cell types from distinct species may respond differently to OP exposure due to differences in maturation times and/or activities of signalling pathways and receptors during development. It could also be that a small sub-population of neurons in RenCell CX cultures does actually respond in the same manner as N2a cells with respect to hyperphosphorylation of NFH.

The observed reductions in NFH phosphorylation in both cell models indicated that disruption of signalling pathways could arise following CPF and CPO exposure. However, in the current study on ReNcell CX cells, both OPs had no detectable effects on the levels of ERK1/2 phosphorylation using the specified concentrations and exposure time. This could be due to the fact that ReNcell CX cells differentiate into mixed populations of neuronal and glial cells with each having a different response with respect to ERK1/2 activation during neural cell differentiation. The different rate of neuronal and glial cell maturation could also correspond to different level of expression of signalling pathway and receptors that activate these pathways. Thus, it may be that this system is not fully in place in ReNcell CX cells at this early stage of differentiation. It may also be that the changes in ERK1/2 activation are occurring in this co-culture model but in a very small population of neurons, and thus, the increased ERK1/2 using cell ELISA could not be observed. Furthermore, regulatory phosphatases could have a key role in the observed reduction in NFH phosphorylation. Therefore, an extension of this work could be conducted to measure phosphatase activity and, if altered, identify specific phosphatases involved in the regulation of NFH phosphorylation following CPF and CPO exposure. Additionally, future work could investigate whether the OP-associated reduction in NFH phosphorylation is a result of the influence of other protein kinases such as cyclin dependent kinase 5 (Cdk5) and p38 MAP kinase.

Exposure of pre-differentiated ReNcell CX cells to CPF and CPO induced concentration-dependent decrease in the activity of AChE. Despite being classed as a weak inhibitor of AChE, the highest concentration of CPF resulted in a significant reduction in AChE activity. This suggests that CPF may partially bio-activated to CPO by some metabolic activity of pre-differentiated ReNcell CX cells. However, the observed inhibition in AChE following CPF treatment would not reflect acute toxicity *in vivo*, since AChE inhibition did not reach the levels (70% AChE inhibition) that have been shown to induce acute cholinergic syndrome (Clegg and van Gemert, 1999b). In this study, it was also apparent that the extent of inhibition of AChE following the exposure of pre-differentiated ReNcell CX cells to CPO was lower than the sustained reductions of AChE observed in pre-differentiated N2a cells (Chapter 3). However, exposure of pre-

differentiated ReNcell CX cells to CPO at higher concentration caused 60-70% AChE inhibition, which is bordering on acute toxicity. The data also showed that there is a sign of less inhibition at 8 h than at 2 h, which may suggest acute toxicity at early time and a recovery of AChE at the later time. This finding indicates that co-culture of neuronal and glial cells could be more resistant to acute toxicity than neuronal cells alone. This could be due to the possibility that CPO is detoxified by the populations of glial cells or undifferentiated stem cells in ReNcell CX model. The ability of glial cells to hydrolyse CPO was previously demonstrated in the study of Sachana et al. (2008), who found lack of significant AChE inhibition in rat C6 glioma cells following 4 h exposure to CPO at similar concentrations to those employed in the current study (Sachana et al., 2008). It is well known that xenobiotic metabolism is mainly located in the liver. However, there is evidence suggesting the presence of some CYP450 isoforms, which are involved in the metabolism of oxons in different brain region in humans (Dutheil et al., 2008). For example, CYP2B6 was present in neuronal and astrocyte cells of the cerebral cortex as identified by Western blot and immunoblot techniques (Miksys et al., 2003, Miksys and Tyndale, 2004). In addition, CYP3A4 and CYP1A2 mRNA has been detected in both neuronal and glial cell types in the cortical tissue of the brain using real time polymerase chain reaction (RT-PCR) (Farin and Omiecinski, 1993). Human CYP2D6 associated with neurological disorders such as Parkinson`s disease was also mainly present in cortical neurons, glial cells of the cortex, and other brain regions (Gilham et al., 1997, Riedl et al., 1998). The presence of such CYP450s in the glial cells demonstrated in the previous studies might explain the discrepancies found between pre-differentiated N2a and ReNcells CX cells in their potential ability for CPO detoxification. Future work on the identification of these CYP450 isoforms in human pre-differentiated ReNcell CX cells would be worthwhile.

The current observation that CPO induced significant reduction in the enzymatic activity of AChE in pre-differentiated ReNcell CX cells at both time points has been demonstrated in a number of previous studies. For example, sustained inhibition of AChE was detected in N2a cells induced to differentiate for 4 and 24 h in the presence of CPO (Flaskos et al., 2011). More than 70% AChE inhibition was also noted in aggregating culture of rat brain cells (Monnet-

Tschudi et al., 2000) and PC12 cells (Das and Barone, 1999) treated with CPO. The finding of this study together with the previous data indicate that the significant reduction in the specific activity of AChE observed following CPO exposure could possibly contribute to the observed neurite retraction and the underlying molecular effects on cytoskeletal proteins. However, it is unlikely that inhibition of AChE alone could be related to the observed changes in the outgrowth of neurites in pre-differentiated ReNcell CX cells, as other studies suggest that lower concentration of CPO that had no effect on AChE can also induce marked impairment in the development of neurites. Indeed, the fall in AChE activity could simply accompany rather than cause the retraction of neurites. In this respect, CPO was found to cause significant inhibition in neurite outgrowth in cultures of embryonic sympathetic (Howard et al., 2005) and sensory neurons (Yang et al., 2008) without affecting the enzymatic activity of AChE. The notion that the neurodevelopmental effects of CPO is not directly caused by AChE inhibition could be explained by the fact that CPO can directly interfere with the morphogenic activity of AChE, which is known to be displayed during the normal process of neurodevelopment, rather than enzymatic activity of AChE protein (Howard et al., 2005, Yang et al., 2008). For example, many types of neurons have been found to transiently express AChE along axons and in growth cones during the period of axonal outgrowth (Robertson, 1987, Bigbee et al., 1999). This expression of AChE has been linked to its morphogenic role during neural development (Yang et al., 2008).

Thus, AChE inhibition may not be the main cause for the CPO-induced morphological and biochemical effects in pre-differentiated ReNcell CX. However, the fact that CPO caused a more severe effect on several parameters suggests that AChE inhibition has at least some influence in the severity of its effect.

In conclusion, this part of the current study investigated the effects of CPF and CPO in a differentiating human neural ReNcell CX stem cell model at an early stage of neuronal differentiation. At sub-cytotoxic concentrations, CPF and CPO were found to cause retraction of neurites in both neuronal and glial cell population, and in neuronal cells these alterations were associated with reduced

level of NFH phosphorylation without affecting the levels of total NFH, βIII-tubulin or MAP kinase ERK1/2. The obtained data also suggested that AChE inhibition may not be directly involved in the process by which CPF induces developmental toxicity in pre-differentiated ReNcell CX cells. However, slightly stronger CPO-induced changes were related to concentrations that inhibit the acute toxicity target by 60-70% of control levels.

7 General discussion

7.1 Summary of findings

In this thesis, I aimed to evaluate the ability of CPF and CPO to induce neurite retraction and cytoskeletal disruption in pre-differentiated mouse N2a cells and the human neural progenitor ReNcell CX stem cell line. Initially, the ability of both compounds to interfere with the outgrowth of pre-formed neurites produced by differentiating N2a cells following 2, 4 and 8 h exposure was evaluated using single concentration (3 µM). MTT reduction assays showed that the specified concentration of CPF and CPO was non-cytotoxic towards pre-differentiated N2a cells. Morphometric analysis of fixed monolayers of OP-treated cells labelled with CFSE showed reduced numbers of axon-like processes compared to the untreated control. Additionally, retraction of neurites was observed within 2 h of exposure by live cell imaging. The enzymatic activity of AChE assay data suggested that the morphological effects on axon-like neurites were not dependent on the inhibition of AChE in case of CPF. However, greater CPO-induced effects were seen at doses that caused severe inhibition of AChE and, thus, may influence the severity of its effects compared to CPF.

The next part of this thesis focused on relating the observed morphological alterations on neurite outgrowth to the levels of expression and activities of cytoskeletal and associated regulatory proteins in pre-differentiated N2a cells. Using indirect immunofluorescence, neurofilament disruption was observed in OP-treated cells stained with anti-pNFH monoclonal antibody SMI34, while the microtubule network was apparently unaffected, suggesting that neurofilaments were specifically targeted by these agents. The lack of effect on microtubules was further confirmed by western blotting analysis with anti-tubulin antibodies, which showed no changes in reactivity. The transiently increased levels of reactivity of Ta51 after 2 h exposure and reduced levels of reactivity of the same antibody following 8 h treatment with both compounds, in the absence of altered reactivity with antibodies to total NFH, suggested that there was a transient hyperphosphorylation of NFH leading to subsequent hypophoshporylation of

NFH in OP-treated cells. The fact that the observed increase in anti-pNFH reactivity at 2 h exposure was associated with increased activation of ERK1/2, suggest that this MAPK was disrupted by OP exposure. The observation of increased levels of phosphatase activity following 8 h OP treatment, could account for the reduction in NFH phosphorylation at the later time point. These findings suggest that OP-induced neurite retraction in N2a cells is associated with early transient increase in NFH phosphorylation and ERK1/2 activation followed by protein phosphatase mediated dephosphorylation. Moreover, the immunoblot analysis using monoclonal antibody GAP7B10 that recognises GAP-43 suggested that CPF and CPO induced a transient reduction in GAP-43 after 4 h exposure. The transiently reduced expression level of GAP-43 could account for the collapse in axon outgrowth observed by live cell imaging following exposure of pre-differentiated N2a cells to both compounds. It will be interesting in future work to determine whether these alterations in cell signalling and reduced levels of GAP-43 are directly related. The precise nature of the phosphatase activities involved in NFH dephosphorylation would also be worth investigating.

The development of high throughput platforms has enabled researchers to evaluate and quantify the neurotoxin exposure effects in a variety of neural cell lines. In this study, a high throughput assay was developed to investigate the effects of several CPF and CPO concentrations on multiple parameters of neurite outgrowth in pre-differentiated N2a cells after 2 and 8 h exposure. Utilising the fully automated approach, measurements of neurite outgrowth were provided based on staining with three different cytoskeleton-specific antibodies used in earlier work (B512, Ta51 and SMI34). The high throughput data indicated that CPF and CPO at sub-cytotoxic doses (1-10 µM) reduced the number of outgrowth, neurite length/cell, number of processes and branches/cell in a concentration-dependent manner, without affecting the cell count or cell body area in pre-differentiated N2a cells at both time points. The data obtained using this technique provide further confirmation for the effects observed for both OPs on neurite outgrowth monitored by manual approaches (e.g. CFSE staining) in previous chapters. Additionally, a cell ELISA approach was conducted to determine the dose-response changes of both compounds on the binding levels of

cytoskeletal proteins and the relevant ERK1/2 MAP kinase signalling pathway. The data showed that treatment of pre-differentiated N2a cells with 3 and 10 µM CPF and CPO resulted in significant increases in NFH phosphorylation at 2 h and a subsequent decrease after 8 h with lack of effects on total NFH and α-tubulin levels at both time points. This observed alteration in NFH phosphorylation at early time point was found to be associated with an increase level of anti-pERK antibody. However, the levels anti-total ERK were unaffected.

Using the same experimental protocol used on N2a cells, the last part of this thesis evaluated the effects of both CPF and CPO in ReNcell CX cells, which is more relevant to the complexities of the developing human nervous system. The neuronal and glial subpopulations of ReNcell CX cells were characterised using the neuronal-specific marker (βIII-tubulin and pNFH) and the astrocyte-specific marker GFAP. Data generated using high throughput assay showed that CPF at 3 and 10 µM and CPO at 1, 3 and 10 µM concentrations were able to reduce the outgrowth of neurites in both cell types following 2 and 8 h exposure. However, the doses used of both OPs had no effects on cell number or cell body area. Moreover, viability of ReNcell CX cells was found not to be affected following treatment with all concentrations of CPF and CPO, as indicated by MTT reduction assay. The molecular changes underlying the neurite inhibitory effects of CPF and CPO in differentiating human neuronal and glial cells were further investigated using cell ELISA. The results obtained suggested a selective inhibition in the levels of NFH phosphorylation with no detectable effects on total NFH, βIII-tubulin and ERK1/2 MAPK transduction pathway after 2 and 8 h exposure to both compounds. Unfortunately, it was unable to assess the effect of both OPs on the binding level of GFAP, as the anti-GFAP antibody reactivity was too weak. This very low expression of GFAP may reflect the early differentiation stage of astro-glial cells at this time point.

In this study, it is also important to mention that the neurotoxic actions of CPF towards pre-differentiated ReNcell CX cells was not related to significant levels of AChE inhibition. However, the fact that, as for N2a cells, CPO-induced morphological and biochemical alterations were greater than those of CPF

suggests that the level of AChE inhibition may affect the severity of the morphological effects.

Figure 7.1 illustrates the common neurotoxic impact of CPF and CPO on pre-differentiated N2a and ReNcell CX-derived neuronal cells. At sub-cytotoxic concentrations, both compounds were able to induce a retraction of neurite outgrowth in both cell models without affecting the microtubule network. The neurite inhibitory effect was associated with decreased level of NFH phosphorylation, which mediated by increased phosphatase activity in pre-differentiated N2a cells. However, further work need to be carried to know if increased phosphatase activity could account for the NFH hypophosphorylation observed in pre-differentiated ReNcell CX cells following CPF and CPO exposure.

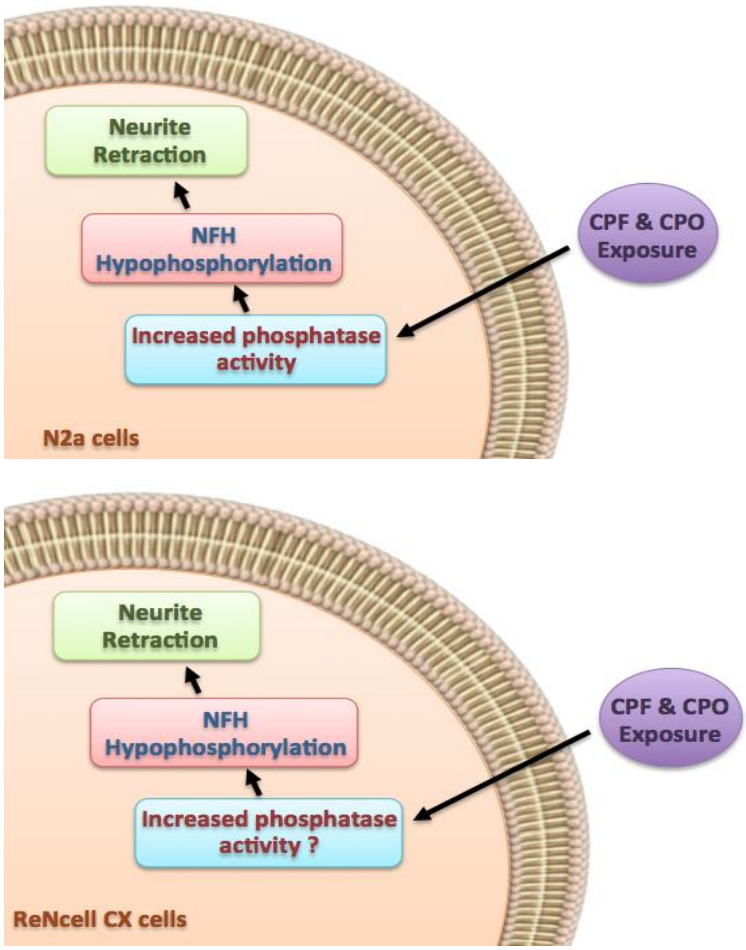

Figure 7.1. Schematic diagram of common CPF and CPO effects in pre-differentiated N2a cells and and ReNcell CX-derived neuronal cells.

The findings obtained in this study may also reflect the potential impacts of both CPF and CPO on memory, since information acquisition and memory storage in the mammalian nervous system are mainly dependent on changes in the synapses and their protein contents. For example, increased levels of GAP43 are important for axonal outgrowth and neuronal connectivity by facilitating the formation of new synapses. GAP43 also plays an essential role in synaptic transmission and plasticity (Holtmaat et al., 1995). Previously, it has been demonstrated that decreased levels of GAP43 were associated with memory impairment in animals (Rekart et al., 2005). Thus, the protein changes observed in the current work could have induced functional and structural alterations in synaptic plasticity, which represents a cellular mechanism of learning and memory processes (Mansuy and Shenolikar, 2006). Therefore, the cytoskeletal disruption observed in both N2a cells and human neural progenitor stem cells following CPF and CPO exposure in this study could reflect a potential to induce memory disorders and cognitive deficits associated with aging, dementias or neurodegenerative disease.

7.2 Correlations between *in vitro* concentrations and *in vivo* exposure

It is difficult to estimate the correlation between *in vivo* exposure and the experimental concentrations used in the current work. However, CPF-induced neurite retraction and cytoskeletal disruption were observed at concentrations similar to those detected *in vivo* in the developing humans. For instance, using meconium analysis (used to estimate the foetal exposure to environmental toxicants), about 22.8 µM of CPF has been detected in samples taken from new-born children (Ostrea et al., 2002). It is important to mention that this cohort study was based on 200 pregnant women who were continuously exposed to CPF via inhalation and dermal absorption. Exposure to CPF via these routes reduced the chance of bio-activating CPF to CPO in the mother`s liver. However, it allowed high concentrations of CPF to reach the foetus without causing maternal toxicity symptoms (Ostrea et al., 2002). In a further study,

Estevan et al. (2013) suggested that CPF at non-cytotoxic concentrations of 10 and 20 µM can cause developmental neurotoxicity *in vivo* if the exposure occurs via skin, which allowed low transformation of CPF to CPO (Estevan et al., 2013). Therefore, the applied CPF concentrations in this study have clinical relevance to human developmental neurotoxicity only if it occurs under similar exposure scenarios to those mentioned above.

With regard to CPO, a previous study indicated that CPO-induced effects on neurite outgrowth and cytoskeletal proteins at similar concentrations (1-10 µM) to those used in this study are clinically relevant to human developmental neurotoxicity (Flaskos et al., 2011). The research group suggested that low micromolar concentrations of CPO were attainable in developing organisms since micromolar levels of CPF (22.8 µM) were detectable in the above-mentioned meconium samples of new-born children (Ostrea et al., 2002). It is well established that CPO has high water solubility compared to CPF, which might reduce its ability to enter the foetus through the lipid membrane of the placenta (Sogorb and Vilanova, 2010). However, the detection of significant cholinesterase inhibition in the mammalian foetus following *in vivo* exposure of pregnant animals to CPF and other OPs (Gupta, 1995) provide further support to the suggestion of Flaskos et al. (2011) findings that foetal exposure to CPO can occur .

Moreover, the foetus is likely to be exposed mainly to the parent compound but possibly also to the oxon metabolite in the maternal tissues. The main enzyme responsible for oxon formation in humans (CYP2B6) is present at relatively low levels in human placenta, suggesting that the placenta does not make a major contribution to oxon formation (Pelkonen et al., 2006, Foxenberg et al., 2007, Croom et al., 2010). However, although CYP2B6 is expressed at low levels in the human foetus compared to later stages of development (Croom et al., 2009, Croom et al., 2010), the level of PON 1, which is responsible for hydrolysing and detoxifying the oxon forms of certain OPs such as CPO, is also relatively low at this stage (Costa et al., 2005). This could allow some oxon formation and/or accumulation in foetal tissue. Additionally, reduced levels of serum PON 1 due to genetic polymorphisms in the *PON1* gene is associated with increased

susceptibility to the toxic effect of the oxon metabolite (Costa et al., 2005). Therefore, the presence of CPO at low micromolar concentrations in developing animals is clinically relevant to developmental neurotoxicity.

There is another possible scenario regarding the potential clinical relevance of CPO concentrations employed in this study. This scenario can be related to OPIDN since the pre-differentiated cell system could also simulate what might occur following OP toxicity in adults. The observed dying back of axons in pre-differentiated N2a and ReNcell CX cells could reflect events following OP acute toxicity in adults. It is highly likely that such a concentration of CPO (1-10 µM), which caused severe inhibition in AChE levels to more than 70% would be lethal to the foetus (Solomon and Moodley, 2007, Heilmair et al., 2008). However, there are numerous case studies of patients who have survived such levels of cholinesterase inhibition with the help of pharmacological intervention, such as adrenaline and/or oximes administration, which develop delayed neuropathy. For example, 19 year old male who ingested a large dose of CPF, was hospitalised suffering from cholinergic crisis. After he was treated with atropine and pralidoxime, he developed respiratory paralysis and required mechanical ventilation for 16 days. Weeks later, he had progressive signs of OPIDN, such as deficits in the lower limbs and muscular atrophy (Nand et al., 2007). Thus, survivors of acute cholinergic crisis can be affected by a delayed neuropathy involving dying back of axons in peripheral/central neurons (Clegg and van Gemert, 1999a, Nand et al., 2007, Thivakaran et al., 2012). Indeed, it has been shown that CPF administered at acute levels in animal models can lead to OPIDN (Gupta, 2006). Therefore the morphological changes in neurite outgrowth following CPO exposure may have potential clinical relevance in terms of delayed neuropathy.

It is important to mention that previous studies by other researchers reported significant AChE inhibition following exposure to CPO at nanomolar levels. For instance, CPO at 2 and 4 nM was reported to cause 50% AChE inhibition (IC_{50}) after 30 min exposure in chicken brain homogenate and SH-SY5Y human neuroblastoma cells, respectively (Sogorb et al., 2010). *In vivo*, Eyer et al. (2009) demonstrated that the ratio of CPO/CPF in blood samples of self-intoxicated

patients was in the range of 0.004-0.025. In this context, cases with 0.3-5 µM CPF were causing 7-200 nM concentration of CPO with about 100% AChE inhibition and very severe toxicity (Eyer et al., 2009). Therefore, if we take the CPO/CPF ratio into consideration, the CPO doses used in the current study may not be easily compatible with life or physiologically relevant. However, it is not known exactly how much of the CPO applied in the current study actually entered the cells, nor the rate at which it was destabilised or degraded *in vitro*.

7.3 Limitations and future work

This study evaluated the effects of pure CPF and CPO compounds (97.6% purity) at similar concentration ranges on neurite outgrowth, cytoskeletal and associated regulatory proteins in two pre-differentiated cellular models. However, exposure of the foetus to levels of CPO causing severe AChE inhibition would be lethal. Therefore, it would be of interest for future work to investigate the ability of CPO at lower concentrations to cause dying back of axon-like process without affecting AChE activity. Additionally, the effects of combined exposure to a mixture of a similar concentration of CPF and a much smaller amount of CPO, together with longer exposure times on neurite outgrowth are merit investigation. This could be carried out using a ratio of 1:20 CPO:CPF because it has been estimated that about 5% of CPF is converting to CPO in humans (Eyer et al., 2009).

In the current study, cells were induced to differentiate for 20 h to reflect the early stages of neurite outgrowth in neural development or nerve regeneration. Longer differentiation times could be applied to obtain a more representative model of OPIDN. Extending the exposure time or using repeat exposures could also have an impact on the extent of neurotoxicity both *in vitro* and *in vivo*.

Cytoskeletal related molecular studies were conducted using Western blotting and cell ELISA approaches. For the most part, data generated from both assays were comparable. However, with the cell ELISA approach, it was not possible to determine the effects of CPF and CPO on the binding level of GFAP in pre-differentiated ReNcell CX cells, due to poor reactivity of GFAP antibody with

fixed cell monolayers. Thus, a more sensitive method is required to repeat to quantify the protein, such as Western blotting. One approach could be to use other anti-GFAP antibodies to determine whether they are more suited to the ELISA approach. Alternatively, the same primary antibody used in the current work could be detected by biotin-labelled secondary antibodies followed by HRP-Extravidin to amplify the signal further.

Cell signalling studies indicated that ERK1/2 MAP kinase activation was increased in pre-differentiated N2a cells treated with both CPF and CPO for 2 h. As NFH is a known substrate for ERK1/2 (Veeranna et al., 1998), the activation status of this MAP kinase could account for the increased levels of NFH phosphorylation. The detrimental effect on this signaling pathway could be further expanded by using ERK 1/2 inhibitors prior to OP exposure. Additional work could also examine the effects of CPF and CPO on upstream regulators of ERK1/2 by using specific MEK1/2 antibodies. Moreover, the exact mechanism underlying the impact of CPF and CPO on pre-differentiated ReNcell CX cells would also be of interest.

In pre-differentiated N2a cells, the increased phosphatase activity could account for the observed reduction in NFH phosphorylation at 8 h. However, this observation was seen using single concentration (3 µM) of CPF and CPO. Therefore, it would be of value to re-evaluate the effect of both OPs on phosphatase activity using the dose range of each toxin. Additionally, an extension of this work could include the assessment of phosphatase activity in ReNcell CX cells following CPF and CPO exposure. Furthermore, future work will also aim to identify specific phosphatases associated with NFH phosphorylation in OP treated cells. For example, protein phosphatase 2A was previously found to reduce NFH phosphorylation following hyper-phosphorylation by cyclin-dependent kinase-5 (cdk5) in animal models (Veeranna et al., 1995). In addition, protein aggregation studies in Alzheimer's disease patients highlighted the association of increased NFH phosphorylation with a decrease in protein phosphatases 2A activity (Vogelsberg-Ragaglia et al., 2001).

High throughput analysis of ReNcell CX cells could be extended to study the effects of OP exposure on individual neuronal and glial cell types in more detail. This would involve the use of additional image analysis software packages to determine the effects of exposure on the proportions of cell expressing specific biomarkers (e.g. myelin basic proteins for oligodendrocytes, choline acetyl transferase for cholinergic neurons, tyrosine hydroxylase for dopaminergic neurons, etc) above the levels found in non-differentiated neural stem cells, which could be further identified by counter-staining monolayers with antibodies to nestin.

7.4 Conclusion

In conclusion, the present study used several morphological and biochemical approaches to study the effects of sub-cytotoxic concentration of CPF and CPO on neurite outgrowth and cytoskeletal proteins in differentiating neural cellular models. Indeed the findings show that pre-differentiated N2a cells represent a useful cellular system for neurotoxicity screening. However, the fact that N2a cells provide a mono-culture cell model, and are derived from a rodent tumour, they may not give a true reflection of the complexity of the human nervous system and its response to OP exposure. The current study also highlights that evaluating the toxicity on human neural progenitor ReNcell CX stem cells reduced the level of uncertainty associated with cells derived from animal models. A further advantage of using such human-derived neural progenitor stem cells is that they differentiate into a co-culture incorporating both neuronal and glial cell types. As such, with further development, it should be more effective at predicting the toxin-related changes *in vivo*.

References

ABDEL RASOUL, G. M., ABOU SALEM, M. E., MECHAEL, A. A., HENDY, O. M., ROHLMAN, D. S. & ISMAIL, A. A. 2008. Effects of occupational pesticide exposure on children applying pesticides. *Neurotoxicology,* 29**,** 833-8.

ABDOLLAHI, M. & KARAMI-MOHAJERI, S. 2012. A comprehensive review on experimental and clinical findings in intermediate syndrome caused by organophosphate poisoning. *Toxicol Appl Pharmacol,* 258**,** 309-14.

ABOU-DONIA, M. B. 1981. Organophosphorus ester-induced delayed neurotoxicity. *Annu Rev Pharmacol Toxicol,* 21**,** 511-48.

ABOU-DONIA, M. B. 1993a. The cytoskeleton as a target for organophosphorus ester-induced delayed neurotoxicity (OPIDN). *Chem Biol Interact,* 87**,** 383-93.

ABOU-DONIA, M. B. 1993b. The cytoskeleton as a target for organophosphorus ester-induced delayed neurotoxicity (OPIDN). *Chemico-biological interactions,* 87**,** 383-393.

ABOU-DONIA, M. B. 2003. Organophosphorus ester-induced chronic neurotoxicity. *Arch Environ Health,* 58**,** 484-97.

ABOU-DONIA, M. B. & LAPADULA, D. M. 1990. Mechanisms of organophosphorus ester-induced delayed neurotoxicity: type I and type II. *Annu Rev Pharmacol Toxicol,* 30**,** 405-40.

ABRAHAM, V. C., TAYLOR, D. L. & HASKINS, J. R. 2004. High content screening applied to large-scale cell biology. *Trends Biotechnol,* 22**,** 15-22.

ACKERLEY, S., THORNHILL, P., GRIERSON, A. J., BROWNLEES, J., ANDERTON, B. H., LEIGH, P. N., SHAW, C. E. & MILLER, C. C. 2003. Neurofilament heavy chain side arm phosphorylation regulates axonal transport of neurofilaments. *J Cell Biol,* 161**,** 489-95.

ACP, A. C. O. P. 2002. ACP annual reports. *Chlorpyrifos.* London.

AGRONEWS. 2013. *2012 China`s major pesticides varieties tracking-chlorpyrifos.* [Online]. Available: http://news.agropages.com/news/newsdetail8993.htm.

ALARCON, W. A., CALVERT, G. M., BLONDELL, J. M., MEHLER, L. N., SIEVERT, J., PROPECK, M., TIBBETTS, D. S., BECKER, A., LACKOVIC, M., SOILEAU, S. B., DAS, R., BECKMAN, J., MALE, D. P., THOMSEN, C. L. & STANBURY, M. 2005. Acute illnesses associated with pesticide exposure at schools. *JAMA,* 294**,** 455-65.

ALBERS, J. W., BERENT, S., GARABRANT, D. H., GIORDANI, B., SCHWEITZER, S. J., GARRISON, R. P. & RICHARDSON, R. J. 2004. The effects of occupational exposure to chlorpyrifos on the neurologic examination of central nervous system function: a prospective cohort study. *J Occup Environ Med,* 46**,** 367-78.

ANDERSEN, H. R., NIELSEN, J. B. & GRANDJEAN, P. 2000. Toxicologic evidence of developmental neurotoxicity of environmental chemicals. *Toxicology,* 144**,** 121-7.

ANDRIEUX, A., SALIN, P. A., VERNET, M., KUJALA, P., BARATIER, J., GORY-FAURE, S., BOSC, C., POINTU, H., PROIETTO, D., SCHWEITZER, A., DENARIER, E., KLUMPERMAN, J. & JOB, D.

2002. The suppression of brain cold-stable microtubules in mice induces synaptic defects associated with neuroleptic-sensitive behavioral disorders. *Genes Dev,* 16**,** 2350-64.

ANTHONY, S. G., SCHIPPER, H. M., TAVARES, R., HOVANESIAN, V., CORTEZ, S. C., STOPA, E. G. & JOHANSON, C. E. 2003. Stress protein expression in the Alzheimer-diseased choroid plexus. *J Alzheimers Dis,* 5**,** 171-7.

ASCHNER, M., ALLEN, J. W., KIMELBERG, H. K., LOPACHIN, R. M. & STREIT, W. J. 1999. Glial cells in neurotoxicity development. *Annu Rev Pharmacol Toxicol,* 39**,** 151-73.

ASPELIN, A. 1997. Pesticide industry sales and usage: 1994 and 1995 Market estimates. *In:* EPA, U. S. E. P. A. (ed.). Washington, DC.

BAGCHI, D., BHATTACHARYA, G. & STOHS, S. J. 1996. In vitro and in vivo induction of heat shock (stress) protein (Hsp) gene expression by selected pesticides. *Toxicology,* 112**,** 57-68.

BAL-PRICE, A. K., SUNOL, C., WEISS, D. G., VAN VLIET, E., WESTERINK, R. H. & COSTA, L. G. 2008. Application of in vitro neurotoxicity testing for regulatory purposes: Symposium III summary and research needs. *Neurotoxicology,* 29**,** 520-31.

BAMBURG, J., BRAY, D. & CHAPMAN, K. 1986. Assembly of microtubules at the tip of growing axons. *Nature,* 321**,** 788-790.

BANKER, G. & GOSLIN, K. 1998. *Culturing nerve cells,* Cambridge, MA, MIT Press.

BANSAL, G. S., NORTON, P. M. & LATCHMAN, D. S. 1991. The 90-kDa heat shock protein protects mammalian cells from thermal stress but not from viral infection. *Exp Cell Res,* 195**,** 303-6.

BARONE, S., JR., DAS, K. P., LASSITER, T. L. & WHITE, L. D. 2000. Vulnerable processes of nervous system development: a review of markers and methods. *Neurotoxicology,* 21**,** 15-36.

BARR, D. B. & ANGERER, J. 2006. Potential uses of biomonitoring data: a case study using the organophosphorus pesticides chlorpyrifos and malathion. *Environ Health Perspect,* 114**,** 1763-9.

BARRES, B. A. & BARDE, Y. 2000. Neuronal and glial cell biology. *Curr Opin Neurobiol,* 10**,** 642-8.

BENDOTTI, C., BALDESSARI, S., PENDE, M., SOUTHGATE, T., GUGLIELMETTI, F. & SAMANIN, R. 1997. Relationship between GAP-43 expression in the dentate gyrus and synaptic reorganization of hippocampal mossy fibres in rats treated with kainic acid. *Eur J Neurosci,* 9**,** 93-101.

BENOWITZ, L. I. & ROUTTENBERG, A. 1997. GAP-43: an intrinsic determinant of neuronal development and plasticity. *Trends Neurosci,* 20**,** 84-91.

BERGER-SWEENEY, J. & HOHMANN, C. F. 1997. Behavioral consequences of abnormal cortical development: insights into developmental disabilities. *Behav Brain Res,* 86**,** 121-42.

BERTRAND, N., CASTRO, D. S. & GUILLEMOT, F. 2002. Proneural genes and the specification of neural cell types. *Nat Rev Neurosci,* 3**,** 517-30.

BIGBEE, J. W., SHARMA, K. V., GUPTA, J. J. & DUPREE, J. L. 1999. Morphogenic role for acetylcholinesterase in axonal outgrowth during neural development. *Environ Health Perspect,* 107 Suppl 1**,** 81-7.

BJORLING-POULSEN, M., ANDERSEN, H. R. & GRANDJEAN, P. 2008. Potential developmental neurotoxicity of pesticides used in Europe. *Environ Health,* 7**,** 50.

BLACK, M. M. & LASEK, R. J. 1980. Slow components of axonal transport: two cytoskeletal networks. *J Cell Biol,* 86**,** 616-23.

BOULTON, T. G., NYE, S. H., ROBBINS, D. J., IP, N. Y., RADZIEJEWSKA, E., MORGENBESSER, S. D., DEPINHO, R. A., PANAYOTATOS, N., COBB, M. H. & YANCOPOULOS, G. D. 1991. ERKs: a family of protein-serine/threonine kinases that are activated and tyrosine phosphorylated in response to insulin and NGF. *Cell,* 65**,** 663-75.

BOULTON, T. G., YANCOPOULOS, G. D., GREGORY, J. S., SLAUGHTER, C., MOOMAW, C., HSU, J. & COBB, M. H. 1990. An insulin-stimulated protein kinase similar to yeast kinases involved in cell cycle control. *Science,* 249**,** 64-7.

BOUQUET, C., SOARES, S., VON BOXBERG, Y., RAVAILLE-VERON, M., PROPST, F. & NOTHIAS, F. 2004. Microtubule-associated protein 1B controls directionality of growth cone migration and axonal branching in regeneration of adult dorsal root ganglia neurons. *J Neurosci,* 24**,** 7204-13.

BRAMANTI, V., TOMASSONI, D., AVITABILE, M., AMENTA, F. & AVOLA, R. 2010. Biomarkers of glial cell proliferation and differentiation in culture. *Front Biosci (Schol Ed),* 2**,** 558-70.

BREIER, J. M., RADIO, N. M., MUNDY, W. R. & SHAFER, T. J. 2008. Development of a high-throughput screening assay for chemical effects on proliferation and viability of immortalized human neural progenitor cells. *Toxicol Sci,* 105**,** 119-33.

BUKAU, B., WEISSMAN, J. & HORWICH, A. 2006. Molecular chaperones and protein quality control. *Cell,* 125**,** 443-51.

BURATTI, F. M., LEONI, C. & TESTAI, E. 2007. The human metabolism of organophosphorothionate pesticides: consequences for toxicological risk assessment. *journal of verbr lebensm,* 2**,** 37-44.

BURGOYNE, R. D. 1991. *The neuronal cytoskeleton,* New York, Wiley-Liss Inc.

CALVERT, G. M., PLATE, D. K., DAS, R., ROSALES, R., SHAFEY, O., THOMSEN, C., MALE, D., BECKMAN, J., ARVIZU, E. & LACKOVIC, M. 2004. Acute occupational pesticide-related illness in the US, 1998-1999: surveillance findings from the SENSOR-pesticides program. *Am J Ind Med,* 45**,** 14-23.

CAMBRAY-DEAKIN, M. 1991a. Cytoskeleton of the growing axon. *The Neuronal Cytoskeleton, Wiley-Liss, New York***,** 233-255.

CAMBRAY-DEAKIN, M. A. 1991b. Cytoskeleton of the growing axon. *In:* BURGOYNE, R. D. (ed.) *The neuronal cytoskeleton.* New York ; Chichester: Wiley-Liss.

CAMPBELL, C. G., SEIDLER, F. J. & SLOTKIN, T. A. 1997. Chlorpyrifos interferes with cell development in rat brain regions. *Brain Res Bull,* 43**,** 179-89.

CARGNELLO, M. & ROUX, P. P. 2011. Activation and function of the MAPKs and their substrates, the MAPK-activated protein kinases. *Microbiol Mol Biol Rev,* 75**,** 50-83.

CARLTON, E. J., MOATS, H. L., FEINBERG, M., SHEPARD, P., GARFINKEL, R., WHYATT, R. & EVANS, D. 2004. Pesticide sales in low-income, minority neighborhoods. *J Community Health,* 29**,** 231-44.

CASARETT, L. J., DOULL, J. & KLAASSEN, C. D. 2001. *Casarett and Doull's toxicology : the basic science of poisons,* New York, McGraw-Hill Medical Pub. Division.

CAUGHLAN, A., NEWHOUSE, K., NAMGUNG, U. & XIA, Z. 2004. Chlorpyrifos induces apoptosis in rat cortical neurons that is regulated by a balance between p38 and ERK/JNK MAP kinases. *Toxicol Sci,* 78**,** 125-34.

CHAMBERS, J. E. & CHAMBERS, H. W. 1989. Oxidative desulfuration of chlorpyrifos, chlorpyrifosâ€ • methyl, and leptophos by rat brain and liver. *Journal of biochemical toxicology,* 4**,** 201-203.

CHANG, L. & KARIN, M. 2001. Mammalian MAP kinase signalling cascades. *Nature,* 410**,** 37-40.

CLEGG, D. J. & VAN GEMERT, M. 1999a. Determination of the reference dose for chlorpyrifos: proceedings of an expert panel. *J Toxicol Environ Health B Crit Rev,* 2**,** 211-55.

CLEGG, D. J. & VAN GEMERT, M. 1999b. Expert panel report of human studies on chlorpyrifos and/or other organophosphate exposures. *J Toxicol Environ Health B Crit Rev,* 2**,** 257-79.

CLEVELAND, D. W. 1993a. Tubulin and associated proteins. *In:* KREIS, T. & VALE, R. (eds.) *Guidebook to the cytoskeletal and motor proteins*
Oxford: Oxford University Press.

CLEVELAND, D. W. 1993b. *tubulin and associated proteins in guidebook to the cytoskeletal and motor proteins,* oxford university press.

COLBORN, T. 2006. A case for revisiting the safety of pesticides: a closer look at neurodevelopment. *Environ Health Perspect,* 114**,** 10-7.

COMPSTON, A., ZAJICEK, J., SUSSMAN, J., WEBB, A., HALL, G., MUIR, D., SHAW, C., WOOD, A. & SCOLDING, N. 1997. Glial lineages and myelination in the central nervous system. *J Anat,* 190 (Pt 2)**,** 161-200.

COOPER, D. C. 2011. *Introduction to neuroscience I,* Donald C. Cooper Ph. D.

COOPER, G. M. 2000. *The cell : a molecular approach,* Washington, D.C.
Sunderland, Mass., ASM Press ;
Sinauer Associates.

COOPER, G. M. & HAUSMAN, R. E. 2000. *The cell,* Sinauer Associates Sunderland.

COOPER, J. A., BOWEN-POPE, D. F., RAINES, E., ROSS, R. & HUNTER, T. 1982. Similar effects of platelet-derived growth factor and epidermal growth factor on the phosphorylation of tyrosine in cellular proteins. *Cell,* 31**,** 263-73.

COSTA, L. G. 2006. Current issues in organophosphate toxicology. *Clin Chim Acta,* 366**,** 1-13.

COSTA, L. G., ASCHNER, M., VITALONE, A., SYVERSEN, T. & SOLDIN, O. P. 2004. Developmental neuropathology of environmental agents. *Annu Rev Pharmacol Toxicol,* 44**,** 87-110.

COSTA, L. G., GIORDANO, G., COLE, T. B., MARSILLACH, J. & FURLONG, C. E. 2013. Paraoxonase 1 (PON1) as a genetic determinant of susceptibility to organophosphate toxicity. *Toxicology,* 307**,** 115-22.

COSTA, L. G., VITALONE, A., COLE, T. B. & FURLONG, C. E. 2005. Modulation of paraoxonase (PON1) activity. *Biochem Pharmacol,* 69**,** 541-50.

COX, C. 1994. Chlorpyrifos, Part 1 (Toxicology). *Journal of pesticide reform,* 14**,** 15-20.

CRAIG, A. M. & BANKER, G. 1994a. Neuronal polarity. *Annual review of neuroscience,* 17**,** 267-310.

CRAIG, A. M. & BANKER, G. 1994b. Neuronal polarity. *Annu Rev Neurosci,* 17**,** 267-310.

CROOM, E. L., STEVENS, J. C., HINES, R. N., WALLACE, A. D. & HODGSON, E. 2009. Human hepatic CYP2B6 developmental expression: the impact of age and genotype. *Biochem Pharmacol,* 78**,** 184-90.

CROOM, E. L., WALLACE, A. D. & HODGSON, E. 2010. Human variation in CYP-specific chlorpyrifos metabolism. *Toxicology,* 276**,** 184-91.

CRUMPTON, T. L., SEIDLER, F. J. & SLOTKIN, T. A. 2000. Developmental neurotoxicity of chlorpyrifos in vivo and in vitro: effects on nuclear transcription factors involved in cell replication and differentiation. *Brain Res,* 857**,** 87-98.

CSERMELY, P. 2001. A nonconventional role of molecular chaperones: involvement in the cytoarchitecture. *News Physiol Sci,* 16**,** 123-6.

DANG, C. V., RESAR, L. M., EMISON, E., KIM, S., LI, Q., PRESCOTT, J. E., WONSEY, D. & ZELLER, K. 1999. Function of the c-Myc oncogenic transcription factor. *Exp Cell Res,* 253**,** 63-77.

DAS, K. P. & BARONE, S., JR. 1999. Neuronal differentiation in PC12 cells is inhibited by chlorpyrifos and its metabolites: is acetylcholinesterase inhibition the site of action? *Toxicol Appl Pharmacol,* 160**,** 217-30.

DAS, K. P., FREUDENRICH, T. M. & MUNDY, W. R. 2004. Assessment of PC12 cell differentiation and neurite growth: a comparison of morphological and neurochemical measures. *Neurotoxicol Teratol,* 26**,** 397-406.

DAVIES, H. G., RICHTER, R. J., KEIFER, M., BROOMFIELD, C. A., SOWALLA, J. & FURLONG, C. E. 1996. The effect of the human serum paraoxonase polymorphism is reversed with diazoxon, soman and sarin. *Nat Genet,* 14**,** 334-6.

DE WAEGH, S. M., LEE, V. M. & BRADY, S. T. 1992. Local modulation of neurofilament phosphorylation, axonal caliber, and slow axonal transport by myelinating Schwann cells. *Cell,* 68**,** 451-63.

DEUMENS, R., KOOPMANS, G. C., DEN BAKKER, C. G., MAQUET, V., BLACHER, S., HONIG, W. M., JEROME, R., PIRARD, J. P., STEINBUSCH, H. W. & JOOSTEN, E. A. 2004. Alignment of glial cells stimulates directional neurite growth of CNS neurons in vitro. *Neuroscience,* 125**,** 591-604.

DONATO, R., MILJAN, E. A., HINES, S. J., AOUABDI, S., POLLOCK, K., PATEL, S., EDWARDS, F. A. & SINDEN, J. D. 2007. Differential development of neuronal physiological responsiveness in two human neural stem cell lines. *BMC Neurosci,* 8**,** 36.

DRAGUNOW, M. 2008. High-content analysis in neuroscience. *Nat Rev Neurosci,* 9**,** 779-88.

DU TOIT, P. W., MULLER, F. O., VAN TONDER, W. M. & UNGERER, M. J. 1981. Experience with the intensive care management of organophosphate insecticide poisoning. *S Afr Med J,* 60**,** 227-9.

DUTHEIL, F., BEAUNE, P. & LORIOT, M. A. 2008. Xenobiotic metabolizing enzymes in the central nervous system: Contribution of cytochrome P450 enzymes in normal and pathological human brain. *Biochimie,* 90**,** 426-36.

EASTER, S. S., JR., ROSS, L. S. & FRANKFURTER, A. 1993. Initial tract formation in the mouse brain. *J Neurosci,* 13**,** 285-99.

EATON, D. L., DAROFF, R. B., AUTRUP, H., BRIDGES, J., BUFFLER, P., COSTA, L. G., COYLE, J., MCKHANN, G., MOBLEY, W. C., NADEL, L., NEUBERT, D., SCHULTE-HERMANN, R. & SPENCER, P. S. 2008. Review of the toxicology of chlorpyrifos with an emphasis on human exposure and neurodevelopment. *Crit Rev Toxicol,* 38 Suppl 2**,** 1-125.

EC, E. C. 2005. Monitoring of pesticide residues in products of plant origin in the European Union, Norway, Iceland and Liechtenstein. *Commision staff working document.*

EDDLESTON, M., BUCKLEY, N. A., EYER, P. & DAWSON, A. H. 2008. Management of acute organophosphorus pesticide poisoning. *Lancet,* 371**,** 597-607.

ELERSEK, T. & FILIPIC, M. 2011. Organophosphorous Pesticides - Mechanisms of Thier Toxicity. *In:* STOYTCHEVA, M. (ed.) *Pesticides - The Impacts of Pesticides Exposure.* Slovenia: Intechopen.

ELLMAN, G. L., COURTNEY, K. D., ANDRES, V., JR. & FEATHER-STONE, R. M. 1961. A new and rapid colorimetric determination of acetylcholinesterase activity. *Biochem Pharmacol,* 7**,** 88-95.

EMERICK, G. L., DEOLIVEIRA, G. H., DOS SANTOS, A. C. & EHRICH, M. 2012. Mechanisms for consideration for intervention in the development of organophosphorus-induced delayed neuropathy. *Chem Biol Interact,* 199**,** 177-84.

ENDO, M., OHASHI, K., SASAKI, Y., GOSHIMA, Y., NIWA, R., UEMURA, T. & MIZUNO, K. 2003. Control of growth cone motility and morphology by LIM kinase and Slingshot via phosphorylation and dephosphorylation of cofilin. *J Neurosci,* 23**,** 2527-37.

ENG, L. F., GHIRNIKAR, R. S. & LEE, Y. L. 2000. Glial fibrillary acidic protein: GFAP-thirty-one years (1969-2000). *Neurochem Res,* 25**,** 1439-51.

ENGEL, S. M., WETMUR, J., CHEN, J., ZHU, C., BARR, D. B., CANFIELD, R. L. & WOLFF, M. S. 2011. Prenatal exposure to organophosphates, paraoxonase 1, and cognitive development in childhood. *Environ Health Perspect,* 119**,** 1182-8.

EPA, U. S. E. P. A. (ed.) 1992. *prevention, Pesticides and Toxic Substances. Pesticides in groundwater database: A compilation of monitoring studies: 1971-1991,* Washington, D.C.: USEPA.

EPA, U. S. E. P. A. 1994. Office of Prevention, Pesticides and Toxic Substances. Review of poison control center data call in. Memo from J. Blondell, Health Statistician Health Effects Division, to Steve Knott, Section Head, and Larry Dorsey, Chief. . Washington, D.C.

EPA, U. S. E. P. A. 1997. Office of prevention, pesticides and toxic substances. Review of chlorpyrifos poisoning data. Washington, DC.

EPA, U. S. E. P. A. 1999. Occupational/residential handler and postapplication residential risk assessment for chlorpyrifos. Washington, DC.

EPA, U. S. E. P. A. 2000. Chlorpyrifos revised risk assessment and agreement with registrants prevention, pesticides and toxic substances. Washington, DC: USEPA.

EPA, U. S. E. P. A. 2013. Chlorpyrifos: Prelimenray evaluation of the potential risks from volatilisation. . Washington DC, USA.

EPA, U. S. E. P. A. 2015. Chlorpyrifos Revised Risk Assessment and Agreement with Registrants Prevention, Pesticides and Toxic Substances. Wshington, DC: USEPA: USEPA.

ESTEVAN, C., VILANOVA, E. & SOGORB, M. A. 2013. Chlorpyrifos and its metabolites alter gene expression at non-cytotoxic concentrations in D3 mouse embryonic stem cells under in vitro differentiation: considerations for embryotoxic risk assessment. *Toxicol Lett,* 217**,** 14-22.

EYER, F., ROBERTS, D. M., BUCKLEY, N. A., EDDLESTON, M., THIERMANN, H., WOREK, F. & EYER, P. 2009. Extreme variability in the formation of chlorpyrifos oxon (CPO) in patients poisoned by chlorpyrifos (CPF). *Biochem Pharmacol,* 78**,** 531-7.

EYER, J. & LETERRIER, J. F. 1988. Influence of the phosphorylation state of neurofilament proteins on the interactions between purified filaments in vitro. *Biochem J,* 252**,** 655-60.

FAO, F. A. A. O. 2013. The state of food and agriculture. Rome.

FARIN, F. M. & OMIECINSKI, C. J. 1993. Regiospecific expression of cytochrome P-450s and microsomal epoxide hydrolase in human brain tissue. *J Toxicol Environ Health,* 40**,** 317-35.

FIEDLER, N., KIPEN, H., KELLY-MCNEIL, K. & FENSKE, R. 1997. Long-term use of organophosphates and neuropsychological performance. *Am J Ind Med,* 32**,** 487-96.

FLANAGAN, L. A., REBAZA, L. M., DERZIC, S., SCHWARTZ, P. H. & MONUKI, E. S. 2006. Regulation of human neural precursor cells by laminin and integrins. *J Neurosci Res,* 83**,** 845-56.

FLASKOS, J. 2012. The developmental neurotoxicity of organophosphorus insecticides: a direct role for the oxon metabolites. *Toxicol Lett,* 209**,** 86-93.

FLASKOS, J. 2014. The neuronal cytoskeleton as a potential target in the developmental neurotoxicity of organophosphorothionate insecticides. *Basic Clin Pharmacol Toxicol,* 115**,** 201-8.

FLASKOS, J., FOWLER, M. J., TEURTRIE, C. & HARGREAVES, A. J. 1999. The effects of carbaryl and trichlorphon on differentiating mouse N2a neuroblastoma cells. *Toxicol Lett,* 110**,** 79-84.

FLASKOS, J., HARRIS, W., SACHANA, M., MUNOZ, D., TACK, J. & HARGREAVES, A. J. 2007. The effects of diazinon and cypermethrin on the differentiation of neuronal and glial cell lines. *Toxicol Appl Pharmacol,* 219**,** 172-80.

FLASKOS, J., MCLEAN, W. G., FOWLER, M. J. & HARGREAVES, A. J. 1998. Tricresyl phosphate inhibits the formation of axon-like processes and disrupts neurofilaments in cultured mouse N2a and rat PC12 cells. *Neurosci Lett,* 242**,** 101-4.

FLASKOS, J., MCLEAN, W. G. & HARGREAVES, A. J. 1994. The toxicity of organophosphate compounds towards cultured PC12 cells. *Toxicol Lett,* 70**,** 71-6.

FLASKOS, J., NIKOLAIDIS, E., HARRIS, W., SACHANA, M. & HARGREAVES, A. J. 2011. Effects of sub-lethal neurite outgrowth inhibitory concentrations of chlorpyrifos oxon on cytoskeletal proteins and acetylcholinesterase in differentiating N2a cells. *Toxicol Appl Pharmacol,* 256**,** 330-6.

FLASKOS, J. & SACHANA, M. 2011. Developmental neuotoxicity of anticholinesterase. *In:* SATOH, T. & GUPTA, R. (eds.) *Anticholinesterase pesticides: metabolism, neurotoxicity, and epidemiology.* Hoboken, New Jersey: John Wiley & Sons Inc.

FOUREST-LIEUVIN, A., PERIS, L., GACHE, V., GARCIA-SAEZ, I., JUILLAN-BINARD, C., LANTEZ, V. & JOB, D. 2006. Microtubule regulation in mitosis: tubulin phosphorylation by the cyclin-dependent kinase Cdk1. *Mol Biol Cell,* 17**,** 1041-50.

FOWLER, M. J., FLASKOS, J., MCLEAN, W. G. & HARGREAVES, A. J. 2001. Effects of neuropathic and non-neuropathic isomers of tricresyl phosphate and their microsomal activation on the production of axon-like processes by differentiating mouse N2a neuroblastoma cells. *J Neurochem,* 76**,** 671-8.

FOWLER, M. J., MCLEAN, G., FLASKOS, J. & HARGREAVES, A. J. 1997. The effects of tricresyl phosphate on axon outgrowth and neurofilament levels in mouse N2a neuroblastoma cells. *Biochem Soc Trans,* 25**,** S574.

FOXENBERG, R. J., MCGARRIGLE, B. P., KNAAK, J. B., KOSTYNIAK, P. J. & OLSON, J. R. 2007. Human hepatic cytochrome p450-specific metabolism of parathion and chlorpyrifos. *Drug Metab Dispos,* 35**,** 189-93.

FURLONG, C. E., HOLLAND, N., RICHTER, R. J., BRADMAN, A., HO, A. & ESKENAZI, B. 2006. PON1 status of farmworker mothers and children as a predictor of organophosphate sensitivity. *Pharmacogenet Genomics,* 16**,** 183-90.

GALLO, G. 2006. RhoA-kinase coordinates F-actin organization and myosin II activity during semaphorin-3A-induced axon retraction. *J Cell Sci,* 119**,** 3413-23.

GARCIA, S. J., SEIDLER, F. J., QIAO, D. & SLOTKIN, T. A. 2002. Chlorpyrifos targets developing glia: effects on glial fibrillary acidic protein. *Brain Res Dev Brain Res,* 133**,** 151-61.

GARTON, H. J. & SCHOENWOLF, G. C. 1996. Improving the efficacy of fluorescent labeling for histological tracking of cells in early mammalian and avian embryos. *Anat Rec,* 244**,** 112-17.

GAVRILESCU, M., DEMNEROVA, K., AAMAND, J., AGATHOS, S. & FAVA, F. 2015. Emerging pollutants in the environment: present and future challenges in biomonitoring, ecological risks and bioremediation. *N Biotechnol,* 32**,** 147-56.

GILHAM, D. E., CAIRNS, W., PAINE, M. J., MODI, S., POULSOM, R., ROBERTS, G. C. & WOLF, C. R. 1997. Metabolism of MPTP by cytochrome P4502D6 and the demonstration of 2D6 mRNA in human foetal and adult brain by in situ hybridization. *Xenobiotica,* 27**,** 111-25.

GINZBURG, I. 1991. Neuronal polarity: targeting of microtubule components into axons and dendrites. *Trends in biochemical sciences,* 16**,** 257-261.

GLYNN, P. 2000. Neural development and neurodegeneration: two faces of neuropathy target esterase. *Prog Neurobiol,* 61**,** 61-74.

GOMI, H., YOKOYAMA, T., FUJIMOTO, K., IKEDA, T., KATOH, A., ITOH, T. & ITOHARA, S. 1995. Mice devoid of the glial fibrillary acidic protein develop normally and are susceptible to scrapie prions. *Neuron,* 14**,** 29-41.

GONG, C. X., SINGH, T. J., GRUNDKE-IQBAL, I. & IQBAL, K. 1993. Phosphoprotein phosphatase activities in Alzheimer disease brain. *J Neurochem,* 61**,** 921-7.

GONZALEZ, M. F., SHIRAISHI, K., HISANAGA, K., SAGAR, S. M., MANDABACH, M. & SHARP, F. R. 1989. Heat shock proteins as markers of neural injury. *Brain Res Mol Brain Res,* 6**,** 93-100.

GOPINATH, R. K., YOU, S. T., CHIEN, K. Y., SWAMY, K. B., YU, J. S., SCHUYLER, S. C. & LEU, J. Y. 2014. The Hsp90-dependent proteome is conserved and enriched for hub proteins with high levels of protein-protein connectivity. *Genome Biol Evol,* 6**,** 2851-65.

GOTTFRIED, B. S., LEE, C. J. & BELL, K. J. 1966. The leidenfrost phenomenon: film boiling of liquid droplets on a flat plate. *International Journal of heat and mass transfer,* 9**,** 1167-1188.

GRANDJEAN, P. & LANDRIGAN, P. J. 2006. Developmental neurotoxicity of industrial chemicals. *Lancet,* 368**,** 2167-78.

GRANDJEAN, P. & LANDRIGAN, P. J. 2014. Neurobehavioural effects of developmental toxicity. *Lancet Neurol,* 13**,** 330-8.

GUNNELL, D., EDDLESTON, M., PHILLIPS, M. R. & KONRADSEN, F. 2007. The global distribution of fatal pesticide self-poisoning: systematic review. *BMC Public Health,* 7**,** 357.

GUPTA, R. C. 2006. *Toxicology of organophosphate and carbamate compounds,* Amsterdam ; London, Elsevier Academic Press.

GUPTA, R. P. 1995. Envioronmental agents and placental toxicity: antcholinesterases and other agents. *In:* SASTRY, R. (ed.) *Placental toxicology.* Boca Raton ; London: CRC Press.

GUPTA, R. P. & ABOU-DONIA, M. B. 1998. Tau proteins-enhanced Ca2+/calmodulin (CaM)-dependent phosphorylation by the brain supernatant of diisopropyl phosphorofluoridate (DFP)-treated hen: tau mutants indicate phosphorylation of more amino acids in tau by CaM kinase II. *Brain Res,* 813**,** 32-43.

GUPTA, S. C., SHARMA, A., MISHRA, M., MISHRA, R. K. & CHOWDHURI, D. K. 2010. Heat shock proteins in toxicology: how close and how far? *Life Sci,* 86**,** 377-84.

HAFFKE, S. C. & SEEDS, N. W. 1975. Neuroblastoma: the E. coli of neurobiology? *Life Sci,* 16**,** 1649-57.

HAMOS, J. E., OBLAS, B., PULASKI-SALO, D., WELCH, W. J., BOLE, D. G. & DRACHMAN, D. A. 1991. Expression of heat shock proteins in Alzheimer's disease. *Neurology,* 41**,** 345-50.

HARGREAVES, A. J. 1997. The cytoskeleton as a target in cell toxicity. *Advanced Molecular cell Biology,* 20**,** 119-144.

HARGREAVES, A. J. 2012. Neurodegenerations induced by organophosphorous compounds. *Adv Exp Med Biol,* 724**,** 189-204.

HARGREAVES, A. J., FOWLER, M. J., SACHANA, M., FLASKOS, J., BOUNTOURI, M., COUTTS, I. C., GLYNN, P., HARRIS, W. & GRAHAM MCLEAN, W. 2006. Inhibition of neurite outgrowth in differentiating mouse N2a neuroblastoma cells by phenyl saligenin phosphate: effects on MAP kinase (ERK 1/2) activation, neurofilament

heavy chain phosphorylation and neuropathy target esterase activity. *Biochem Pharmacol,* 71**,** 1240-7.

HARRILL, J. A., FREUDENRICH, T. M., ROBINETTE, B. L. & MUNDY, W. R. 2011. Comparative sensitivity of human and rat neural cultures to chemical-induced inhibition of neurite outgrowth. *Toxicol Appl Pharmacol,* 256**,** 268-80.

HARRILL, J. A. & MUNDY, W. R. 2011. Quantitative assessment of neurite outgrowth in PC12 cells. *Methods Mol Biol,* 758**,** 331-48.

HARRIS, W., SACHANA, M., FLASKOS, J. & HARGREAVES, A. J. 2009a. Neuroprotection from diazinon-induced toxicity in differentiating murine N2a neuroblastoma cells. *Neurotoxicology,* 30**,** 958-64.

HARRIS, W., SACHANA, M., FLASKOS, J. & HARGREAVES, A. J. 2009b. Proteomic analysis of differentiating neuroblastoma cells treated with sub-lethal neurite inhibitory concentrations of diazinon: identification of novel biomarkers of effect. *Toxicol Appl Pharmacol,* 240**,** 159-65.

HARRY, G. J., BILLINGSLEY, M., BRUININK, A., CAMPBELL, I. L., CLASSEN, W., DORMAN, D. C., GALLI, C., RAY, D., SMITH, R. A. & TILSON, H. A. 1998. In vitro techniques for the assessment of neurotoxicity. *Environ Health Perspect,* 106 Suppl 1**,** 131-58.

HARTL, F. U. & HAYER-HARTL, M. 2002. Molecular chaperones in the cytosol: from nascent chain to folded protein. *Science,* 295**,** 1852-8.

HEIDEMANN, S. R., LANDERS, J. M. & HAMBORG, M. A. 1981a. Polarity orientation of axonal microtubules. *The Journal of cell biology,* 91**,** 661-665.

HEIDEMANN, S. R., LANDERS, J. M. & HAMBORG, M. A. 1981b. Polarity orientation of axonal microtubules. *J Cell Biol,* 91**,** 661-5.

HEILMAIR, R., EYER, F. & EYER, P. 2008. Enzyme-based assay for quantification of chlorpyrifos oxon in human plasma. *Toxicol Lett,* 181**,** 19-24.

HENSCHLER, D., SCHMUCK, G., VAN AERSSEN, M. & SCHIFFMANN, D. 1992. The inhibitory effect of neuropathic organophosphate esters on neurite outgrowth in cell cultures: A basis for screening for delayed neurotoxicity. *Toxicol In Vitro,* 6**,** 327-35.

HIROKAWA, N., GLICKSMAN, M. A. & WILLARD, M. B. 1984. Organization of mammalian neurofilament polypeptides within the neuronal cytoskeleton. *J Cell Biol,* 98**,** 1523-36.

HISANAGA, S.-I. & HIROKAWA, N. 1989. The effects of dephosphorylation on the structure of the projections of neurofilament. *The Journal of Neuroscience,* 9**,** 959-966.

HISANAGA, S.-I., KUSUBATA, M., OKUMURA, E. & KISHIMOTO, T. 1991. Phosphorylation of neurofilament H subunit at the tail domain by CDC2 kinase dissociates the association to microtubules. *Journal of Biological Chemistry,* 266**,** 21798-21803.

HISANAGA, S. & HIROKAWA, N. 1990. Dephosphorylation-induced interactions of neurofilaments with microtubules. *J Biol Chem,* 265**,** 21852-8.

HJORTH, J. J., VAN PELT, J., MANSVELDER, H. D. & VAN OOYEN, A. 2014. Competitive dynamics during resource-driven neurite outgrowth. *PLoS One,* 9**,** e86741.

HOEFEL, D., GROOBY, W. L., MONIS, P. T., ANDREWS, S. & SAINT, C. P. 2003. A comparative study of carboxyfluorescein diacetate and

carboxyfluorescein diacetate succinimidyl ester as indicators of bacterial activity. *J Microbiol Methods,* 52**,** 379-88.

HOLTMAAT, A. J., DIJKHUIZEN, P. A., OESTREICHER, A. B., ROMIJN, H. J., VAN DER LUGT, N. M., BERNS, A., MARGOLIS, F. L., GISPEN, W. H. & VERHAAGEN, J. 1995. Directed expression of the growth-associated protein B-50/GAP-43 to olfactory neurons in transgenic mice results in changes in axon morphology and extraglomerular fiber growth. *J Neurosci,* 15**,** 7953-65.

HONORATO DE OLIVEIRA, G., MOREIRA, V. & RIBEIRO GOES, S. P. 2002. Organophosphate induced delayed neuropathy in genetically dissimilar chickens: studies with tri-ortho-cresyl phosphate (TOCP) and trichlorfon. *Toxicol Lett,* 136**,** 143-50.

HOWARD, A. S., BUCELLI, R., JETT, D. A., BRUUN, D., YANG, D. & LEIN, P. J. 2005. Chlorpyrifos exerts opposing effects on axonal and dendritic growth in primary neuronal cultures. *Toxicol Appl Pharmacol,* 207**,** 112-24.

ICENOGLE, L. M., CHRISTOPHER, N. C., BLACKWELDER, W. P., CALDWELL, D. P., QIAO, D., SEIDLER, F. J., SLOTKIN, T. A. & LEVIN, E. D. 2004. Behavioral alterations in adolescent and adult rats caused by a brief subtoxic exposure to chlorpyrifos during neurulation. *Neurotoxicol Teratol,* 26**,** 95-101.

JAKEL, R. J., SCHNEIDER, B. L. & SVENDSEN, C. N. 2004. Using human neural stem cells to model neurological disease. *Nat Rev Genet,* 5**,** 136-44.

JAMAL, G. A. 1995. Long term neurotoxic effects of organophosphate compounds. *Adverse Drug React Toxicol Rev,* 14**,** 85-99.

JANKE, C. & KNEUSSEL, M. 2010. Tubulin post-translational modifications: encoding functions on the neuronal microtubule cytoskeleton. *Trends Neurosci,* 33**,** 362-72.

JENSEN, K. F., LAPADULA, D. M., ANDERSON, J. K., HAYKAL-COATES, N. & ABOU-DONIA, M. B. 1992. Anomalous phosphorylated neurofilament aggregations in central and peripheral axons of hens treated with tri-ortho-cresyl phosphate (TOCP). *J Neurosci Res,* 33**,** 455-60.

JESSEN, K. R. 2004. Glial cells. *Int J Biochem Cell Biol,* 36**,** 1861-7.

JETT, D. A., NAVOA, R. V., BECKLES, R. A. & MCLEMORE, G. L. 2001. Cognitive function and cholinergic neurochemistry in weanling rats exposed to chlorpyrifos. *Toxicol Appl Pharmacol,* 174**,** 89-98.

JIN, K., MAO, X. O., ZHU, Y. & GREENBERG, D. A. 2002. MEK and ERK protect hypoxic cortical neurons via phosphorylation of Bad. *J Neurochem,* 80**,** 119-25.

JOHNSON, G. L. & LAPADAT, R. 2002. Mitogen-activated protein kinase pathways mediated by ERK, JNK, and p38 protein kinases. *Science,* 298**,** 1911-2.

JOHNSON, M. K. 1969. The delayed neurotoxic effect of some organophosphorus compounds. Identification of the phosphorylation site as an esterase. *Biochem J,* 114**,** 711-7.

JOHNSON, M. K. 1975. The delayed neuropathy caused by some organophosphorus esters: mechanism and challenge. *CRC Crit Rev Toxicol,* 3**,** 289-316.

JOHNSON, M. K. 1982. Initiation of organophosphate-induced delayed neuropathy. *Neurobehav Toxicol Teratol,* 4**,** 759-65.

JOHNSON, M. K. 1990. Organophosphates and delayed neuropathy--is NTE alive and well? *Toxicol Appl Pharmacol,* 102**,** 385-99.

JOHNSON, M. K. & LAUWERYS, R. 1969. Protection by some carbamates against the delayed neurotoxic effects of di-isopropyl phosphorofluoridate. *Nature,* 222**,** 1066-7.

JOKANOVIC, M., KOSANOVIC, M., BRKIC, D. & VUKOMANOVIC, P. 2011. Organophosphate induced delayed polyneuropathy in man: an overview. *Clin Neurol Neurosurg,* 113**,** 7-10.

JORTNER, B. S., PERKINS, S. K. & EHRICH, M. 1999. Immunohistochemical study of phosphorylated neurofilaments during the evolution of organophosphorus ester-induced delayed neuropathy (OPIDN). *Neurotoxicology,* 20**,** 971-5.

JULIEN, J.-P. & MUSHYNSKI, W. E. 1998. Neurofilaments in health and disease. *Progress in nucleic acid research and molecular biology,* 61**,** 1-23.

KAMEL, F., ROWLAND, A. S., PARK, L. P., ANGER, W. K., BAIRD, D. D., GLADEN, B. C., MORENO, T., STALLONE, L. & SANDLER, D. P. 2003. Neurobehavioral performance and work experience in Florida farmworkers. *Environ Health Perspect,* 111**,** 1765-72.

KARALLIEDDE, L. 1999. Organophosphorus poisoning and anaesthesia. *Anaesthesia,* 54**,** 1073-88.

KARALLIEDDE, L. 2006. Carbon monoxide poisoning. *Int J Clin Pract,* 60**,** 1523-4.

KARANTH, S. & POPE, C. 2000. Carboxylesterase and A-esterase activities during maturation and aging: relationship to the toxicity of chlorpyrifos and parathion in rats. *Toxicol Sci,* 58**,** 282-9.

KEARNS, G. L., ABDEL-RAHMAN, S. M., ALANDER, S. W., BLOWEY, D. L., LEEDER, J. S. & KAUFFMAN, R. E. 2003. Developmental pharmacology--drug disposition, action, and therapy in infants and children. *N Engl J Med,* 349**,** 1157-67.

KEILBAUGH, S. A., PRUSOFF, W. H. & SIMPSON, M. V. 1991. The PC12 cell as a model for studies of the mechanism of induction of peripheral neuropathy by anti-HIV-1 dideoxynucleoside analogs. *Biochem Pharmacol,* 42**,** R5-8.

KESAVAPANY, S., PATEL, V., ZHENG, Y. L., PAREEK, T. K., BJELOGRLIC, M., ALBERS, W., AMIN, N., JAFFE, H., GUTKIND, J. S., STRONG, M. J., GRANT, P. & PANT, H. C. 2007. Inhibition of Pin1 reduces glutamate-induced perikaryal accumulation of phosphorylated neurofilament-H in neurons. *Mol Biol Cell,* 18**,** 3645-55.

KETSCHEK, A. & GALLO, G. 2010. Nerve growth factor induces axonal filopodia through localized microdomains of phosphoinositide 3-kinase activity that drive the formation of cytoskeletal precursors to filopodia. *J Neurosci,* 30**,** 12185-97.

KI, Y. W., PARK, J. H., LEE, J. E., SHIN, I. C. & KOH, H. C. 2013. JNK and p38 MAPK regulate oxidative stress and the inflammatory response in chlorpyrifos-induced apoptosis. *Toxicol Lett,* 218**,** 235-45.

KIM, S. U. 2004. Human neural stem cells genetically modified for brain repair in neurological disorders. *Neuropathology,* 24**,** 159-71.

KIRKPATRIC, L. L. & BRADY, S. T. 1999. Molecular components of the neuronal cytoskeleton. *In:* SIEGEL, G. J., AGRANOFF, B. W., ALBERS, R. W., FISHER, S. K. & UHLER, M. D. (eds.) *Basic neurochemistry: molecular, cellular and medical aspects.* Philadelphia: Lippincott-Raven.

KLEBE, R. J. & RUDDLE, F. H. 1969. Neuroblastoma: cell culture analysis of a differentiating stem cell system. *Journal of Cell Biology,* 43**,** 69.

KLEMM, M. & SCHRATTENHOLZ, A. 2004. Neurotoxicity of active compounds--establishment of hESC-lines and proteomics technologies for human embryo- and neurotoxicity screening and biomarker identification. *ALTEX,* 21 Suppl 3**,** 41-8.

KOELLE, G. B. 1992. Erythrocyte and tissue AChE inhibition. *J Appl Toxicol,* 12**,** 305.

KOLAROVA, M., GARCÃ-A-SIERRA, F., BARTOS, A., RICNY, J. & RIPOVA, D. 2012. Structure and pathology of tau protein in Alzheimer disease. *International journal of Alzheimerâ€™s disease,* 2012.

KORNBLUM, H. I. 2007. Introduction to neural stem cells. *Stroke,* 38**,** 810-6.

KRUG, A. K., KOLDE, R., GASPAR, J. A., REMPEL, E., BALMER, N. V., MEGANATHAN, K., VOJNITS, K., BAQUIE, M., WALDMANN, T., ENSENAT-WASER, R., JAGTAP, S., EVANS, R. M., JULIEN, S., PETERSON, H., ZAGOURA, D., KADEREIT, S., GERHARD, D., SOTIRIADOU, I., HEKE, M., NATARAJAN, K., HENRY, M., WINKLER, J., MARCHAN, R., STOPPINI, L., BOSGRA, S., WESTERHOUT, J., VERWEI, M., VILO, J., KORTENKAMP, A., HESCHELER, J., HOTHORN, L., BREMER, S., VAN THRIEL, C., KRAUSE, K. H., HENGSTLER, J. G., RAHNENFUHRER, J., LEIST, M. & SACHINIDIS, A. 2013. Human embryonic stem cell-derived test systems for developmental neurotoxicity: a transcriptomics approach. *Arch Toxicol,* 87**,** 123-43.

KUCZMARSKI, E. R. & ROSENBAUM, J. L. 1979. Studies on the organization and localization of actin and myosin in neurons. *J Cell Biol,* 80**,** 356-71.

KWON, C. H., LUIKART, B. W., POWELL, C. M., ZHOU, J., MATHENY, S. A., ZHANG, W., LI, Y., BAKER, S. J. & PARADA, L. F. 2006. Pten regulates neuronal arborization and social interaction in mice. *Neuron,* 50**,** 377-88.

LARNER, A. J. 1995. Axonal sprouting and synaptogenesis in temporal lobe epilepsy: possible pathogenetic and therapeutic roles of neurite growth inhibitory factors. *Seizure,* 4**,** 249-58.

LAUDER, J. M. & SCHAMBRA, U. B. 1999. Morphogenetic roles of acetylcholine. *Environ Health Perspect,* 107 Suppl 1**,** 65-9.

LEE, M. K. & CLEVELAND, D. W. 1994. Neurofilament function and dysfunction: involvement in axonal growth and neuronal disease. *Curr Opin Cell Biol,* 6**,** 34-40.

LEE, M. K. & CLEVELAND, D. W. 1996. Neuronal intermediate filaments. *Annu Rev Neurosci,* 19**,** 187-217.

LEVIN, H. S., RODNITZKY, R. L. & MICK, D. L. 1976. Anxiety associated with exposure to organophosphate compounds. *Arch Gen Psychiatry,* 33**,** 225-8.

LI, X., DANCAUSSE, H., GRIJALVA, I., OLIVEIRA, M. & LEVI, A. D. 2003. Labeling Schwann cells with CFSE-an in vitro and in vivo study. *J Neurosci Methods,* 125**,** 83-91.

LICHTENBERG-KRAAG, B., MANDELKOW, E. M., BIERNAT, J., STEINER, B., SCHROTER, C., GUSTKE, N., MEYER, H. E. & MANDELKOW, E. 1992. Phosphorylation-dependent epitopes of neurofilament antibodies on tau protein and relationship with Alzheimer tau. *Proc Natl Acad Sci U S A,* 89**,** 5384-8.

LIEDTKE, W., EDELMANN, W., BIERI, P. L., CHIU, F.-C., COWAN, N. J., KUCHERLAPATI, R. & RAINE, C. S. 1996. GFAP is necessary for the integrity of CNS white matter architecture and long-term maintenance of myelination. *Neuron,* 17**,** 607-615.

LIN, L.-F. H. 1996. Glial cell line-derived neurotrophic factor (GDNF): a comperhensive review. *Neural notes,* 11**,** 1-7.

LIU, C., LI, Y., LEIN, P. J. & FORD, B. D. 2012. Spatiotemporal patterns of GFAP upregulation in rat brain following acute intoxication with diisopropylfluorophosphate (DFP). *Current neurobiology,* 3**,** 90.

LOCK, E. A. & JOHNSON, M. K. 1990. Delayed neuropathy and acute toxicity studies with pirimiphos-methyl in the hen. *J Appl Toxicol,* 10**,** 17-21.

LODISH, H., BERK, A., ZIPURSKY, S. L., MATSUDAIRA, P., BALTIMORE, D. & DARNELL, J. 2000a. The actin cytoskeleton.

LODISH, H., BERK, A., ZIPURSKY, S. L., MATSUDAIRA, P., BALTIMORE, D. & DARNELL, J. 2000b. Protein structure and function.

LODISH, H. F. 2000. *Molecular cell biology,* New York, NY ; Basingstoke, Freeman.

LOPEZ-MADERUELO, M. D., FERNANDEZ-RENART, M., MORATILLA, C. & RENART, J. 2001. Opposite effects of the Hsp90 inhibitor Geldanamycin: induction of apoptosis in PC12, and differentiation in N2A cells. *FEBS Lett,* 490**,** 23-7.

LOTTI, M. 1991. The pathogenesis of organophosphate polyneuropathy. *Crit Rev Toxicol,* 21**,** 465-87.

LOTTI, M. 2000. Organophosphorus compounds. *In:* SPENCER, P. S., SCHAUMBURG, H. H. & LUDOLPH, A. C. (eds.) *Experimental and clinical neurotoxicology*

2nd ed. New York: Oxford University Press.

LOTTI, M. 2001. Clinical toxicology of anticholinesterase agents in humans. *Handbook of pesticide toxicology,* 2**,** 1043-1085.

LOTTI, M. & MORETTO, A. 2005. Organophosphate-induced delayed polyneuropathy. *Toxicol Rev,* 24**,** 37-49.

LOTTI, M., MORETTO, A., ZOPPELLARI, R., DAINESE, R., RIZZUTO, N. & BARUSCO, G. 1986. Inhibition of lymphocytic neuropathy target esterase predicts the development of organophosphate-induced delayed polyneuropathy. *Archives of toxicology,* 59**,** 176-179.

LOWERY, L. A. & VAN VACTOR, D. 2009. The trip of the tip: understanding the growth cone machinery. *Nat Rev Mol Cell Biol,* 10**,** 332-43.

LOWRY, O. H., ROSEBROUGH, N. J., FARR, A. L. & RANDALL, R. J. 1951. Protein measurement with the Folin phenol reagent. *J Biol Chem,* 193**,** 265-75.

LUDUENA, R. F. 1993. Are tubulin isotypes functionally significant. *Mol Biol Cell,* 4**,** 445-57.

LYONS, A. B. 1999. Divided we stand: tracking cell proliferation with carboxyfluorescein diacetate succinimidyl ester. *Immunol Cell Biol,* 77**,** 509-15.

MANDELL, J. & BANKER, G. 1995. The microtubule cytoskeleton and the development of neuronal polarity. *Neurobiology of aging,* 16**,** 229-237.

MANSUY, I. M. & SHENOLIKAR, S. 2006. Protein serine/threonine phosphatases in neuronal plasticity and disorders of learning and memory. *Trends Neurosci,* 29**,** 679-86.

MARTIN, M. A., OSMANI, S. A. & OAKLEY, B. R. 1997. The role of gamma-tubulin in mitotic spindle formation and cell cycle progression in Aspergillus nidulans. *J Cell Sci,* 110 (Pt 5)**,** 623-33.

MATTINGLY, J. E., SULLIVAN, J. E., SPILLER, H. A. & BOSSE, G. M. 2003. Intermediate syndrome after exposure to chlorpyrifos in a 16-month-old girl. *J Emerg Med,* 25**,** 379-81.

MCGOUGH, A. & CHIU, W. 1999. ADF/cofilin weakens lateral contacts in the actin filament. *J Mol Biol,* 291**,** 513-9.

MEARNS, J., DUNN, J. & LEES-HALEY, P. R. 1994. Psychological effects of organophosphate pesticides: a review and call for research by psychologists. *J Clin Psychol,* 50**,** 286-94.

MEIRI, K. F., PFENNINGER, K. H. & WILLARD, M. B. 1986. Growth-associated protein, GAP-43, a polypeptide that is induced when neurons extend axons, is a component of growth cones and corresponds to pp46, a major polypeptide of a subcellular fraction enriched in growth cones. *Proc Natl Acad Sci U S A,* 83**,** 3537-41.

MEIRI, K. F., SAFFELL, J. L., WALSH, F. S. & DOHERTY, P. 1998. Neurite outgrowth stimulated by neural cell adhesion molecules requires growth-associated protein-43 (GAP-43) function and is associated with GAP-43 phosphorylation in growth cones. *J Neurosci,* 18**,** 10429-37.

MENSE, S. M., SENGUPTA, A., LAN, C., ZHOU, M., BENTSMAN, G., VOLSKY, D. J., WHYATT, R. M., PERERA, F. P. & ZHANG, L. 2006. The common insecticides cyfluthrin and chlorpyrifos alter the expression of a subset of genes with diverse functions in primary human astrocytes. *Toxicol Sci,* 93**,** 125-35.

MIKSYS, S., LERMAN, C., SHIELDS, P. G., MASH, D. C. & TYNDALE, R. F. 2003. Smoking, alcoholism and genetic polymorphisms alter CYP2B6 levels in human brain. *Neuropharmacology,* 45**,** 122-32.

MIKSYS, S. & TYNDALE, R. F. 2004. The unique regulation of brain cytochrome P450 2 (CYP2) family enzymes by drugs and genetics. *Drug Metab Rev,* 36**,** 313-33.

MILLECAMPS, S. & JULIEN, J.-P. 2013. Axonal transport deficits and neurodegenerative diseases. *Nat Rev Neurosci,* 14**,** 161-176.

MONNET-TSCHUDI, F., ZURICH, M. G., SCHILTER, B., COSTA, L. G. & HONEGGER, P. 2000. Maturation-dependent effects of chlorpyrifos and parathion and their oxygen analogs on acetylcholinesterase and neuronal and glial markers in aggregating brain cell cultures. *Toxicol Appl Pharmacol,* 165**,** 175-83.

MOSER, V. C., CHANDA, S. M., MORTENSEN, S. R. & PADILLA, S. 1998. Age- and gender-related differences in sensitivity to chlorpyrifos in the rat reflect developmental profiles of esterase activities. *Toxicol Sci,* 46**,** 211-22.

MOSMANN, T. 1983. Rapid colorimetric assay for cellular growth and survival: application to proliferation and cytotoxicity assays. *J Immunol Methods,* 65**,** 55-63.

MUNDY, W. R., RADIO, N. M. & FREUDENRICH, T. M. 2010. Neuronal models for evaluation of proliferation in vitro using high content screening. *Toxicology,* 270**,** 121-30.

MUNOZ-QUEZADA, M. T., IGLESIAS, V., LUCERO, B., STEENLAND, K., BARR, D. B., LEVY, K., RYAN, P. B., ALVARADO, S. & CONCHA, C. 2012. Predictors of exposure to organophosphate pesticides in schoolchildren in the Province of Talca, Chile. *Environ Int,* 47**,** 28-36.

NAND, N., AGGARWAL, H. K., BHARTI, K. & CHAKRABARTI, D. 2007. Organophosphate induced delayed neuropathy. *J Assoc Physicians India,* 55**,** 72-3.

NCFAP, N. C. F. F. A. A. P. 2000. Pesticide use in U.S. crop production: 1997 national summary report. *In:* LEONARD P, G. A. M. B. M. (ed.). Wachington, DC.

NIXON, R. A., BROWN, B. A. & MAROTTA, C. A. 1982. Posttranslational modification of a neurofilament protein during axoplasmic transport: implications for regional specialization of CNS axons. *J Cell Biol,* 94**,** 150-8.

NIXON, R. A. & MAROTTA, C. A. 1984. Degradation of neurofilament proteins by purified human brain cathepsin D. *J Neurochem,* 43**,** 507-16.

O'CALLAGHAN, J. P. 1988. Neurotypic and gliotypic proteins as biochemical markers of neurotoxicity. *Neurotoxicol Teratol,* 10**,** 445-452.

ODELL, I. D. & COOK, D. 2013. Immunofluorescence techniques. *J Invest Dermatol,* 133**,** e4.

OLMSTED, J. 1986. Microtubule-associated proteins. *Annual review of cell biology,* 2**,** 421-457.

OMARY, M. B., KU, N. O., TAO, G. Z., TOIVOLA, D. M. & LIAO, J. 2006. "Heads and tails" of intermediate filament phosphorylation: multiple sites and functional insights. *Trends Biochem Sci,* 31**,** 383-94.

OSTERLOH, J., LOTTI, M. & POND, S. M. 1983. Toxicologic studies in a fatal overdose of 2, 4-D, MCPP, and chlorpyrifos. *Journal of analytical toxicology,* 7**,** 125-129.

OSTREA, E. M., MORALES, V., NGOUMGNA, E., PRESCILLA, R., TAN, E., HERNANDEZ, E., RAMIREZ, G. B., CIFRA, H. L. & MANLAPAZ, M. L. 2002. Prevalence of fetal exposure to environmental toxins as determined by meconium analysis. *Neurotoxicology,* 23**,** 329-39.

PAK, C. W., FLYNN, K. C. & BAMBURG, J. R. 2008. Actin-binding proteins take the reins in growth cones. *Nat Rev Neurosci,* 9**,** 136-47.

PARISH, C. R. 1999. Fluorescent dyes for lymphocyte migration and proliferation studies. *Immunol Cell Biol,* 77**,** 499-508.

PARRAN, D. K., MAGNIN, G., LI, W., JORTNER, B. S. & EHRICH, M. 2005. Chlorpyrifos alters functional integrity and structure of an in vitro BBB model: co-cultures of bovine endothelial cells and neonatal rat astrocytes. *Neurotoxicology,* 26**,** 77-88.

PEKINER, C., DENT, E. W., ROBERTS, R. E., MEIRI, K. F. & MCLEAN, W. G. 1996. Altered GAP-43 immunoreactivity in regenerating sciatic nerve of diabetic rats. *Diabetes,* 45**,** 199-204.

PELKONEN, O., VAHAKANGAS, K. & GUPTA, R. C. 2006. Placental toxicity of organophosphate and carbamate pesticides. *In:* GUPTA, R. C.

(ed.) *Toxicology of organophosphate and carbamate compounds.* Amsterdam ; Boston: Elsevier Academic Press.

PERRON, J. C. & BIXBY, J. L. 1999. Distinct neurite outgrowth signaling pathways converge on ERK activation. *Mol Cell Neurosci,* 13**,** 362-78.

PERROT, R. & EYER, J. 2009. Neuronal intermediate filaments and neurodegenerative disorders. *Brain Res Bull,* 80**,** 282-95.

POPE, C. N. & CHAKRABORTI, T. K. 1992. Dose-related inhibition of brain and plasma cholinesterase in neonatal and adult rats following sublethal organophosphate exposures. *Toxicology,* 73**,** 35-43.

POPE, C. N., CHAKRABORTI, T. K., CHAPMAN, M. L., FARRAR, J. D. & ARTHUN, D. 1991. Comparison of in vivo cholinesterase inhibition in neonatal and adult rats by three organophosphorothioate insecticides. *Toxicology,* 68**,** 51-61.

PRASHAD, N. & ROSENBERG, R. N. 1978. Induction of cyclic AMP-binding proteins by dibutyryl cyclic AMP in mouse neuroblastoma cells. *Biochim Biophys Acta,* 539**,** 459-69.

PRENDERGAST, M. A., SELF, R. L., SMITH, K. J., GHAYOUMI, L., MULLINS, M. M., BUTLER, T. R., BUCCAFUSCO, J. J., GEARHART, D. A. & TERRY JR, A. V. 2007. Microtubule-associated targets in chlorpyrifos oxon hippocampal neurotoxicity. *Neuroscience,* 146**,** 330-339.

RADIO, N. M., BREIER, J. M., SHAFER, T. J. & MUNDY, W. R. 2008. Assessment of chemical effects on neurite outgrowth in PC12 cells using high content screening. *Toxicol Sci,* 105**,** 106-18.

RADIO, N. M., FREUDENRICH, T. M., ROBINETTE, B. L., CROFTON, K. M. & MUNDY, W. R. 2010. Comparison of PC12 and cerebellar granule cell cultures for evaluating neurite outgrowth using high content analysis. *Neurotoxicol Teratol,* 32**,** 25-35.

RADIO, N. M. & MUNDY, W. R. 2008. Developmental neurotoxicity testing in vitro: models for assessing chemical effects on neurite outgrowth. *Neurotoxicology,* 29**,** 361-76.

RAMAKERS, G. J. 2002. Rho proteins, mental retardation and the cellular basis of cognition. *Trends Neurosci,* 25**,** 191-9.

RAMAN, M., CHEN, W. & COBB, M. H. 2007. Differential regulation and properties of MAPKs. *Oncogene,* 26**,** 3100-12.

RAO, M. V., CAMPBELL, J., YUAN, A., KUMAR, A., GOTOW, T., UCHIYAMA, Y. & NIXON, R. A. 2003. The neurofilament middle molecular mass subunit carboxyl-terminal tail domains is essential for the radial growth and cytoskeletal architecture of axons but not for regulating neurofilament transport rate. *J Cell Biol,* 163**,** 1021-31.

RAUH, V. A., PERERA, F. P., HORTON, M. K., WHYATT, R. M., BANSAL, R., HAO, X., LIU, J., BARR, D. B., SLOTKIN, T. A. & PETERSON, B. S. 2012. Brain anomalies in children exposed prenatally to a common organophosphate pesticide. *Proc Natl Acad Sci U S A,* 109**,** 7871-6.

REKART, J. L., MEIRI, K. & ROUTTENBERG, A. 2005. Hippocampal-dependent memory is impaired in heterozygous GAP-43 knockout mice. *Hippocampus,* 15**,** 1-7.

RICCERI, L., VENEROSI, A., CAPONE, F., COMETA, M. F., LORENZINI, P., FORTUNA, S. & CALAMANDREI, G. 2006. Developmental neurotoxicity of organophosphorous pesticides: fetal and neonatal

exposure to chlorpyrifos alters sex-specific behaviors at adulthood in mice. *Toxicol Sci,* 93**,** 105-13.

RICE, D. & BARONE, S., JR. 2000. Critical periods of vulnerability for the developing nervous system: evidence from humans and animal models. *Environ Health Perspect,* 108 Suppl 3**,** 511-33.

RICHARDSON, R. J. 1995. Assessment of the neurotoxic potential of chlorpyrifos relative to other organophosphorus compounds: a critical review of the literature. *J Toxicol Environ Health,* 44**,** 135-65.

RICHARDSON, R. J., MOORE, T. B., KAYYALI, U. S. & RANDALL, J. C. 1993. Chlorpyrifos: assessment of potential for delayed neurotoxicity by repeated dosing in adult hens with monitoring of brain acetylcholinesterase, brain and lymphocyte neurotoxic esterase, and plasma butyrylcholinesterase activities. *Fundam Appl Toxicol,* 21**,** 89-96.

RICHARDSON, R. M., HOLLOWAY, K. L., BULLOCK, M. R., BROADDUS, W. C. & FILLMORE, H. L. 2006. Isolation of neuronal progenitor cells from the adult human neocortex. *Acta Neurochir (Wien),* 148**,** 773-7.

RIEDL, A. G., WATTS, P. M., JENNER, P. & MARSDEN, C. D. 1998. P450 enzymes and Parkinson's disease: the story so far. *Mov Disord,* 13**,** 212-20.

ROBERTSON, R. T. 1987. A morphogenic role for transiently expressed acetylcholinesterase in developing thalamocortical systems? *Neurosci Lett,* 75**,** 259-64.

ROBINSON, M. J. & COBB, M. H. 1997. Mitogen-activated protein kinase pathways. *Curr Opin Cell Biol,* 9**,** 180-6.

ROHLMAN, D. S., ARCURY, T. A., QUANDT, S. A., LASAREV, M., ROTHLEIN, J., TRAVERS, R., TAMULINAS, A., SCHERER, J., EARLY, J., MARIN, A., PHILLIPS, J. & MCCAULEY, L. 2005. Neurobehavioral performance in preschool children from agricultural and non-agricultural communities in Oregon and North Carolina. *Neurotoxicology,* 26**,** 589-98.

ROHLMAN, D. S., BAILEY, S. R., ANGER, W. K. & MCCAULEY, L. 2001. Assessment of neurobehavioral function with computerized tests in a population of hispanic adolescents working in agriculture. *Environ Res,* 85**,** 14-24.

ROHLMAN, D. S., LASAREV, M., ANGER, W. K., SCHERER, J., STUPFEL, J. & MCCAULEY, L. 2007. Neurobehavioral performance of adult and adolescent agricultural workers. *Neurotoxicology,* 28**,** 374-80.

ROINESTAD, K. S., LOUIS, J. B. & ROSEN, J. D. 1993. Determination of pesticides in indoor air and dust. *J AOAC Int,* 76**,** 1121-6.

ROSENSTOCK, L., KEIFER, M., DANIELL, W. E., MCCONNELL, R. & CLAYPOOLE, K. 1991. Chronic central nervous system effects of acute organophosphate pesticide intoxication. The Pesticide Health Effects Study Group. *Lancet,* 338**,** 223-7.

RUDRABHATLA, P., JAFFE, H. & PANT, H. C. 2011. Direct evidence of phosphorylated neuronal intermediate filament proteins in neurofibrillary tangles (NFTs): phosphoproteomics of Alzheimer's NFTs. *FASEB J,* 25**,** 3896-905.

SACHANA, M., FLASKOS, J., ALEXAKI, E., GLYNN, P. & HARGREAVES, A. J. 2001. The toxicity of chlorpyrifos towards differentiating mouse N2a neuroblastoma cells. *Toxicol In Vitro,* 15**,** 369-72.

SACHANA, M., FLASKOS, J., ALEXAKI, E. & HARGREAVES, A. J. 2003. Inhibition of neurite outgrowth in N2a cells by leptophos and carbaryl: effects on neurofilament heavy chain, GAP-43 and HSP-70. *Toxicol In Vitro,* 17**,** 115-20.

SACHANA, M., FLASKOS, J. & HARGREAVES, A. J. 2005. Effects of Chlorpyrifos and Chlorpyrifos-Methyl on the Outgrowth of Axon-Like Processes, Tubulin, and GAP-43 in N2a Cells. *Toxicol Mech Methods,* 15**,** 405-10.

SACHANA, M., FLASKOS, J., SIDIROPOULOU, E., YAVARI, C. A. & HARGREAVES, A. J. 2008. Inhibition of extension outgrowth in differentiating rat C6 glioma cells by chlorpyrifos and chlorpyrifos oxon: effects on microtubule proteins. *Toxicol In Vitro,* 22**,** 1387-91.

SACHANA, M., SIDIROPOULOU, E., FLASKOS, J., HARRIS, W., ROBINSON, A. J., WOLDEHIWET, Z. & HARGREAVES, A. J. 2014. Diazoxon disrupts the expression and distribution of betaIII-tubulin and MAP 1B in differentiating N2a cells. *Basic Clin Pharmacol Toxicol,* 114**,** 490-6.

SAKAMOTO, M., KUBOTA, M., LIU, X. J., MURATA, K., NAKAI, K. & SATOH, H. 2004. Maternal and fetal mercury and n-3 polyunsaturated fatty acids as a risk and benefit of fish consumption to fetus. *Environ Sci Technol,* 38**,** 3860-3.

SALVI, R. M., LARA, D. R., GHISOLFI, E. S., PORTELA, L. V., DIAS, R. D. & SOUZA, D. O. 2003. Neuropsychiatric Evaluation in Subjects Chronically Exposed to Organophosphate Pesticides. *Toxicological Sciences,* 72**,** 267-271.

SALYHA, Y. 2010. Biological effects assessment of chlorpyrifos and some aspects of its neurotoxicity. *Biology Series,* 54**,** 3-14.

SANCHEZ-SANTED, F., CANADAS, F., FLORES, P., LOPEZ-GRANCHA, M. & CARDONA, D. 2004. Long-term functional neurotoxicity of paraoxon and chlorpyrifos: behavioural and pharmacological evidence. *Neurotoxicol Teratol,* 26**,** 305-17.

SAVAGE, E. P., KEEFE, T. J., MOUNCE, L. M., HEATON, R. K., LEWIS, J. A. & BURCAR, P. J. 1988. Chronic neurological sequelae of acute organophosphate pesticide poisoning. *Arch Environ Health,* 43**,** 38-45.

SCHETTLER, T. 2001. Toxic threats to neurologic development of children. *Environ Health Perspect,* 109 Suppl 6**,** 813-6.

SCHMUCK, G. & AHR, H. J. 1997. Improved in vitro method for screening organophosphate-induced delayed polyneuropathy. *Toxicol In Vitro,* 11**,** 263-70.

SCHOENFELD, T. A. & OBAR, R. A. 1994. Diverse distribution and function of fibrous microtubule-associated proteins in the nervous system. *Int Rev Cytol,* 151**,** 67-137.

SCHUBERT, D., HUMPHREYS, S., BARONI, C. & COHN, M. 1969. In vitro differentiation of a mouse neuroblastoma. *Proc Natl Acad Sci U S A,* 64**,** 316-23.

SEABERG, R. M. & VAN DER KOOY, D. 2003. Stem and progenitor cells: the premature desertion of rigorous definitions. *Trends Neurosci,* 26**,** 125-31.

SENANAYAKE, N. & KARALLIEDDE, L. 1987. Neurotoxic effects of organophosphorus insecticides. An intermediate syndrome. *N Engl J Med,* 316**,** 761-3.

SHAUL, Y. D. & SEGER, R. 2007. The MEK/ERK cascade: from signaling specificity to diverse functions. *Biochim Biophys Acta,* 1773**,** 1213-26.

SHAW, A. S. & FILBERT, E. L. 2009. Scaffold proteins and immune-cell signalling. *Nat Rev Immunol,* 9**,** 47-56.

SHAW, G. 1991. Neurofilament proteins. *In:* BURGOYNE, R. D. (ed.) *The neuronal cytskeleton.* New York: Wiley-Liss Inc.

SIDIROPOULOU, E., SACHANA, M., FLASKOS, J., HARRIS, W., HARGREAVES, A. J. & WOLDEHIWET, Z. 2009a. Diazinon oxon affects the differentiation of mouse N2a neuroblastoma cells. *Arch Toxicol,* 83**,** 373-80.

SIDIROPOULOU, E., SACHANA, M., FLASKOS, J., HARRIS, W., HARGREAVES, A. J. & WOLDEHIWET, Z. 2009b. Diazinon oxon interferes with differentiation of rat C6 glioma cells. *Toxicol In Vitro,* 23**,** 1548-52.

SIHAG, R. K., INAGAKI, M., YAMAGUCHI, T., SHEA, T. B. & PANT, H. C. 2007. Role of phosphorylation on the structural dynamics and function of types III and IV intermediate filaments. *Exp Cell Res,* 313**,** 2098-109.

SILVA, R. F., FALCAO, A. S., FERNANDES, A., GORDO, A. C., BRITO, M. A. & BRITES, D. 2006. Dissociated primary nerve cell cultures as models for assessment of neurotoxicity. *Toxicol Lett,* 163**,** 1-9.

SINGH, S. & SHARMA, N. 2000. Neurological syndromes following organophosphate poisoning. *Neurol India,* 48**,** 308-13.

SINGLETON, D. W., LU, C. L., COLELLA, R. & ROISEN, F. J. 2000. Promotion of neurite outgrowth by protein kinase inhibitors and ganglioside GM1 in neuroblastoma cells involves MAP kinase ERK1/2. *Int J Dev Neurosci,* 18**,** 797-805.

SKENE, J. H. 1989. Axonal growth-associated proteins. *Annu Rev Neurosci,* 12**,** 127-56.

SLOTKIN, T. A. 2004. Cholinergic systems in brain development and disruption by neurotoxicants: nicotine, environmental tobacco smoke, organophosphates. *Toxicol Appl Pharmacol,* 198**,** 132-51.

SLOTKIN, T. A., LEVIN, E. D. & SEIDLER, F. J. 2006. Comparative developmental neurotoxicity of organophosphate insecticides: effects on brain development are separable from systemic toxicity. *Environ Health Perspect,* 114**,** 746-51.

SMITH, C. & EISENSTEIN, M. 2005. Automated imaging: data as far as the eye can see. *Nature methods,* 2**,** 547-55.

SOBUE, K. 1993. Actin-based cytoskeleton in growth cone activity. *Neurosci Res,* 18**,** 91-102.

SOGORB, M. A., GONZALEZ-GONZALEZ, I., PAMIES, D. & VILANOVA, E. 2010. An alternative in vitro method for detecting neuropathic compounds based on acetylcholinesterase inhibition and on inhibition and aging of neuropathy target esterase (NTE). *Toxicol In Vitro,* 24**,** 942-52.

SOGORB, M. A. & VILANOVA, E. 2010. Detoxication of anticholineserase pesticides. *In:* SATOH, T., GUPTA, R. C. & EBRARY INC. (eds.) *Anticholinesterase pesticides metabolism, neurotoxicity, and epidemiology.* Hoboken, N.J.: Wiley,.

SOLOMON, G. M. & MOODLEY, J. 2007. Acute chlorpyrifos poisoning in pregnancy: a case report. *Clin Toxicol (Phila),* 45**,** 416-9.

SREEDHAR, A. S., SOTI, C. & CSERMELY, P. 2004. Inhibition of Hsp90: a new strategy for inhibiting protein kinases. *Biochim Biophys Acta,* 1697**,** 233-42.

STEENLAND, K., JENKINS, B., AMES, R. G., O'MALLEY, M., CHRISLIP, D. & RUSSO, J. 1994. Chronic neurological sequelae to organophosphate pesticide poisoning. *American Journal of Public Health,* 84**,** 731-736.

STEEVENS, J. A. & BENSON, W. H. 1999. Toxicological interactions of chlorpyrifos and methyl mercury in the amphipod, Hyalella azteca. *Toxicol Sci,* 52**,** 168-77.

STEPHENS, R., SPURGEON, A., CALVERT, I. A., BEACH, J., LEVY, L. S., BERRY, H. & HARRINGTON, J. M. 1995. Neuropsychological effects of long-term exposure to organophosphates in sheep dip. *Lancet,* 345**,** 1135-9.

STRACK, S., WESTPHAL, R. S., COLBRAN, R. J., EBNER, F. F. & WADZINSKI, B. E. 1997. Protein serine/threonine phosphatase 1 and 2A associate with and dephosphorylate neurofilaments. *Brain Res Mol Brain Res,* 49**,** 15-28.

SUWITA, E., LAPADULA, D. M. & ABOU-DONIA, M. B. 1986. Calcium and calmodulin-enhanced in vitro phosphorylation of hen brain cold-stable microtubules and spinal cord neurofilament triplet proteins after a single oral dose of tri-o-cresyl phosphate. *Proc Natl Acad Sci U S A,* 83**,** 6174-8.

TATA, A. M., VELLUTO, L., D'ANGELO, C. & REALE, M. 2014. Cholinergic system dysfunction and neurodegenerative diseases: cause or effect? *CNS Neurol Disord Drug Targets,* 13**,** 1294-303.

THERIOT, J. A. 1994. Regulation of the actin cytoskeleton in living cells. *Semin Cell Biol,* 5**,** 193-9.

THIERMANN, H., SZINICZ, L., EYER, F., WOREK, F., EYER, P., FELGENHAUER, N. & ZILKER, T. 1999. Modern strategies in therapy of organophosphate poisoning. *Toxicol Lett,* 107**,** 233-9.

THIVAKARAN, T., GAMAGE, R., GUNARATHNE, K. S. & GOONERATNE, I. K. 2012. Chlorpyrifos-induced delayed myelopathy and pure motor neuropathy: a case report. *Neurologist,* 18**,** 226-8.

THOMA, K. & NICHOLSON, B. C. 1989. Pesticide losses in runoff from a hurticultural catchment in South Australia and their relevance to stream and reservoir water quality. *Environmental Technology Letters,* 10**,** 117-129.

TILNEY, L. G., BRYAN, J., BUSH, D. J., FUJIWARA, K., MOOSEKER, M. S., MURPHY, D. B. & SNYDER, D. H. 1973. Microtubules: evidence for 13 protofilaments. *J Cell Biol,* 59**,** 267-75.

TIMCHALK, C., NOLAN, R. J., MENDRALA, A. L., DITTENBER, D. A., BRZAK, K. A. & MATTSSON, J. L. 2002. A Physiologically Based Pharmacokinetic and Pharmacodynamic (PBPK/PD) Model for the Organophosphate Insecticide Chlorpyrifos in Rats and Humans. *Toxicological Sciences,* 66**,** 34-53.

TISCHFIELD, M. A. & ENGLE, E. C. 2010. Distinct alpha- and beta-tubulin isotypes are required for the positioning, differentiation and survival of neurons: new support for the 'multi-tubulin' hypothesis. *Biosci Rep,* 30**,** 319-30.

TOWBIN, H., STAEHELIN, T. & GORDON, J. 1979. Electrophoretic transfer of proteins from polyacrylamide gels to nitrocellulose sheets: procedure and some applications. *Proc Natl Acad Sci U S A,* 76**,** 4350-4.

TUSH, G. M. & ANSTEAD, M. I. 1997. Pralidoxime continuous infusion in the treatment of organophosphate poisoning. *Ann Pharmacother,* 31**,** 441-4.

VALLEE, R. & BLOOM, G. 1991. Mechanisms of fast and slow axonal transport. *Annual review of neuroscience,* 14**,** 59-92.

VEERANNA, AMIN, N. D., AHN, N. G., JAFFE, H., WINTERS, C. A., GRANT, P. & PANT, H. C. 1998. Mitogen-activated protein kinases (Erk1,2) phosphorylate Lys-Ser-Pro (KSP) repeats in neurofilament proteins NF-H and NF-M. *J Neurosci,* 18**,** 4008-21.

VEERANNA, KAJI, T., BOLAND, B., ODRLJIN, T., MOHAN, P., BASAVARAJAPPA, B. S., PETERHOFF, C., CATALDO, A., RUDNICKI, A., AMIN, N., LI, B. S., PANT, H. C., HUNGUND, B. L., ARANCIO, O. & NIXON, R. A. 2004. Calpain mediates calcium-induced activation of the erk1,2 MAPK pathway and cytoskeletal phosphorylation in neurons: relevance to Alzheimer's disease. *Am J Pathol,* 165**,** 795-805.

VEERANNA, SHETTY, K. T., LINK, W. T., JAFFE, H., WANG, J. & PANT, H. C. 1995. Neuronal cyclin-dependent kinase-5 phosphorylation sites in neurofilament protein (NF-H) are dephosphorylated by protein phosphatase 2A. *J Neurochem,* 64**,** 2681-90.

VESCOVI, A. L., PARATI, E. A., GRITTI, A., POULIN, P., FERRARIO, M., WANKE, E., FROLICHSTHAL-SCHOELLER, P., COVA, L., ARCELLANA-PANLILIO, M., COLOMBO, A. & GALLI, R. 1999. Isolation and cloning of multipotential stem cells from the embryonic human CNS and establishment of transplantable human neural stem cell lines by epigenetic stimulation. *Exp Neurol,* 156**,** 71-83.

VIDAIR, C. A. 2004. Age dependence of organophosphate and carbamate neurotoxicity in the postnatal rat: extrapolation to the human. *Toxicol Appl Pharmacol,* 196**,** 287-302.

VOGELSBERG-RAGAGLIA, V., SCHUCK, T., TROJANOWSKI, J. Q. & LEE, V. M. 2001. PP2A mRNA expression is quantitatively decreased in Alzheimer's disease hippocampus. *Exp Neurol,* 168**,** 402-12.

WALL, M. J. 2005. Short-term synaptic plasticity during development of rat mossy fibre to granule cell synapses. *Eur J Neurosci,* 21**,** 2149-58.

WANG, X., MARTINDALE, J. L., LIU, Y. & HOLBROOK, N. J. 1998. The cellular response to oxidative stress: influences of mitogen-activated protein kinase signalling pathways on cell survival. *Biochem J,* 333 (Pt 2)**,** 291-300.

WAUCHOPE, R. D., BUTTLER, T. M., HORNSBY, A. G., AUGUSTIJN-BECKERS, P. W. & BURT, J. P. 1992. The SCS/ARS/CES pesticide properties database for environmental decision-making. *Rev Environ Contam Toxicol,* 123**,** 1-155.

WEBB, S. J., MONK, C. S. & NELSON, C. A. 2001. Mechanisms of postnatal neurobiological development: implications for human development. *Dev Neuropsychol,* 19**,** 147-71.

WHANG, J. M., SCHOMBURG, C. J., GLOTFELTY, D. E. & TAYLOR, A. W. 1992. Volatilization of fonfos, chlorpyrifos, and atrazine from conventional and no-till surface soils in the field. *Journal of Environmental Quality,* 22**,** 173-180.

WHITNEY, K. D., SEIDLER, F. J. & SLOTKIN, T. A. 1995. Developmental neurotoxicity of chlorpyrifos: cellular mechanisms. *Toxicol Appl Pharmacol,* 134**,** 53-62.

WHO 2001. Organophosphorus pesticides in the environment- Integrated risk assessment. Geneva.

WHO 2008. The global burden of disease- 2004 updated. Geneva.

WHYATT, R. M. & BARR, D. B. 2001. Measurement of organophosphate metabolites in postpartum meconium as a potential biomarker of prenatal exposure: a validation study. *Environ Health Perspect,* 109**,** 417-20.

WIDMANN, C., GIBSON, S., JARPE, M. B. & JOHNSON, G. L. 1999. Mitogen-activated protein kinase: conservation of a three-kinase module from yeast to human. *Physiol Rev,* 79**,** 143-80.

WILLIAMSON, T. L., MARSZALEK, J. R., VECHIO, J. D., BRUIJN, L. I., LEE, M. K., XU, Z., BROWN, R. H., JR. & CLEVELAND, D. W. 1996. Neurofilaments, radial growth of axons, and mechanisms of motor neuron disease. *Cold Spring Harb Symp Quant Biol,* 61**,** 709-23.

WILSON, M. S., GRAHAM, J. R. & BALL, A. J. 2014. Multiparametric High Content Analysis for assessment of neurotoxicity in differentiated neuronal cell lines and human embryonic stem cell-derived neurons. *Neurotoxicology,* 42**,** 33-48.

WRIGHT, L. S., PROWSE, K. R., WALLACE, K., LINSKENS, M. H. & SVENDSEN, C. N. 2006. Human progenitor cells isolated from the developing cortex undergo decreased neurogenesis and eventual senescence following expansion in vitro. *Exp Cell Res,* 312**,** 2107-20.

YANG, C. C. & DENG, J. F. 2007. Intermediate syndrome following organophosphate insecticide poisoning. *J Chin Med Assoc,* 70**,** 467-72.

YANG, D., HOWARD, A., BRUUN, D., AJUA-ALEMANJ, M., PICKART, C. & LEIN, P. J. 2008. Chlorpyrifos and chlorpyrifos-oxon inhibit axonal growth by interfering with the morphogenic activity of acetylcholinesterase. *Toxicol Appl Pharmacol,* 228**,** 32-41.

YANG, J., MUTKUS, L. A., SUMNER, D., STEVENS, J. T., ELDRIDGE, J. C., STRANDHOY, J. W. & ASCHNER, M. 2001. Transendothelial permeability of chlorpyrifos in RBE4 monolayers is modulated by astrocyte-conditioned medium. *Brain Res Mol Brain Res,* 97**,** 43-50.

YANG, Z. & WANG, K. K. 2015. Glial fibrillary acidic protein: from intermediate filament assembly and gliosis to neurobiomarker. *Trends Neurosci,* 38**,** 364-74.

YUAN, A., NIXON, R. A. & RAO, M. V. 2006. Deleting the phosphorylated tail domain of the neurofilament heavy subunit does not alter neurofilament transport rate in vivo. *Neurosci Lett,* 393**,** 264-8.

YUAN, A., RAO, M. V., VEERANNA & NIXON, R. A. 2012. Neurofilaments at a glance. *J Cell Sci,* 125**,** 3257-63.

ZABIK, J. M. & SEIBER, J. N. 1993. Atmospheric transport of organophosphate pesticides from California`s Central Valley to the Sierra Nevada Mountains. *Journal of Environmental Quality,* 22**,** 80-90.

ZECH, R. & CHEMNITIUS, J. M. 1987. Neurotoxicant sensitive esterase. Enzymology and pathophysiology of organophosphorus ester-induced delayed neuropathy. *Prog Neurobiol,* 29**,** 193-218.

ZHANG, H. S., XIAO, J. H., CAO, E. H. & QIN, J. F. 2005. Homocysteine inhibits store-mediated calcium entry in human endothelial cells:

evidence for involvement of membrane potential and actin cytoskeleton. *Mol Cell Biochem,* 269**,** 37-47.

ZHANG, Z., ZOLTEWICZ, J. S., MONDELLO, S., NEWSOM, K. J., YANG, Z., YANG, B., KOBEISSY, F., GUINGAB, J., GLUSHAKOVA, O., ROBICSEK, S., HEATON, S., BUKI, A., HANNAY, J., GOLD, M. S., RUBENSTEIN, R., LU, X. C., DAVE, J. R., SCHMID, K., TORTELLA, F., ROBERTSON, C. S. & WANG, K. K. 2014. Human traumatic brain injury induces autoantibody response against glial fibrillary acidic protein and its breakdown products. *PLoS One,* 9**,** e92698.

ZHENG, Q., OLIVIER, K., WON, Y. K. & POPE, C. N. 2000. Comparative cholinergic neurotoxicity of oral chlorpyrifos exposures in preweanling and adult rats. *Toxicol Sci,* 55**,** 124-32.

8 Appendix

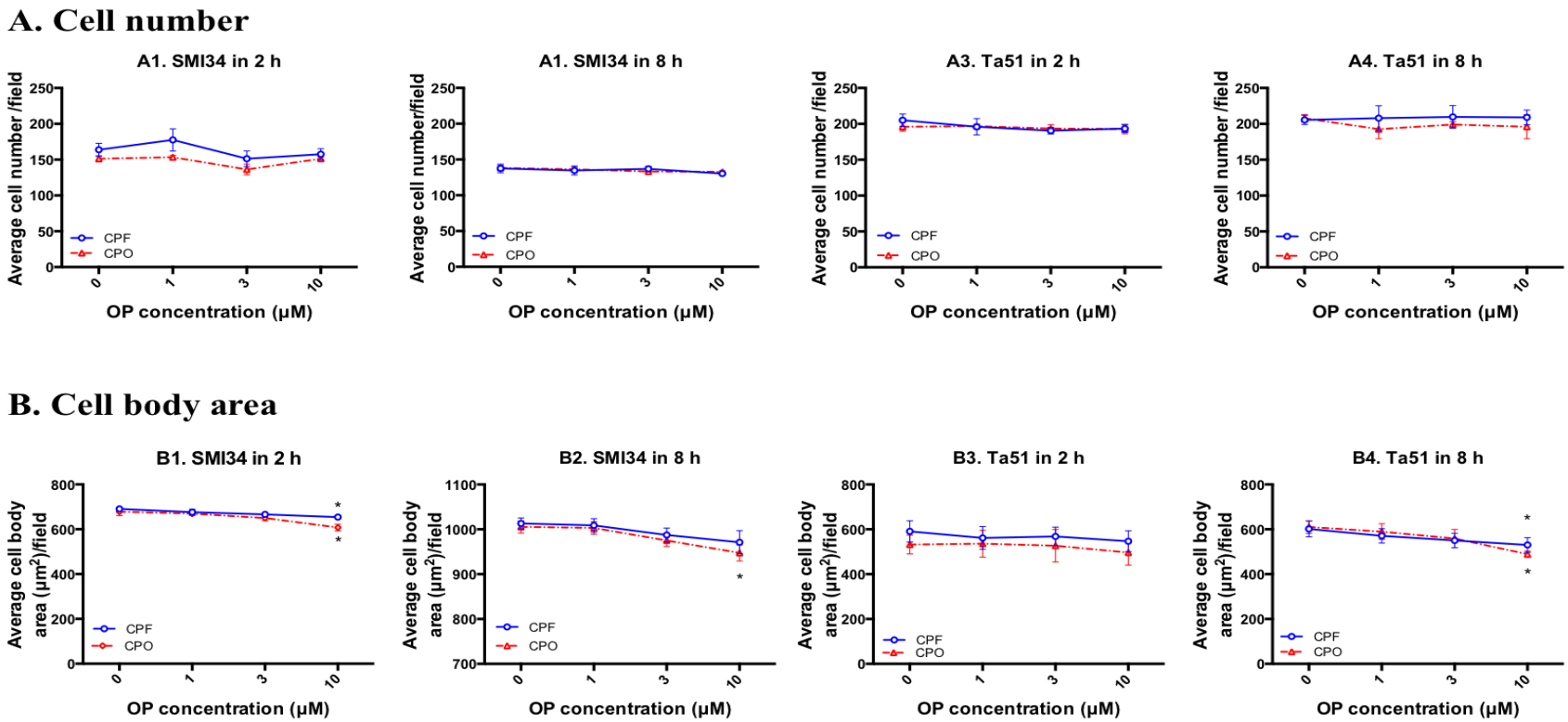

Figure 8.1. Effects of CPF and CPO on cell number and cell body area in pre-differentiated N2a cells as assessed by high throughput assays. Cell were then fixed and stained with SMI34 and Ta51, after which data were acquired using the ImageXpress Micro system and the average cell number/field and the average cell body area/field were measured using MetaXpress imaging and analysis software. Data show dose-related effects of both CPF and CPO on cell number (A) and cell body area (µm) (B) with SMI34 and Ta51 staining at 2 h and 8 h. High throughput data are represented as mean values ± SEM from four independent experiments. Data were analysed using two-way ANOVA. The CPF effects are presented as blue solid lines with circles; the CPO effects are presented as red dashed lines with triangles. Asterisks indicate changes that are statistically different from the non OP-treated controls (*$p < 0.05$). When SEM bars are not apparent, this means that error is smaller than the symbol size.

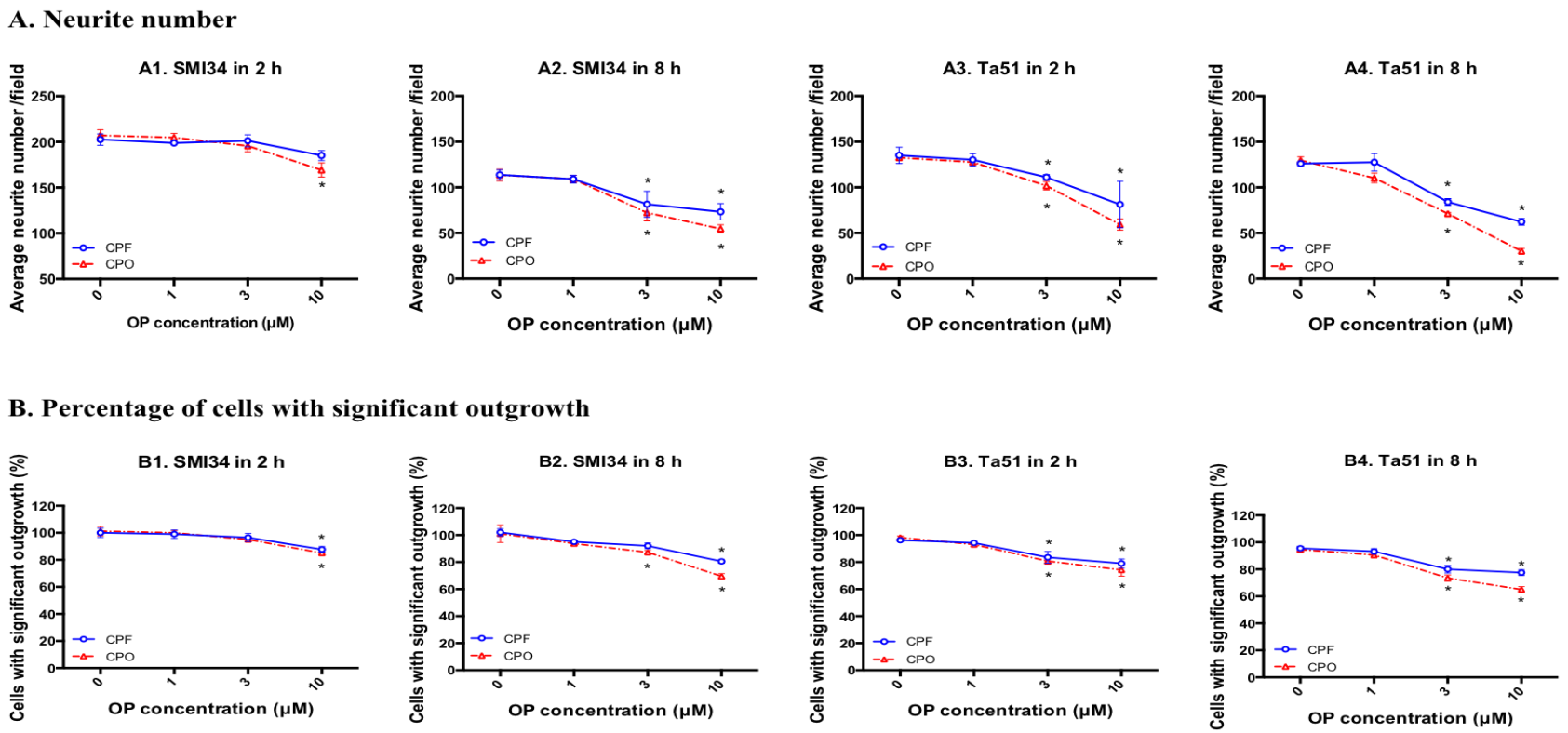

Figure 8.2. Effects of CPF and CPO on neurite number and percentage of cells with significant outgrowth in pre-differentiated N2a cells as assessed by high throughput analysis. Cells were stained with SMI34 and Ta51, after which data were acquired using ImageXpress Micro system and measured using MetaXpress imaging and analysis software. Data show dose-related effects of both CPF and CPO on the average neurite number/field (A) and the percentage of cells with significant outgrowth (B) at 2 and 8 h with SMI34 and Ta51 staining. Data are presented as mean values ± SEM from four independent experiments for both time points. Data were analysed using two-way ANOVA. The CPF effects are presented as blue solid lines with circles; the CPO effects are presented as red dashed lines with triangles. Asterisks indicate changes that are statistically different from the non OP-treated controls ($p < 0.05$). When SEM bars are not apparent, this means that error is smaller than the symbol size.

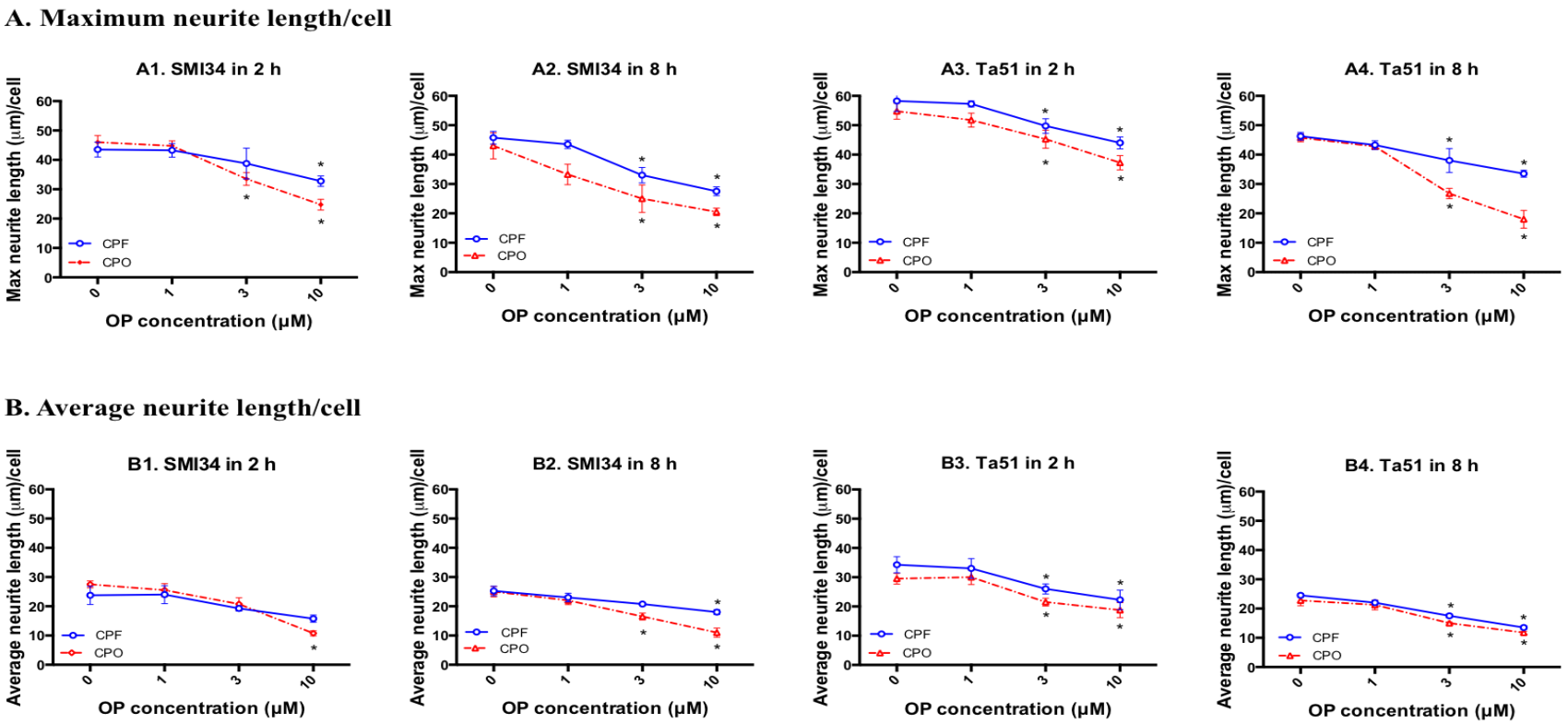

Figure 8.3. Effects of CPF and CPO on maximum and average neurite length/cell in pre-differentiated N2a cells as assessed by high throughput analysis. Cells were stained with SMI34 and Ta51, after which data were acquired using ImageXpress Micro system and measured using MetaXpress imaging and analysis software. Data show dose-related effects of both CPF and CPO on the maximum neurite length/cell (A) and the average neurite length/cell (B) at 2 and 8 h with SMI34 and Ta51 staining. Data are presented as mean values ± SEM from four independent experiments for both time points. Data were analysed using two-way ANOVA. The CPF effects are presented as blue solid lines with circles; the CPO effects are presented as red dashed lines with triangles. Asterisks indicate changes that are statistically different from the non OP-treated controls (*$p < 0.05$). When SEM bars are not apparent, this means that error is smaller than the symbol size.

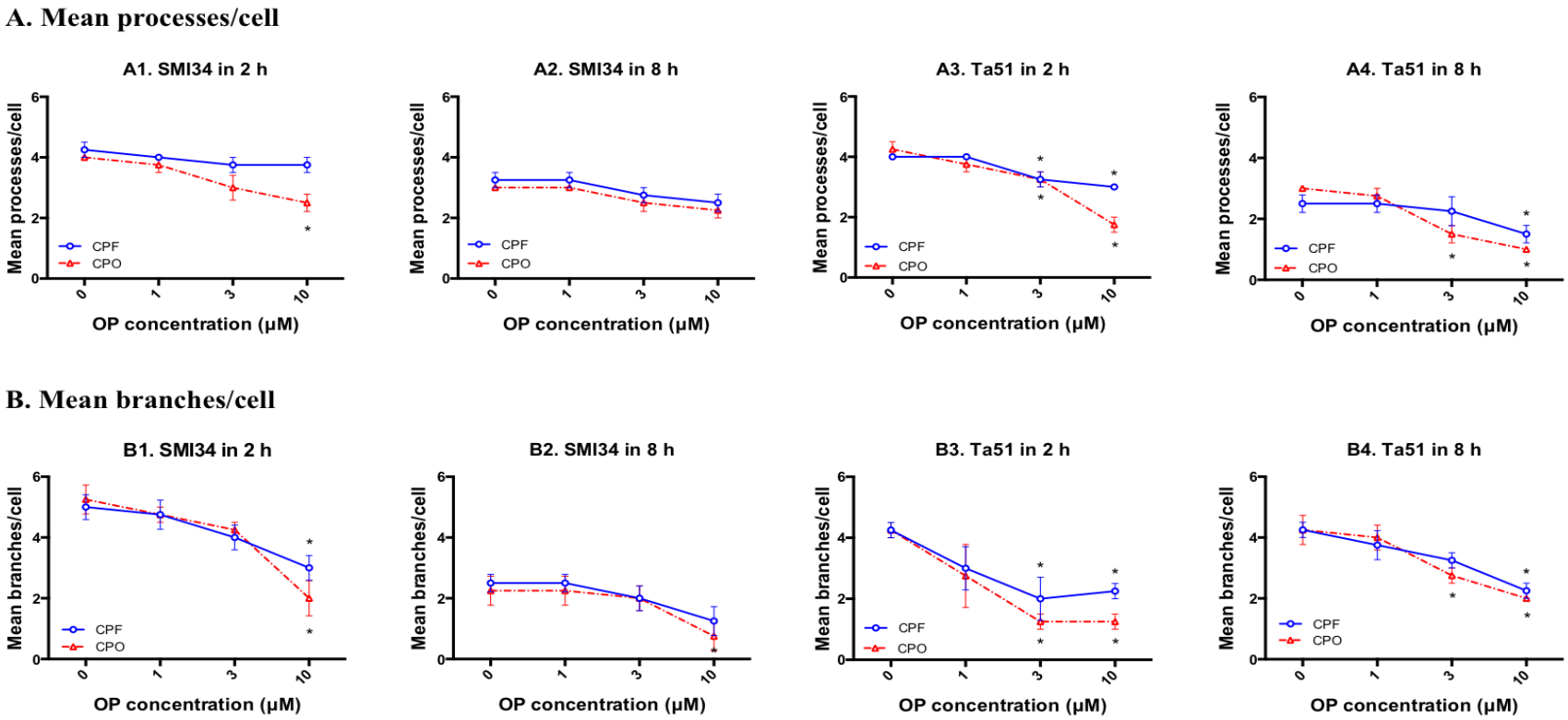

Figure 8.4. Effects of CPF and CPO on the mean number of processes and branches/cell in pre-differentiated N2a cells as assessed by high throughput analysis. Cells were stained with SMI34 and Ta51, after which data were acquired using ImageXpress Micro system and measured using MetaXpress imaging and analysis software. Data show dose-related effects of both CPF and CPO on the mean processes/cell (A) and the mean branches/cell (B) at 2 and 8 h with SMI342 and Ta51 staining. Data are presented as mean values ± SEM from four independent experiments for both time points. Data were analysed using two-way ANOVA. The CPF effects are presented as blue solid lines with circles; the CPO effects are presented as red dashed lines with triangles. Asterisks indicate changes that are statistically different from the non OP-treated controls (*$p < 0.05$). When SEM bars are not apparent, this means that error is smaller than the symbol size.